SMALL SIGNAL STABILITY ASSESSMENT OF THE ESKOM NETWORK BASED ON MEASUREMENTS

Steven Siphesihle Mvuyana

A dissertation submitted to the Faculty of Engineering and the Built Environment, University of the Witwatersrand, Johannesburg, in fulfillment of the requirements for the degree of Master of Science in Engineering.

Faculty of Engineering and the Built Environment
University of the Witwatersrand

Johannesburg, 2014

I declare that this dissertation is my own unaided work. Some of the information presented in this dissertation has been obtained working under the aegis of Eskom Holdings SOC Limited. This dissertation is being submitted to the Degree of Master of Science in Engineering, to the University of the Witwatersrand, Johannesburg. It has not been submitted before for any other degree or examination to any other University.

Signature:

Student: Steven Siphesihle Mvuyana

Student Number: 700051

Date: 31 October 2014

Dedicated To God, who formed me in my mothers womb, who knew me before the foundations of the world were set and who's plans and purposes for me are excellent in every way. His Grace endures forever!

Acknowledgments

The work presented in this dissertation was carried out under the supervision of Dr John van Coller of the School of Electrical and Information Engineering, University of the Witwatersrand, Johannesburg and Mr Thabo Modisane, of Eskom Holdings SOC, System Operations. I wish to thank Dr van Coller and Thabo Modisane for their constant support, patient guidance, and co-operation throughout the course of this research.

I also wish to thank Mr Manny Magro of Eskom Holdings SOC, Protection, Testing and Measurements, Excitation Control Systems, for the many times that he availed himself selflessly to my aid and for his patience, constant support and encouragement which were very much appreciated. Mr Brian Berry of Eskom Holdings SOC, System Operations, for granting me access to the phasor measurement monitoring system and helpful guidance in understanding the various intricacies of simulating large electric power systems.

In addition I would also like to thank:

- my beloved mother Lulu Mvuyana, who taught me the value of hard work and my father Mduduzi Mvuyana, for the discipline he instilled in me;

- my wife Phenyo Mvuyana who encouraged me through the most difficult times and always believed in me when I could not see the forest for the trees. Thank you for your patience, for the love and prayers. You have never ceased to believe in me.

- my family for their patience, support and love;

- my friends for their encouragement;

- my postgraduate friends for their assistance and in helping to create a friendly and stimulating work environment;

- the Eskom Power Plant Engineering Institute (EPPEI) for their financial sponsorship, of special mention are Malcolm Fawkes, Nick Basson, professor Louis Jestin and Robert Jones;

- my home cell members for their constant prayers and support;

- last but certainly not least, my manager Lomile Ngqendesha, who supported me constantly throughout the duration of this research. Thank you.

Abstract

Low frequency oscillations between the ranges of 0.1Hz and 3.0Hz are inherent in power systems. These low frequency oscillations are directly related to the small signal stability of the power system and its ability to function as designed under their constant presence within the power system. This dissertation presents an investigation into the small signal stability performance of the Eskom network with the aim of improving the damping performance of a known inter-area network oscillation mode between the (South-) Western Cape and the North-Eastern Mpumalanga regions. The most cost effective method of damping out these low frequency oscillations is through the use of power system stabilizers. The damping performance of the inter-area oscillation mode of concern was achieved through re-designing the power system stabilizer parameters for stabilizers currently installed within the Eskom network. The designed power system stabilizers were then tested under various network contingencies to ensure that their performance was optimal over a wide range of system conditions.

Contents

List of Appendices

List of Figures

List of Tables

List of symbols

$(\boldsymbol{p} = \frac{d}{dt})$ is the differentiation operator

Δ- deviation

Ψ - generator rotor flux linkage

L_S - is the sub-matrix of the stator self and mutual inductances,

L_R - is a submatrix of the rotor self and mutual inductances,

M_{RS} - is a submatrix of the rotor to stator mutual inductances

M_{SR} - is a sub-matrix of the stator to rotor mutual inductances

R_a, R_b, R_c - generator stator phase resistances

A - state matrix

P_E - generator electrical power

P_M - turbine mechanical power

T'_{do}, T'_{qo} - d-axis, q-axis transient open circuit time constants

T''_{do}, T''_{qo} - d-axis, q-axis sub-transient open circuit time constants

e_d, e_q - d-axis, q-axis terminal voltage components

i_d, i_d - d-axis, q-axis terminal current components

H - shaft inertia constant

K_d - damping torque coefficient

L_{FD} - field winding leakage inductance

L_L - stator leakage inductance

L_{ad}, L_{fd} - d-axis, q-axis stator to rotor mutual inductance

L_d, L_q - d-axis, q axis synchronous inductance

L'_d, L'_q - d-axis, q axis transient inductance

L''_d, L''_q - d-axis, q axis sub-transient inductance

R_{FD} - Field resistance

ζ - damping ratio

δ - rotor angle

ω - rotor angular velocity

AVR - Automatic Voltage Regulator

$SMIB$ - Single Machine Infinite Bus

λ - eigenvalue of power system oscillation mode

pu - per unit

PSS - Power System Stabilizer

f - power system frequency in Hertz (Hz)

ψ- left eigenvector of power system oscillation mode

ϕ- right eigenvector of power system oscillation mode

Note: The notation used for complex numbers in this dissertation is j.

Chapter 1

Introduction

1.1 Background

The human growth rate over the last century has been unprecedented and has had a large impact on all of the main sectors contributing directly to the growth of economies around the world, these sectors being agriculture, industries, commercial, residential and transport. With the global population forecast to increase by twenty five percent (25%) by the year 2040 [25], all sectors within the economy will experience large amounts of growth hence increasing energy demand globally. According to a study presented in [25], the energy demand between 2010 and 2040 is expected to double. This will be driven by developing countries around the world such as China and India with Africa also playing a more prominent role on the global markets.

Within the energy sector itself there are a host of challenges which delay and prevent the growth of the electric network, such as transmission line right of way, high-cost capacity expansion projects and the move away from traditional fossil fuel power plants. These compounded factors force the electric network to operate much closer to its original design limits and reduce the operational security of the network. The consequence of such operating conditions is reduced operational grid security which could lead to increased grid instability or grid blackouts similar to those experienced in North America (2003) [26, 27], India (2012) [28] and South Africa (2007) [29].

The estimated loss of revenue during the blackouts which plagued South Africa was R50 billion [29]. While the drive in the energy sector is to ensure reduced emissions from fossil fuel power plants and increased usage of renewable energy sources, it has also become more important to optimize the existing network infrastructure namely generation, transmission and distribution. The research work carried out within this dissertation solely focuses on the optimization of the generation part of the power network.

Power system networks are among the most complex structures invented by man. They are highly non linear and dynamic systems. Power networks are continuously subjected to disturbances in the form of load fluctuations, various network faults, equipment outages, etc. Hence it is vital that power systems are able to remain stable for most network operating conditions, topologies and contingencies. Reference [11] gives the most widely accepted definition of power system stability:

> "Power system stability is the ability of an electric power system for a given initial operating condition, to regain a state of operating equilibrium after

being subjected to physical disturbance, with most system variables bounded so that practically the entire system remains intact"

1.2 Introduction to Power System Stability

The earliest documented cases of power system instability were recorded as early as in 1920 [1, 5]. These were observed as spontaneous, sporadic oscillations and generator hunting [1]. These were mitigated by using damper windings in generators and turbine-type prime movers with desirable torque-speed characteristics. Power system stability has since evolved into a very specific field and discipline which encompasses a host of specific stability challenges which are faced in modern-day power systems. Figure 1.1 shows the universally accepted classification of power system stability as given in [11]. Generator rotor angle stability is defined as the ability of synchronous machines to remain in synchronism with one another after being subjected to a disturbance, while operating in an interconnected power system [11].

Depending upon the type of disturbance to which the power system is subjected, the response of the generator rotor angle may be described as either transient stability or small signal stability (also known as dynamic stability). Transient stability of a power system is defined as the ability of the power system to remain in synchronism after being subjected to a severe disturbance. Large disturbances may be classified as disturbances which result in large generator rotor angle fluctuations. Conditions which give rise to such operating conditions are normally fault conditions on the grid, large fluctuations of load on the grid, etc. In order to assess whether a power system is transiently stable, it is vital that the initial operating state of the power system and the severity of the fault condition are known and assessed, as transient stability is highly dependent on these conditions [5, 11].

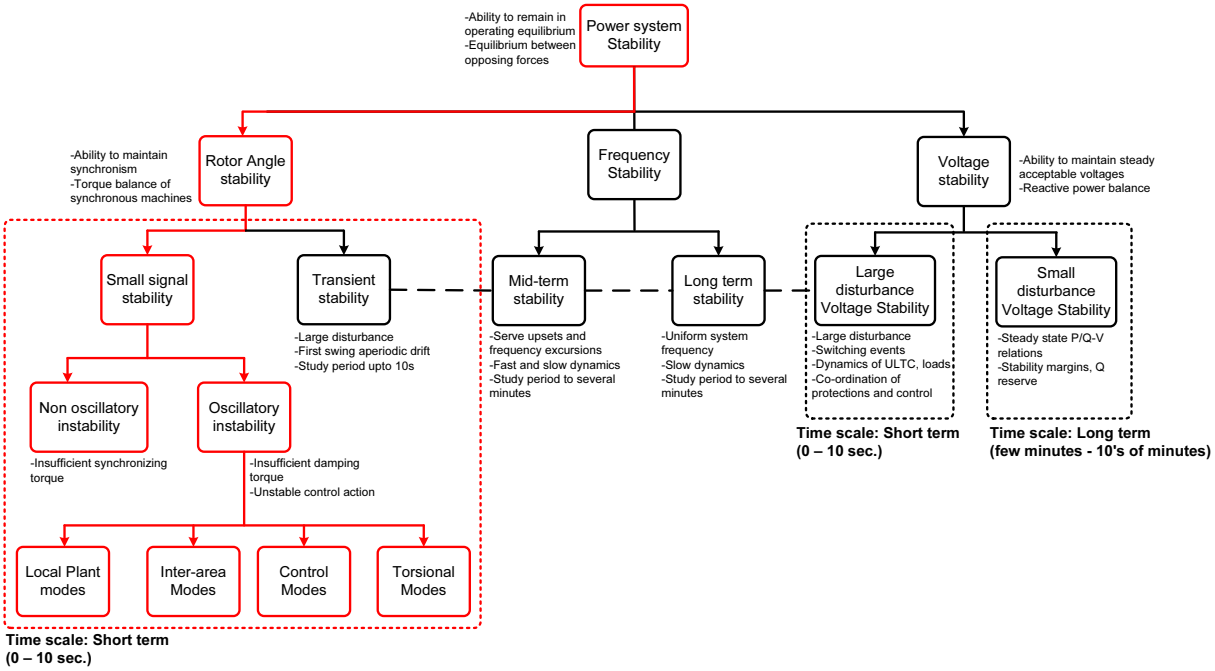

Figure 1.1: Classification of power system stability adapted from [11]

Transient instability in power systems is usually observed as aperiodic angular separation between one or a few synchronous generators within the power system after being subjected to a severe disturbance. This is due to a lack of synchronizing torque within the system and manifests as generator first swing instability [5, 11]. In large networks, transient instability may not always be observed as first swing instability associated with one particular power system mode. In some instances it may be as a result of the superposition of slower acting inter-area modes or local plant swing modes which result in large rotor angle excursions beyond the first swing [5].

Transient instability may also be as a result of non-linear effects affecting a particular swing mode resulting in transient instability well beyond the first swing [11]. Hence the time frame of interest in the study of transient stability phenomena may be three to five (3 to 5) seconds in radial power systems which are not highly meshed and dominated by poorly damped inter-area modes. In such networks the time frame of interest ranges from ten to twenty (10 to 20) seconds.

Small Signal Stability (SSS) in power systems is defined as the ability of a power system to remain in synchronism for small disturbances. "Small disturbances" in this context are classified as disturbances which are small enough to allow the system equations to be linearized about an operating point [5]. As the number of interconnections between power systems of various countries has grown, stability challenges affecting power systems have also become prominent, with SSS being one of the main challenges limiting

the power transfer capabilities of some interconnections. Reference [30] gives various cases of utility experience with small signal instability resulting from various interconnections. Similar to transient stability, in order to assess whether a network will be SSS after being subjected to a disturbance, the initial system operating conditions must be known and the exact disturbance acting on the power system must also be known [11].

SSS constraints in power systems may manifest in two ways, as shown in Figure 1.1, namely non - oscillatory instability and oscillatory instability:

1. Non-Oscillatory Instability (Aperiodic Instability): results from an increasing rotor angle due to a lack of sufficient synchronizing torque (also known as drifting), this has been eliminated through the use of continuously acting Automatic Voltage Regulators (AVRs) installed on most generators as of the 1960s [1].
2. Oscillatory Instability: results from a lack of sufficient damping torque within the power system and often manifests as growing rotor angle oscillations or non-decaying or sustained rotor angle oscillations.

1.3 Electromechanical Oscillation Modes in Power Systems [1, 2]

The various electromechanical oscillation modes which are associated with oscillatory instability are shown in Figure 1.1 and these are:

1. Local Plant Oscillation Modes
2. Inter-area Oscillation Modes
3. Control Oscillation Modes
4. Torsional Oscillation Modes
5. Intra-plant Oscillation Modes.

1.3.1 Local Plant Oscillation Modes

In this mode, a single generator oscillates against the rest of the power system. The power system can be viewed as an infinite bus (constant voltage and constant frequency). When a generator is delivering power into an infinite bus via a long radial line, or through a high impedance, it will be highly susceptible to local plant mode oscillations [18]. The typical oscillation frequency of local plant modes ranges from $0.9Hz$ to $2.0Hz$. Local plant mode oscillations generally tend to be well damped by the power system [18]. Figure 1.2 adapted from [2], shows a simplified single generator unit connected to an infinite bus through a step up transformer and a transmission line, the typical oscillation frequency for local mode oscillations is also shown.

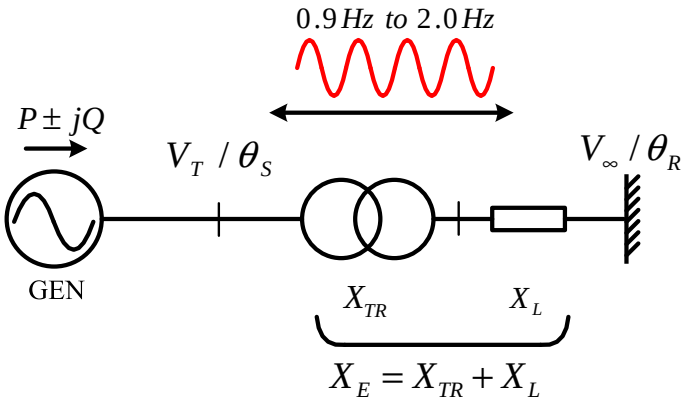

Figure 1.2: Local plant oscillation mode adapted from [2].

1.3.2 Inter-area Oscillation Modes

Inter-area oscillation modes involve coherent groups of generators within a particular area oscillating against other coherent groups of generators within another area of the power system. When particular areas or power systems are connected together through a relatively weak transmission system, the areas will oscillate with respect to one another. The oscillations result from an energy exchange between the two areas. The energy exchange occurs in a cyclical manner with the oscillation frequency ranging from $0.2Hz$ to $0.9Hz$. Figure 1.3 adapted from [12, 2] shows a simplified representation of the inter-area phenomena, whereby generators in Area 1 behave coherently and similarly the generators in Area 2. The two areas are connected via two relatively weak transmission lines resulting in poorly damped inter-area oscillations between Areas 1 and 2

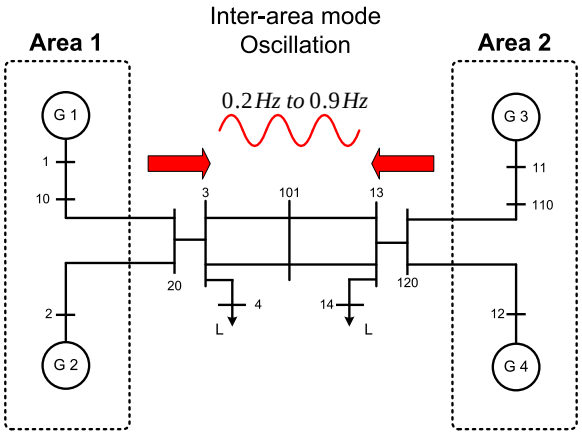

Figure 1.3: Inter-area oscillation modes, adapted from [12, 2].

1.3.3 Control Mode Oscillations

Control mode oscillations in power systems, arise as a result of poorly tuned controllers and also as a result of complex interactions of various power system components. The various system components which give rise to poorly damped control modes in power systems are:

1. Poorly tuned Static Var Compensator (SVC) controllers [31]
2. Poorly tuned High Voltage Direct Current (HVDC) controllers [1]
3. Poorly tuned generator Automatic Voltage Regulator (AVR) controls
4. Poorly tuned governor control loops
5. Cyclical non - linear loads interacting with tap changing transformers in a complex manner [18, 32].

Figure 1.4 shows a simplified oscillation power system with all of the various components which give rise to poorly damped control modes in power systems highlighted. The typical oscillation frequency associated with control modes ranges from $0.02 Hz$ to $0.09 Hz$. Poorly damped control mode oscillations may also be as a result of various control systems interacting with one another through the power system in a complex manner.

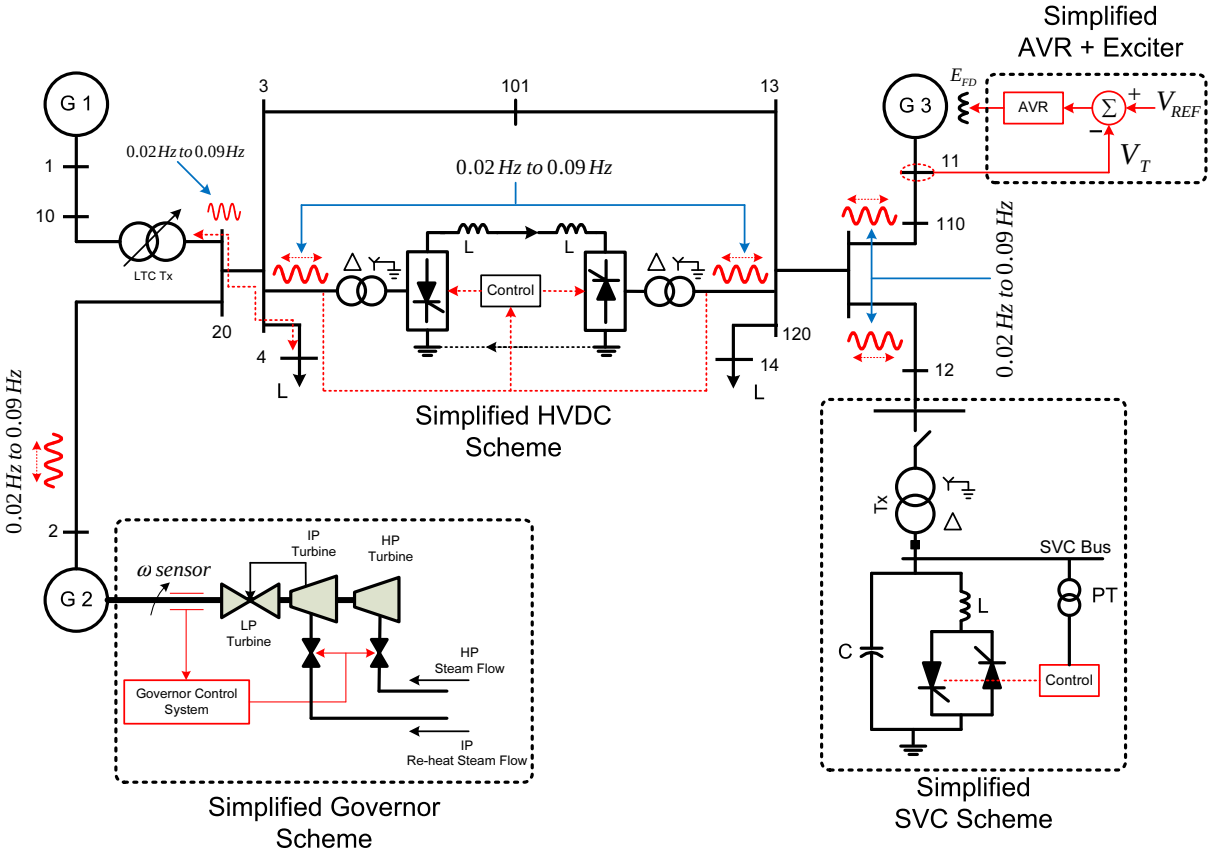

Figure 1.4: Simplified power system showing components and systems which give rise to control mode oscillation in power systems.

Governor Control Loops

Generator governor control systems operate so as to minimize frequency deviations in power systems by adjusting the prime mover so as to control the speed deviations and hence frequency of the power system. The governors at any particular power plant have a set droop characteristic which allows the generators to share power system load according to their respective sizes [18]. Incorrect governor control settings on any one of the units in a power plant would result in the generators competing for load changes in the power system, hence giving rise to power oscillations with a frequency in the control mode oscillation range.

High Voltage Direct Current (HVDC) Controllers

HVDC controllers can cause frequency and power oscillations in power systems. It is vital that the HVDC control system operation is well coordinated with the AC network

generation levels at the rectifier and the inverter ends. Through modulating the active power at the rectifier end, HVDC systems can add damping into the AC network.

Static Var Compensator (SVC) Controllers

SVC controllers, if not tuned properly, can cause voltage oscillations at critical buses within the power system. When disturbances within the grid occur, the SVC response affects the bus voltages, exciting the oscillation modes further and hence exacerbating oscillations in the grid. Similarly the SVC can also add damping in power systems through the use of a supplemental controller and supplemental input signals [30].

Generator Automatic Voltage Regulator (AVR) Controller

The use of continuously acting voltage regulators in order to control generator terminal voltages was initially adopted in the 1940s and 1950s. This greatly improved the operating steady-state limits but it was soon evident that this was detrimental to low frequency oscillations, which were observed to be persistent and poorly damped [30]. The use of high-gain excitation systems improved the transient stability of power systems and has also improved the steady-state stability limit of units connected to very long radial transmission lines. But they have also proved detrimental to SSS as they reduce the damping effect introduced by synchronous generators [30]. Hence in tuning the AVR it is important that the exciter gain is chosen so as not to significantly reduce the inherent positive damping of the generator.

Cyclical Loads interacting with On-Load Tap Changing Transformers

Within a power system, cyclic loads are similar to power system oscillations. When large loads are operated in a cyclical manner they will result in voltage oscillations seen within the power system and On-Load Tap Changer (OLTC) transformers may operate so as to try and restore power system voltages within an acceptable level which may exacerbate the oscillations [32]. Hence it becomes vital that loads are modelled accurately in order to understand their impact on system voltages and hence network oscillations.

1.3.4 Torsional Mode Oscillations

Torsional mode oscillations in power systems arise as a result of the interaction of the mechanical (multistage turbine generator shaft) resonances and the electrical network (series compensated line) resonances. Figure 1.5 shows a simplified multistage turbine-generator shaft train. The mechanical resonances of the various turbine shafts can interact with the series capacitor of the transmission line at the natural frequency of the electrical network, hence giving rise to the resonance condition whereby the turbine rotors can be damaged [33]. Reference [13] states that torsional mode oscillation frequencies range from $4.0Hz$ and above but below synchronous frequency, while [1] states

that the frequency range of interest is between $10Hz$ to $46Hz$. Hence it would be prudent to evaluate each case individually in order to determine the various turbine natural frequencies.

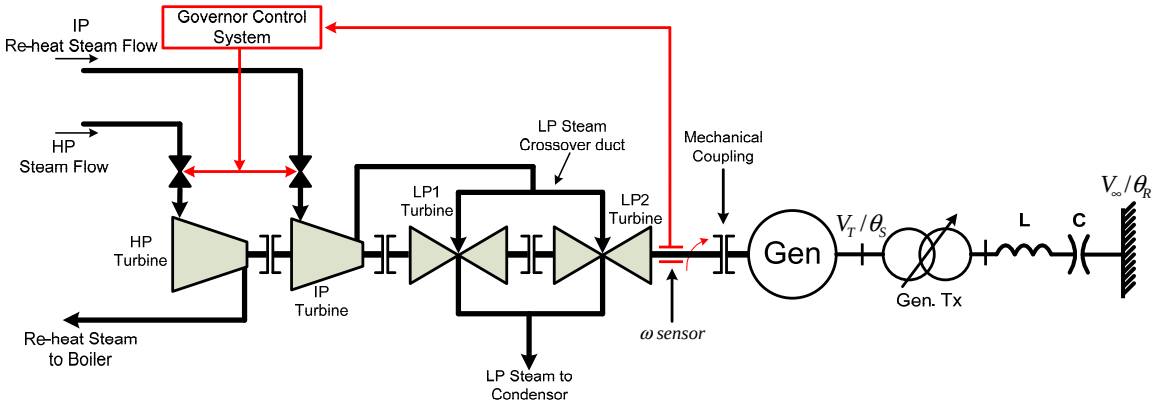

Figure 1.5: Simplified multistage turbine-generator shaft train and series compensated electrical network.

1.3.5 Intra-plant Oscillation Modes

Intra-plant oscillations in power systems occur within a single power plant whereby the units within the plant oscillate against each other. Figure 1.6 adapted from [2] shows a simplified network with the generators at a power plant oscillating against one another. The typical oscillation frequency range is $2.0Hz$ to $3.0Hz$. Intra-plant oscillations can be very poorly damped and at times can be excited by unit controllers interacting with one another, e.g. poorly tuned governor controllers resulting in Intra-plant oscillations.

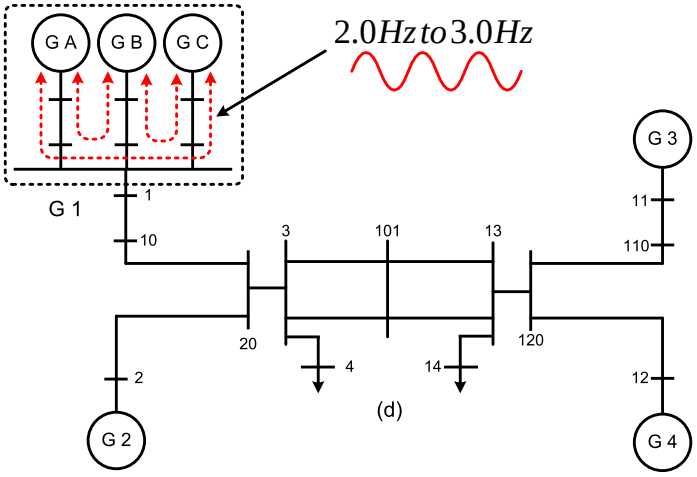

Figure 1.6: Simplified Intra-plant oscillations at a power plant, adapted from [2].

1.4 Control of Power System Oscillations

It is essential to ensure that power system oscillations are controlled and damped effectively in order to ensure that the reliability of the electric power system is not compromised. In order to introduce the required damping into the power system, the control of various power system parameters and variables is critical. There are various methods which have been used to introduce damping into power systems. Reference [30] gives a wide array of power system components which have been used to achieve this. Reference [30] gives the following as some of the methods used in power systems to mitigate power system oscillations:

1. Generator Voltage Regulation:
    a) Through the use of continuously acting AVRs it was noted that transient stability and steady state stability could be improved
    b) After the introduction of continuously acting AVRs, power system oscillations were noted to last much longer and to be predominant
    c) Reference [30] presents a case where a high gain exciter in the Ontario power system limited the power transfer of an interconnection within the network. It was found that by reducing the AVR gain it was possible to improve the damping of network oscillations.
2. Generator AVR Output Modulation:
    a) It is possible to introduce positive damping into the network through the use of supplemental control. Power System Stabilizers (PSSs) were designed in the 1960s when it was noted that the use of continuously acting AVRs had a detrimental effect on the damping of the network
    b) PSSs were designed to act through the AVR and modulate the AVR voltage output in order to implement the damping.
3. Generator Mechanical Power Control:
    a) The use of hydro generators in power systems in order to introduce damping is a well established practice. The fly-wheel effect of the hydro generator provides appropriate modulation of the energy flow in the grid [30].
4. HVDC Control:
    a) HVDC control systems can be used to increase the amount of damping in the AC system. This can be done through modulation of the current order at the rectifier end or through modulating both the current and the voltage order at the inverter end [5].

5. Modulating Shunt Admittance:

    a) Modulating shunt admittance can be done through the use of a voltage regulator, but the power oscillations observed on the network may still have poor damping, hence supplementary controls may be needed.

    b) References [5, 30] state that an SVC offers a very high degree of shunt admittance modulation and the ability to add supplemental controls which allow for sufficient introduction of the necessary damping into the power system.

6. Modulating Shunt Current:

    a) Shunt current modulation in power systems was mainly thought to be for the purposes of reactive power injection, but this concept is not only limited to reactive power injection or control since active power control and injection is also possible.

    b) Static Compensators (STATCOMs) have the ability to allow for shunt current modulation and this adds damping into networks.

7. Modulating Transfer Impedance:

    a) The transfer impedance modulation in power systems is achieved through the use of a Thyristor Controlled Series Capacitor (TCSC). Modulating the impedance of a transmission line based on the dynamic network conditions improves both the transient stability capability of the power system and can also improve the SSS of the network.

    b) The design of the TCSC controllers can be such that a specific oscillation mode or a frequency range of interest is targeted [30]. The controller has to be designed so as to ensure that specific targets are met, e.g. increasing damping or increasing synchronizing torque.

8. Modulating Transmission Phase Angle:

    a) The rapid modulation of the transmission phase angle can greatly enhance the transient and SSS of a power system [30]. In power systems this is achieved through the use of a Thyristor Controlled Phase Shifter (TCPS) or a Unified Power Flow Controller (UPFC).

    b) Modulating the transmission phase angle about an operating point or about an equilibrium point with the appropriate feedback control can greatly enhance the SSS of the power system whereby oscillation modes with poor system damping can be damped.

9. Modulating Load:

a) Varying load center voltage in phase with local frequency variations produces power system damping by superimposing damping torques on remote generators which are supplying the load centers [30]. In order for this concept to work successfully reference [30] states that the various damping torques produced must be in phase with the frequency difference across the power system.

1.5 Research Motivation

The damping of power system oscillations has been studied by many researchers and there exists a large pool of information on the subject. The application of various design techniques and equipment to damp out power system oscillations has not been widely applied within the power industry due to the lack of confidence and practical application. But as the power system evolves and a new host of challenges arise, it becomes necessary that some of these techniques are applied to real world power systems in order to increase power system resilience and reliability.

Within the Eskom network there have been recent network incidents which have resulted in unstable network conditions and power oscillations. Of particular concern in recent network incidents has been the South-Western Cape and Mpumalanga, 0.65Hz oscillation mode. In some incidents the oscillation mode has been found to have poor damping which has resulted in sustained oscillations being observed at some power plants. Hence it has become necessary that a thorough investigation into the instability incidents be conducted and methods to improve operational and dynamic grid stability be proposed using currently existing grid infrastructure. The last documented assessment of the SSS of the Eskom network performed was presented in [34] which was done in 1996. The network has since changed with new transmission lines and loads added onto the network, affecting the network damping and SSS.

The research presented in this dissertation focuses on:

1. Assessing the current state of the SSS of the Eskom network in relation to the instability incidents which have been observed
2. Recreating the instability incidents which have been observed on the network and validating the simulated network response with measured data
3. Using currently existing grid controls and infrastructure to improve the damping response of the network over a range of operating conditions.

References [5, 30, 35] state that PSSs are the most cost effective manner of introducing damping into power systems; hence the research presented in this dissertation focuses solely on the use of PSSs in the Eskom network in order to improve the SSS performance of the network. With all modern AVRs implemented using microprocessor-based hardware and the PSSs included in the control system, the challenge faced by power system

operators is no longer one of power system stabilizer placement within the network but one of optimal tuning to ensure good damping of all oscillation modes of interest. Hence the main focus on improving the damping of the network in this dissertation is the optimal tuning of existing PSSs in order to achieve the desired damping response within the network.

1.6 Goals and Objectives of the Research

In order to conduct the proposed research effectively, research questions were developed to aid and guide the research, these are:

1. What is the current state of the Eskom network with regards to small signal stability?
2. What are the global effects of re-tuning PSSs which are currently installed so as to achieve:
   a) Effective local mode damping?
   b) Effective inter-area damping?
3. Which conventional techniques would be the best suited for re-designing of the PSS within the entire network so as to ensure optimal stability of the network?
4. Would it be beneficial to apply more advanced techniques to improve the stability of the global network versus purely that which can be achieved through conventional design techniques?
5. Investigating the optimal tuning of the PSSs within the Eskom network in order to ensure minimum controller inter-action which may have negative effects on the network stability.

A methodology was developed so as to aid in answering the proposed questions. The methodology presented is modified to suit the desired outcomes of this study, the methodology is based on reference [36]. The proposed methodology is:

Step 1: Full network model verification [22, 21]

Before simulation models can be used it is important that they be validated and that they are able to mimic actual network behaviour. The network model validation procedure used is adapted from [22, 21] and is outlined as follows:

- Steady-state network assessment,
- Dynamic model response assessment,
- Integrated model response.

The performance of the simulation model is validated using actual measurements. Grid incidents which have been identified as having poor damping will be recreated using simulation and the model validated through linear analysis and non-linear time domain simulation.

Step 2: Eigenvalue study and step input response study for individual generator units

In order to study the network instability incidents, it is vital to ensure that all generator units which have been identified as important in this study are modelled accurately and that the behaviour of each of these simulation models is verified with actual measurements. In order to verify each of the generator controllers of concern in this study, namely AVR and PSS, the generators of concern will be tested individually at no load and connected to an infinite bus. The Single Machine Infinite Bus (SMIB) tests results of importance in this step are:

- The system eigenvalue solution, with and without the original stabilizers,
- Through the assessment of the Generator, Excitation system and Power system transfer function, ($GEP\,(s)$, phase lag of system), calculate preliminary values of the PSS phase lead requirement,
- Calculating the time constants and the gains of each PSS, assuming that each of these is derived from the generator rotor speed,
- Calculating each of the PSS gains such that the electromechanical mode to be damped has a minimum damping factor of 10% ($\zeta = 0.1$),
- Calculating the PSSs gain, so that the exciter mode presents a damping factor greater than 15% ($\zeta = 0.15$),
- In order to verify that the PSS gain is not too high, analyse the step response functions $\frac{\triangle V_T(s)}{\triangle V_{REF}(s)}$ and $\frac{\triangle P_T(s)}{\triangle P_{REF}(s)}$, with and without the PSS. The function step response analysis will indicate the improvement introduced by the stabilizer,
- Analysis of the effect of tuning the PSS on the reactive power output of the generators in order to ensure that the PSS gain is not too small. This will be achieved through analysis of $\frac{\triangle Q_T(s)}{\triangle P_{REF}(s)}$ with and without the PSS.

This is a crucial step and will ensure minimization of any controller and generator errors within the model. This step will also ensure good PSS preliminary values are selected.

Step 3: Assessment of three base case scenarios

The tuned controller performance has to be assessed for a host of conditions in order to ensure that the PSS is able to meet the set objectives for each of the conditions identified. The steps which will be carried out to achieve this goal are:

- Establish the minimum damping values for all of the oscillatory modes, with emphasis on the most critical modes identified in Step 2. The experience presented in [30] will be used to aid the process. Set minimum damping values for a chosen base case, for an N-1 case and also for an N-2 case. All other modes associated with other controllers must have a minimum damping which must also be predetermined based on experience presented in [30]
- In order to ensure that all oscillation modes associated with the generators of interest are within the required damping range determined, the eigenvalue solution of the entire system will be computed
- Insert the various PSSs one at a time or all simultaneously, according to the ranking established in Step 2 for each PSS established through the analysis of the transfer function $\frac{\Delta\omega(s)}{\triangle P_{REF}(s)}$ at the oscillation mode of interest. For the parameters used for each PSS determined in Step 2, each PSS is then tuned so as to minimize the dominant oscillation mode of interest at that location
- Each PSS which has been re-tuned must be verified to ensure that it damps the identified oscillation mode without affecting any other oscillation modes in an adverse manner

The design of each of the PSSs will be carried out independently for all of the chosen base cases. One of the main goals in the design process of the PSSs will be to ensure a robust controller performance.

Step 4: Coordinated tuning and optimization of PSSs

Coordinated design of the PSSs is essential for all of the critical modes identified in Step 2. This will be ensured through the accurate modeling of the power system performed in Step 1. The steps to be carried out for coordinated tuning are:

- Accurate design of the PSS will be ensured by determining the departure angle of the root locus for each of the dominant poles of the transfer function $\frac{\Delta\omega(s)}{\triangle P_{REF}(s)}$. In order to ensure that the PSS gain is satisfactory, the root locus of these specific poles will be determined for a variable gain.
- Through coordinated design, parameters of the PSS may be changed in order to ensure the optimal performance of the various PSSs.

A change to the PSS of a power plant, which impacts the inter-area modes, may affect the performance of stabilizers at other power plants. Hence it is vital that all modes within which the generators of interest participate remain stable and are sufficiently damped.

Step 5: Robustness assessments of the re-tuned PSS

The minimum criteria of the damping values determined through case studies presented in [30] is to be analysed for all contingency cases identified in Step 3. Within each

scenario identified in Step 3, the critical modes of interest must have sufficient damping for all contingency cases. The steps to be carried out to assess the robustness of the tuned PSSs are:

- Assess PSS performance for scenarios with depressed transmission voltages, as oscillation damping is sensitive to this variable as stated in Step 2 [36, 37]
- If the identified mode is not damped effectively (below criteria), the PSS which is responsible for damping of that mode will be re-tuned for that specific scenario. The new parameters will then be used for all the chosen base cases and the performance of the system evaluated

Analysis of the selected scenarios identified in Step 3 will be used to determine the impact on the damping of major system modes with:

- Different load modeling (other than constant current, used in all the studies)
- Stabilizer parameter deviations
- The loss of the stabilizer action in critical power stations

Step 6: Non-linear time domain assessment for large signal disturbances

After re-designing of the PSS it is essential to ensure that the large signal disturbance (transient) stability of the network is not compromised. In order to ensure that the transient stability of the network is not compromised, the following analysis will be carried out:

- Based on contingencies identified in Step 3, a transient stability assessment of the network will be carried out and if necessary the stabilizer limiters will be adjusted and the impact of the limit adjustment on the non-linear time domain response will be assessed
- Due to the limits imposed and other system factors which restrict the full operation of the PSS, a minimum reduction on the damping on the transient stability simulation must be set
- Within the full network model, applying a small step disturbance (mechanical power) to plants which oscillate in anti-phase for the oscillation modes of concern

If the transient stability performance of the power system is compromised by the tuned PSS it may be necessary that the PSS be re-tuned so as to reduce the amount of phase compensation introduced [16].

1.7 Thesis Outline

The research presented in this dissertation is organized as follows:

Chapter 1

A general background is presented on the impact of power systems on society and the challenges facing power system engineers with emphasis on power system stability. A brief introduction to power system stability is presented with a focus on rotor angle stability and the classification of various electromechanical modes which arise in power systems and the various components which affect these modes. The control of the various electromechanical modes and the equipment used in power systems, the research motivation and the goals which are to be achieved based on the research questions which were constructed and the methodology which will be used to carry out the research will be presented.

Chapter 2

This chapter presents the concept of power systems represented using mathematical descriptions and the various components and systems within power systems which are important in small signal stability analysis. Fundamental theory associated with small signal stability analysis is presented and various other fundamental concepts are introduced and developed. The excitation control system of power plants which are to be analysed in the dissertation are presented and analysed. The use of a single machine infinite bus model in the assessment of excitation control systems as presented in [7] is analysed and extended using the concepts presented in [38].

Chapter 3

This chapter presents a review of the electromechanical modes of concern within the Eskom network, with a focus on the inter-area oscillation modes, in particular the Southern African Power Pool network oscillation mode and the (South-) Western Cape - Mpumalanga oscillation. The detailed Eskom network model is validated through the use of steady-state and dynamic network parameters and measurements. Network controllability and participation factors are analysed using network incidents and these are compared with the simulated network parameters. Open loop and closed loop measurements are then used to validate the excitation control system performance of one of the generators within the Eskom network. These are compared with the simulated model so as to optimize the model.

Chapter 4

This chapter presents the tuning of power system stabilizers. Various methods are presented and three methods which are the most commonly used in industry for the tuning of power system stabilizers are applied. Eigenvalue assessment along with nonlinear time domain simulation methods are used to verify the performance of the tuned power system stabilizer. The impact of the tuned stabilizer on the generator response is also analysed and the methods which have the least adverse effect on the generator are chosen for further analysis.

Chapter 5

Various network contingencies are presented in this chapter. The use of advanced methods in order to determine exact paths which the inter-area oscillation modes of concern travel within the network is presented, and the persistence of these paths is also analysed. The corridors which are found to have the highest content of the inter-area oscillation energy are analysed. The impact of load dynamics on the oscillation mode damping performance is analysed by introducing a dynamic component into all of the loads within the detailed Eskom network. The total composition of the load is such that it has a dynamic component of approximately 22.5% of the total load content. The designed stabilizers are then assessed within each of the various contingencies identified in order to assess the improved performance which the power system stabilizers offer.

Chapter 6

This chapter presents the conclusions deduced from the results obtained in the various chapters and also presents various suggestions for future research.

Chapter 2

Small Signal Stability Analysis in Power Systems and Modelling Techniques - Literature Review

2.1 Introduction

Power systems can be modelled mathematically through the use of algebraic and differential equations [37, 4]. In carrying out SSS studies, the disturbance acting on the power system is considered to be sufficiently small that the system equations can be linearized about the operating point while still yielding an accurate solution [11]. In linearizing the power system equations about an operating point, the power system behavior can be represented using derived state variables and redundant system variables can be eliminated. Power system component models which are considered in the analysis of SSS and the justification for the exclusion of certain system components in the analysis are presented. The main components which are considered as important in SSS studies are:

- Synchronous generators,
- Excitation Control Systems (ECS),
- Power System Stabilizers (PSSs),
- System loads.

Dynamic component models which have a large impact on SSS, namely synchronous generators, excitation control systems and PSSs are verified through actual measurements. Modal analysis of power systems is a very well defined and accepted practice. It is well known that the use of non-linear time domain simulations for SSS assessment can be deceptive as unstable modes cannot be identified and depending on the system signals being studied, instability may not be observed [30]. A simple Single Machine Infinite Bus (SMIB) model is analysed and modal analysis is used, and this is also extended to multi-machine power systems in order to study the characteristics of multi-machine power systems through analysis of system eigenvalues, left and right eigenvectors, participation factors, modal observability and controllability are determined.

2.2 Power System Component Modeling

2.2.1 Synchronous Machine Model [3, 4]

There are numerous sources of electromechanical oscillation modes in power system as stated in Chapter 1. These oscillations involve the exchange of energy between various components within the grid through the transmission network. Synchronous machines can serve as a source or a sink of oscillation energy within a power system network. The interaction of synchronous machines with various modes within a power system must be modelled accurately to ascertain the exact response and impact of the oscillations on the synchronous machines. Synchronous machines may be modelled with varying degrees of complexity depending on the various studies which are conducted and the level of accuracy required for the studies being conducted. It has become accepted practice to model synchronous machines which are involved directly in the oscillation mode of concern using a relatively detailed machine model (6^{th} order model or higher) and the rest of the synchronous machines using the classical machine model (4^{th} order model). The synchronous machine models used throughout the dissertation are 6^{th} order models unless it is explicitly stated otherwise.

Figure 2.1 adapted from [3] shows a cross section of a generator with the various windings and labelled axes. This model is characterized by the presence of the sub-transient components of the various generator reactances and voltages. Synchronous machine models can be represented mathematically by various equations which describe the electromagnetic behaviour of the rotor, the motion of the rotor, and the stator voltage equations. The generator shown in Figure 2.1 shows a three-phase generator with a three-phase stator armature winding ($\boldsymbol{a,\ b,\ c}$), rotor field winding ($\boldsymbol{f}$) and two damper windings, one in the d-axis ($\boldsymbol{D}$) and one in the q-axis ($\boldsymbol{Q}$).

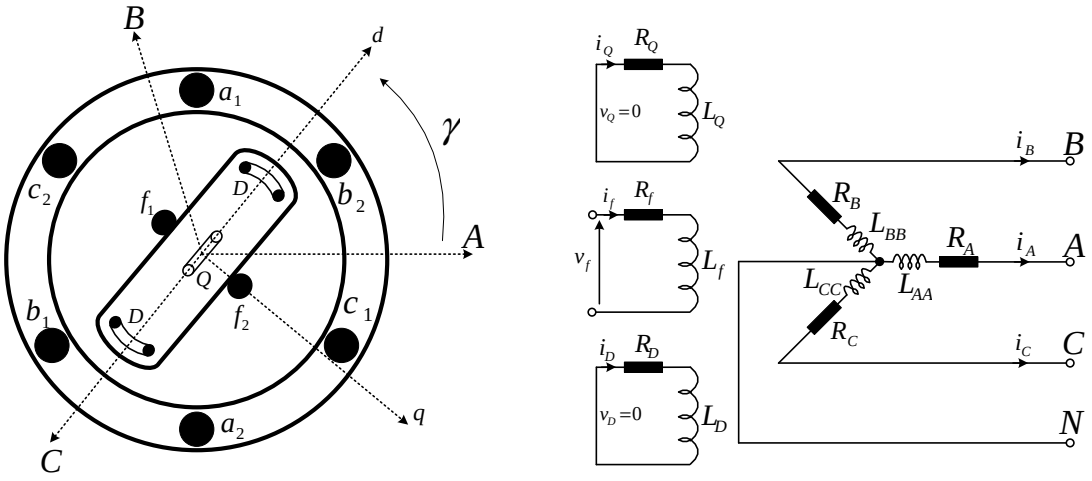

Figure 2.1: Schematic cross section of synchronous machine windings and their axes, adapted from [3].

The following assumptions are made in the derivation of the mathematical model [3]:

1. The three-phase stator windings are symmetrical.
2. The capacitance of all windings can be ignored.
3. Each of the distributed windings may be represented by a concentrated coil.
4. The inductance of the stator windings due to rotor position is sinusoidal and does not contain higher harmonics.
5. Hysteresis losses are negligible but the influence of eddy currents can be included in the model of the damper windings.
6. In the transient and sub-transient states, the rotor speed is near synchronous speed ($\omega \approx \omega_S$).
7. The magnetic circuits are linear and the inductance does not depend on the current flowing.

Analysis of Figure 2.1 shows that the voltage matrix equation for all the windings can be obtained as:

$$\begin{bmatrix} v_A \\ v_B \\ v_C \\ \cdots \\ v_f \\ 0 \\ 0 \end{bmatrix} = \begin{bmatrix} R_A & 0 & 0 & \vdots & 0 & 0 & 0 \\ 0 & R_B & 0 & \vdots & 0 & 0 & 0 \\ 0 & 0 & R_C & \vdots & 0 & 0 & 0 \\ \cdots & \cdots & \cdots & \cdots & \cdots & \cdots & \cdots \\ 0 & 0 & 0 & \vdots & R_f & 0 & 0 \\ 0 & 0 & 0 & \vdots & 0 & R_D & 0 \\ 0 & 0 & 0 & \vdots & 0 & 0 & R_Q \end{bmatrix} \begin{bmatrix} -i_A \\ -i_B \\ -i_C \\ \cdots \\ i_f \\ i_D \\ i_Q \end{bmatrix} + p \begin{bmatrix} \Psi_A \\ \Psi_B \\ \Psi_C \\ \cdots \\ \Psi_f \\ \Psi_D \\ \Psi_Q \end{bmatrix} \tag{2.1}$$

- where $(\boldsymbol{p} = \frac{d}{dt})$ is the differentiation operator, and the flux linkage (Ψ) of each winding can be given in terms of the various self inductances and mutual inductances of the synchronous machine:

$$\begin{bmatrix} \Psi_A \\ \Psi_B \\ \Psi_C \\ \cdots \\ \Psi_f \\ \Psi_D \\ \Psi_Q \end{bmatrix} = \begin{bmatrix} L_{AA} & M_{AB} & M_{AC} & \vdots & M_{Af} & M_{AD} & M_{AQ} \\ M_{BA} & L_{BB} & M_{BC} & \vdots & M_{Bf} & M_{BD} & M_{BQ} \\ M_{CA} & M_{CB} & L_{CC} & \vdots & M_{Cf} & M_{CD} & M_{CQ} \\ \cdots & \cdots & \cdots & \cdots & \cdots & \cdots & \cdots \\ M_{fA} & M_{fB} & M_{fC} & \vdots & L_{ff} & M_{fD} & M_{fQ} \\ M_{DA} & M_{DB} & M_{DC} & \vdots & M_{Df} & L_{DD} & M_{DQ} \\ M_{QA} & M_{QB} & M_{QC} & \vdots & M_{Qf} & M_{QD} & L_{QQ} \end{bmatrix} \begin{bmatrix} -i_A \\ -i_B \\ -i_C \\ \cdots \\ i_f \\ i_D \\ i_Q \end{bmatrix},$$

or

$$\begin{bmatrix} \Psi_{ABC} \\ \cdots \\ \Psi_{fDQ} \end{bmatrix} = \begin{bmatrix} L_S & \vdots & M_{SR} \\ \cdots & \cdots & \cdots \\ M_{RS} & \vdots & L_R \end{bmatrix} \begin{bmatrix} -i_{ABC} \\ \cdots \\ i_{fDQ} \end{bmatrix} \tag{2.2}$$

- where L_S is the sub-matrix of the stator self and mutual inductances. Similarly L_R is a submatrix of the rotor self and mutual inductances. M_{RS} is a submatrix of the rotor to stator mutual inductances. Similarly M_{SR} is a sub-matrix of the stator to rotor mutual inductances.

Based on the assumptions it can be shown that Eq. (2.2) is symmetrical. Analysis of Figure 2.1 shows that the reluctance of the magnetic circuit for the windings varies as a result of rotor position; hence the various stator inductances (L_S) and stator to rotor mutual inductances ($M_{SR}\, and\, M_{RS}$) of the machine are a function of rotor position.

Eq. (2.2) is a time varying differential equation which is computationally intensive; hence

to convert these into time invariant equations, *Park's* modified equations are used. At any instant of time the rotor position relative to the stator reference (phase ***A*** chosen as the reference phase), can be described by the angle (γ) as shown in Figure 2.1. All of the various machine parameters, currents, voltages, reactances, flux linkages etc. can be transformed from the stator reference frame (***a, b, c***) into the (***d, q***, 0) reference frame by projecting one reference frame onto the other through the trigonometric functions of γ. It can be shown that the various self and mutual inductances of the machine can be expressed using the (***d, q***, 0) reference frame by transforming Eq. (2.2) to:

$$\begin{bmatrix} \Psi_0 \\ \Psi_d \\ \Psi_q \\ \cdots \\ \Psi_f \\ \Psi_D \\ \Psi_Q \end{bmatrix} = \begin{bmatrix} L_0 & 0 & 0 & \vdots & 0 & 0 & 0 \\ 0 & L_d & 0 & \vdots & kM_f & kM_D & 0 \\ 0 & 0 & L_q & \vdots & 0 & 0 & kM_Q \\ \cdots & \cdots & \cdots & \cdots & \cdots & \cdots & \cdots \\ 0 & kM_f & 0 & \vdots & L_f & M_{fD} & 0 \\ 0 & kM_D & 0 & \vdots & M_{fD} & L_D & 0 \\ 0 & 0 & kM_Q & \vdots & 0 & 0 & L_Q \end{bmatrix} \begin{bmatrix} -i_0 \\ -i_d \\ -i_q \\ \cdots \\ i_f \\ i_D \\ i_Q \end{bmatrix} \tag{2.3}$$

- where $k = \sqrt{\frac{3}{2}}$. Eq. (2.3) can be rewritten as three independent sets of equations as follows:

$$\Psi_o = L_o i_o \tag{2.4}$$

$$\begin{bmatrix} \Psi_d \\ \Psi_f \\ \Psi_D \end{bmatrix} = \begin{bmatrix} L_d & kM_f & kM_D \\ kM_f & L_f & L_{fD} \\ kM_D & L_{fD} & L_D \end{bmatrix} \begin{bmatrix} -i_d \\ i_f \\ i_D \end{bmatrix} \tag{2.5}$$

$$\begin{bmatrix} \Psi_q \\ \Psi_Q \end{bmatrix} = \begin{bmatrix} L_q & kM_Q \\ kM_Q & L_Q \end{bmatrix} \begin{bmatrix} -i_q \\ i_Q \end{bmatrix} \tag{2.6}$$

Eq. (2.4) to Eq. (2.6) describe three sets of magnetically coupled windings. The windings are shown in Figure 2.2 adapted from [3]. Each set of windings is independent of the others in that there is no magnetic coupling between the sets of windings. The (***f and D***) windings shown in Figure 2.2 and also given by Eq. (2.5) represent the actual field and damper windings of the rotor, and (***d***) winding is a fictitious winding which rotates with the rotor and represents the effect of the three-phase stator winding in the ***d-axis*** of the rotor.

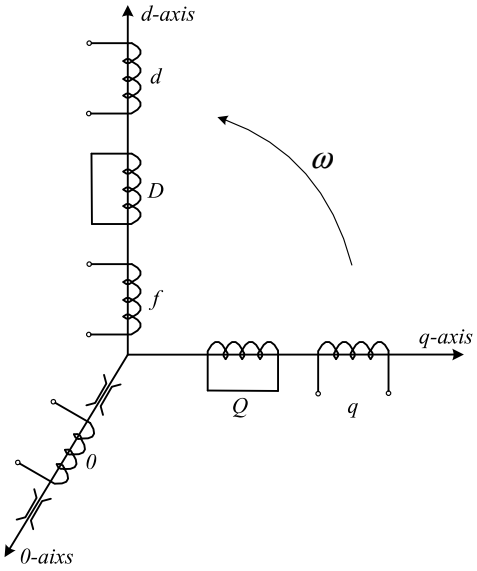

Figure 2.2: Three sets of fictitious windings perpendicular to one another representing synchronous machine windings, adapted from [3].

The two windings on the ***q-axis*** shown in Figure 2.2 (***Q*** and ***q***) also given by Eq. (2.6) represent the actual damper winding on the rotor. Where (***q***) is a fictitious winding which represents the effect of the three-phase stator winding on the ***q-axis***. Eq. (2.4) depicted on the ***0-axis*** as shown in Figure 2.2 represents the third winding which is made up of a single coil which is magnetically decoupled from all other windings. It must be noted that the current flowing in this winding is zero.

The synchronous machine transient and sub-transient parameters can also be represented accordingly using the ***d and q axes***, the machine terminal voltage can similarly be represented using the ***d and q axes*** as given by:

$$\begin{bmatrix} V_d \\ V_q \end{bmatrix} = \begin{bmatrix} E''_d \\ E''_q \end{bmatrix} - \begin{bmatrix} R & X''_q \\ -X''_d & R \end{bmatrix} \begin{bmatrix} I_d \\ I_q \end{bmatrix} \tag{2.7}$$

The equivalent generator circuit showing the ***d and q axes*** terminal voltages using the various sub-transient reactances is shown in Figure 2.3 adapted from [3]. The differential equations describing the various ***d and q axis*** sub-transient and transient voltages are given by Eq. (2.8) to Eq. (2.11).

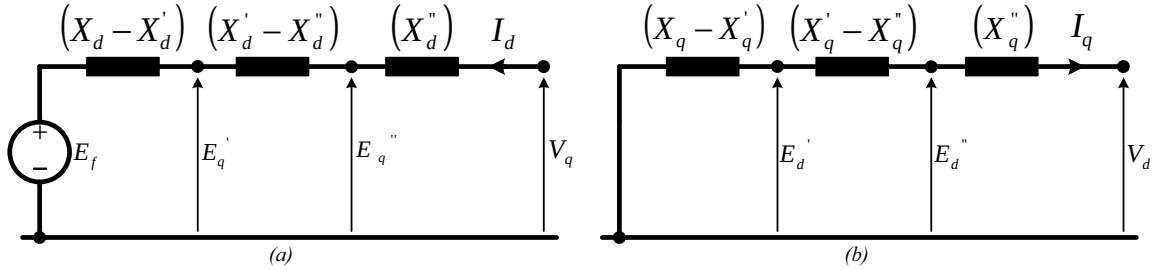

Figure 2.3: Synchronous machine equivalent circuits with resistances neglected, showing ***q and d axis*** terminal voltages, adapted from [3].

$$T_{do}''\dot{E}_q'' = E_q' - E_q'' + I_d\left(X_d' - X_d''\right) \tag{2.8}$$

$$T_{qo}''\dot{E}_d'' = E_d' - E_d'' - I_q\left(X_q' - X_q''\right) \tag{2.9}$$

$$T_{do}'\dot{E}_q' = E_f - E_q' + I_d\left(X_d - X_d'\right) \tag{2.10}$$

$$T_{qo}'\dot{E}_d' = -E_d' - I_q\left(X_q - X_q'\right) \tag{2.11}$$

Eq. (2.8) to Eq. (2.11) describe the change of the synchronous machine electromotive forces (emfs) as the flux linking the various rotor circuits change with time. In order to fully describe the sixth order model of a synchronous machine, the speed and rotor angle deviations must be included with Eq. (2.8) to Eq. (2.11). Hence the inclusion of Eq. (2.12) and Eq. (2.13) (values now in per unit) fully describes the behaviour of a sixth order synchronous machine.

$$\dot{\Delta\omega} = \frac{1}{2H}\left(P_M - P_E - P_D\right) \tag{2.12}$$

$$\dot{\Delta\delta} = \omega_S\left(\omega - 1\right) \tag{2.13}$$

2.2.2 Excitation Control System Model

A number of different excitation control systems are used in industry, with each specific system differing from one manufacturer to the next. Figure 2.4 adapted from [13] shows a simplified block diagram representing the Excitation Control System (ECS), the excitation system and the synchronous machine voltage regulator also known as the Automatic Voltage Regulator (AVR).

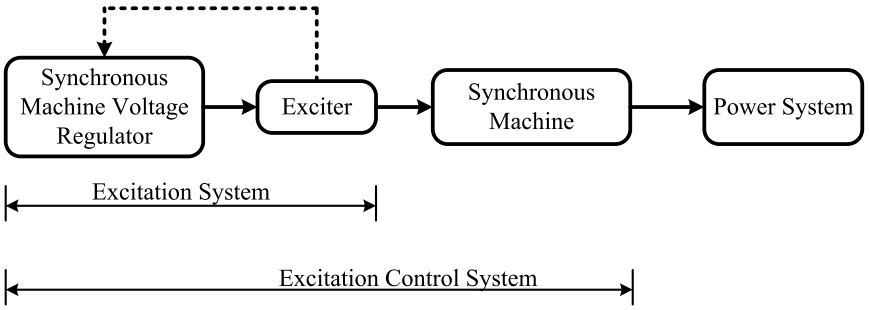

Figure 2.4: Block diagram of an excitation control system, adapted from [13].

Figure 2.5 adapted from [14] shows a more detailed block diagram of a synchronous machine ECS. The chief aim of this section is to present an analysis of the ECS which forms the predominant ECS for most of the generators which are treated throughout the dissertation. Generally in SSS studies the effects of limiters, namely Over-Excitation Limiters (*OELs*), Under-Excitation Limiters (*UELs*) and Volts/Hertz (*V/Hz*) limiters are ignored, and most SSS commercial software packages do not handle the inclusion of generator limiters in the system eigenvalue solution [39]. Hence the effects of *OELs*, *UELs* and *V/Hz* limiter will also be ignored in the analysis carried out in this dissertation.

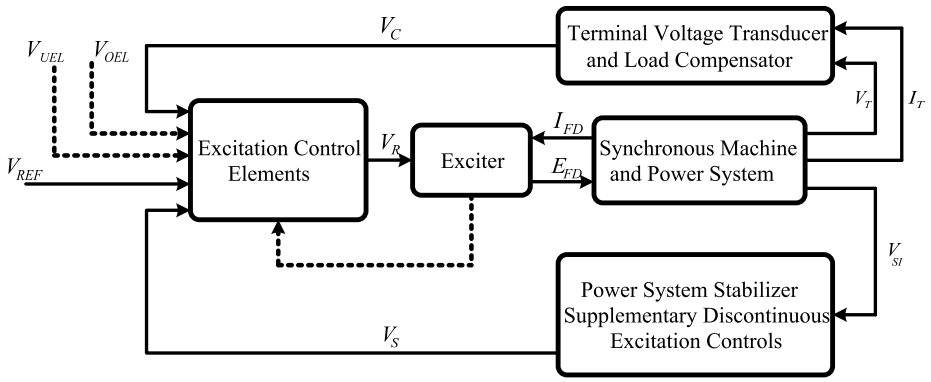

Figure 2.5: General block diagram of synchronous machine excitation control system, adapted from [14].

Figure 2.6 adapted from [15], shows a simplified computer representation of the excitation system which forms part of the main ECS which is used throughout the dissertation. Figure 2.6 (*a*) represents the synchronous machine automatic voltage regulator and (*b*) the main exciter model. The operation of the excitation system is identical to that depicted in Figure 2.4, whereby the AVR output is fed to the synchronous machine rotor field winding via an exciter.

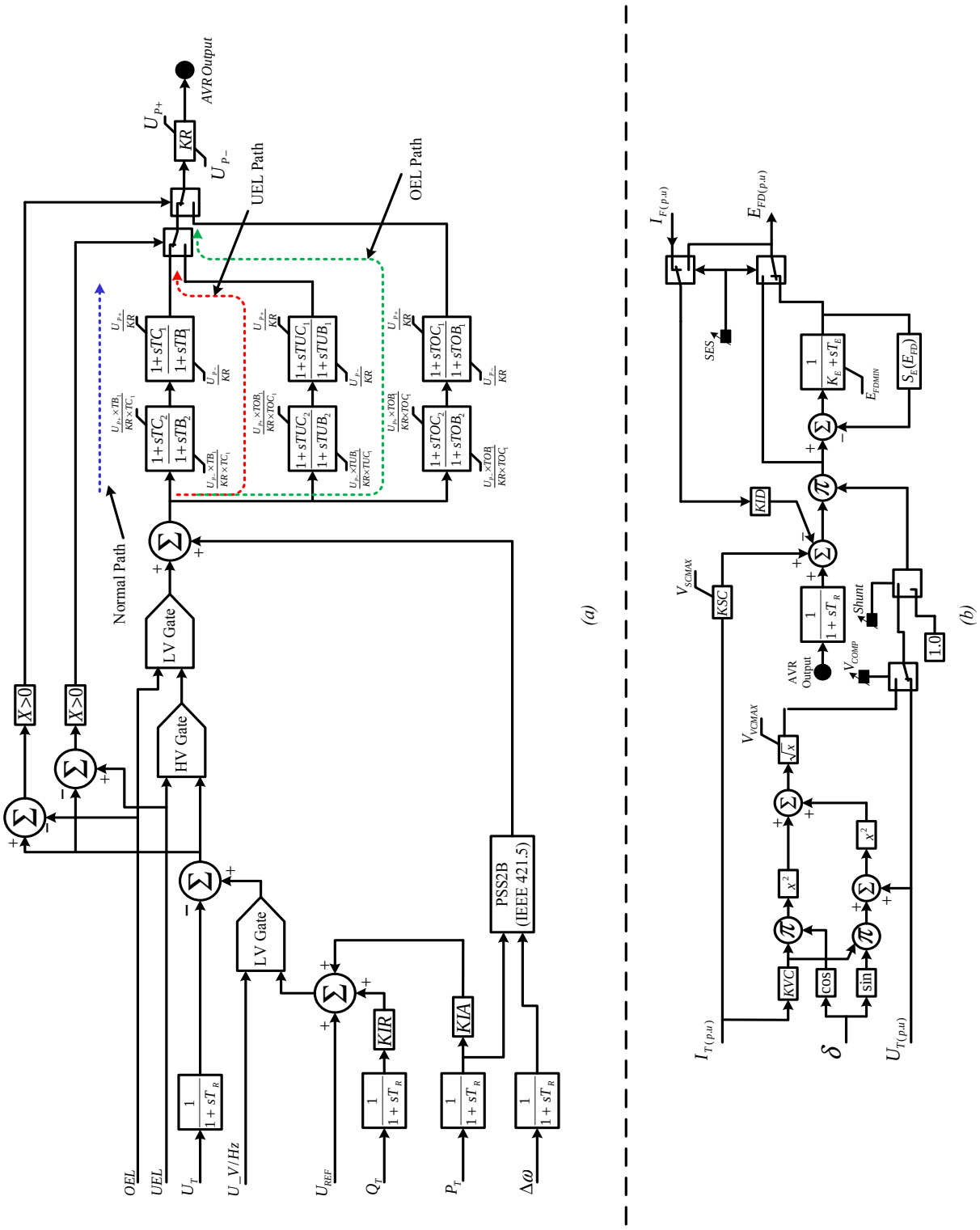

Figure 2.6: Computer representation of the UNITROL 5000 AVR, adapted from [15].

The AVR shown in Figure 2.6 has three operating states which are governed by the operating condition of the generator. Each operating state follows a different compensation path through the AVR:

1. Normal Path: This path is the path which is used as the compensation path within the AVR as long as the operating point of the generator is well within the defined loading capability chart of the synchronous machine. This path is highlighted in Figure 2.6 (a).
2. UEL Path: This path is the main path which is used for compensation within the AVR when the synchronous machine operates in the under-excited state. The logic circuitry shown in Figure 2.6 (a) selects the appropriate AVR compensation channel based on the input from the UEL. The UEL path is highlighted in (a).
3. OEL Path: Similarly this is the path which is used for compensation within the AVR when the synchronous machine operates in the over-excited state. The logic circuitry shown in Figure 2.6 (a) selects the appropriate AVR compensation channel based on the input from the OEL. The OEL path is highlighted in (a).

The OEL and UEL compensators act as transient gain reducers, ensuring that the overall AVR gain is reduced under certain operating conditions thus ensuring that the ECS is not destabilized by the AVR high gain. Each of the compensation paths within the AVR was analysed for each of the scenarios presented within the dissertation. The transfer function, of the plant was derived from the AVR drawing as shown in Figure 2.6 (a), $\frac{Y(s)}{U_T(s)}$ where $Y(s)$ represents the AVR output and $U_T(s)$ represents the machine terminal voltage input. A simplified transfer function, whereby the logic control circuitry is ignored, can be represented by Eq. (2.14) to Eq. (2.16) for each of the various AVR control modes:

$$\frac{Y(s)}{U_T(s)} = \left[\frac{1}{1+sT_R}\right]\left[K_R\left(\frac{1+sT_{C1}}{1+sT_{B1}}\right)\left(\frac{1+sT_{C2}}{1+sT_{B2}}\right)\right] \tag{2.14}$$

$$\frac{Y(s)}{U_T(s)} = \left[\frac{1}{1+sT_R}\right]\left[K_R\left(\frac{1+sTU_{C1}}{1+sTU_{B1}}\right)\left(\frac{1+sTU_{C2}}{1+sTU_{B2}}\right)\right] \tag{2.15}$$

$$\frac{Y(s)}{U_T(s)} = \left[\frac{1}{1+sT_R}\right]\left[K_R\left(\frac{1+sTO_{C1}}{1+sTO_{B1}}\right)\left(\frac{1+sTO_{C2}}{1+sTO_{B2}}\right)\right] \tag{2.16}$$

.

Figure 2.7 shows the Bode plots for each of the AVR paths (U_T ***to AVR output***), the parameters used for the AVR are given in Appendix A.

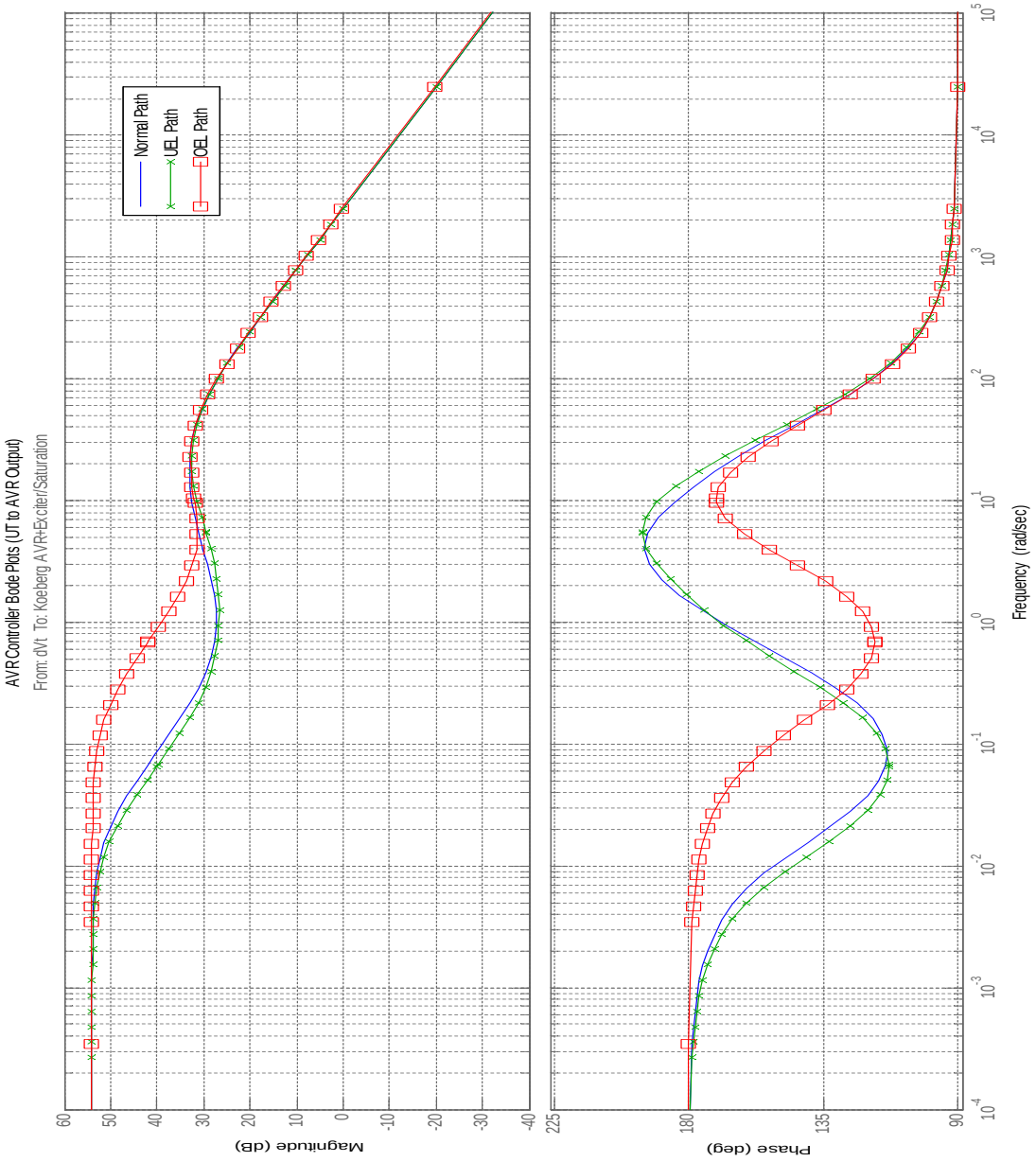

Figure 2.7: AVR controller path Bode plots (U_T ***to AVR output***).

The simplified block diagram shown in Figure 2.6 was used to derive the Bode plot of the excitation system (AVR and exciter) for each of the AVR controller paths (Normal path, UEL path and OEL path) for the path (U_T *to* E_{FD}). The parameters used for the excitation system are presented in Appendix A.

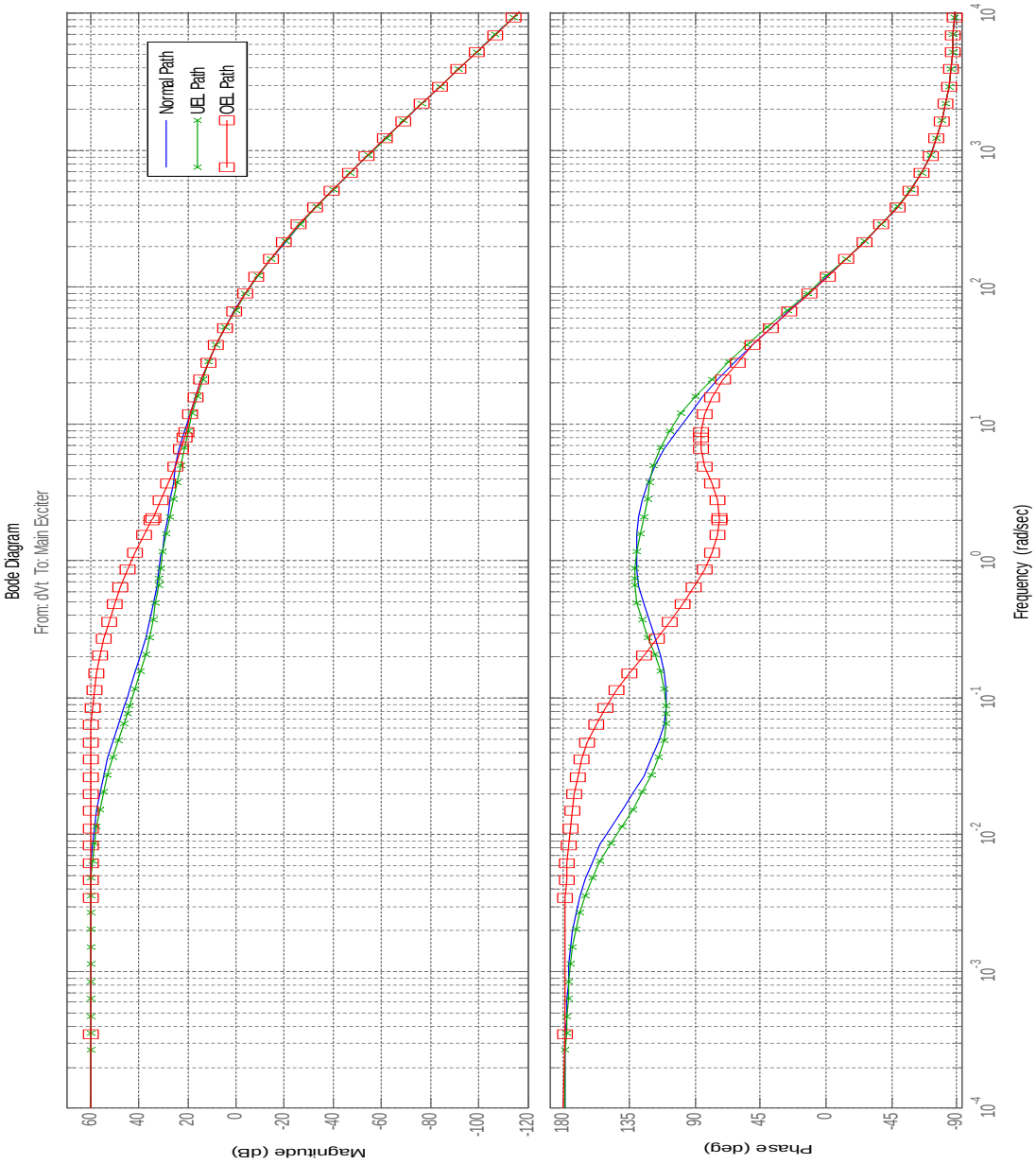

Figure 2.8: Excitation system Bode plots for various paths ($\boldsymbol{U_T}$ ***to*** $\boldsymbol{E_{FD}}$).

2.2.3 Power System Stabilizer

The main aim of a Power System Stabilizer (PSS) is to improve the stability and the dynamic performance of the power system. It does this by introducing a component of electrical torque in phase with the generator rotor speed deviations hence resulting in the introduction of a damping torque [5]. The PSS signal is input into a summing junction in the AVR in a similar manner to that shown in Figure 2.6. There are various types of structures which are used to implement PSSs, each with its own advantages and disadvantages based on the application and technical constraints of each individual case. Reference [14] presents the four types which are the most commonly used within industry.

Three of the stabilizer structures are based on the simplified PSS representation shown in Figure 2.9. The simplest PSS structure has a single input (PSS1A), where the stabilizer input can be power, frequency or rotor speed. This is fed through a high-pass washout filter in order to ensure that the PSS has no effect when no disturbance is present. For two input type PSSs (PSS2A or PSS2B) the filters have an additional role of synthesizing the desired control signal, which is normally rotor speed. The role of the phase compensator is to provide the necessary amount of phase lead which has to be introduced through the PSS, to compensate for the phase lag introduced by the generator field, exciter and the power system. The gain serves to amplify the signal which is then limited in order to ensure that it does not have an adverse impact on the generator terminal voltage [16].

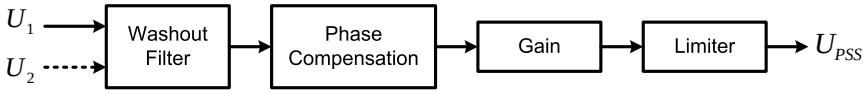

Figure 2.9: Simplified block diagram representation of a typical Lead-Lag type power system stabilizer.

The final type of PSS has a structure which operates as three single-input PSSs in parallel (PSS4B), whereby each of the loops within the PSS is used to target a specific frequency of interest in the power system and the various outputs are summed together yielding the final PSS output.

2.2.3.1 Theoretical Basis of Power System Stabilizer Operation

When a power system is subjected to a disturbance acting on the network, the electrical torque (T_E) of the synchronous machines is perturbed and the imbalance between the electrical and mechanical torque acting on the rotor results in oscillations. These oscillations can be described conceptually by splitting the resultant electrical torque deviation ΔT_E into two components as follows [7, 5]:

$$\Delta T_E = T_S \Delta\delta + T_D \Delta\omega \tag{2.17}$$

where:

$T_S \Delta\delta$ represents the generator synchronizing torque component

$T_D \Delta\omega$ represents the generator damping torque component.

The synchronizing torque component can be viewed as the torque component which serves to hold the generator rotor in synchronism with the rotating field of the stator. The synchronizing torque component plays a very important role in ensuring the transient stability of a power system following a large disturbance. When the power system is subjected to a small disturbance, the synchronizing torque component determines the frequency of oscillation [7]. The damping torque component determines the rate of decay of the oscillations which arise as a result of the disturbances acting on the power system. Damping torque analysis is crucial in small signal stability analysis of power systems.

The analysis of the stability of synchronous machines under small perturbations is based on the work presented in [7]. In analyzing the electromechanical low frequency oscillations in power systems, both the electrical and the mechanical generator loops have to be considered. Figure 2.10 (a) shows a simplified Single Machine Infinite Bus (SMIB) model used to describe how oscillations in power system are controlled. As previously stated, when a power system is subjected to a small disturbance there is an immediate imbalance of the instantaneous electrical and mechanical torques, (T_E) and (T_M). This imbalance results in rotor speed deviations $(\Delta\omega)$, generator load angle deviations $(\Delta\delta)$ and electrical output power deviations (ΔP_E). In order to dampen the oscillations resulting from the disturbances, the amount of damping introduced by the generator has to be sufficient. Analysis of Eq. (2.17) shows that in order to increase oscillation energy damping, a torque component in phase with generator speed deviations produces the desired effect of increased positive damping.

The PSS must compensate for the phase and gain characteristics of the plant through which it must act, which consists of the Generator, Excitation system, and Power system (*GEP(s)*). Figure 2.10 *(a)* shows a representation of the components which are considered in the analysis of *GEP(s)*. Figure 2.10 *(b)* adapted from [16] shows a simplified representation of the SMIB block diagram depicting the relationships between the various ECS variables.

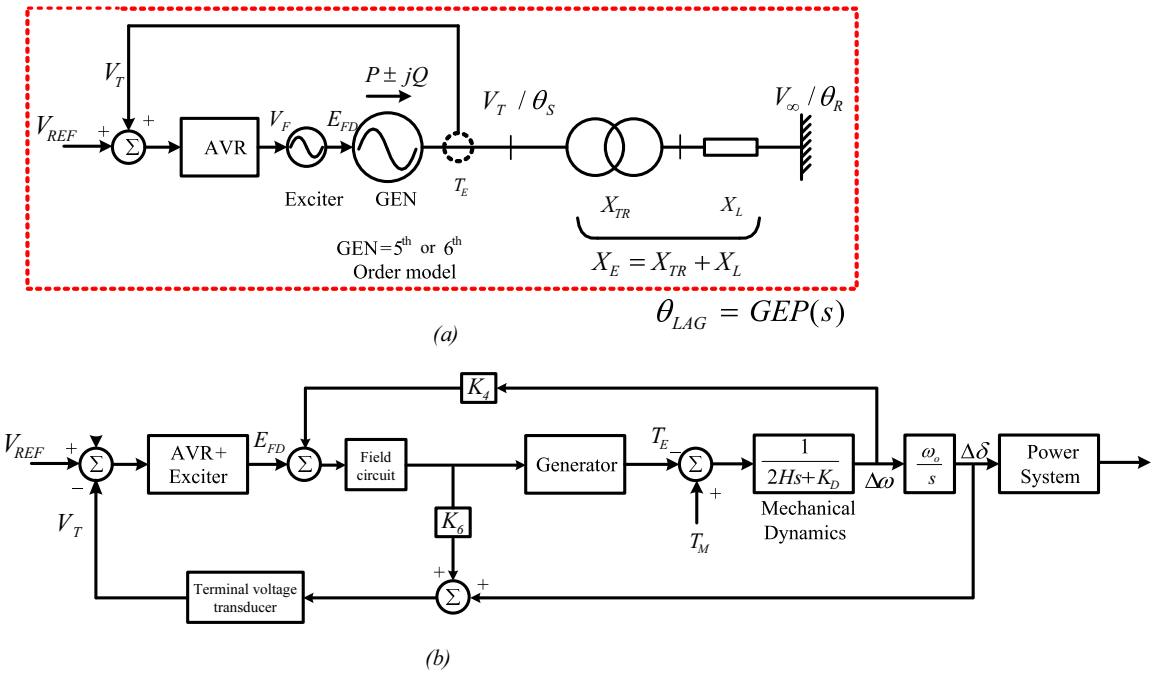

Figure 2.10: Single Machine Infinite Bus Model, adapted from [16].

Eq. (2.17) can be represented schematically as shown in Figure 2.11. The electrical torque is decomposed into its various components and the phase lag of *GEP(s)* represented by θ_{LAG}.

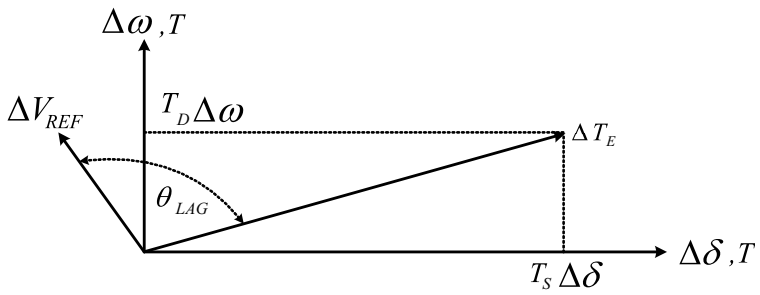

Figure 2.11: Generator electrical torque deviation decomposition.

The phase lag of the transfer function *GEP(s)*, must be compensated for by the introduction of a PSS. Figure 2.12 shows a simplified SMIB model with a PSS, compensating for the gain and phase characteristic of the $GEP(s)$ transfer function.

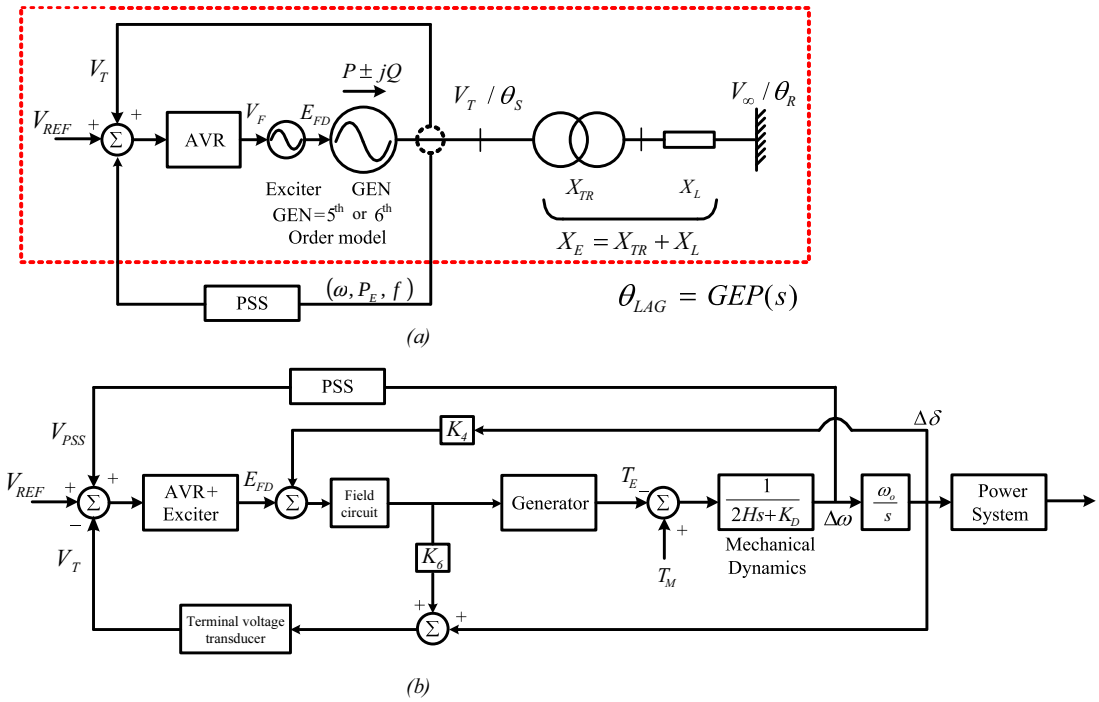

Figure 2.12: Single Machine Infinite Bus Model with PSS adapted from [16].

The PSS introduces a torque component in phase with the speed deviation which acts on the rotor circuit and hence damps the rotor oscillations. Figure 2.13 shows the generator electrical torque decomposition. ΔT_{PSS} is the electrical torque introduced by the PSS at the oscillation frequency of interest. The resultant electrical torque within the generator is given by the vector sum of ΔT_{PSS} and ΔT_E, shown as ΔT_{EP} in Figure 2.13 and α represents the net phase lag between ΔT_{EP} and $\Delta\omega$ after the tuned PSS has been introduced into the plant.

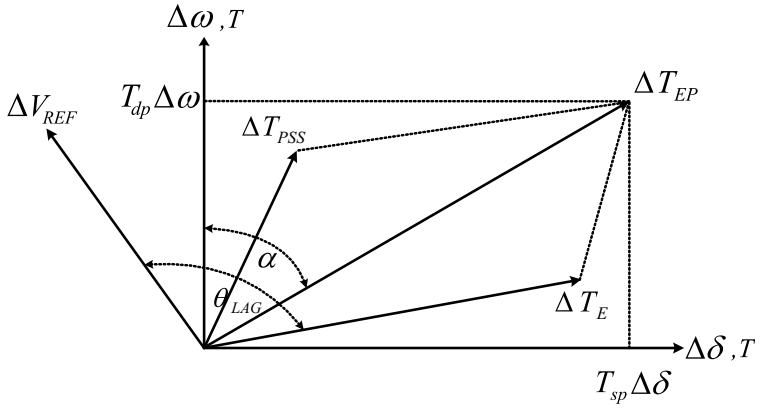

Figure 2.13: Generator torque electrical torque decomposition with PSS.

The PSS design has to ensure that the tuned PSS introduces the required damping and does not have any undesired effect on the excitation system mode, or on the synchronizing torque of the generator. The net phase lag (α) for the tuned PSS must generally be [30, 40]:

1. Less than 90 degrees for as broad a frequency range as possible. If it is allowed to become larger than 90 degrees the PSS will introduce negative damping. α must also be larger than 0 degrees to ensure that the PSS does not have a de-synchronizing effect on the generator synchronizing torque [41].
2. Between the electromechanical frequency ranges of interest (lowest inter-area and local mode or intra-plant mode frequencies) α must be maintained between 0 and 45 degrees. Analysis of Figure 2.13 using trigonometric identities reveals that the damping torque T_{dp} is proportional to the *cosine* of α. Hence for a net phase lag within 0 and 45 degrees, any discrepancies of α will have a small detrimental effect.
3. For higher frequency modes such as the intra-plant oscillation modes, it is important to ensure that there is no overcompensation in this region. To avoid overcompensation α must be larger than -5 degrees.

Ideally from eigenvalue analysis, the compensation which is to be added by the PSS must provide enough phase lead such that the eigenvalue of interest will be shifted perpendicular to the imaginary axis or that the eigenvalue shifts slightly upward from the real axis but with the largest displacement being perpendicular to the imaginary axis [40]. This ensures that the damping torque provided by the PSS is high while also maintaining a high synchronizing torque component and maintaining stability of higher frequency modes such as intra-plant modes. If the eigenvalue motion is downward towards the real axis, this implies that the PSS provides too much phase lead and this results in the PSS detracting from the synchronizing torque hence compromising the transient stability performance of the generator. [42] states that this would result in

the excitation system mode becoming unstable at relatively low values of synchronizing torque.

The PSS used in the project will use the integral of accelerating power, also known as PSS2B [14]. Figure 2.14 shows the basic structure of the PSS2B stabilizer. The PSS2B stabilizers utilize rotor speed ω and electrical power P_E, to synthesize an equivalent speed deviation signal which is given by Eq. (2.18):

$$\Delta\omega_{EQ} = \Delta P_A \bullet \frac{1}{2Hs} = (\Delta P_M - \Delta P_E) \bullet \frac{1}{2Hs} \tag{2.18}$$

where:

$\Delta\omega_{EQ}$ is the equivalent rotor speed deviation,

ΔP_A is the accelerating power deviation acting on the rotor,

H is the inertia constant of the generator shaft,

ΔP_E is the electrical power output deviation of the generator,

ΔP_M is the mechanical power input deviation.

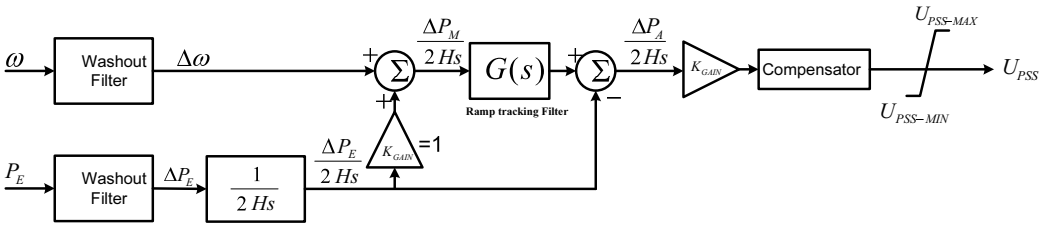

Figure 2.14: Basic structure of the dual input PSS.

The ramp tracking filter in the PSS2B structure shown in Figure 2.14 is represented by:

$$G(s) = \left[\frac{1 + sT_8}{(1 + sT_9)^M}\right]^N$$

The characteristics of the ramp tracking filter have to be chosen so as to ensure that all high frequency components in the speed signal are attenuated accordingly. This is done by choosing T_9, N and M such that the desired behaviour is achieved. T_8 is calculated as $T_8 = M \times T_9$. Hence this ensures that all rapid changes of mechanical and electrical power input signals can be tracked quickly thus minimizing the terminal voltage modulation which may be caused by the PSS [43, 44].

2.2.4 System Load representation

Load models have a significant impact on power system dynamics and have to be represented using dynamic models as the voltage and frequency characteristics of the loads play an important role in small signal stability analysis of power systems. [17] presents an investigation into the small signal instability incident which occurred in 1996 which resulted in the separation of large parts of the Western Electric Coordinating Council (WECC) formally known as the Western System Coordinating Council (WSCC) grid in North America. One of the primary findings presented in [17] was the lack of adequate load representation in the software simulation model used. Figure 2.15 adapted from [17, 18] shows the actual measured WECC response and the simulated response. The actual measured response shows unstable growing oscillations whereas the simulation model stabilized after the disturbance. This prompted various studies within the WECC to determine the composition of the loads to be used for various studies [17]. An "interim" load model is presented in [45] whereby 80% of the total load was modelled as static and 20% was modelled using an induction machine.

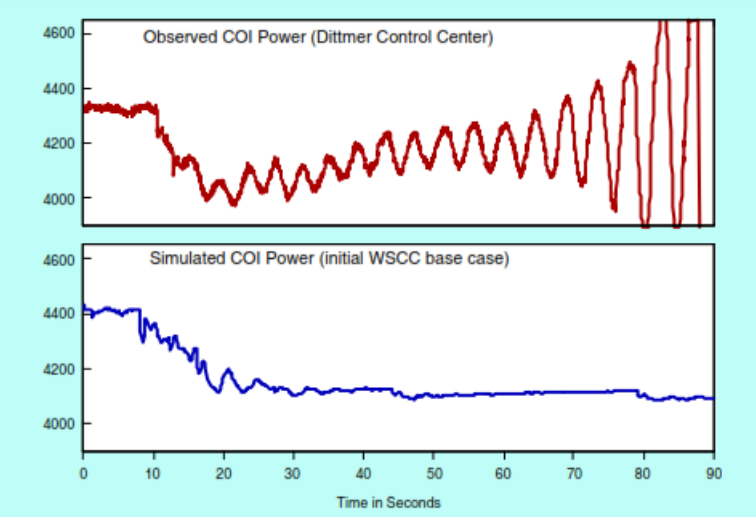

Figure 2.15: 10 August 1996, WECC system disturbance measured and simulated response adapted from [17, 18].

Most power systems loads are composite in nature and creating accurate load models can be complex. In most studies, loads are usually lumped together at the high voltage transmission system busbars. Typical in most simulation studies, loads are represented using *ZIP* models (constant impedance, constant current and constant power loads) as shown by Eq. (2.19). The constant impedance component of the load is proportional to the square of the voltage.The constant current component is directly proportional to the voltage. The constant power component of the load is not affected or related to the

busbar voltage.

$$\begin{aligned} P &= P_0 \left[p_1 \bar{V}^2 + p_2 \bar{V} + p_3 \right] \\ Q &= Q_0 \left[q_1 \bar{V}^2 + q_2 \bar{V} + q_3 \right] \end{aligned} \tag{2.19}$$

Reference [46] states that for SSS studies, especially inter-area mode oscillations, there are large variations in voltage and frequency within the power system, hence the load voltage and frequency characteristics will have a significant impact on the damping of small signal oscillations. Reference [46] cites [47] in stating that representing loads using a constant impedance model for small SSS studies over estimates the damping in a power system by as much as 25%. Thus it is imperative to investigate the influence of load voltage and frequency characteristics on the damping performance of the power systems in SSS studies. The frequency and voltage dynamics of the power system loads which are found to have a significant impact on the oscillation modes of concern will be investigated. Eq. (2.19) will be modified to include the frequency dependency of the load characteristics as follows:

$$\begin{aligned} P &= P_0 \left[p_1 \bar{V}^2 + p_2 \bar{V} + p_3 \right] (1 + K_{pf} \Delta f) \\ Q &= Q_0 \left[q_1 \bar{V}^2 + q_2 \bar{V} + q_3 \right] (1 + K_{qf} \Delta f) \end{aligned} \tag{2.20}$$

- where:

Δf gives the frequency deviation $(f - f_0)$

K_{pf} and K_{qf} give the frequency dependency of the active and reactive power components of the load.

Figure 2.16 adapted from [5] shows a generalized composite load model which is used to represent typical power system loads as viewed from a typical substation busbar. The static load model parameters K_{pf}, K_{qf}, p_1 to p_3 and q_1 to q_3 are taken from [48]. The data used for the dynamic model induction machine is adapted from [45]. Transformer saturation and the capacitors will also be modelled. Discharge lighting loads and thermostatically controlled loads will not be modelled. The frequency and voltage characteristics of the various loads of concern will be based on actual measurements presented by [48].

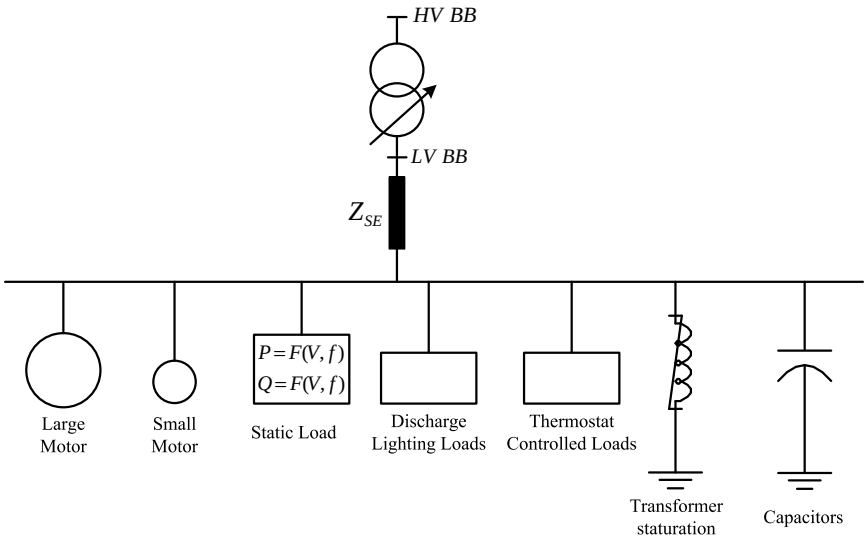

Figure 2.16: Composite static and dynamic load model adapted from[5].

2.3 Fundamental Theory for Small Signal Stability Analysis [5, 4]

Power systems can be represented using differential and algebraic equations as previously stated. These equations can be represented in state space format as follows:

$$\dot{x} = f(x, u) \tag{2.21}$$

- where

$x = [x_1, x_2, \cdots, x_n]^T$, is the state vector with n state variables

$u = [u_1, u_2, \cdots, u_m]^T$ is the input vector to the system with m inputs.

The output variables of interest can be expressed in state space format as follows:

$$y = g(x, u) \tag{2.22}$$

- where:

$y = [y_1, y_2, \cdots, y_k]^T$, is an output vector of the power system with k outputs,

$g = [g_1, g_2, \cdots, g_k]^T$, is the vector of k non-linear functions relating the state and input variables to the output variables

The derivatives of the state variables $\dot{x}$ are all simultaneously zero at equilibrium points, hence

$$\dot{x_0} = f(x_0, u_0) = 0 \tag{2.23}$$

In Eq. (2.23) x_0 and u_0 are the steady state values of the state and input vectors respectively. If the system is perturbed from an equilibrium point, the state and input vectors can be described as follows:

$$\begin{aligned} x &= x_0 + \Delta x \\ u &= u_0 + \Delta u \end{aligned} \tag{2.24}$$

- where Δ denotes small deviations. Eq. (2.21) can be written as follows:

$$\dot{x} = \dot{x_0} + \Delta\dot{x} = f\left[(x_0 + \Delta x), (u_0 + \Delta u)\right] \tag{2.25}$$

The perturbations acting on the system are assumed to be very small and the non-linear function $f(x, u)$ can be expressed using Taylor's series expansion and all of the higher order terms in the expression can be neglected. Hence Eq. (2.25) can be expressed as:

$$\begin{aligned} \dot{x} &= \dot{x_{i0}} + \Delta\dot{x_i} = f_i\left[(x_0 + \Delta x), (u_0 + u)\right] \\ &= f_i(x_0, u_0) + \left(\frac{\partial f_i}{\partial x_1}\Delta x_1 + \cdots + \frac{\partial f_i}{\partial x_n}\Delta x_n\right) + \left(\frac{\partial f_i}{\partial u_1}\Delta u_1 + \cdots + \frac{\partial f_i}{\partial u_m}\Delta u_m\right) \end{aligned}$$

Since $\dot{x_{i0}} = f_i(x_0, u_0)$, we have that:

$$\Delta\dot{x_i} = \left(\frac{\partial f_i}{\partial x_1}\Delta x_1 + \cdots + \frac{\partial f_i}{\partial x_n}\Delta x_n\right) + \left(\frac{\partial f_i}{\partial u_1}\Delta u_1 + \cdots + \frac{\partial f_i}{\partial u_m}\Delta u_m\right)$$

- with *i=1, 2 . . . , n.* Similarly Eq. (2.22) can also be expressed using Taylor's series as follows:

$$\Delta y_j = \left(\frac{\partial g_j}{\partial x_1}\Delta x_1 + \cdots + \frac{\partial g_j}{\partial x_n}\Delta x_n\right) + \left(\frac{\partial g_j}{\partial u_1}\Delta u_1 + \cdots + \frac{\partial g_j}{\partial u_m}\Delta u_m\right)$$

- with *j=1,2, . . . , k.* Hence Eq. (2.21) to Eq. (2.22) can be expressed in linearized form as:

$$\Delta\dot{x} = A\Delta x + B\Delta u \tag{2.26}$$

$$\Delta y = C\Delta x + D\Delta u \tag{2.27}$$

- where:

$$
\begin{aligned}
A &= \begin{bmatrix} \frac{\partial f_1}{\partial x_1} & \dots & \frac{\partial f_1}{\partial x_n} \\ \vdots & \dots & \vdots \\ \frac{\partial f_n}{\partial x_1} & \dots & \frac{\partial f_n}{\partial x_n} \end{bmatrix} B = \begin{bmatrix} \frac{\partial f_1}{\partial u_1} & \dots & \frac{\partial f_1}{\partial u_m} \\ \vdots & \dots & \vdots \\ \frac{\partial f_n}{\partial u_1} & \dots & \frac{\partial f_n}{\partial u_m} \end{bmatrix} \\
C &= \begin{bmatrix} \frac{\partial g_1}{\partial x_1} & \dots & \frac{\partial g_1}{\partial x_n} \\ \vdots & \dots & \vdots \\ \frac{\partial g_k}{\partial x_1} & \dots & \frac{\partial g_n}{\partial x_n} \end{bmatrix} D = \begin{bmatrix} \frac{\partial g_1}{\partial u_1} & \dots & \frac{\partial g_1}{\partial u_m} \\ \vdots & \dots & \vdots \\ \frac{\partial g_k}{\partial u_1} & \dots & \frac{\partial g_m}{\partial u_m} \end{bmatrix}
\end{aligned} \tag{2.28}
$$

All of the partial derivatives of the matrices A *to* D in Eq. (2.28) are evaluated at the equilibrium point for small perturbations acting on the system, in Eq. (2.26) to Eq. (2.27),

Δx is the state vector deviation of the system, with dimension n

Δy is the output vector deviation of the system, with dimension k

Δu is the input vector deviation of the system, with dimension m

A is the state or the plant matrix of the system, with size $n \times n$

B is the control or the input matrix of the system, with size $n \times m$

C is the output matrix of the system, with size $k \times n$

D is the feed forward matrix which defines the proportion of the input which appears directly in the output, with size $k \times m$.

2.3.1 Modal Analysis of Power Systems

In order to be able to extract information about the system which is being analysed, the state space model of the system has to be formulated. From the state space model the eigenvalues, eigenvector properties and participation factors can be determined.

2.3.1.1 Eigenvalues and Eigenvector Analysis in Power Systems

The eigenvalues of the state matrix given by A can be calculated from the scalar parameter λ for which there exists a non-trivial solution that satisfies:

$$
A\phi = \lambda\phi \tag{2.29}
$$

- where ϕ is an $n \times 1$ column vector. For any eigenvalue λ_j, the $n \times 1$ column vector ϕ_j, which satisfies Eq. (2.29) is called the right eigenvector of A, associated with λ_j. Hence Eq. (2.29) can be written as:

$$A\phi_j = \lambda_j \phi_j \tag{2.30}$$

$$\phi_j = [\phi_{1j}, \phi_{2j}, \cdots, \phi_{nj}]^T \tag{2.31}$$

- where $j = 1, 2 \ldots, n$. The right eigenvector given by Eq. (2.31) for any particular j gives the mode shape of the mode of interest, λ_j. The mode shape of λ_j defines the distribution of the mode through the various system state variables. All of the components of the mode shape contain information about the observability of the mode of interest in the various state variables corresponding to the power system.

In a similar manner, a $1 \times n$ row vector ψ_j that satisfies:

$$\psi_j A = \lambda_j \psi_j$$

$$\psi_j = [\psi_{1j}, \psi_{2j}, \cdots, \psi_{nj}] \tag{2.32}$$

- where $j = 1, 2 \ldots, n$. ψ_j is called the left eigenvector of the system, associated with eigenvalue λ_j. The left eigenvector of the system defines the distribution of state variables of a specific mode of interest. The left eigenvector has a direct effect on the amplitude of the mode of interest excited by a specific state variable. The various components of the left eigenvector contain information regarding the controllability of the mode of interest with respect to the component of interest.

The stability of the dynamic system about an operating point (x_0, u_0) can be determined through analysis of the system eigenvalues. The eigenvalues of the system are analysed using root locus techniques. The system is said to be stable for a particular operating point if all of the eigenvalues of the system are in the left-hand side of the complex plane. Otherwise the system is said to be unstable. A real eigenvalue corresponds to a non-oscillatory mode (if the eigenvalue is positive it represents aperiodic instability, if the eigenvalue is negative it represents a decaying mode, where the larger the magnitude the faster the mode decay). Complex eigenvalues $(\delta \pm j\omega)$, occur in conjugate pairs, the real component of the eigenvalue gives an indication of the system damping, the imaginary component gives the frequency of the oscillation in rad/sec. The damping ratio of the oscillation mode of interest is given by:

$$\zeta = \frac{-\delta}{\sqrt{\delta^2 + \omega^2}} \tag{2.33}$$

The oscillation frequency of a complex pair of eigenvalues is given by:

$$f = \frac{\omega}{2\pi} \tag{2.34}$$

2.3.1.2 Participation Factor Analysis in Power Systems

The main drawback in the use of left and right eigenvectors for determining system stability and the various relationships between the state variables and oscillation modes of interest is that the eigenvectors are dependent on units and scaling factors associated with the various state variables. This is avoided by introducing the (dimensionless) participation matrix P, which combines the left and the right eigenvectors as follows:

$$p_{ij} = \phi_{ij}\psi_{ij} \tag{2.35}$$

- where p_{ij} gives the participation factor for the i^{th} state variable in the j^{th} oscillation mode, and ϕ_{ij} is the i^{th} entry of the j^{th} right eigenvector of the system. ϕ_{ij} provides observability information regarding the i^{th} state variable in the j^{th} oscillation mode of the system. ψ_{ij} provides a measure of the j^{th} oscillation mode activity regarding the i^{th} state variable. Participation factors can be viewed as the sensitivity of the j^{th} eigenvalue to a change in the i^{th} diagonal element of the state matrix A. Participation factors are indicative of the relative participations of the respective state variables in the corresponding oscillation modes.

The participation vector p_j, is defined as the vector containing all the participation factors for the j^{th} oscillation mode of interest. The participation matrix, P, is defined as follows:

$$P = [p_1, p_2, \ldots, p_n] \tag{2.36}$$

with (column vector)

$$p_i = [p_{1j}, p_{2j}, \ldots, p_{nj}] \tag{2.37}$$

2.4 Single Machine Infinite Bus Model Linearization

In order to be able to study the behaviour of the SMIB model, Figure 2.10 is linearized about an operating point. The linearized SMIB model used is based on the Heffron-Phillips model presented in [49]. The derivation of the model is presented in [7, 5]. The main aim of using the Heffron-Phillips model is that the phase characteristic of the plant can be modelled and studied in detail. Figure 2.17 adapted from [5], shows the Heffron-Phillips model which is used to study the small deviations in power systems.

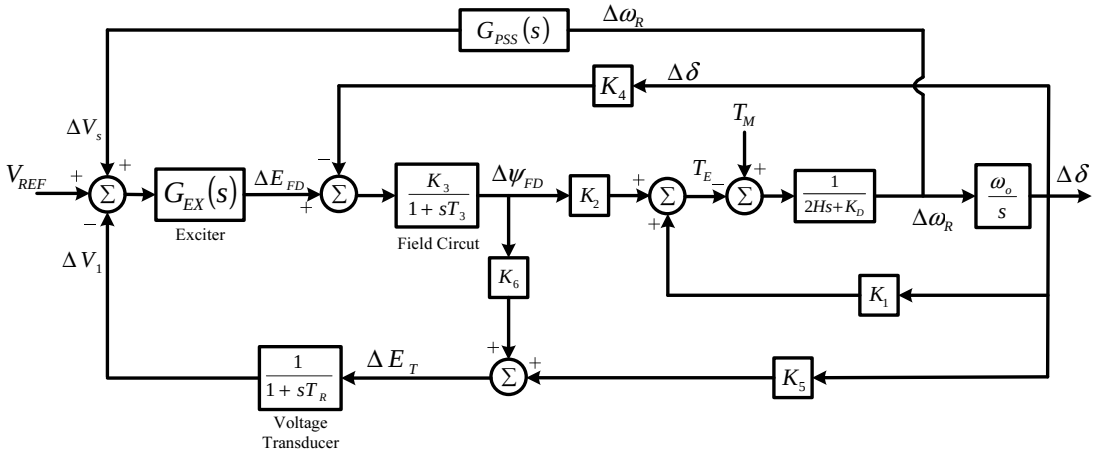

Figure 2.17: Block diagram of the Heffron-Phillips SMIB model with AVR and PSS adapted from [5].

The various parameters shown in Figure 2.17 are defined as:

$K_1 = \frac{\Delta T_E}{\Delta\delta}\,|_{E'_q}$ which represents the change in electrical torque for a change in the rotor angle with constant flux linkages in the d-axis.

$K_2 = \frac{\Delta T_E}{\Delta E'_q}\,|_{\delta}$ which represents the change in electrical torque for a change in the d-axis flux linkages with constant rotor angle.

$K_3 = \frac{X'_d + X_E}{X_d + X_E}$ represents the case where the external impedance is modelled as a pure reactance; K_3 represents the impedance factor.

$K_4 = \frac{1}{K_3}\frac{\Delta E_q}{\Delta\delta}$ represents the demagnetizing effect for a change in the rotor angle.

$K_5 = \frac{\Delta E_T}{\Delta\delta}\,|_{E'_q}$ represents the change in the terminal voltage with a change in rotor angle for a constant $\Delta E'_q$.

$K_6 = \frac{\Delta E_T}{\Delta E'_q}\,|_{\delta}$ represents the change in the terminal voltage with a change in $\Delta E'_q$ for constant rotor angle.

The Heffron-Phillips model assumes a 4^{th} order synchronous machine model and [50] has shown that for SSS studies it is important to use a detailed synchronous machine model in order to accurately capture the network dynamics associated with the damping introduced by the synchronous machine damper windings (which is excluded in low order models) and certain network transients which are important in the analysis of SSS and transient stability analysis. Hence the Heffron-Phillips model will be extended to a 5^{th}order model in order to capture all of the necessary network dynamics and transients. A higher synchronous machine model also captures the ECS characteristics accurately hence allowing for accurate control design of the PSS.

Extension of the Heffron-Phillips model is based on the approach presented by [38]. [38] extends the Heffron-Phillips model to a 5^{th} order model. Based on the synchronous machine theory presented earlier, Eq. (2.7) to Eq. (2.12) are used to develop a simplified block diagram transfer function model of a SMIB model with a 6^{th} order synchronous machine model. The assumption made in the derivation of the model is that the generator is feeding into an infinite busbar via a reactive tie-line as shown in Figure 2.10. The various constituents of the generator model can be expressed in terms of transfer functions $g_1(s)$ to $g_3(s)$ as given by Eq. (2.38) to Eq. (2.40):

Generator Transfer Function Expressions:

$$g_1(s) = \frac{\left(X_d'' + X_l\right)\left(1 + sT_{d0}''\right)}{(X_d + X_l) + \left[T_{d0}'\left(X_d' + X_l\right) + T_{d0}''\left(X_d'' + X_l + X_d - X_d'\right)\right]s + T_{d0}'T_{d0}''\left(X_d'' + X_l\right)s^2} \tag{2.38}$$

$$g_2(s) = \frac{-V_{\infty d0}\left[\left(X_d - X_d''\right) + \left\{T_{d0}'\left(X_d' - X_d''\right) + T_{d0}''\left(X_d - X_d'\right)\right\}s\right]}{(X_d + X_l) + \left[T_{d0}'\left(X_d' + X_l\right) + T_{d0}''\left(X_d'' + X_l + X_d - X_d'\right)\right]s + T_{d0}'T_{d0}''\left(X_d'' + X_l\right)s^2} \tag{2.39}$$

$$g_3(s) = V_{\infty d0}\frac{\left(X_q - X_q''\right)}{(X_q + X_l)}\frac{1}{\left(1 + sT_q''\right)} \tag{2.40}$$

-where

$$T_q'' = \frac{X_q'' + X_l}{X_q + X_l}T_{q0}'' \tag{2.41}$$

$$K_1 = \frac{V_{\infty d0}^2}{(X_l + X_d'')} + I_{d0}V_{\infty q0} + \frac{V_{\infty q0}^2}{X_l + X_q''} - I_{q0}V_{\infty d0} \tag{2.42}$$

$$K_2 = \frac{V_{\infty d0}}{(X_l + X_d'')} \qquad K_{2d} = \frac{V_{\infty q0}}{\left(X_l + X_q''\right)} \tag{2.43}$$

$$K_5 = \frac{V_{td0}}{V_{t0}}\left\{\frac{X_q''V_{\infty q0}}{\left(X_l + X_q''\right)}\right\} - \frac{V_{tq0}}{V_t}\left\{\frac{X_d''V_{\infty d0}}{(X_l + X_d'')}\right\} \tag{2.44}$$

$$K_6 = \frac{V_{tq0}}{V_{t0}}\frac{X_l}{(X_l + X_d'')} \qquad K_{6d} = \frac{V_{td0}}{V_{t0}}\frac{X_l}{\left(X_l + X_q''\right)} \tag{2.45}$$

Observations which can be made from analysis of the expression for K_5, $V_{tq0} \times V_{\infty d0}$ is always greater than $V_{td0} \times V_{\infty q0}$. As can be seen from Eq. (2.44), this is always independent of the generator operating condition since $X_q'' \leqslant X_d''$. .

2.5 Summary

This chapter presented the mathematical modeling techniques which are used in small signal stability analysis, namely modal analysis. Modal analysis complemented by the use of time domain simulation studies is generally the most effective manner of carrying out small signal oscillation studies in power system networks.

In general PSSs are the most cost effective manner of introducing damping into power systems, because of the simplicity and the financial benefits which they offer. The phase tuning objectives and the fundamental theory of PSSs were presented. The use of a SMIB model in order to study phase and gain characteristics of the main excitation control system in power plants was presented and the extension of the general SMIB model was also presented in order to be able to comprehensively study the behaviour and hence tuning requirements which any proposed compensator must meet.

Chapter 3

Power System Model Validation for Power System Studies

3.1 Introduction

Studies of large power networks are conducted using suitable simulation software packages which are relevant to the studies being conducted. For SSS it is crucial to ensure that the dynamic models which are used for AVRs, generators, PSSs and loads are accurate and reflect the performance of the actual components, especially under transient and highly loaded network conditions. This chapter focuses on a review of the Eskom network in order to identify inter-area mode oscillations of concern and the various components which participate in the modes of interest and the validation of the software models of the Eskom network based on steady state and network disturbance data. Network model validity is also assessed for components having a high participation factor for oscillation modes of interest. This is achieved through analysis of the various network solutions as the parameters of various components are varied. Finally a summary of the chapter is presented.

3.2 Review of Electromechanical Modes of concern in the Eskom Network

The Eskom network is characterized by a large generation pool which is geographically situated in the north-eastern part of the country and mainly consists of large coal-fired power plants and load centers which are situated very far away from the generating stations and hence there are a large number of transmission lines to deliver power to various load centers within the network. One of the largest load centers within the Eskom national grid is the South-Western Cape load of the network which is situated approximately 1200km away from the Mpumalanga generation pool. The south-western region of the network also has a small amount of generation which consists of a small amount of gas-fired power plants, a small amount of pump storage plants, and a single large nuclear power plant. The local generation in the South-Western Cape is smaller than the load demand and the balance of the power between generation and load is imported from Mpumalanga, via 765kV interconnectors to the South-Western grid.

Figure 3.1 shows the main Eskom transmission network. Highlighted in the diagram is the Southern African Power Pool (SAPP) oscillation mode, 0.30 Hz, which has been studied in depth through modal analysis and the findings presented in [20]. Phasor Measurement Units (PMUs) were installed as part of a pilot project within the Eskom network in order to study the oscillatory stability of the Eskom network. There were

three locations where PMUs were installed. These are shown in Figure 3.1. The PMU locations are labelled as PMU-GR, PMU-PG and PMU-MV. The network model used to perform the studies presented in this dissertation does not contain enough detail of the various constituent SAPP members in order to be able to model the 0.3Hz inter-area oscillation or study it adequately.

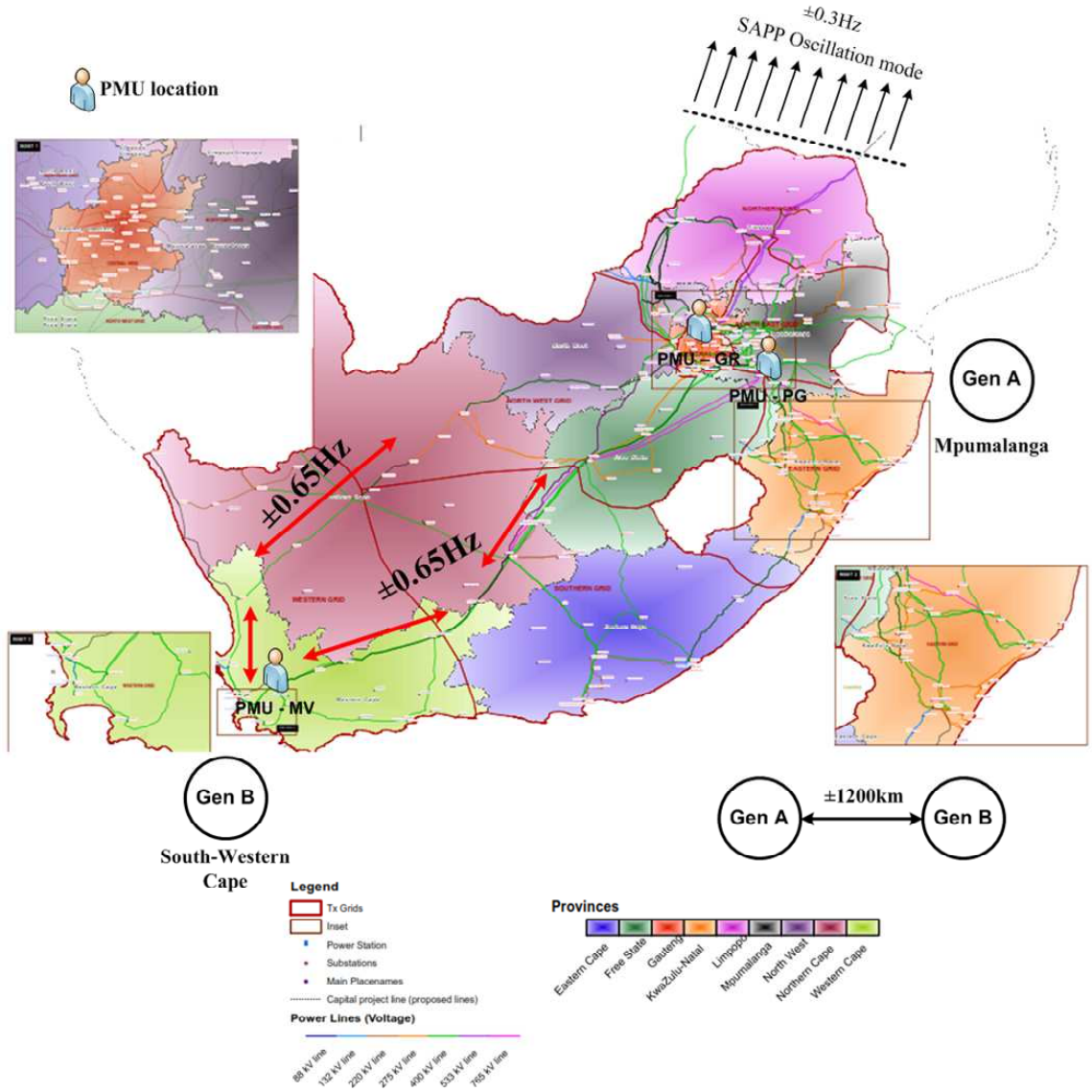

Figure 3.1: Main Eskom transmission network, also showing the SAPP oscillation mode.

Reference [20] showed that the 0.3Hz oscillation is primarily the generators in Zimbabwe

(ZESA), Zambia (ZESCO) and Zaire (SNEL) swinging against the Eskom and Nampower generators. The generators which have the highest participation in the mode are those located in the southern region of the ZESCO grid and within the Eskom network the generators which have the highest participation in this mode are the PS-KRG generators. The mode has also been captured on measurements on the 400kV Matimba-Phokoje tie-line. Controllability analysis of the mode presented in [20] revealed that the mode is not controllable from the Eskom network and that generators in the ZESA, ZESCO and SNEL grids offer a higher degree of controllability.

Within the Eskom network there also exist a number of other modes. One of the most commonly known modes is that between the South-Western Cape and the north-eastern (Mpumalanga) networks, which has an oscillation frequency of approximately 0.65Hz. The mode mainly consists of generators in the South-Western Cape swinging against generators in the Mpumalanga region. The oscillations have been measured in some of the corridors which carry power to the South-Western Cape.

The modes which are of concern within the Eskom network have been observed in measurements of incidents which have occurred on the network. The steady state and dynamic models which are to be used to perform the study will be verified through modal analysis and time domain analysis using PMU measurements and measurements which were taken from the Supervisory Control and Data Acquisition (SCADA) system. The electromechanical modes which will be of primary focus in this dissertation are the South-Western Cape and Mpumalanga, 0.65Hz oscillation mode and the other modes which are affected by the oscillation mode through non-linear modal interaction which may occur.

3.2.1 SAPP Oscillation Mode (0.3Hz) Verification

The PMUs used in the Eskom network measure the oscillatory behavior of various parameters within the network at the various substations at which they are located. Parameters which are considered vital in PMU oscillatory monitoring are frequency, f, and active power, P. The SAPP mode is normally well damped and can be observed from PMU data analysis. Figure 3.2 adapted from [19] shows a three month histogram of the frequency (Figure 3.2 *(a)*), and active power (Figure 3.2 *(b)*) signals measured by the PMUs. The PMU power signals are measured at selected transmission lines in the same substation. Figure 3.2 *(b)* shows the active power oscillations measured by the PMUs, PMU-MV measures the oscillations of two transmission lines and the line oscillation measurements are labelled as PMU-MV-DRO and PMU-MV-BAC.

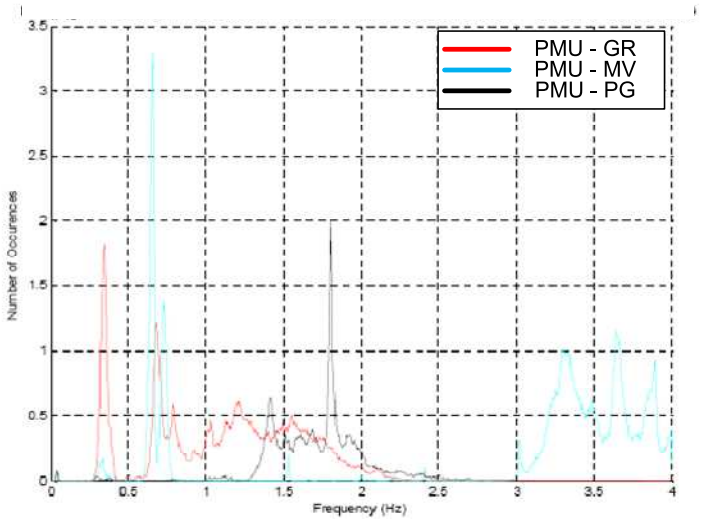

(a)

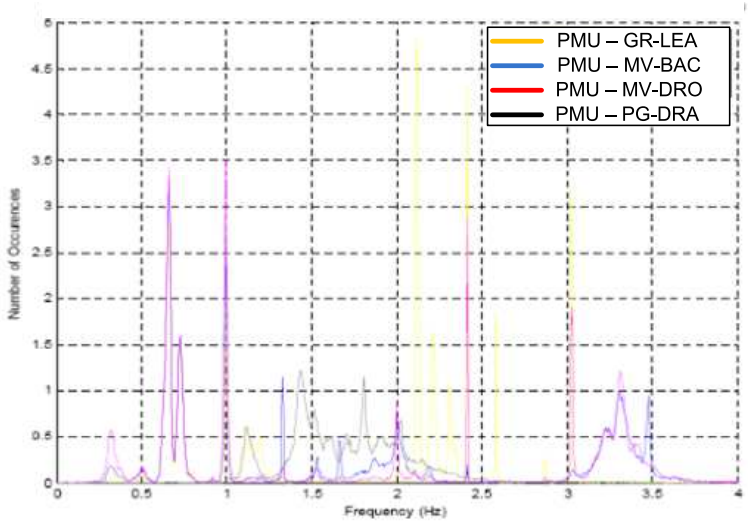

(b)

Figure 3.2: Histogram of mode frequencies observed in: *(a)* frequency signal, *(b)* power signal. (October-December), adapted from [19].

The 0.3Hz mode is mainly observed in the frequency component at location, PMU-GR, and is normally well damped. When the amplitude of the mode is large or when the mode has poor damping it is observable at all PMU locations, Figure 3.3 shows the SAPP mode shape. Reference [20] presented the SAPP mode shape from modal analysis which is shown in Figure 3.3 *(a)*. Figure 3.3 *(b)* shows the SAPP mode shape as observed in the Eskom network from the PMU measurements.

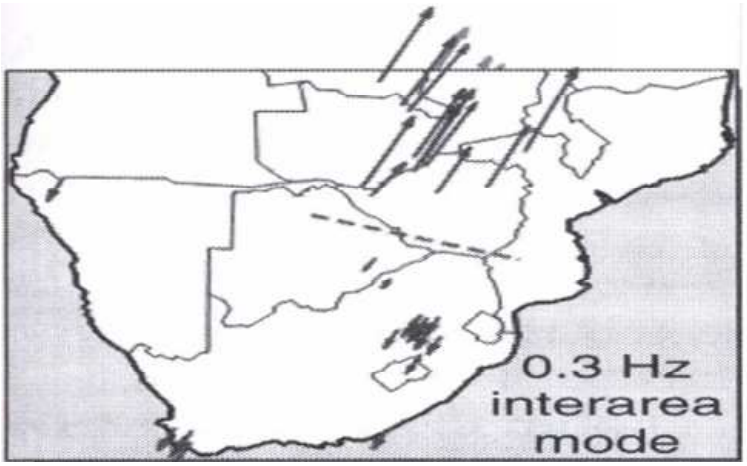

(a)

(b)

Figure 3.3: Mode observability of SAPP mode, *(a)* Calculated using software [20], *(b)* PMU measured observability.

Table 3.1 shows the average data statistics of the SAPP mode as observed by the PMUs within the Eskom network from frequency and active power oscillations derived from the histogram shown in Figure 3.2. The SAPP mode was found to be observable 45% of the time at location PMU-GR, from the frequency signal analysis. The average frequency amplitude was found to be higher at location PMU-MV even though the mode was only observable for 3.5% of the time. This confirms the results presented in [20], which show that generators which have the highest participation in the SAPP mode within

the Eskom network are situated in the South-Western Cape. Similarly the frequency amplitude at location PMU-PG is also high even though it is only observable for 0.9% of the time during the time period considered. Analysis of the SAPP mode frequency signal confirms that the mode is predominantly observable at locations PMU-MV and PMU-PG only when the amplitude of the mode is high or when the mode has poor damping.

In a similar manner analysis of the power signals measured by the PMUs shows that the generators in the South-Western Cape have the highest participation. The active power oscillations observed at locations PMU-MV-BAC and PMU-MV-DRO have the highest content of active power oscillations, based on the average MW amplitude. The active power oscillations observed at location PMU-GR-LEA have a smaller amplitude compared to the PMUs in the South-Western Cape network. Based on the data presented in Table 3.1, the active power oscillations contrary to frequency oscillations are observed for longer periods of time in the South-Western Cape network. This can be attributed to the higher degree of participation which the generators in that part of the network have in the mode. Other factors which influence the presence of the SAPP mode in the Mpumalanga and South-Western Cape regions will have to be investigated in order to draw any further conclusions regarding the observations made from PMU data.

Table 3.1: SAPP mode frequency and power measurements from PMU data.

Frequency Signals				
	Average Frequency (Hz)	Average Decay Time - τ (sec)	Average Amplitude (mHz)	% Present
PMU-GR	0.35	2.7	0.5	45.0
PMU-MV	0.35	3.8	1.0	3.5
PMU-PG	0.34	6.1	0.9	0.9
Power Signals				
	Average Frequency (Hz)	Average Decay Time - τ (sec)	Average Amplitude (MW)	% Present
PMU-GR-LEA	0.34	2.8	0.41	2.5
PMU-MV-BAC	0.33	2.6	0.50	6.4
PMU-MV-DRO	0.33	2.5	0.79	18
PMU-PG-DRA	-	-	-	-

Figure 3.4 shows the SAPP mode amplitude as measured from the active power oscillations using PMUs. The active power oscillations are greater in the South-Western Cape region than in Mpumalanga. Location PMU-PG-DRA has very low active power observability, less than 1%.

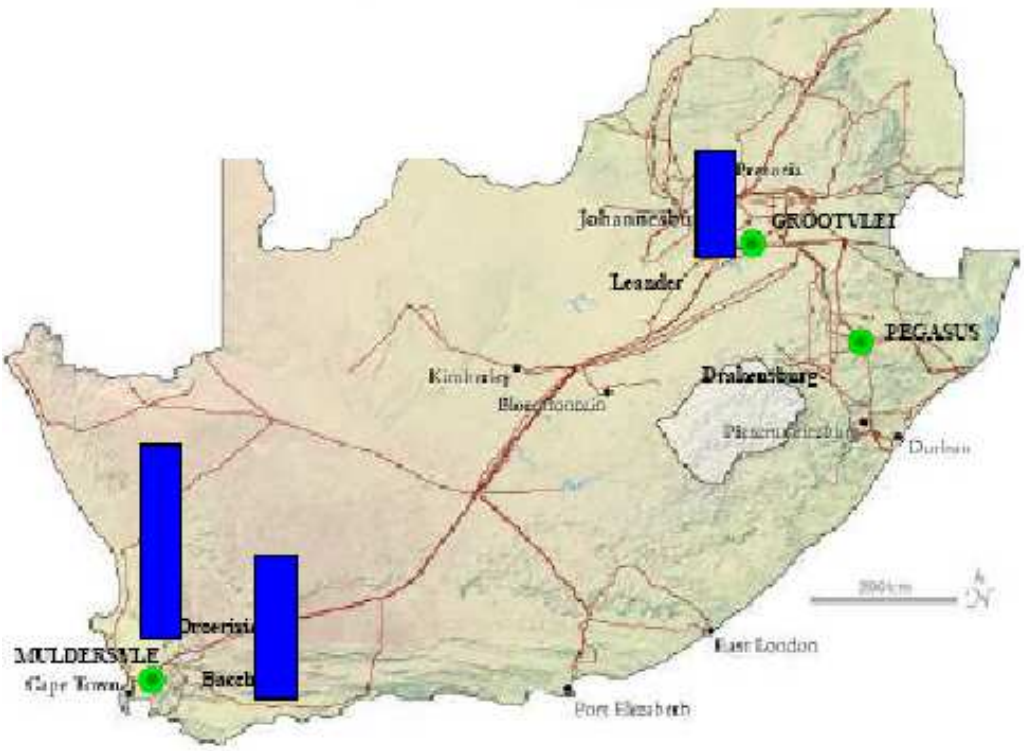

Figure 3.4: SAPP mode amplitude calculated from power signals.

3.2.2 South-Western Cape and Mpumalanga Mode (0.65Hz) Verification

The presence of the South-Western Cape and Mpumalanga oscillation has also been verified through measurements which were taken using PMUs which have confirmed observations made using software simulation packages. This mode is normally observed between PMU-GR and PMU-MV. Analysis of the data presented in Figure 3.2 confirms the presence of the oscillation mode. The mode is strongly observable in both the frequency and power measurements. The active power oscillations on both transmission lines monitored, PMU-MV-DRO and PMU-MV-BAC, are identical as can be seen in Figure 3.2. Figure 3.5 shows the South-Western Cape and Mpumalanga oscillation mode. Figure 3.5 *(a)* shows the oscillation mode which was observed from software simulations of the Eskom network, *(b)* shows the mode observability as seen by the PMUs.

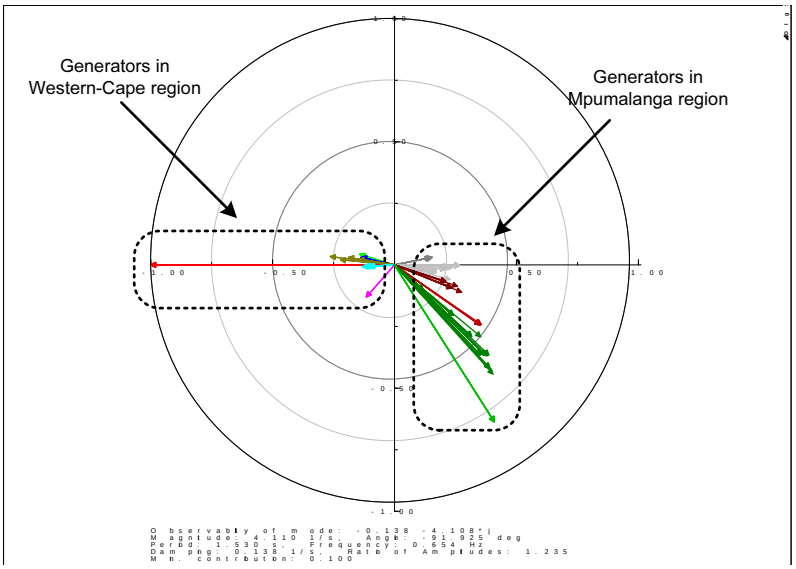

(a)

(b)

Figure 3.5: South-Western Cape and Mpumalanga mode observability, *(a)* Calculated using software, *(b)* PMU measured observability.

The mode observability of the South-Western Cape and Mpumalanga mode found using software shows a clear phase angle distinction between the two areas within the network. The generators in the South-Western Cape all form a group of coherent generators. Similarly the Mpumalanga region generators also form a group of coherent generators with some generators having a higher degree of observability of the mode. The mode shape observed from software for the Mpumalanga region is mainly distributed in the fourth quadrant as shown in Figure 3.5 which coincides with the mode shape observed

from PMU measurements for that region. Similarly the South-Western Cape mode observed from software is mainly distributed between the second and third quadrant. The mode distribution of the South-Western Cape mode shown in Figure 3.5 *(a)* lies mainly in the second quadrant. The mode shape observed from PMU measurements is in the third quadrant. In order to obtain a better mode shape distribution more PMUs would have to be installed in the South-Western Cape region.

Table 3.2 shows the average data statistics of the South-Western Cape mode observed from PMUs within the Eskom network from frequency and active power oscillations derived from the histogram shown in Figure 3.2. The oscillation mode captured by the PMUs shows that the mode frequency varies from 0.65Hz to 0.75Hz and the average data dominant oscillation frequencies are presented in Table 3.2. From the frequency data in Table 3.2 it can be seen that the mode has the highest amplitude observability at location PMU-MV and the mode has a longer presence at the same location. Average power signal data presented in Table 3.2, shows that the average power signal amplitude is larger in the South-Western Cape mode and that the mode presence at the PMU locations seems to be distributed equally at all locations within the network.

Table 3.2: South-Western Cape and Mpumalanga, average frequency and active power measurements from PMU.

Frequency Measurement Signals				
0.66Hz	Average Frequency (Hz)	Average Decay Time - τ (sec)	Average Amplitude (mHz)	% Present
PMU-GR	0.67	2.1	0.3	19.8
PMU-MV	0.66	3.5	0.9	59.3
PMU-PG	-	-	-	-
0.72Hz	Average Frequency (Hz)	Average Decay Time - τ (sec)	Average Amplitude (mHz)	% Present
PMU-GR	0.73	2.0	0.3	24.5
PMU-MV	0.72	3.3	1.0	31.1
PMU-PG	-	-	-	-
Power Measurement Signals				
0.66Hz	Average Frequency (Hz)	Average Decay Time - τ (sec)	Average Amplitude	% Present
PMU-GR-LEA	0.66	3.3	0.55	60.1
PMU-MV-BAC	0.65	3.4	0.80	61.0
PMU-MV-DRO	0.65	3.4	1.40	63.3
PMU-PG-DRA	0.66	3.7	0.43	0.005
0.72Hz	Average Frequency (Hz)	Average Decay Time - τ (sec)	Average Amplitude (MW)	% Present
PMU-GR-LEA	0.72	3.3	0.49	32.3
PMU-MV-BAC	0.72	3.2	0.71	33.0
PMU-MV-DRO	0.72	3.3	1.25	33.1
PMU-PG-DRA	-	-	-	-

Figure 3.6 shows the South-Western Cape mode amplitude as measured from the active power oscillations using PMUs. The active power oscillations are greater in the South-Western Cape region than in Mpumalanga. Location PMU-PG-DRA has very low active power observability, less than 1%.

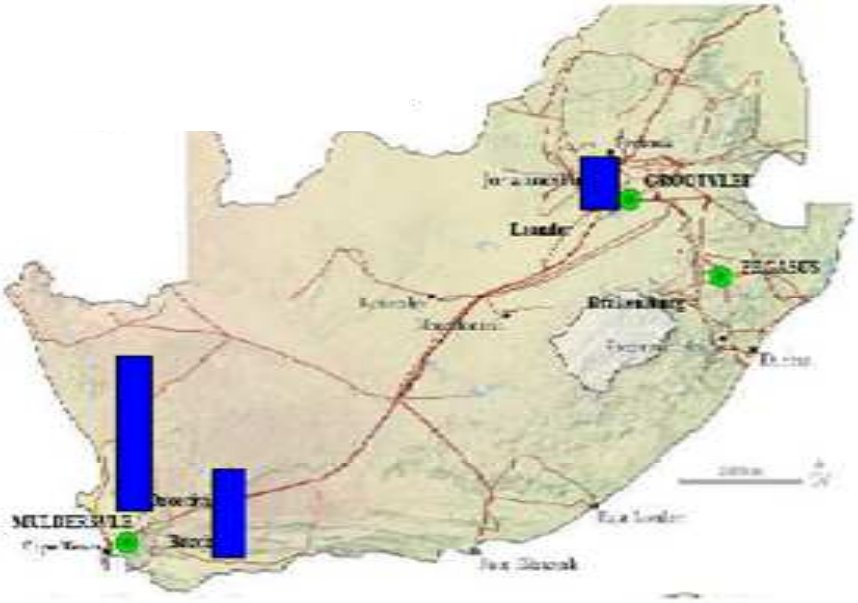

Figure 3.6: South-Western Cape and Mpumalanga mode amplitude calculated from power signals.

3.3 Eskom Network Model Validation

Software model validation is a crucial exercise which has to be performed in order to ensure that the computer models used in studies are an accurate representation of the actual performance of the network. In order to validate the performance of the actual network, a formal process adapted from [21] is shown in Figure 3.7. The model validation process consists of a steady-state model validation component and a dynamic model validation process. Once the model behaviour has been confirmed, the steady-state and dynamic models are then combined and the combined model behaviour is then validated.

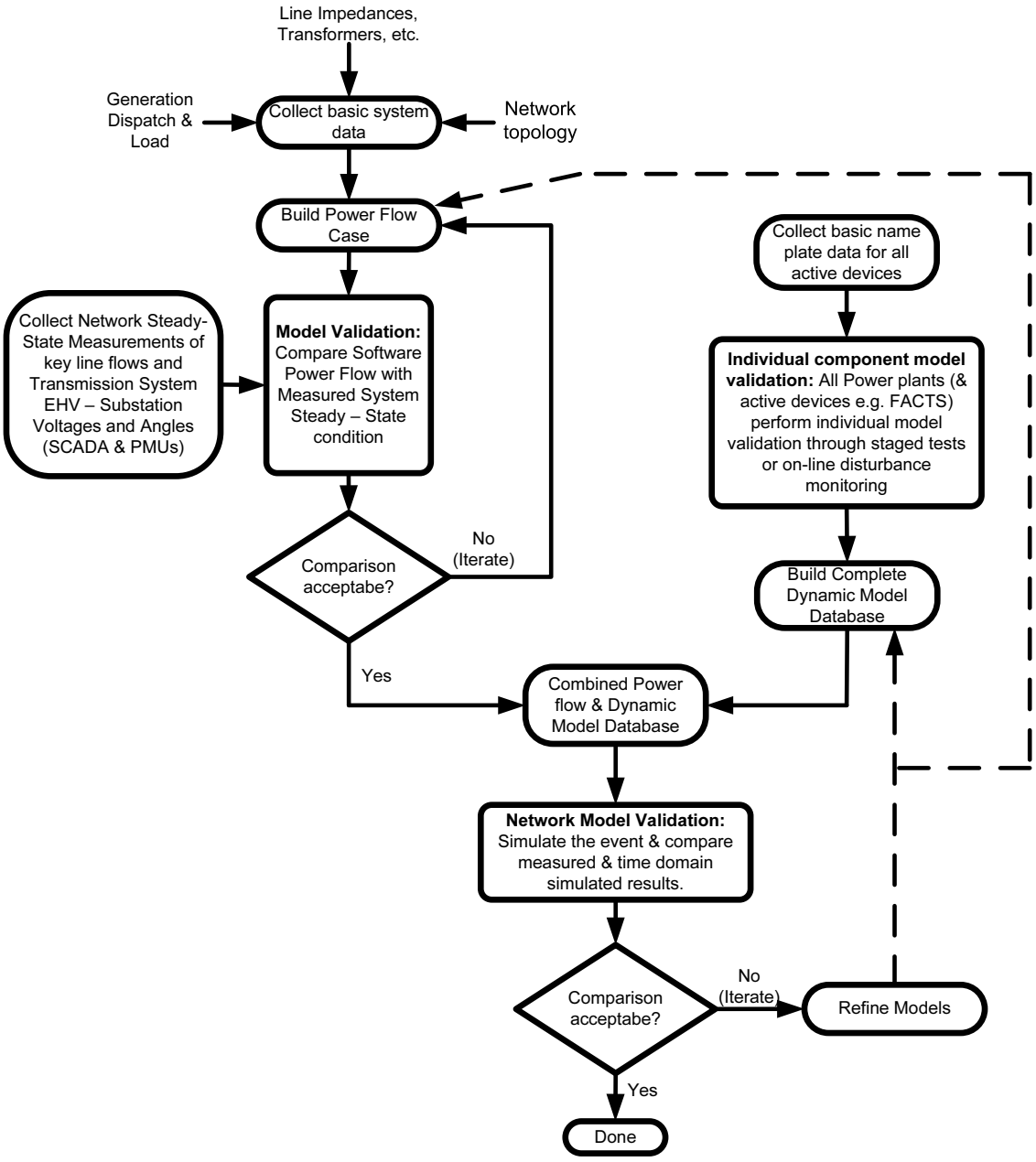

Figure 3.7: SSS network model validation procedure, adapted from [21].

3.3.1 Steady-State Network Model Validation (Component Model Validation)

The steady-state model behaviour is validated by collecting basic system data for system wide components such as transmission lines, transformers, generation dispatch, network topology and busbar load data in order to build a load flow case study. The simulated

steady-state behaviour is then compared with measured network behaviour for the same components (e.g. transmission lines, generation dispatch, etc.). Comparisons of the simulated network behaviour with actual measurements must be reasonably accurate for confidence in the model.

Figure 3.8 shows a simplified transmission line schematic used to represent a transmission corridor within a network. Steady-state active and reactive power flow simulations were performed for the transmission line for a snapshot of the actual Eskom network flows and these were compared and the results are shown in Table 3.3.

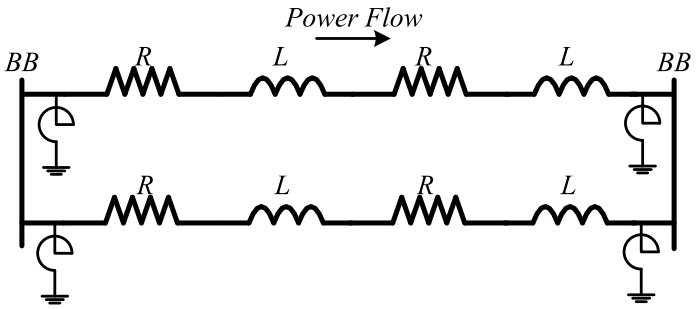

Figure 3.8: Simplified schematic representation of transmission corridor in the Eskom network.

Separate snapshots of the Eskom network were simulated using software and the steady-state conditions of a corridor were captured and validated. Table 3.3 shows the results obtained from network measurements. Network state parameters are captured using the SCADA system and the network state estimator. These results are then compared with the simulated network response. Kirchhoff's current law is applied to all nodes within the network to ensure the validity of the load flow solution obtained from simulation results using network data. A similar process is carried out for all of the network components within the transmission network on an individual basis, whereby either measured data or state estimator data is used.

Table 3.3: Steady-state transmission line corridor result comparison.

		State Estimator	Measured Results	Simulated Results
Sending End				
Line 1	P (MW)	861	808	865
	Q (MVAr)	492	507	446.91
Line 2	P (MW)	866	818	871.30
	Q (MVAr)	489	514	443.38
Receiving End				
Line 1	P (MW)	856	803	859.1
	Q (MVAr)	543	558	499.83
Line 2	P (MW)	862	812	864.58
	Q (MVAr)	542	563	497.21

The load flow solution obtained is crucial as it forms the basis on which the modal analysis is performed. Hence the following process was performed as a load flow sanity check:

1. Check all generators to ensure that they are not importing or exporting more than their nominal rating.
    a) Lower any reactive power export which is at its maximum or close to the maximum continuous rating.
2. Check the slack bus generator and ensure the following:
    a) It always has positive active power output.
    b) Check that the active power does not exceed the generator rating.
    c) The generator rating may operate at its emergency rating.
    d) Ensure that the reactive power output is within the generator limits.
3. Check all busbar voltages and all SVC voltages and ensure the following:
    a) Try to maintain the buses at 1.0 pu voltages.
    b) Try to limit the upper voltages to 1.05 pu.
    c) Try to limit the lower voltage limit to 0.97 pu.
4. For transmission systems with voltages above 275kV, the voltages may be as high as 1.07 pu. This is to ensure that the 132kV network is maintained at about 1.0 pu.
5. Ensure that there are no components within the simulation which are saturated or operating at the limits, as this will result in incorrect values in the system linearization.

Once all of the requirements for the components and busbars given above are met, only then can dynamic studies be conducted as the steady-state solutions obtained can be trusted.

3.3.2 Dynamic Network Model Validation

In performing dynamic network model validation studies, specifically for models to be used in SSS studies, it is essential that time-domain studies are coupled with modal analysis. This is to ensure that any control design implemented does not adversely affect the time-domain response as stated in [16] and that any unstable modes which may be present in the network are found through modal analysis as stated in [30]. Discussions presented by reviewers of [22] give a systems analysis approach to model validation which involves SSS studies. Figure 3.9 adapted from [22], shows a systems analysis approach for model validation for SSS studies.

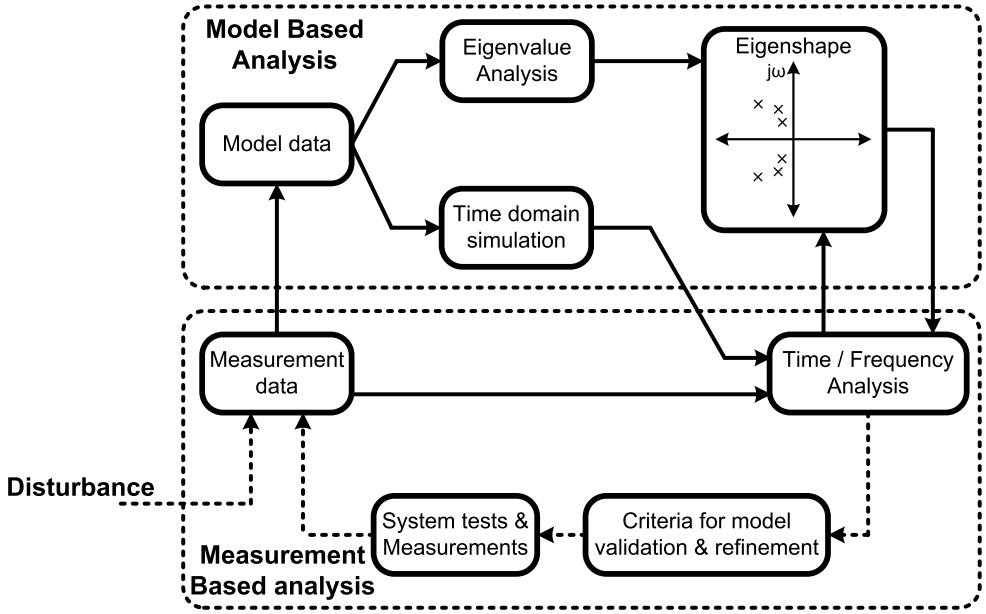

Figure 3.9: System analysis model validation for SSS studies, adapted from [22].

Figure 3.7 also gives a formal procedure for the validation of dynamic models (time-domain based validation). This same procedure was adopted for the dynamic model validation which was carried out. Various dynamic and active component nameplate data must be assimilated, and the various staged tests of power plants, SVC etc. must be validated on an individual component level basis. Models which are generally used in power system studies generally tend to be generic models issued by equipment manufactures, hence dynamic model behaviour must be verified through staged testing or

through the use of recorded component responses to various disturbances. A complete dynamic model database is then compiled and combined with the steady-state model and the complete model validated.

3.3.2.1 Oscillation Incident Model Validation

Incident based model validation is a very important exercise as staged network testing for large power system networks is not always possible. Hence incident based model validation becomes crucial in ensuring that software models are a true reflection of power system performance. There have been small-signal instability events which have occurred on the Eskom network and data captured from these incidents will be used to verify the dynamic performance of the software network model using the validation approach shown in Figure 3.9.

One such particular SSS related incident occurred on 10 January 2011, whereby under a certain network topology small signal oscillations were observed at certain locations in the network and at certain power plants within the network. Figure 3.10 shows a simplified single line diagram of the study area in the Eskom network prior to the events which led to instability. Of particular importance in this study is the power plant labelled PS-MAJ, whereby the busbar topology of the power plant with the grid resulted in the plant oscillation mode becoming negatively damped.

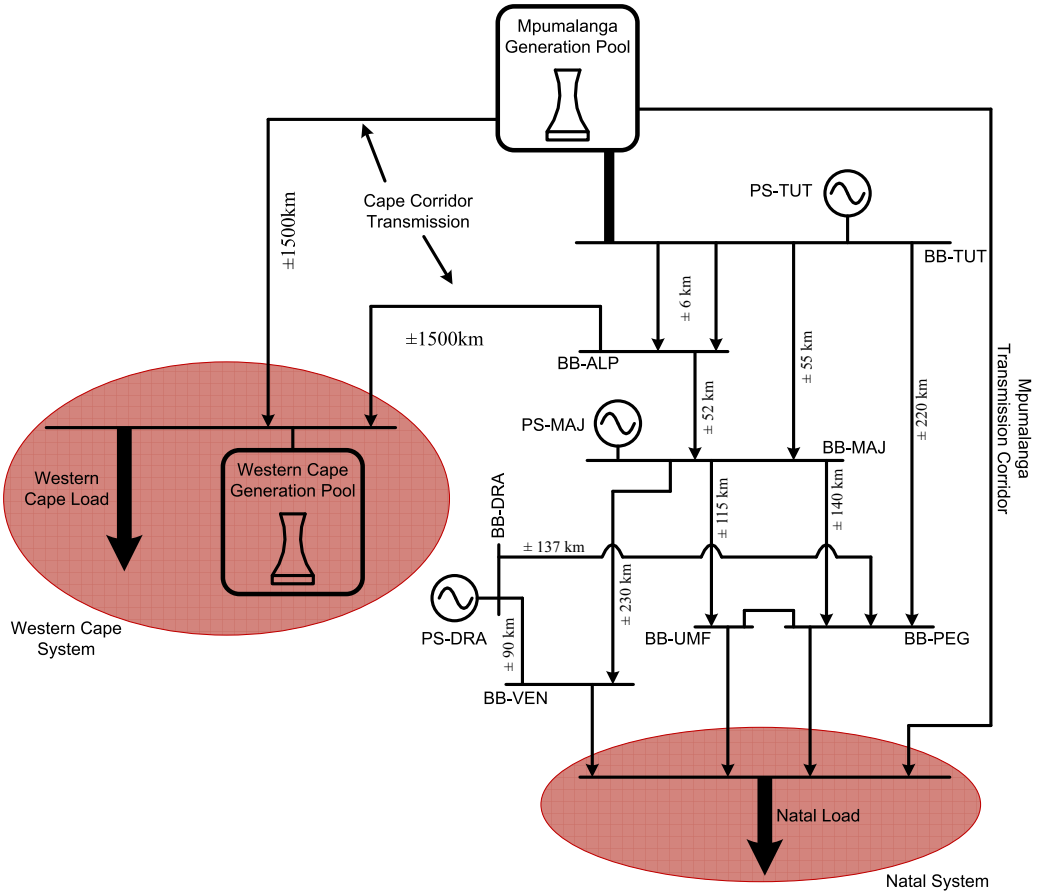

Figure 3.10: Simplified single line diagram of the study area prior to the emergence of unstable oscillations in the network.

Figure 3.11 shows the power plant busbar configuration prior to the instability. Six units within the power plant were on load and delivering power to the network. The transmission line labelled ALP was out of service for maintenance work. This same transmission line in Figure 3.10 is that between BB-ALP and BB-MAJ. A snapshot of the network conditions prior to the unstable mode appearing was modelled using a detailed model of the Eskom network, and a summary of the network conditions is given in Appendix B.

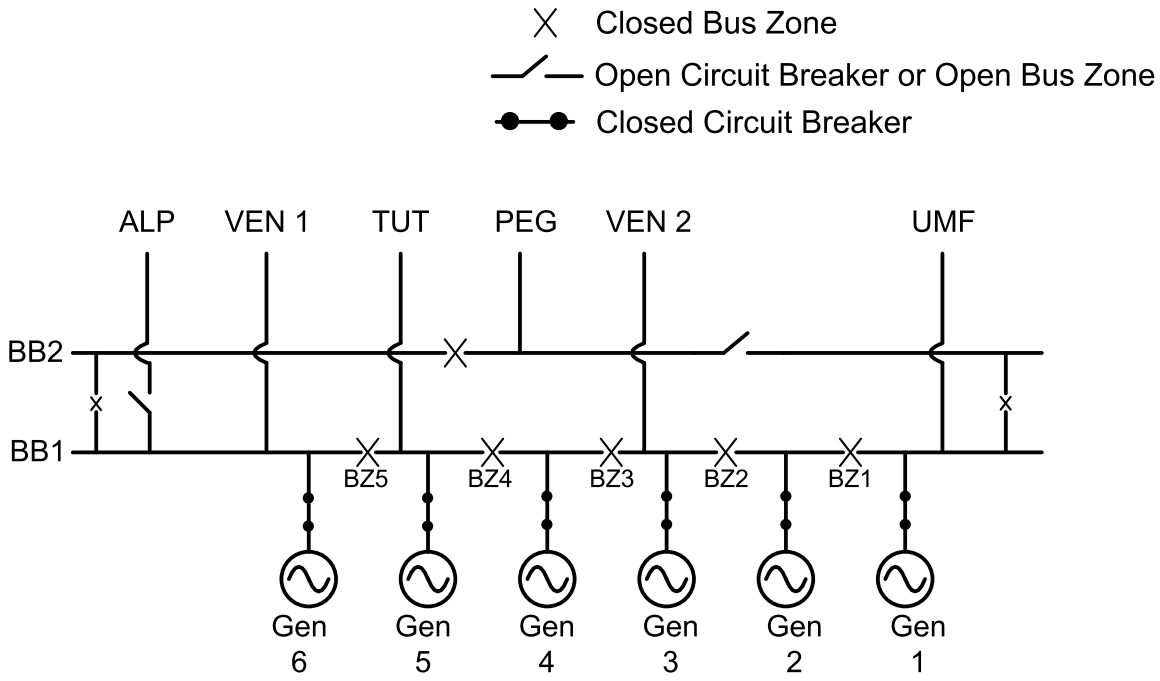

Figure 3.11: Power plant busbar configuration prior to network instability.

In order to confirm the stability of the simulation model prior to the network incident, time-domain simulations and eigenvalue analysis were conducted and the results are shown in Figure 3.12. Figure 3.12 (a) shows the eigenvalue results obtained for when the network was still healthy. Analysis of the eigenvalues shows that all of the eigenvalues are contained in the left hand plane of the frequency domain. Hence the system is stable, Figure 3.12 (b) shows the frequency measured on the transmission line between BB-MAJ and BB-PEG in Figure 3.10, also labelled as PEG in Figure 3.11. Eigenvalue analysis was performed using the QR algorithm which calculates the eigenvalues of a system by decomposing the state matrix and expressing it as a product of an orthogonal matrix and an upper triangular matrix. The decomposed matrices are multiplied by one another and the process is repeated iteratively.

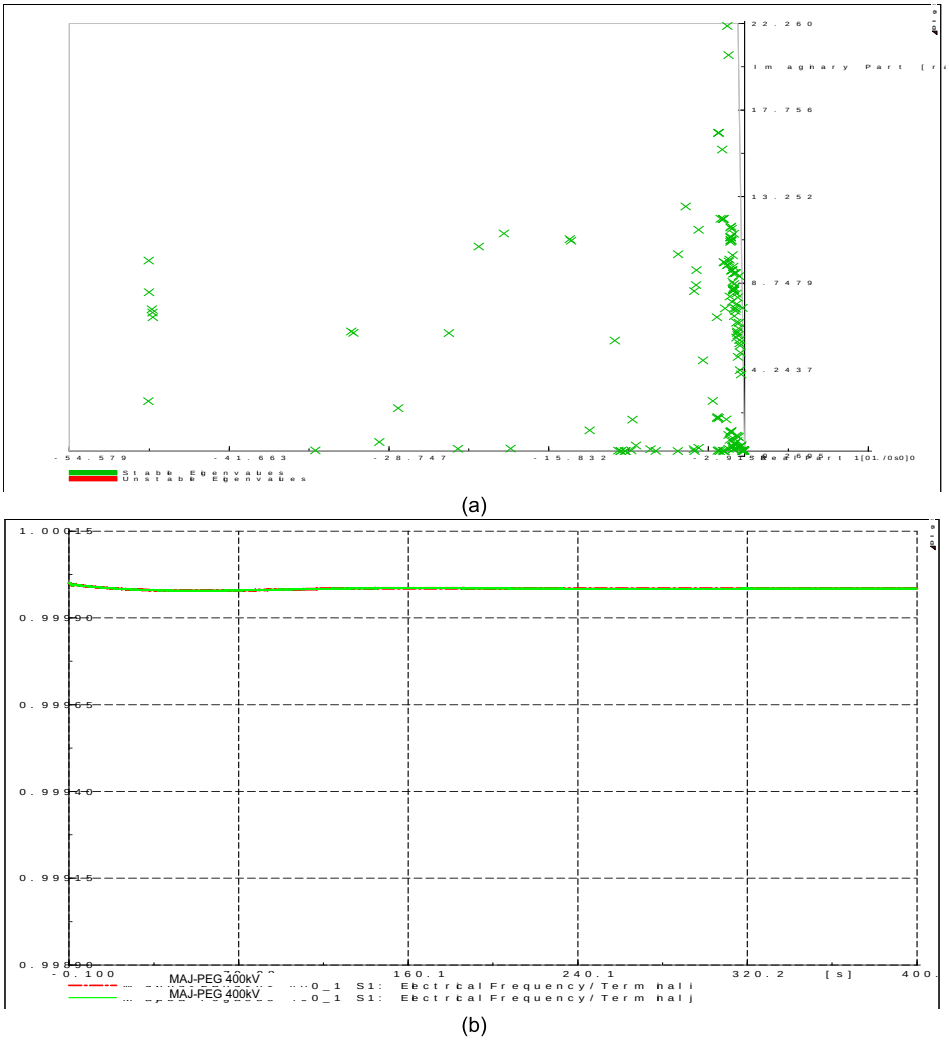

Figure 3.12: Power plant PS-MAJ time domain and modal analysis, (a) Eigenvalue analysis results, (b) Measured frequency.

PMU results measured by PMU-PG and PMU-GR are shown in Figure 3.13 for the time period between 05:00am and 10:00am on the day of the incident. The mode which was found to have become unstable and excited as a result of various network incidents was found to be in the frequency range of 0.75Hz to 0.95Hz. Hence this was the frequency range which was analysed for the time period presented in Figure 3.13. Analysis of the mode frequency, damping and amplitude presented in Figure 3.13, for the time period between 05:00am and 05:20am reveals that the amplitude was very low and the mode was hardly visible or even present in the network. Hence the network was stable within the time period, as has been confirmed by the snapshot simulation results presented in Figure 3.12.

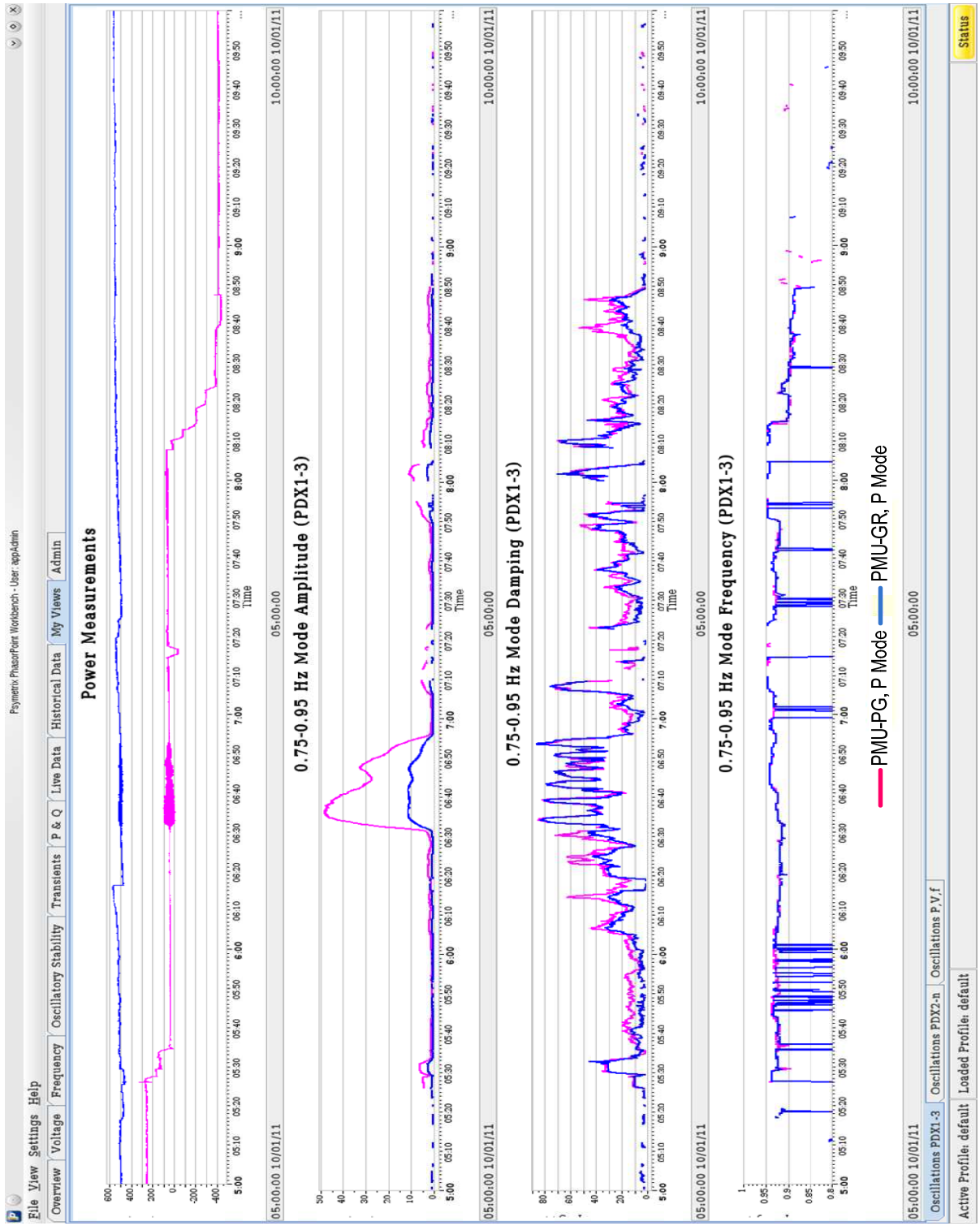

Figure 3.13: PMU-PG and PMU-GR measured data for a oscillation mode of concern.

Unit 6 (Gen 6) at power plant PS-MAJ tripped from 654MW at 05:24am. The grid frequency was reduced from 50.01Hz to 49.91Hz as a result of the unit trip. Loss of the unit did not result in mode instability.

The frequency of the Eskom grid is controlled via primary frequency control and secondary frequency control. Primary frequency control consists of a select number of units within the network which are strategically selected to respond first to deviations in network frequency through control signals which are issued remotely from the national control center. Governor droop control is also used to control the frequency within the network. Secondary frequency control is performed by what is known as Automatic Generation Control (AGC). Specific units are selected to participate in the AGC within the network. These units are issued control signals which change the operational set-point of the unit within a specified operational limit in order to control network frequency deviations within a specified frequency band. Hence the response of generators is controlled in order to ensure that frequency and network stability are not affected drastically by allowing all units within the network to attempt to restore frequency in the event of a fault or an incident on the network. The software simulation model used to conduct the studies presented does not incorporate these various forms of control, hence their exclusion in the following analysis.

At 05:26am, the transmission line between busbars BB-TUT and BB-MAJ tripped on bus zone protection. Further bus zone trips also occurred and the bus zone breakers labelled BZ4 and BZ5 in Figure 3.11 opened resulting in unit 5 (Gen 5) also tripping from the network. Figure 3.14 shows the configuration of the busbars at power plant PS-MAJ. This busbar configuration resulted in power plant PS-MAJ being weakly coupled to the network, Figure 3.15 shows a simplified single line diagram of the study area after the various bus zones and units at power plant PS-MAJ had tripped.

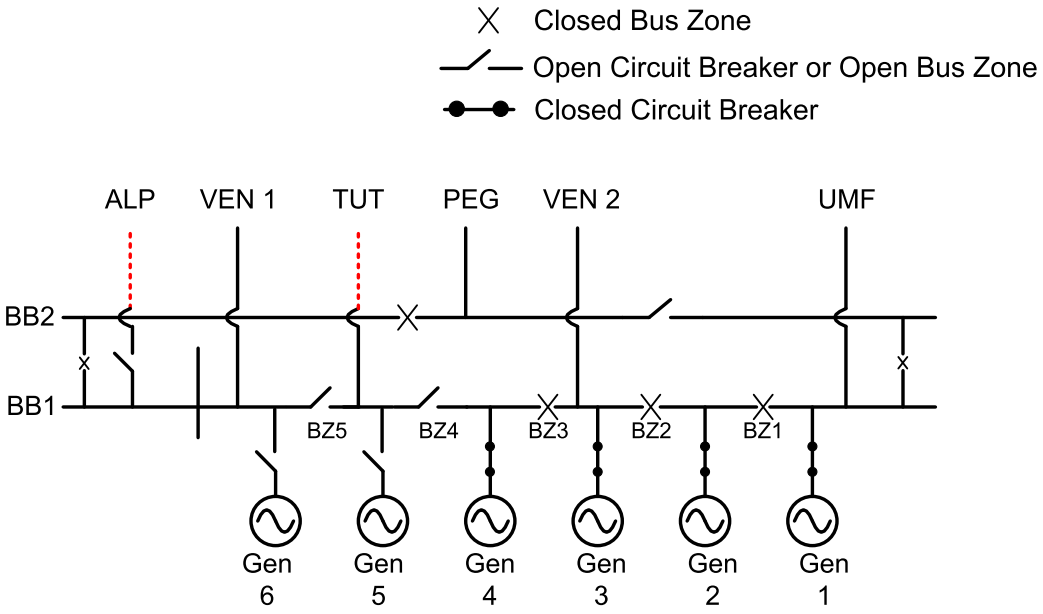

Figure 3.14: Power plant busbar configuration after bus zone operation and unit tripping.

The loss of the units and the transmission lines (ALP and TUT) connecting PS-MAJ to various parts of the network resulted in the power plant being weakly coupled. The effective impedance seen by PS-MAJ increased as a result of the loss of the transmission lines. Units 1 to 4 continued operating at the same output levels.

Analysis of the PMU data presented in Figure 3.13 shows that immediately after 05:26am, the mode becomes more visible as can be seen in the mode frequency plot, the mode has a relative good amount of damping initially maintaining consistently above 10%. Between 05:40 and 06:30am PMU-GR and PMU-PG have different damping values for the same oscillation mode, this is to be expected as this is highly dependent on the power flows and network conditions where the PMU is located. Between 06:30am and 07:00am the oscillation mode amplitude (measured in MW) drastically increased and this is evidence of the mode being excited, it must also be noted that during this same period the mode damping (measured in percentage) also increased. The exact event which resulted in the oscillation mode being excited is unknown as there were no network topology changes or drastically increased power flows from one region to another. At approximately 06:40am two units tripped due to network oscillations and at approximately the same time the oscillation mode amplitude decreased. It is suspected that loss of these units must have provided some form of electrical damping (based on network topology and system conditions) to the oscillation mode resulting in a reduction of the mode amplitude. At some points it was observed that the mode damping in Figure 3.13 fluctuated and at some time periods becomes very poor (below 5%).

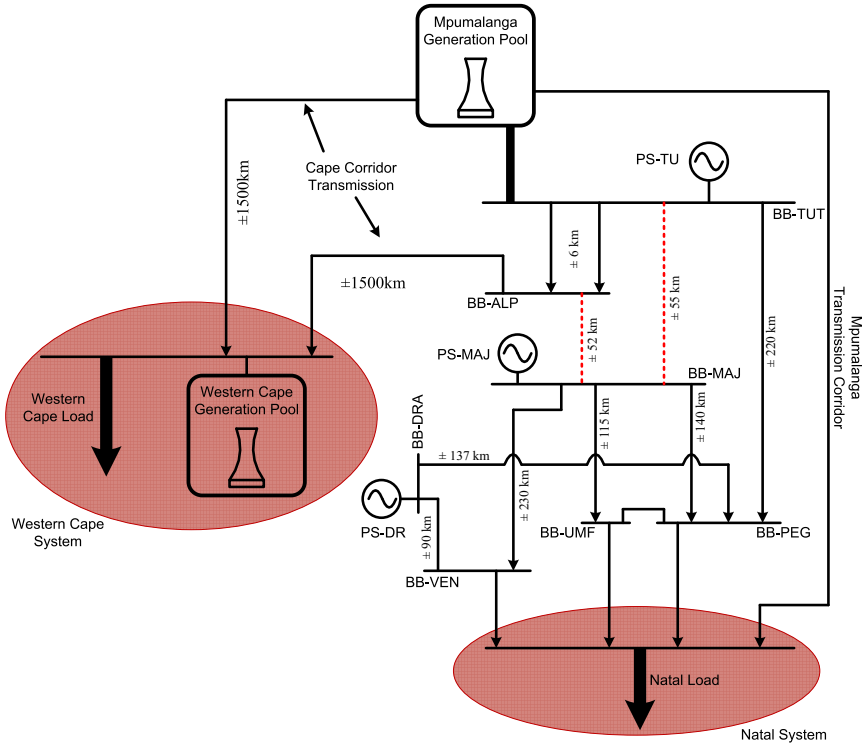

Figure 3.15: Simplified single line diagram of the area of study after bus zone operation.

The snapshot of the actual network after the busbar configuration at PS-MAJ had changed was simulated in order to recreate the incident. Modal analysis and time domain simulation of certain network parameters was performed. Eigenvalue analysis results of the network obtained from the simulation are shown in Figure 3.16. One of the modes of the system lies in the right hand side of the frequency domain, hence indicating the presence of an unstable mode in the network.

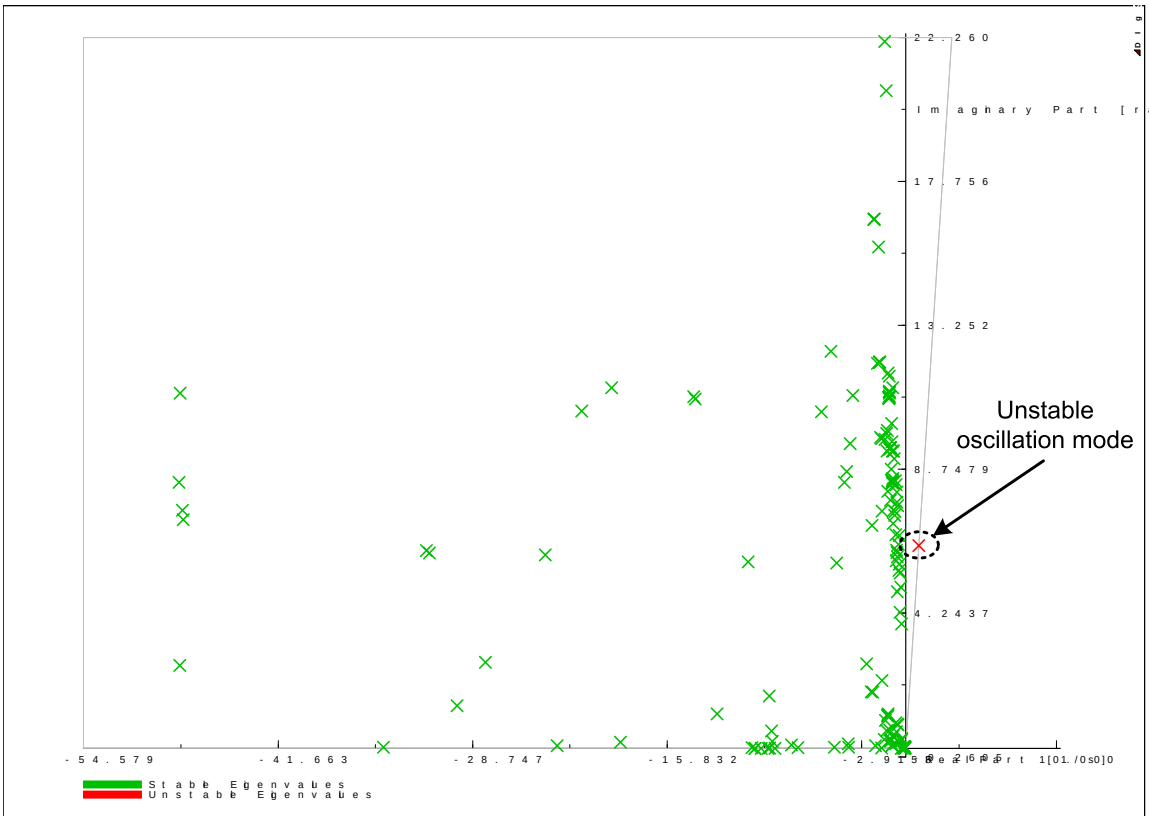

Figure 3.16: Eigenvalue analysis of power system after buszone trip.

Table 3.4 presents the eigenvalue analysis results of the unstable oscillation mode observed in the simulation. The oscillation mode frequency found in the simulation results is slightly higher than that measured by the PMUs. The difference between the actual and measured frequency indicates a difference of inertia between the actual Eskom network and the simulated model of the network. This is to be expected as the load models which are used in the software model are ZIP load models and do not account for the inertia introduced by induction motors which are connected to the network. Similarly the mode damping calculated by the PMUs is positive and the mode amplitude is also relatively small. This implies the mode initially remained stable and was not initially excited. Oscillation mode damping in power systems is influenced by various factors. Reference [51] shows that various load voltage dynamics aspects significantly influence mode damping and hence it becomes vital to ensure that the load models used are able to accurately capture load voltage dynamics. This aspect is beyond the scope of this dissertation and will not be investigated further.

Table 3.4: Eigenvalue results of the unstable oscillation mode observed in the software model.

Eigenvalue	Frequency	Damping Ratio	Damping Time Constant
-	(Hz)	ζ (%)	(sec)
+0.872+j6.352	1.011	-13.603	1.1464

At approximately 06:30am, the oscillation mode is excited by an unknown source or event. There were no recorded network changes or events at this time, but as can be seen in Figure 3.13 the mode amplitude increases significantly at locations PMU-PG and PMU-GR, . This results in the large active power oscillations being observed at various points within the network. Analysis of the active power plots provided by PMU-PG, shown in Figure 3.13, shows large active power oscillations. Between 06:30am and 07:00am large active power oscillations were measured at various point within the network. Figure 3.17 (a) gives a detailed view of the active power oscillations which were measured on the transmission line DRA-PEG as shown in Figure 3.15. Figure 3.17 (b) gives the active power oscillations which were reproduced using a simulation model compared with measured oscillation in (a). The actual active power oscillations along transmission line DRA-PEG were measured to be 100MW immediately after 06:30am as shown in Figure 3.17 (a), these were verified through simulation and the results of the simulation model along the same transmission line are shown in (b).

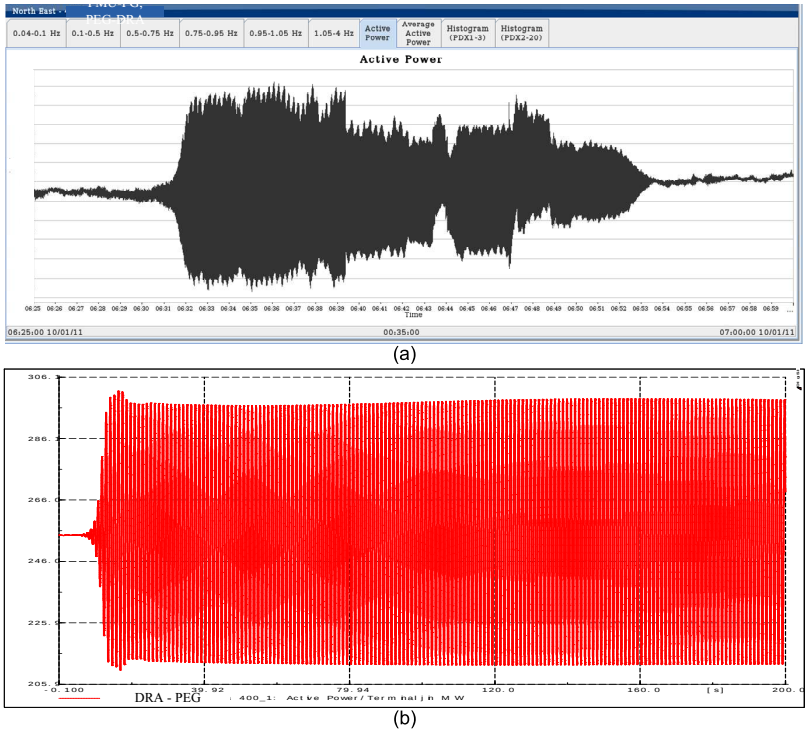

Figure 3.17: Active power oscillations on transmission line DRA-PEG, (a) PMU measured oscillations, (b) Software model simulated oscillations.

Active power oscillations of approximately 60MW were reported at certain power plants in the Western Cape. Figure 3.18 shows measured and simulated active power oscillations for a particular unit in the Western Cape. Figure 3.18 (a) shows the actual measured active power oscillations and Figure 3.18 (b) shows the simulated active power response on the same unit. The active power oscillation magnitudes between the measured and simulated responses were found to be of the same order.

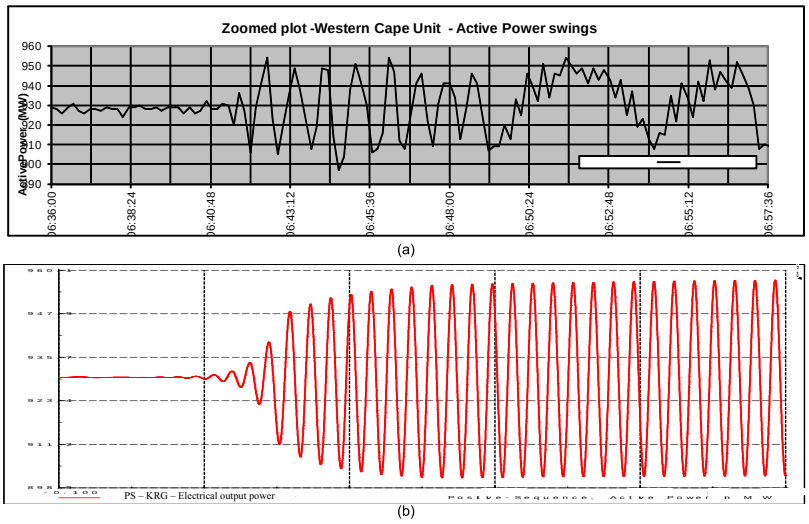

Figure 3.18: Active power oscillations observed on a unit in the Western Cape. (a) Measured active power oscillations, (b) Software model simulated oscillations.

In order to further analyse the oscillations which were measured within the network, Fast Fourier Transforms (FFTs) were performed on the measured signals. The FFT results were then used to calculate the Power Spectral Density (PSD). PSD analysis provides information regarding the "strength" of a signal, and how this "strength" is distributed in the frequency domain. Figure 3.19 shows the PSD results of the unit in the Western Cape which experienced active power oscillations. Figure 3.19 (a) shows the simulated active power response of the Western Cape unit prior to the oscillation mode appearance at 05:24am (with all lines and units at PS-MAJ in service). Figure 3.19 (b) shows the PSD for the active power measurement shown in (a). The frequency spectrum considered in the analysis ranged from 0.1Hz to 2.0Hz, and it was found that the dominant mode in the frequency spectrum occurred at 0.422Hz in the frequency domain. The amplitude of the oscillation mode was found to be very small. Figure 3.19 (c) shows the simulated active power response of the Western Cape unit after the appearance of the oscillation mode at 06:30am (with the two units and transmission lines out of service, the station being weakly coupled) and the PSD of the active power response was calculated and is shown in Figure 3.19 (d). The network snapshot used to simulate this condition was at 06:30am. The frequency spectrum considered in the analysis ranged from 0.1Hz to 2.0Hz, and it was found that the dominant mode in the frequency spectrum occurred at 0.90Hz as shown in Figure 3.19 (d).

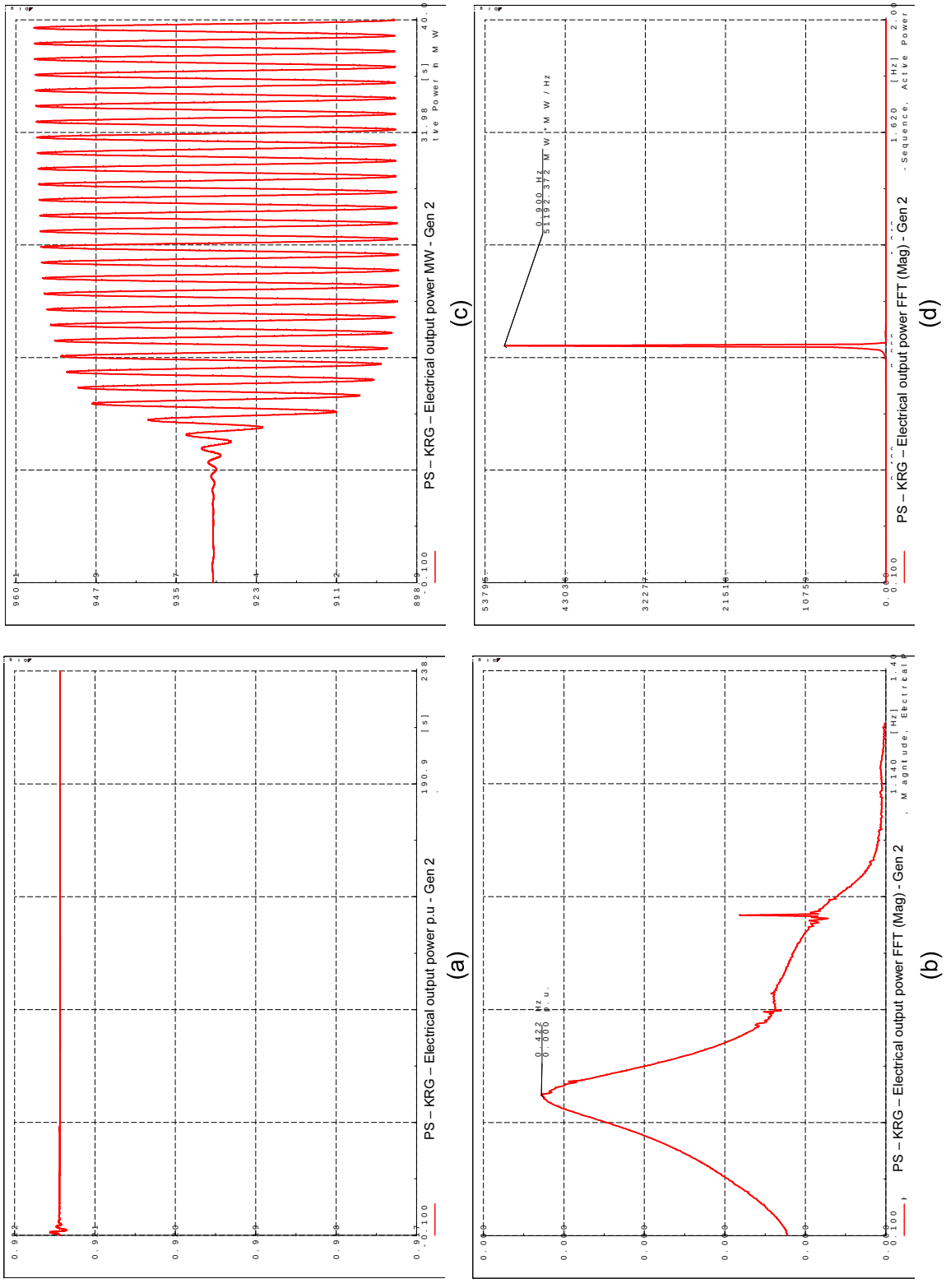

Figure 3.19: Power Spectral Density analysis of Western Cape unit active power. (a)-(b) PSD prior to unstable mode appearance, (c)-(d) PSD after unstable mode appearance.

Similar analysis was also carried out on the signals measured at PS-MAJ. The PSD of the active power and frequency signals was calculated for both steady-state network conditions before the appearance of the unstable oscillation mode and after the appearance of the unstable oscillation mode. Figure 3.20 shows the PSD analysis of the transmission line power flow between BB-MAJ and BB-PEG. Figure 3.20 (a) shows the frequency plot of the transmission line MAJ-PEG power flow prior to the appearance of the oscillation mode. The PSD of this same signal is shown in (b). The frequency spectrum considered in the analysis ranged from 0.1Hz to 2.0Hz, and it was found that the dominant mode in the frequency spectrum occurred at 0.410Hz. The amplitude of the oscillation mode was found to be very small. Figure 3.20 (c) shows the simulated frequency response of the transmission line MAJ-PEG power flow after the appearance of the oscillation mode at 06:30am and the PSD response was calculated and is shown in Figure 3.19 (d). The frequency spectrum considered in the analysis ranged from 0.1Hz to 2.0Hz, and it was found that the dominant mode in the frequency spectrum occurred at 0.90Hz as shown in Figure 3.19 (d).

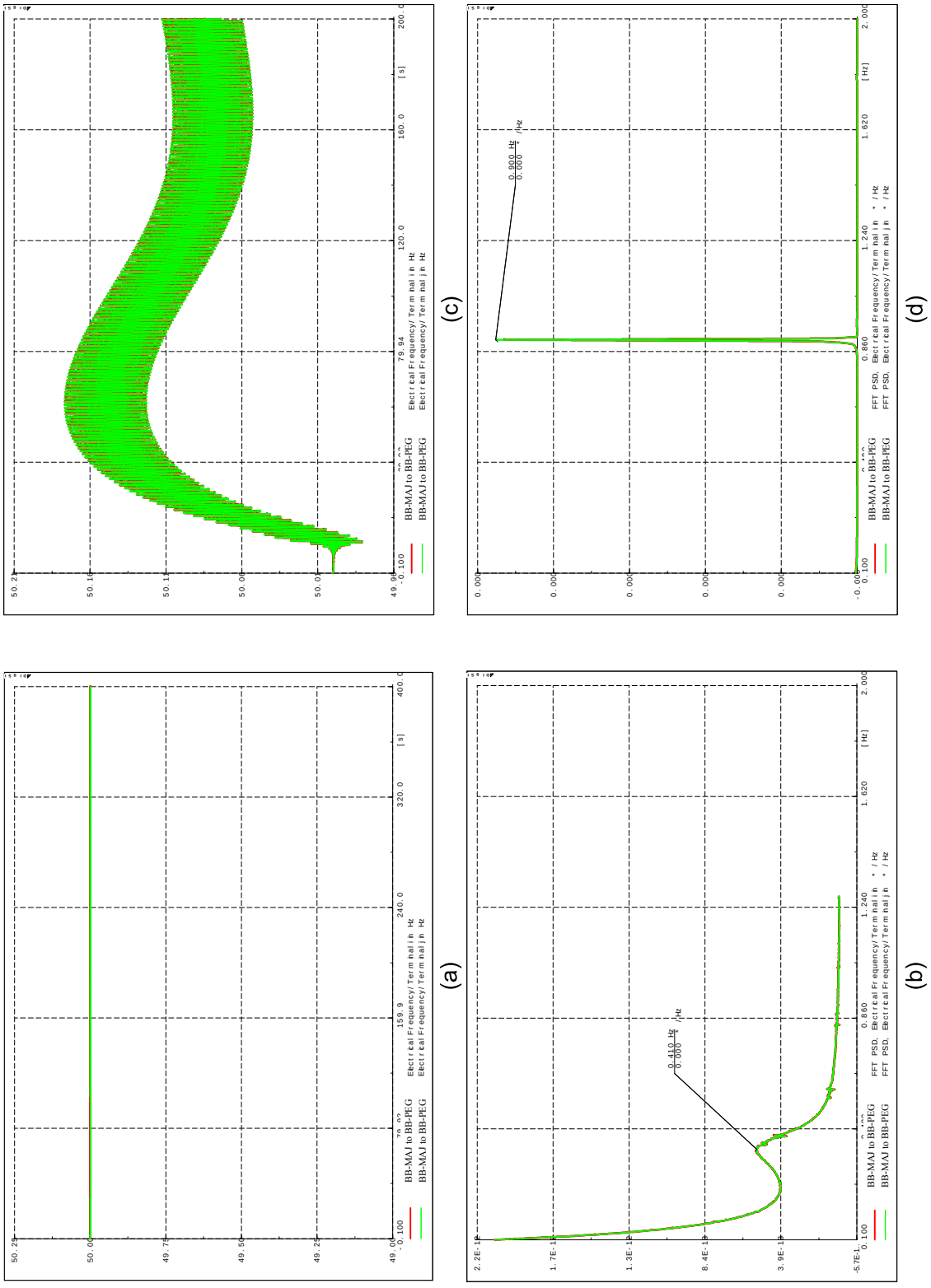

Figure 3.20: Power Spectral Density analysis of PS-MAJ frequency. (a)-(b) PSD prior to unstable mode appearance, (c)-(d) PSD after unstable mode appearance.

The same analysis was also performed on the transmission line DRA-PEG power flow which had experienced large active power oscillations. Figure 3.21 (a) shows the simulated active power response prior to the oscillation mode appearing in the network at 05:24am, and as can be seen in Figure 3.21 (b), the dominant oscillation mode frequency in the active power signal occurs at 0.425Hz. But similar to all of the other PSD plots the mode amplitude prior to the appearance of the unstable eigenvalue is very small and can be considered as negligible. Figure 3.21 (b) shows the active power response of the same transmission line after the appearance of the oscillation mode at 06:30am. Analysis of the PSD plot for the active power oscillations in Figure 3.21 (c) is given in Figure 3.21 (d), and shows that the dominant oscillation mode frequency is 0.90Hz.

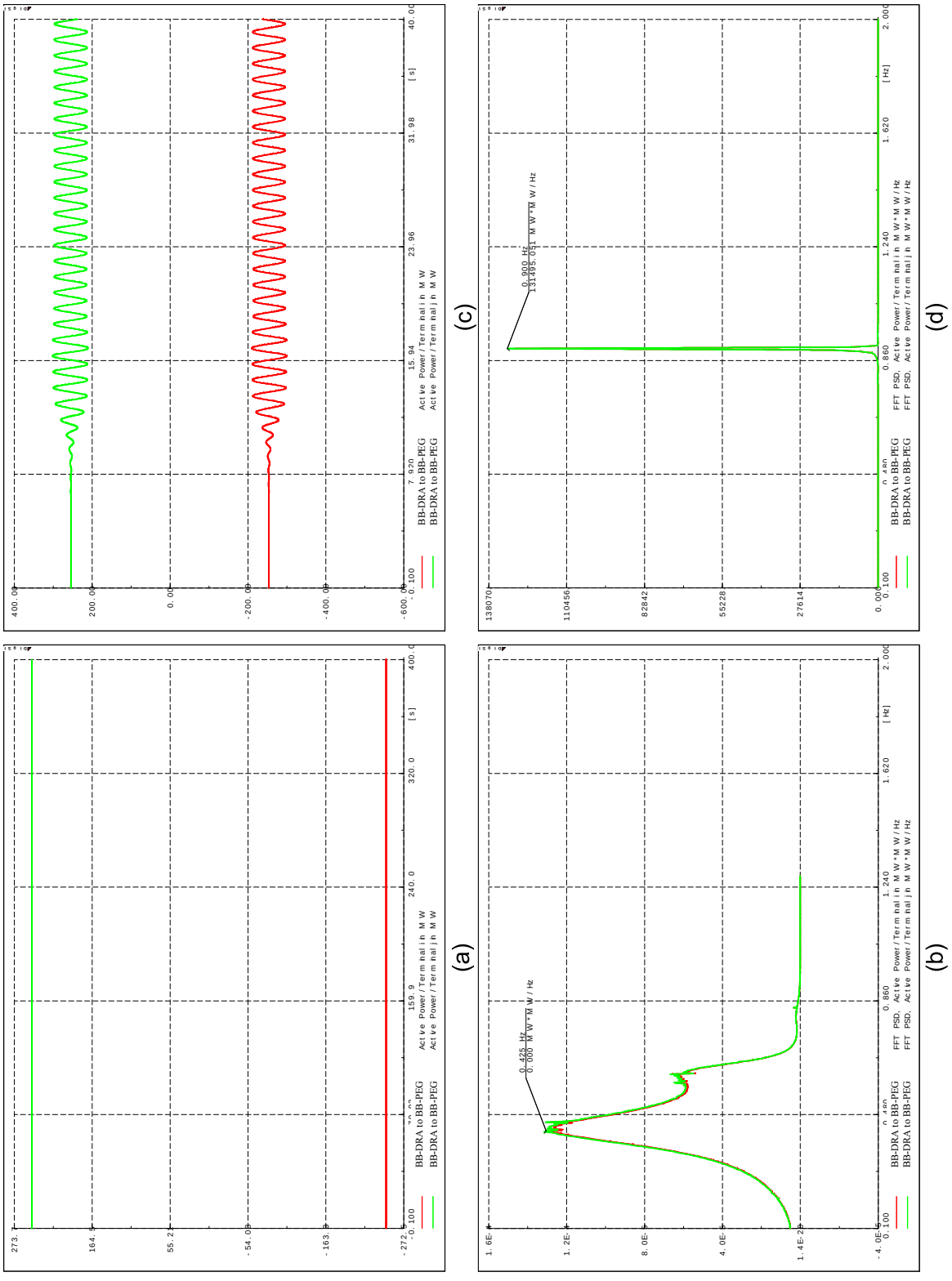

Figure 3.21: Power Spectral Density analysis of DRA-PEG active power. (a)-(b) PSD prior to unstable mode appearance, (c)-(d) PSD after unstable mode appearance.

Based on the PSD result analysis presented in Figure 3.19 to Figure 3.21, it can be seen that the generators at power plant PS-MAJ and those in the Western Cape participate in the unstable oscillation mode at a frequency of 0.90Hz, based on the various signals analysed (frequency and active power). The PMU measurements obtained for the same disturbance shown in Figure 3.13, indicated that the oscillation mode frequency measured on the actual network had a frequency range of 0.75Hz to 0.95Hz , Hence the oscillation mode frequency obtained from the PSD software analysis is within this range. This indicates that the detailed software model of the Eskom network used to recreate the network oscillations represents the actual Eskom network to a sufficient level of accuracy. The oscillation mode frequency obtained from modal analysis was 1.011Hz. The software used the QR algorithm to perform the modal analysis. The linearization methodology and perturbation size used in the software are not known to the user and it is possible that they influenced the solution. Reference [52] suggests that the accuracy of the solutions obtained using the QR algorithms can be improved through the application of inverse iteration methods.

3.4 Analysis of Controllability and Participation Factors

The SSS oscillations observed in the network on 10 January 2011 arose mainly as a result of the busbar topology at power plant PS-MAJ caused by various equipment trips at the plant. The busbar topology and transmission line outages resulted in the plant having a weak connection to the grid and hence the relatively poor damping of the subsequent oscillation mode which appeared on the network as a result. Participation factor analysis of the unstable oscillation mode and analysis of the mode controllability will be presented based on the network snapshot data which includes analysis of the Western Cape - Mpumalanga oscillation observed.

3.4.1 10 January 2011 Oscillation Incident Participation and Controllability factors

Figure 3.22 shows the participation and controllability factors of the unstable oscillation mode observed in the network at 06:30am. Figure 3.22 (a) shows the participation factors. The generators with the highest level of participation in the oscillation mode are the generators situated at PS-MAJ, namely generators 1 to 4. Participation factor analysis of the oscillation mode suggests that the mode is a local mode, since it is mainly dominated by the generators at PS-MAJ. Other generators within the network do also participate in the mode but at a low level, approximately 0.01pu. The low participation of the other generators observed in Figure 3.22 (a) is consistent with the events which were reported by various other power plants within the network, namely the large active power oscillations measured on units in the Western Cape shown in Figure 3.18. Appendix B.2 presents a full description of the network events observed.

Fast voltage transients were reported at PS-MAJ. Based on the mode participation factor analysis, the generator field voltage state variables at power plant PS-MAJ have a participation factor higher than 0.2pu on all of the generators still connected to the grid (units 1 to 4).

The unstable mode controllability was calculated and is shown in Figure 3.22 (b). The state variables which offer the highest degree of controllability of the unstable mode are the speed variables at the power plant. Hence this implies that if properly designed/tuned PSSs had been installed at PS-MAJ, sufficient damping would have been introduced into the network and the oscillations would have been well damped.

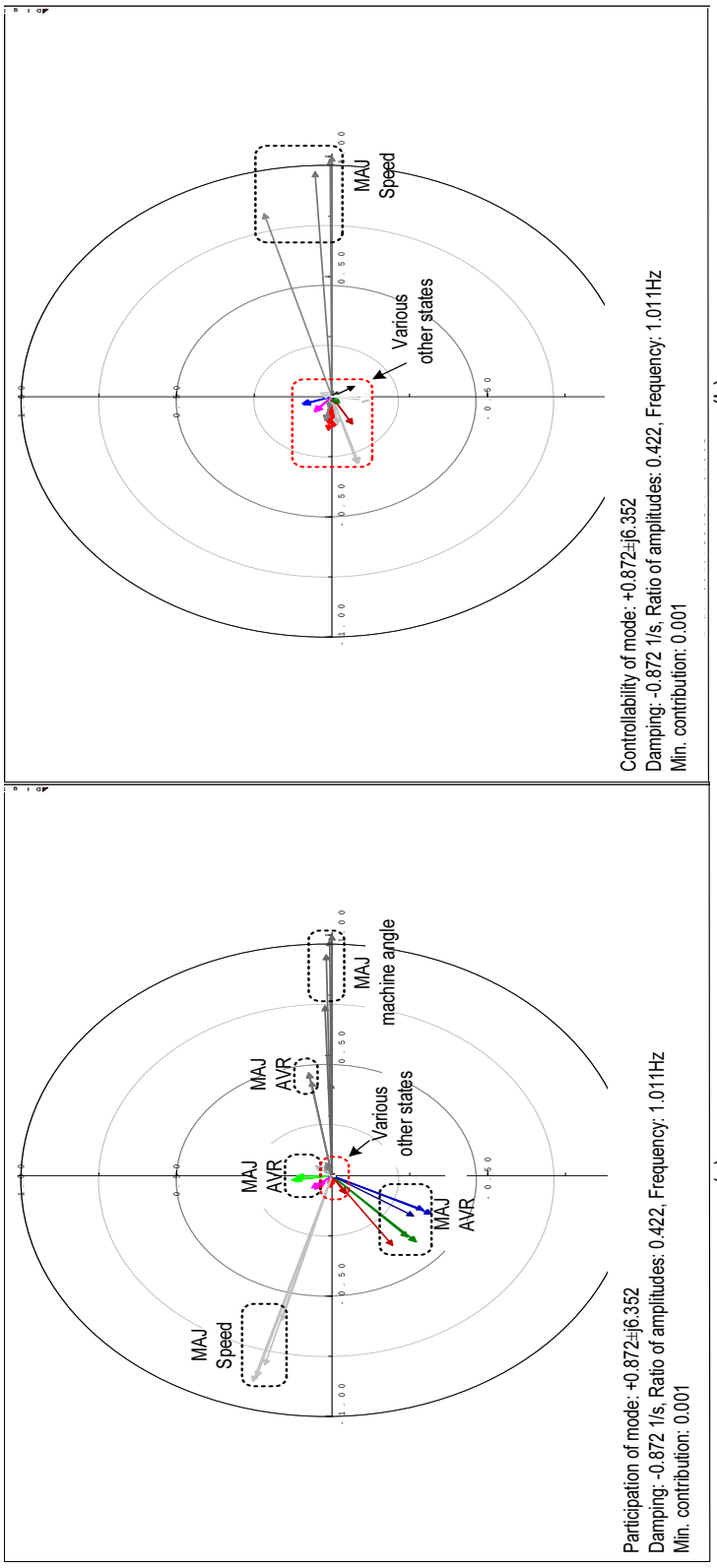

Figure 3.22: Unstable mode participation and controllability factors.

3.4.2 Western Cape - Mpumalanga mode Participation and Controllability factors

Figure 3.23 shows the participation and controllability factors of the Western Cape - Mpumalanga oscillation mode. Figure 3.23 (a) shows the participation factors. It can be seen that the generators with the highest level of participation in the oscillation mode are the generators at power plant PS-KRG in the Western Cape (both units 1 and 2). Participation factor analysis of the oscillation mode suggests that the mode is an inter-area mode, as the generators in the Western Cape are in anti phase with those in the Mpumalanga region. This same observation was also made from PMU observability results shown in Figure 3.5.

The Western Cape - Mpumalanga mode controllability was calculated, and is shown in Figure 3.23 (b). It can be seen that the generators which have the highest degree of controllability are located at power plant PS-KRG. The state variables which offer the highest degree of controllability of the mode are the speed variables at PS-KRG. This similarly implies that if properly designed/tuned PSSs had been installed at PS-KRG, sufficient damping would have been introduced to the Western Cape - Mpumalanga mode.

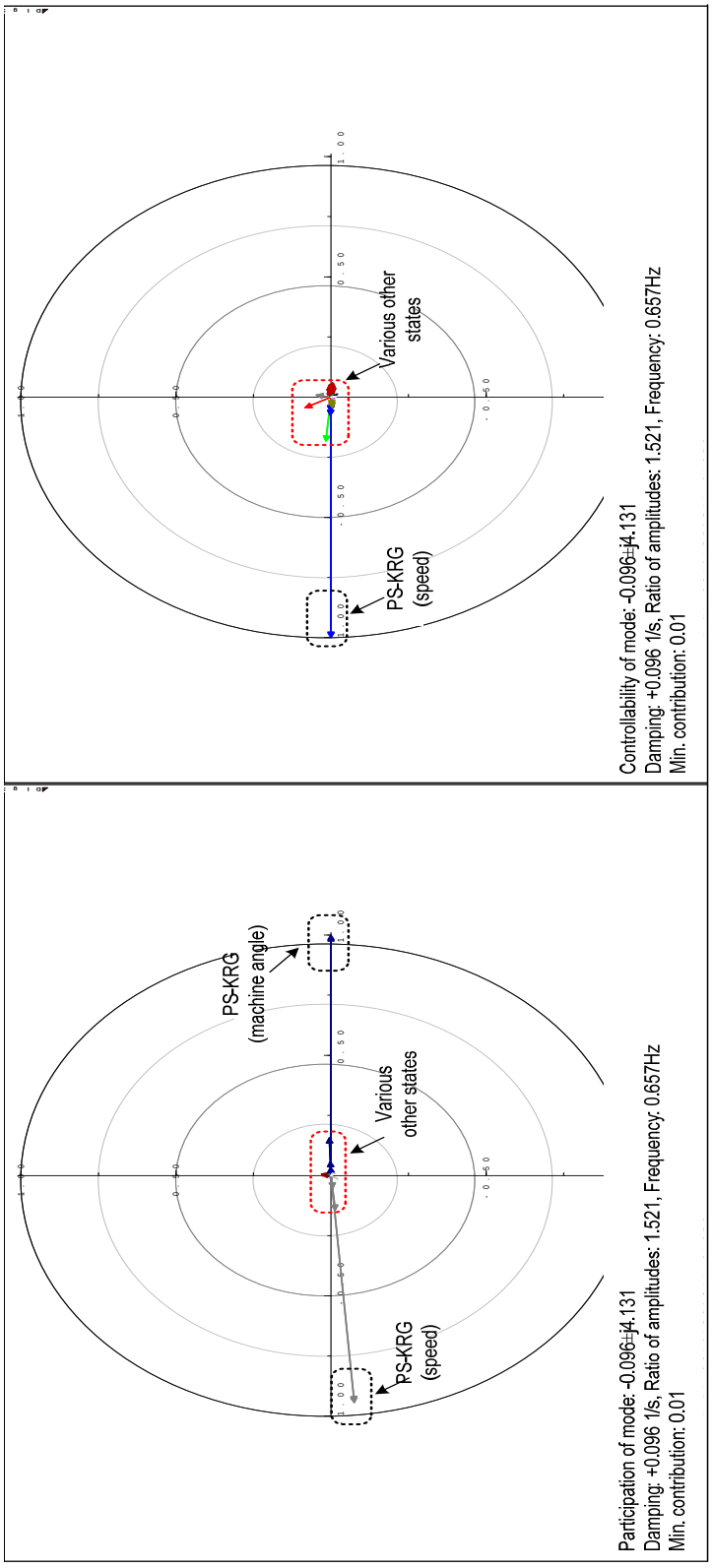

Figure 3.23: Western Cape - Mpumalanga mode participation and controllability factors.

3.4.3 Western Cape - Mpumalanga and SAPP mode interaction

PMU data presented in Figure 3.2 was analysed in order to determine modal interactions present within the network. It was found that the SAPP oscillation mode of 0.3Hz has a clearly observable interaction with the Western Cape - Mpumalanga 0.65Hz oscillation mode. Reference [53] found that modal interaction in power systems is highly non-linear. Resonance between two power system modes occurs when the frequency of the sum of two (or more) modes is nearly equal to the frequency of another natural mode occurring within the network. Reference [54] demonstrated that the non-linearity governing the power system electromechanical mode interactions, "is quadratic in nature according to Taylor's series expansion of the power system's dynamic equations", [54]. Hence this implies that the use of linear analysis techniques, such as linearization of power system equations about an operating point and linear control design methods, is not well suited to modal resonances in power systems.

Since most commercially available software tools predominantly use linear analysis and design methods, the modal resonance of the SAPP and Western Cape - Mpumalanga modes cannot be studied or addressed comprehensively in this dissertation. Also the simulation model used in this dissertation does not include any generation outside of the Eskom network. Reference [54] states that modal resonance conditions tend to become much more severe under conditions of poor system damping (of one or both modes), large signal disturbance, and heavily stressed power systems.

On 10 May 2013, a large disturbance occurred in the SAPP network, whereby a large unit in the ZESA network tripped and one of the bridges on the Mozambique HVDC converter station tripped resulting in a bridge trip at the South African converter station. This particular operating condition resulted in the SAPP mode becoming unstable. Figure 3.24 shows the frequency measured by the PMUs located at PMU-MV and PMU-PG. As can be seen, the frequency drops from 49.94Hz to 49.69Hz following the loss of a large unit and the HVDC bridges tripping.

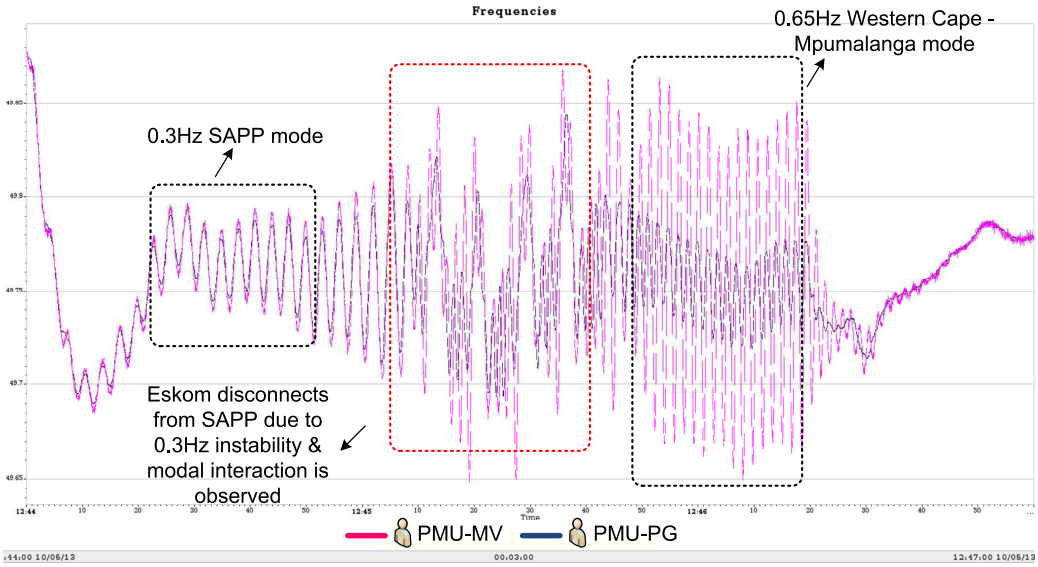

Figure 3.24: Frequency measured at PMU-MV showing the SAPP and Western Cape - Mpumalanga modes interacting.

The grid frequency does increase as the generators on primary frequency control respond. But as can be seen shortly afterward, the frequency contains growing oscillations at a frequency of 0.3Hz. These oscillations continue to increase for a period of approximately 70 seconds until the SAPP interconnector is tripped by opening the tie-line breakers. With the SAPP interconnector severed, the 0.3Hz mode becomes unobservable. But the poorly damped 0.3Hz mode excited the 0.65Hz mode resulting in oscillations slightly lower than 0.65Hz due to modal interaction. The oscillations persist for a period of approximately 40 seconds and then subside. There were no changes in the network topology, but various generators within the network were responding to frequency deviations and this could have resulted in increased damping of the oscillating mode. Figure 3.25 shows the measured active power flow on the PHO-MAT tie-line during the incident, which is the largest AC tie-line between South-Africa and ZESA.

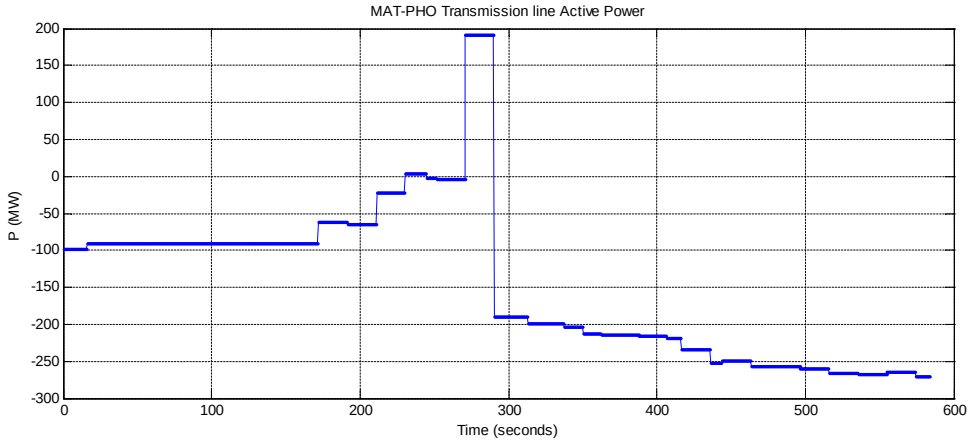

Figure 3.25: Actual MAT-PHO trasmission line active power.

Figure 3.26 shows the PMU-MV measurements taken on 10 May 2013, showing grid frequency measurements, mode amplitude, mode damping and frequency for the SAPP mode. The active power flow in Figure 3.25 is that of the transmission line on the day mentioned. Highlighted in Figure 3.26 is the time period when the SAPP mode became excited. As can be seen in Figure 3.26, the mode amplitude increased drastically and the mode damping was reduced to about 1%, resulting in large oscillations in the frequency as measured by PMU-MV.

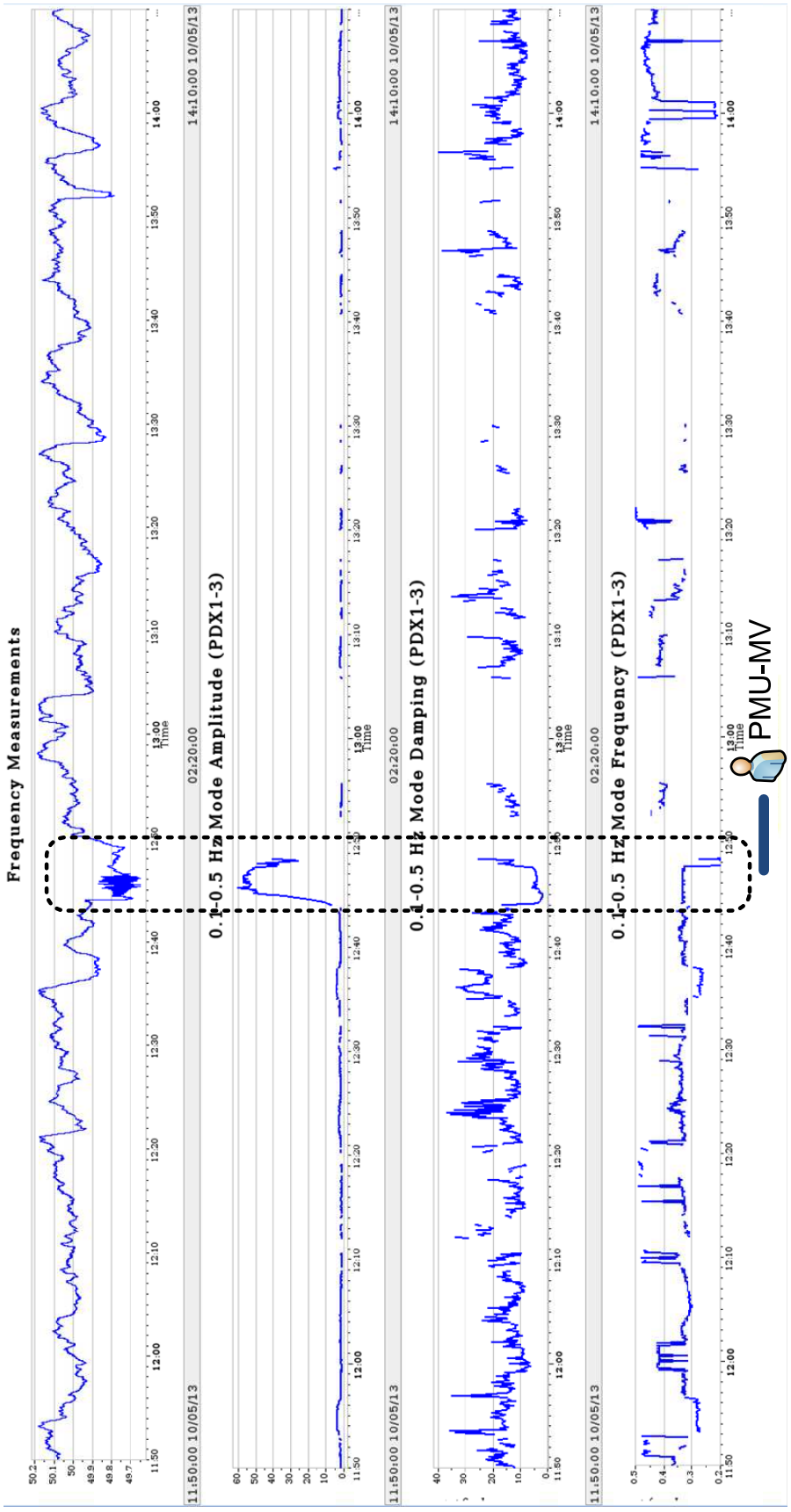

Figure 3.26: PMU-MV data for the frequency range 0.1Hz - 0.5Hz.

Figure 3.27 shows the PMU-MV measurements for the Western Cape - Mpumalanga mode, showing grid frequency measurements, mode amplitude, mode damping and frequency for the disturbance incident. Also highlighted in Figure 3.27 is the time period of interest whereby the Western Cape - Mpumalanga mode became excited as a result of modal resonance with the SAPP mode. As can be seen in Figure 3.27 the mode amplitude increased drastically and the mode damping was reduced to about 1%, resulting in large oscillations in the frequency as measured by PMU-MV. This can also be deduced from analysis of Figure 3.24, whereby the initial dominant oscillation mode in the frequency was the SAPP mode and some resonance condition occurs between the two modes with the Western Cape - Mpumalanga mode then having a slightly reduced mode frequency. As can be seen in Figure 3.27, the mode frequency is reduced from approximately 0.65Hz to approximately 0.575Hz during this time period while the mode damping remains well below 5% and the mode amplitude is still very high.

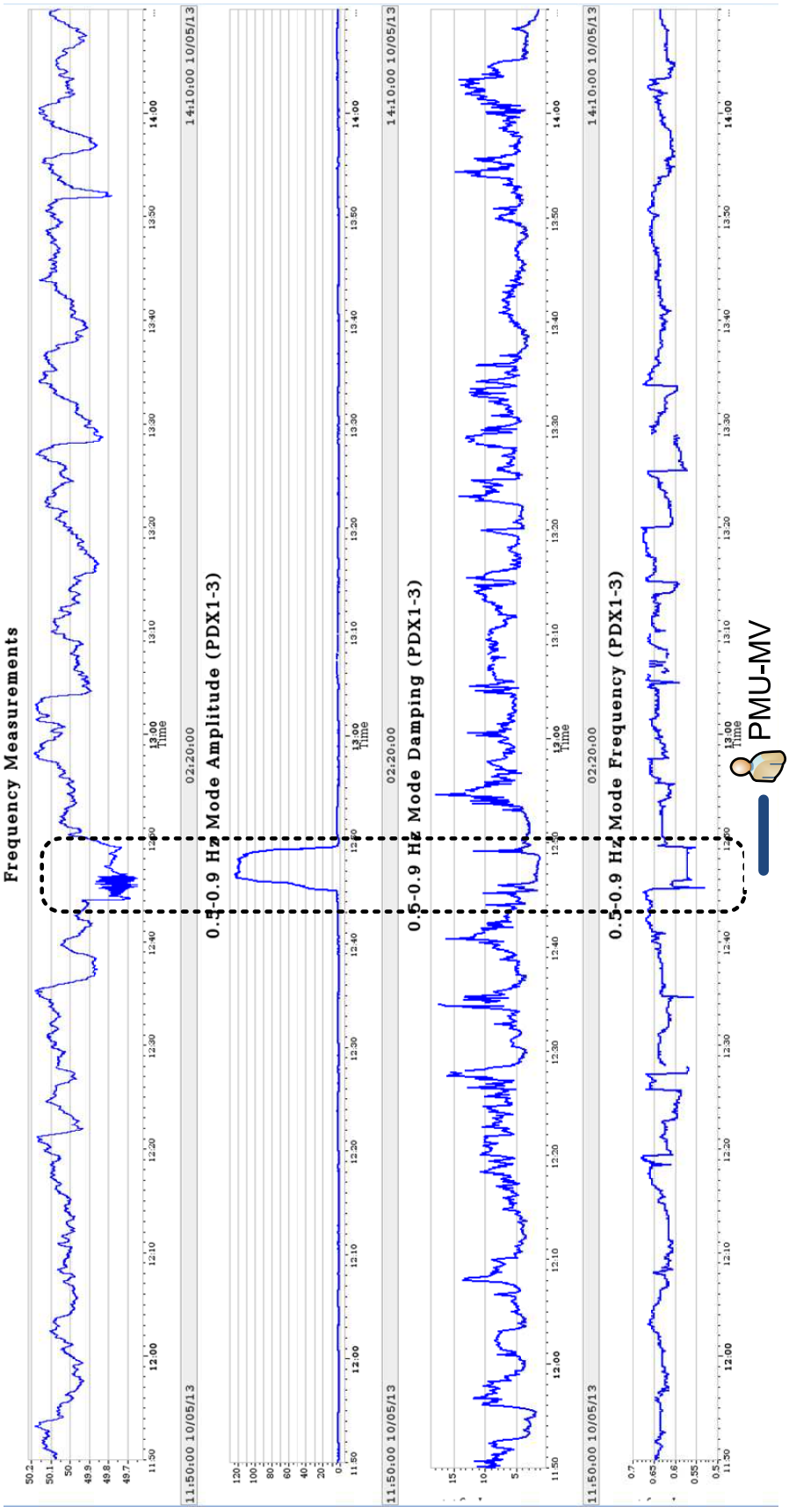

Figure 3.27: PMU-MV measured data for frequency range 0.5Hz - 1.0Hz.

The manner in which the modal interaction between the Western Cape and Mpumalanga mode will be handled in this dissertation will be to ensure that the damping introduced through phase compensation is able to increase the amount of damping over a wide frequency range. The main disadvantage regarding this approach is that power system linearization tools will still be used to simulate network snapshot conditions. The frequency domain performance of the PSS will be analysed over the electromechanical frequency range, 0.2Hz to 3.0Hz.

3.5 Measurement Based Unit Model Validation

Analysis of the Western Cape - Mpumalanga oscillation mode presented Figure 3.23 (a) shows that the generators at PS-KRG have the highest participation in the oscillation mode. The participation of the generators at plant PS-KRG was found to be 100% (machine angle having the highest participation). Various network snapshot conditions were simulated in order to ensure that the mode participation was not highly influenced by the load flow conditions at any point. Various other generators in the Western Cape also have significant participation in the oscillation mode. The mode controllability of the Western Cape - Mpumalanga oscillation mode shown in Figure 3.23 (b) shows that the best generators suited to controlling the oscillation mode are at PS-KRG. The state variable offering the highest degree of controllability of this mode is the machine speed variable. This implies that a properly designed/tuned PSS would be able to introduce the required amount of damping of the mode. Hence it is important that the PSS settings at PS-KRG be reviewed in order to improve the amount of damping of the oscillation mode over the frequency range of interest.

In order to be able to design/tune the PSS situated at power plant PS-KRG, the software model response must be verified to be the same as that of the actual unit. In order to be able to perform this model validation, staged tests were carried out on the units at PS-KRG. The tests conducted were open circuit (open loop) model tests and closed circuit (closed loop) model tests. The software model response was compared with the actual unit measurements.

3.5.1 Unit Response Model Validation with Generator offline

Figure 3.28 shows a single line diagram of a SMIB model with the generator circuit breaker open, the unit still running. The PSS was disabled during this test. The excitation control system model is identical to that shown in Figure 3.28 and the AVR model is shown in Figure 2.6. The unit was subjected to step input changes through the AVR set-point. The response of the actual unit was compared with the software model in order to verify its performance.

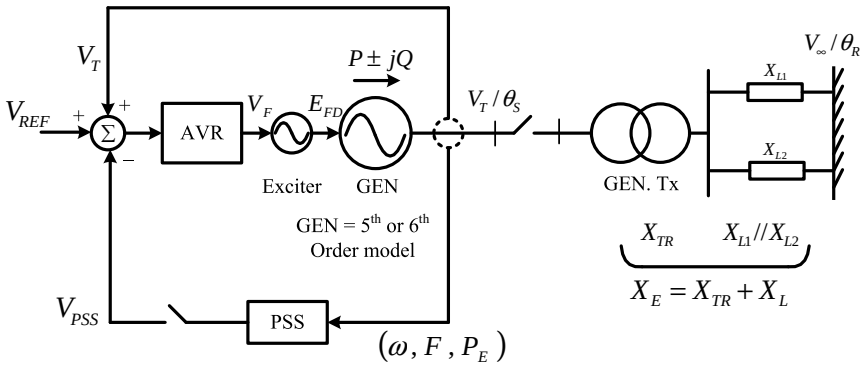

Figure 3.28: Single line diagram of SMIB with the unit open circuit.

Figure 3.29 shows the open loop ECS response measured on the unit for step inputs into the AVR. Figure 3.29 (a) shows the terminal voltage response and (b) shows the field voltage response. Comparisons of the measured response with the model response shows that the model matches the performance of the unit quite well with an error margin of less than 4% (Figure 3.29 (a)) on the terminal voltage response. The field voltage model response matches the measured field voltage response but it was found that the measured response has a much quicker settling time after the disturbance. The field voltage response on both the positive and negative steps are higher on the model than the actual plant measurement, this could be as a result of the damping effect of the main exciter which are not captured by the derived model shown in Figure 2.6 (b). It must be mentioned that the models used in this dissertation are standard user models similar to those presented in [13] and the derivation of exact model responses for the excitation systems used in this dissertation is beyond the scope of this dissertation.

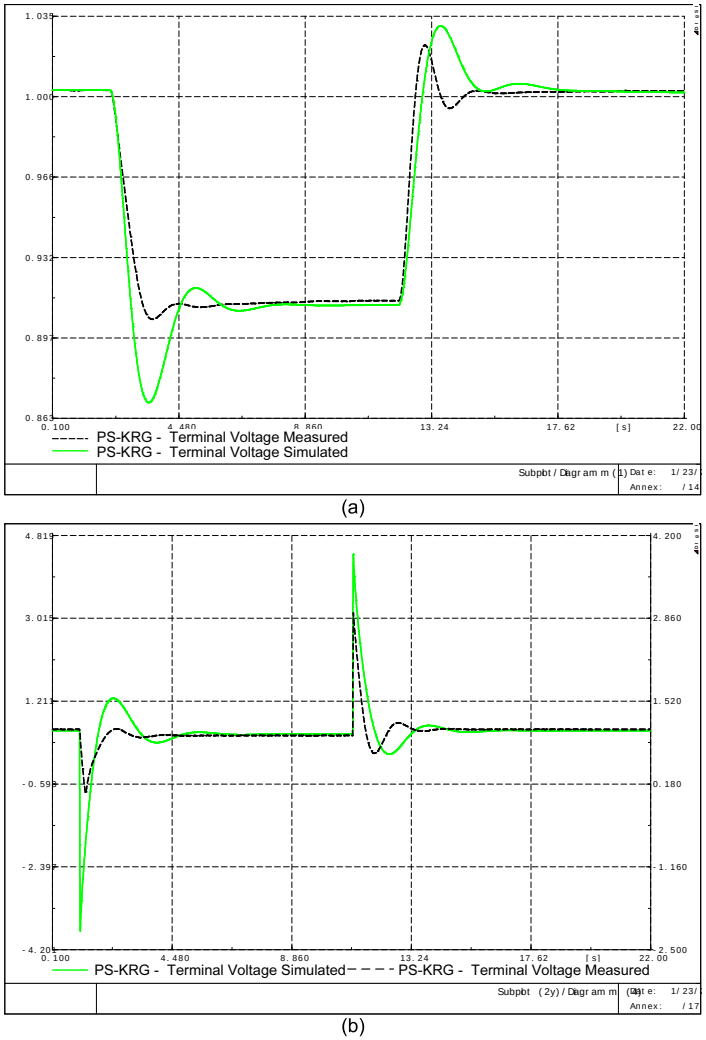

Figure 3.29: Open circuit unit response to AVR step input changes. (a) Unit terminal voltage response, (b) Unit field voltage response.

3.5.2 Unit Response Model Validation with Generator on-line

Figure 3.30 shows the closed loop ECS response performed on the unit for step inputs into the AVR with the unit operating at half load. Figure 3.30 (a) shows the terminal voltage response and (b) shows the field voltage response. Comparisons of the measured response with the model response shows that the model matches the unit quite well on the terminal voltage response. The field voltage response on both the positive and negative steps are higher on the model than the actual plant measurement, this could be as a result of the damping effect of the main exciter which are not captured by the derived model shown in Figure 2.6 (b)

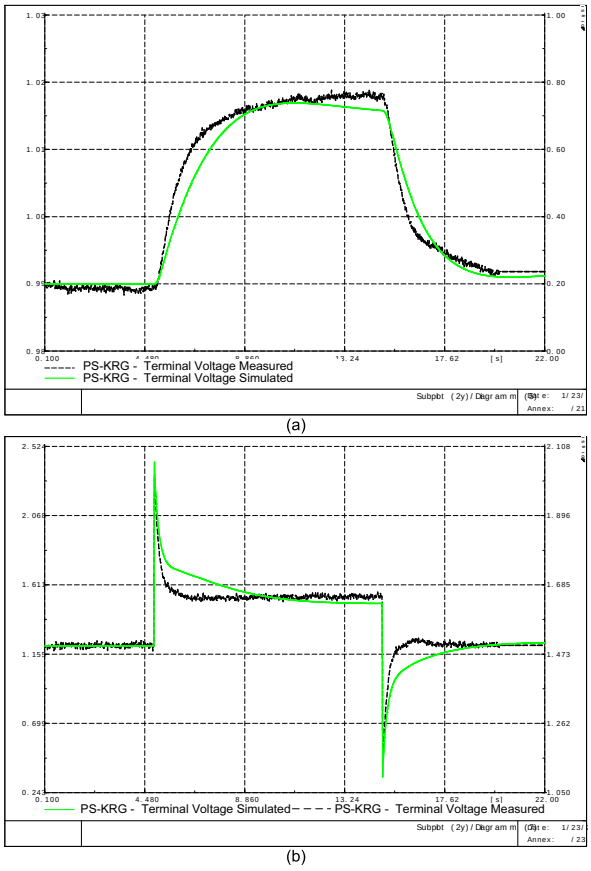

Figure 3.30: Closed circuit response to AVR step input changes. (a) Unit terminal voltage response, (b) Unit field voltage response.

Further tests were conducted on the unit to verify the software model performance. These tests were all conducted with the unit operating at various points, full load, and low load, and the results are shown in Appendix C. For all tests performed on the unit, it was found that the model was able to sufficiently mimic the measured response.

3.6 Summary

This chapter presented the model validation techniques which are used in small signal stability analysis, namely modal and time domain analysis. A review of the critical electromechanical modes in the Eskom network was presented. Electromechanical modes of interest which were identified were the Western Cape - Mpumalanga and the SAPP modes. PMU measurements were presented confirming results which have been observed from simulations conducted. Dynamic network model behaviour based on network incidents which have been observed were presented and simulation results were found to

match well with the PMU measurements.

The mode controllability and participation factors were presented and the units at power plant PS-KRG were identified as the best location to control the Western Cape - Mpumalanga mode. Modal interaction between the SAPP and Western Cape - Mpumalanga modes were shown through the PMU measurements. The ECS model performance of the units at power plant PS-KRG was verified through staged tests which were performed on the actual unit and it was found that the model was able to adequately mimic the performance of the actual plant ECS.

Chapter 4

Power System Stabilizer Design/Tuning

4.1 Introduction

As previously stated, PSSs are the most cost effective manner of introducing damping into power systems. The main aim of this dissertation is to design PSS lead/lag parameters in order to target a specific oscillation mode in the Eskom network. The designed PSS is expected to provide damping over a wide frequency range. The PSS structure to be used is PSS2B which was presented in 2.2.3. This PSS structure is designed for single mode damping. Through the use of conventional control design techniques and assessing the performance of the proposed controller, it is possible for the designed controller to act over a wide operating frequency range. Reference [16] states that the frequency range of concern in SSS studies is approximately 0.2Hz to 3.0Hz. This will be the electromechanical frequency range analysed. The effect of various parameters on the designed PSS will also be evaluated in order to ensure that the PSS does not have an adverse affect on the generator torsional modes, intra-plant modes and generator terminal voltage while the generator is being ramped by the turbine. All analysis will be carried out through eigenvalue analysis and non-linear time domain simulations as suggested in [30], so as to ensure that the designed PSS is the most optimal stabilizer.

4.2 Power System Stabilizer Tuning/Design Methods

There exists a host of controller design and tuning techniques which have been applied to PSSs. These techniques can be classified into two categories, namely linear and non-linear design methods. Various PSS design methodologies have been proposed over the past decade, but not many have been widely accepted in the design of conventional PSS controls. This is due to their rather complex nature, non practicability (in some cases) and assumptions which are required in their application. Some of the most common techniques which are used in PSS design and tuning are reviewed in order to demonstrate and compare the benefits and advantages of each. The methods analysed are those which are known to have been applied to actual stabilizers.

4.2.1 H_∞ (H-infinity) design method

H_∞ controllers are designed in the frequency domain to determine optimal controller parameters, offering controllers which are robust over a wide range of system conditions

and which minimize disturbances to the plant output subject to closed loop stability. One of the main disadvantages of H_∞ controllers is that they are of the same order as the plant. Hence in the application of H_∞, the plant model must be reduced in order to minimize the controller order. Thus H_∞ design relies heavily on highly accurate model reduction.

Another challenge associated with the application of H_∞ design is the selection of the weighting functions used in the optimization of the controller parameters. This relation has been reported throughout the literature [55]. Reference [56] states that uncertainty in the reduced model creates a situation whereby the controller cannot respond and a system becomes unstable after it has been disturbed. Reference [57] demonstrates that the pole-zero cancellation which is important in the application of this method can produce closed loop poles which have damping which is directly dependent on the open loop system poles. This is not necessarily desirable as the open loop poles could be poorly damped. Hence the application of H_∞ controller design techniques has not been widely accepted in the practical application and design of PSSs.

4.2.2 Pole placement design method

Similar to H_∞ design, pole placement design is performed in the frequency domain. The pole placement design approach focuses on using root locus design techniques to move a pair of poles to a new desired location. The pole placement technique provides good graphical representation of system poles which is a desirable attribute to design engineers. This approach works directly with the closed loop poles of the system. Reference [58] states that this technique may lead to very high values of PSS gain which could result in poor non-linear time domain behaviour. Large PSS gains also lead to quick saturation of the stabilizer output which is undesirable as it could lead to controller windup.

The pole placement technique does not necessarily ensure that the poles move to the desired location and this method is also not robust over a wide range of system conditions. Reference [5] states that this technique is not suitable for large networks whereby multiple inter-area modes may exist due to the inherent complexity. Another disadvantage of this method is that it only focuses on a single pole pair; hence any other modes which may be adversely affected as a result of the pole shift can only be discovered after the design is complete. Hence reducing adverse pole interactions in the frequency domain relies on a trial and error approach.

4.2.3 Frequency response design methods

Frequency response based controller design is the most common controller design method used in industry due to its simplicity. The amount of compensation which is to be added

by the controller can be obtained through residue analysis or through participation factor analysis. The main advantage of this method is that it is not affected by the size of the plant and is insensitive to varying system conditions, [8]. Reference [8] states that a compromise is necessary to ensure an acceptable level of phase compensation exists over the frequency range of interest over a range of system conditions.

This also offers initial design-stage counter-measures against any adverse effects which may result due to the controller tuning and also offers insight into the exact controller response. The controller gain is chosen to achieve an acceptable gain margin and to ensure that the controller is able to introduce the required amount of phase compensation at the desired frequency without amplifying the controller input noise, [43].

4.3 Frequency Response Power System Stabilizer Design

4.3.1 Residue based design [6]

The general structure of a PSS was initially presented in 2.9, and its transfer function can be expressed as:

$$\begin{aligned} G_{PSS}(s) &= K_{GAIN} \times G_{WASHOUT}(s) \times G_{PHASE-COMP}(s) \\ &= K_{GAIN} \times \left(\frac{sT_w}{1+sT_w}\right) \times \left(\frac{1+sT_1}{1+sT_2}\right) \times \left(\frac{1+sT_3}{1+sT_4}\right) \\ &= K_{GAIN} \times G_W(s) \times G_P(s) \end{aligned} \tag{4.1}$$

-where $G_W(s)$ is the transfer function of the washout filter, and $G_P(s)$ is the transfer function of the phase compensator. The residues of a power system are determined using the transfer function of the linearized power system model given by Eq. (2.26) and Eq. (2.27) as follows:

$$\begin{aligned} G(s) &= \frac{y(s)}{u(s)} \\ &= C(sI_n - A)^{-1} B \end{aligned} \tag{4.2}$$

If we let the modal matrices of the right and left eigenvectors ϕ , ψ and the diagonal matrix Λ, be given by:

$$\Phi = [\phi_1, \cdots \phi_n] \quad \Psi = [\psi_1, \cdots, \psi_n]^T \quad \Lambda = diag(\lambda_j), \; j = 1, ...n$$

-it can be shown using eigenvector properties presented in 2.3.1.1 that:

$$A\Phi = \Phi\Lambda, \tag{4.3}$$
$$\Psi^T A = \Lambda\Psi^T, \tag{4.4}$$

hence by definition we have $\Psi^T\Phi = I_n$

-where I_n is an identity matrix.

Using matrix manipulations, the modal matrices may be rearranged to yield:

$$\Psi^T A\Phi = \Psi^T\Phi\Lambda = I_n\Lambda \tag{4.5}$$
$$A = \left[\Psi^T\right]^{-1}\Lambda\Psi^T = \Phi\Lambda\Psi \tag{4.6}$$

Eq. (4.2) can now be written as in Eq. (4.7) by using the matrix property $f(A) = \Phi f(\Lambda)\Psi^T$, where f an arbitrary matrix function:

$$G(s) = C\Phi\left(sI_n - \Lambda\right)^{-1}\Psi^T B \tag{4.7}$$

Since $(sI_n - \Lambda)$ is a diagonal matrix, its inverse therefore is also a diagonal matrix. Hence Eq. (4.7) can be expressed as:

$$G(s) = \sum_{j=1}^{n}\frac{C\phi_j\psi_j^T B}{s-\lambda_h} = \sum_{j=1}^{n}\frac{R_j}{s-\lambda_j} \tag{4.8}$$

-where

$$R_j = C\phi_j\psi_j^T B \tag{4.9}$$

-is the residue of the transfer function Eq. (4.7) at eigenvalue λ_j.

For a power system with a critical eigenvalue λ_j with poor damping which is to be improved, let λ_j have its residue given by R_j for a specific single input and single output of the system. The sensitivity of λ_j to the stabilizer gain, K_{GAIN} can be expressed as, [6]:

$$\frac{\partial\lambda_j}{\partial K_{GAIN}} = R_j\frac{\partial G_{PSS}(\lambda_j)}{\partial K_{GAIN}} = R_j G_W(\lambda_j) G_P(\lambda_j) \tag{4.10}$$

Eq. (4.10) can now be used to determine the change in the eigenvalue of λ_j as a result of the PSS:

$$\Delta\lambda_j = R_j G_W(\lambda_j) G_P(\lambda_j) K_{GAIN} \tag{4.11}$$

(Note: Strictly speaking Eq. (4.11) must have ΔK_{GAIN} on the right hand side of the equation, but inserting a PSS is equivalent to increasing ΔK_{GAIN} from 0. Hence $\Delta K_{GAIN} = K_{GAIN}$).

It must be noted that all components of Eq. (4.11) are complex except for K_{GAIN} which is a real constant. The residue R_j and the PSS transfer function at eigenvalue λ_j, are all multiplied by a particular gain value to produce a shift in the eigenvalue to the desired location. Figure 4.1 adapted from [23] shows how the eigenvalue λ_j is moved to a new desired position y whereby $\Delta\lambda_j$ makes a right angle triangle as shown in Figure 4.1. Moving λ_j to y ensures that the eigenvalue has the required amount of damping while moving λ_j the shortest distance. λ_j normally has a very small real component, implying that κ in Figure 4.1 has a small value. This implies that if λ_j is moved parallel to the $x - axis$, the additional distance added is insignificant.

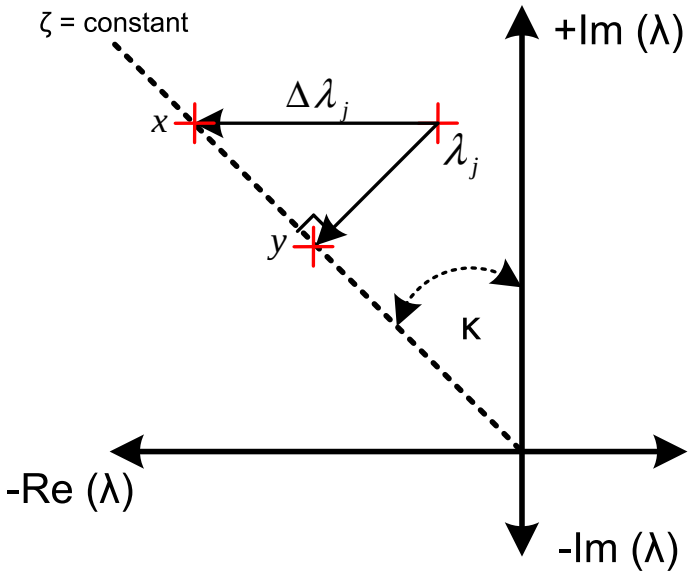

Figure 4.1: Eigenvalue shift to preferred location, adapted from [23].

For the application of residue based design to PSSs, [40] states that the compensation to be added by the PSS must provide enough phase lead such that the modes of interest will be shifted perpendicular to the imaginary axis or that the mode shifts slightly upward from the real axis but with the largest displacement being perpendicular to the imaginary

axis, represented by $\Delta\lambda_j$ in Figure 4.1. This ensures that the damping torque provided by the PSS is high while also maintaining a high synchronizing torque component.

If the eigenvalue motion is downward towards the real axis, this implies that the PSS provides too much phase lead. This results in the PSS detracting from the synchronizing torque of the generator and thereby compromising the transient stability performance of the generator in some cases. Reference [42] states that this would result in the excitation system mode becoming unstable at relatively low values of synchronizing torque even though the gain value may be high. Hence to ensure that λ_j moves parallel to the $x-axis$, $\angle \triangle \lambda_j = \pi$.

The necessary phase compensation which is to be added by the PSS can be computed using Eq. (4.11) as follows:

$$\begin{aligned} \angle G_P(\lambda_j) &= \angle\Delta\lambda_j - \angle R_j - \angle G_W(\lambda_j) && (4.12) \\ &= \pi - \angle R_j - \angle G_W(\lambda_j) && (4.13) \end{aligned}$$

The number of phase compensation blocks, each consisting of a pole zero pair, is determined by the amount of phase compensation to be added. Reference [2] suggests that the largest phase compensation to be added by a single lead/lag block must be limited to 55^o (degrees) to prevent the amplification of any unwanted noise. This noise may appear on the signal from the speed transducer. References [23, 55] suggest that the maximum allowable compensation limit of a single lead/lag stage is 65^o (degrees). The maximum allowable phase compensation will be taken as 65^o in this dissertation. The PSS gain can also be calculated using Eq. (4.11), as follows:

$$K_{GAIN} = \frac{|\Delta\lambda_j|}{|R_j|\,|G_W(\lambda_j)|\,|G_P(\lambda_j)|} \quad (4.14)$$

In some cases the eigenvalue λ_j may not move to the desired location because of system non-linearity. Hence it may be necessary to adjust the phase compensation and gain slightly to meet the desired specification. In the application of the stabilizer, the phase lag to be compensated is computed based on the type of stabilizer used. For example, for a PSS using rotor speed as its input the phase lag of the plant is computed between the rotor speed output and the AVR input reference voltage.

4.3.2 Participation factor based design [7, 8, 9]

This design method is based on the analysis of generator speed participation factors and assumes the PSS uses the rotor speed as its input. The sensitivity of an eigenvalue λ_j, with respect to the transfer function, a_{ii}, between the generator speed and the

generator speed derivative coincides with the generator participation factor. Similar to the methodology used in 4.3.1, the sensitivity of λ_j to the transfer function, a_{ii}, between the generator speed and the generator speed derivative can be expressed as [9]:

$$\frac{\partial \lambda_j}{\partial a_{ii}} = p_{ij} \tag{4.15}$$

-where p_{ij} represents the participation factor of the i^{th} rotor speed (i^{th} state variable in the state matrix) when considering the j^{th} eigenvalue (oscillation mode) and a_{ii} is the transfer function between the generator speed and its speed derivative. It must be noted that this method assumes that the generator speed will be used as a stabilizing signal, and this is analysed on the Heffron-Phillips SMIB model. Hence using Figure 2.12, the sensitivity of λ_j with respect to the stabilizer transfer function, a_{ii}, where $a_{ii} = \frac{1}{2H}\left[-K_{GAIN}G_{PSS}\left(\lambda_j\right)G_{EXC}\left(\lambda_j\right)G_{GEN}\left(\lambda_j\right)\right]$, can be expressed as:

$$\frac{\partial \lambda_j}{\partial K_{GAIN}} = \frac{\partial \lambda_j}{\partial a_{ii}}\frac{\partial a_{ii}}{\partial K_{GAIN}} = \frac{1}{2H}\left[-p_{ij}G_{PSS}\left(\lambda_j\right)G_{EXC}\left(\lambda_j\right)G_{GEN}\left(\lambda_j\right)\right] \tag{4.16}$$

-where $G_{GEN}\left(\lambda_j\right)$ and $G_{EXC}\left(\lambda_j\right)$ are the values of the transfer functions of the generator and excitation system at mode frequency λ_j. Similarly it should be ΔK_{GAIN} on the right hand side, but inserting the PSS is equivalent to increasing K_{GAIN} from 0, so $\Delta K_{GAIN} = K_{GAIN}$. Therefore the eigenvalue change after the PSS has been introduced can be represented as:

$$\Delta\lambda_j = \frac{1}{2H}\left[-p_{ij}K_{GAIN}G_W\left(\lambda_j\right)G_P\left(\lambda_j\right)G_{EXC}\left(\lambda_j\right)G_{GEN}\left(\lambda_j\right)\right] \tag{4.17}$$

Similar to the residue based design approach, K_{GAIN} and H are real values.

The exact phase shift which needs to be introduced by the stabilizer resulting in the eigenvalue displacement of $\Delta\lambda_j$ can be expressed as:

$$\angle\Delta\lambda_j = \pi + \angle p_{ij} + \angle G_W\left(\lambda_j\right) + \angle G_P\left(\lambda_j\right) + \angle G_{EXC}\left(\lambda_j\right) + \angle G_{GEN}\left(\lambda_j\right) \tag{4.18}$$

Since $\angle\Delta\lambda_j = \pi$, Eq. (4.18) can be rearranged to obtain the amount of phase compensation to be added:

$$\begin{aligned} \pi &= \pi + \angle p_{ij} + \angle G_W\left(\lambda_j\right) + \angle G_P\left(\lambda_j\right) + \angle G_{EXC}\left(\lambda_j\right) + \angle G_{GEN}\left(\lambda_j\right) \\ 0 &= \angle p_{ij} + \angle G_W\left(\lambda_j\right) + \angle G_P\left(\lambda_j\right) + \angle G_{EXC}\left(\lambda_j\right) + \angle G_{GEN}\left(\lambda_j\right) \\ \angle G_P\left(\lambda_j\right) &= -\left[\angle p_{ij} + \angle G_W\left(\lambda_j\right) + \angle G_{EXC}\left(\lambda_j\right) + \angle G_{GEN}\left(\lambda_j\right)\right] \end{aligned} \tag{4.19}$$

The PSS gain is also calculated using Eq. (4.16) as follows:

$$K_{GAIN} = \frac{2H\left|\Delta\lambda_j\right|}{\left|p_{ij}\right|\left|G_W\left(\lambda_j\right)\right|\left|G_P\left(\lambda_j\right)\right|\left|G_{EXC}\left(\lambda_j\right)\right|\left|G_{GEN}\left(\lambda_j\right)\right|} \tag{4.20}$$

In a similar manner to the residue based design approach, the eigenvalue λ_j may not move to the desired location because of system non-linearity; hence it may be necessary to adjust the phase shift and gain slightly to meet the desired specification. In this design method, the phase lag for which the stabilizer must compensate is also that between the AVR input reference voltage and the electrical torque produced in the generator air-gap (exciter and the generator time constants).

Reference [59] states that the residue for a nonreciprocal system can be defined as the product of the right eigenvector and the left eigenvector. Hence residues and participation factors can only be said to be similar for nonreciprocal systems and a system must be proven to be either reciprocal or nonreciprocal. This implies that the use of residues and participation factors in the design of compensator parameters for systems can be seen as two separate approaches as the two methods can give vastly different answers depending on the nature of the system being analysed, which is the case in this dissertation.

4.3.3 Conventional stabilizer design method [9]

The conventional design approach used to design PSSs uses the participation factor approach but some assumptions are made in order to simplify the design process. The conventional design approach assumes that the participation factor of the rotor speed of the respective eigenvalue (oscillation mode) is real [7, 16, 8, 60, 61]. The phase lag component associated with the washout filter is also ignored, since it is relatively small at the mode frequency of concern. Hence the required phase compensation is approximated as:

$$\angle G_{PSS}\left(\lambda_j\right) \approx \left[\angle G_{EXC}\left(\lambda_j\right) + \angle G_{GEN}\left(\lambda_j\right)\right] = \left[\angle G_{ECS}\left(\lambda_j\right)\right] \tag{4.21}$$

Analysis of Eq. (4.21), shows that the PSS compensates only for the phase lag of the generator and the exciter (ECS). Based on the underlying assumptions and analysis of Eq. (4.21), the PSS provides the required damping for the critical mode λ_j, only if the phase of the participation factor is close to zero.

Reference [16] showed that the phase compensation which is to be provided by the stabilizer must compensate for the phase lag between the AVR input reference voltage V_{REF} and the generator electrical torque T_E as presented in 2.2.3. In calculating the frequency response characteristic it is essential to ensure that the inertia of the generator is assumed to be very large in order to ensure that any feedback due to generator rotor

angle is ignored. This ensures that the frequency response characteristic obtained only reflects the phase lag of the ECS. The stabilizer gain is calculated in exactly the same manner as the participation factor method, using Eq. (4.20).

4.4 Eigenvalue Assessment of the Tuned Power System Stabilizers

In order to evaluate the performance of the tuned PSS using residue, participation factor and conventional design methods, two software models were used to assess the local, intra, and inter-area oscillation modes. Figure 4.2 shows a detailed busbar configuration of power plant PS-KRG feeding into the network. This configuration was used to assess the performance of the PSS in the detailed Eskom network model.

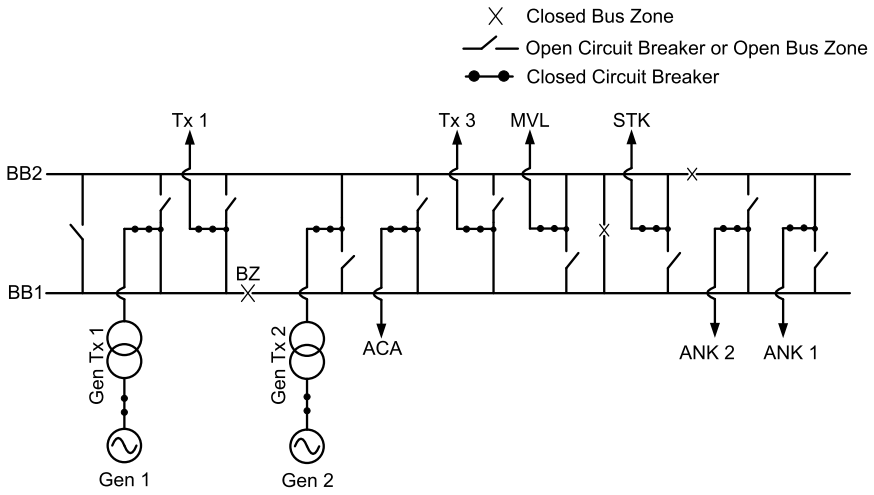

Figure 4.2: Simplified power plant busbar configuration feeding into network.

The power plant was also modelled feeding into an infinite bus, which was used to study the local mode and intra-plant oscillation modes, Figure 4.3 shows a single line diagram representation of the model used to study the modes mentioned. Reference [16] demonstrated that in tuning PSSs, different generator operating points need to be chosen depending on the stabilizer type applied. Speed based stabilizers are tuned using $P \pm jQ = 1.0 + j0.0$, feeding into a strong AC transmission network (effective network impedance is generally assumed to be approximately 0.2pu). This generator operating condition results in maximum phase lag observed in the path which the stabilizer compensates. Frequency based stabilizers are tuned feeding into a weak AC transmission system. This results in maximum phase lag with regards to the stabilizer [16].

The PSS2B is an "integral of accelerating power stabilizer", which uses speed and electrical power as controller inputs. Hence the tuning operating point which results in the

maximum phase lag of the ECS according to [16], is $P \pm jQ = 1.0 + j0.0$. Also the generator feeds into a very strong transmission system (low output impedance seen by the generator).

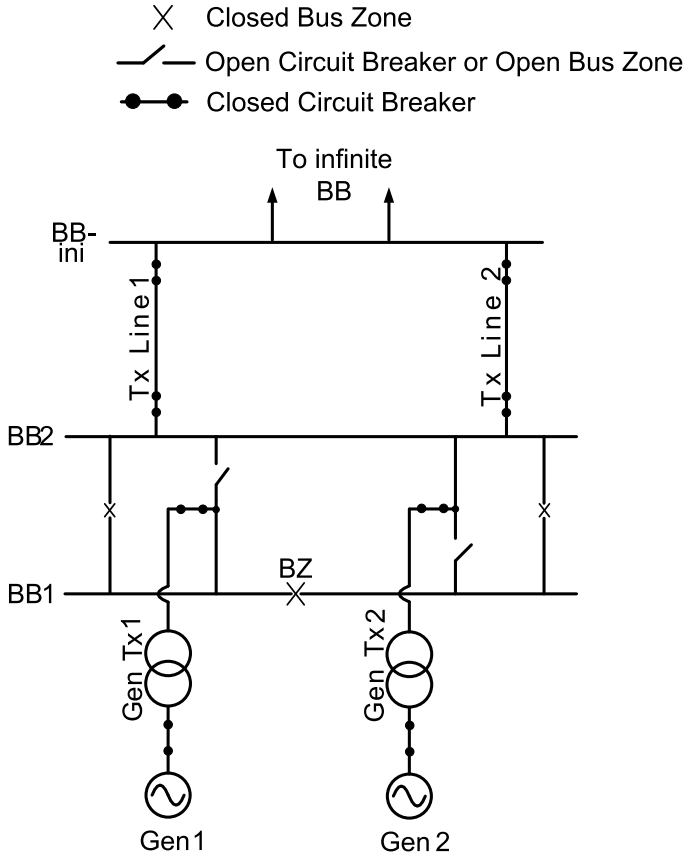

Figure 4.3: Simplified power plant busbar configuration feeding into an infinite bus.

Appendix D shows detailed calculations with each of the previously stated design techniques. The PSS stabilizers were designed at three operational functional frequencies. These were inter-area mode, local mode, and at the highest electromechanical operational frequency of 3.0Hz. The latter was performed based on observations presented in [16], stating that tuning compensators at higher frequencies allows better phase compensation to be provided at the lower frequencies and ensures that the phase roll off at higher electromechanical frequencies is not severe, thus ensuring a better phase compensation over the frequency range.

The stabilizer performance assessment criteria which were set were based on the following factors adapted from [30, 36] :

- Ensure that the local mode has good damping, $\zeta \geq 15\%$,

- Ensure that the inter-area mode has moderate damping, $\zeta \geq 5\%$,
- Ensure that the stabilizer does not detract from the performance of other system modes having $\zeta \geq 10\%$.
- Ensure that the stabilizer parameters do not cause excessive terminal voltage transients.

The PSS which was able to effectively meet the set requirements was taken as the best performing stabilizer. The challenge presented by the requirements was the tradeoffs which had to be made. During PSS tuning it was found that the PSS parameter that ensured maximum local mode damping did not necessarily ensure good inter-area mode damping. Hence the PSS was then optimized to increase the inter-area mode damping by increasing the stabilizer gain. It was found that this detracted from the local mode damping, but the optimal gain was chosen to ensure that $\zeta \geq 5\%$.

Figure 4.4 shows a simplified diagram used in order to explain pole movement in the complex frequency plane as a result of the tuned PSS parameters.

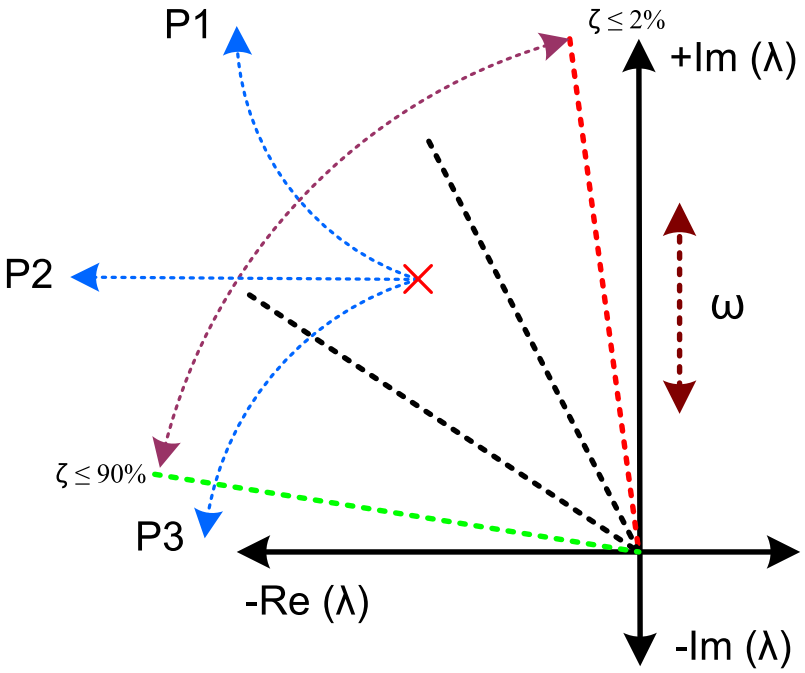

Figure 4.4: Pole movement in the complex frequency plane due to tuned PSS parameters.

As previously described in 4.3.1, the ideal case for PSS design is for the pole with poor damping to move parallel to the negative $x - axis$ following the line labelled P2. But this is not always the case due to system non-linearity. The pole could move following

the line P1 or P2. In the case whereby the line follows the P1 route, the stabilizer introduces damping and synchronizing torque to the pole, but the pole moves quickly towards the right hand plane in the frequency domain and could become unstable. In the case whereby the pole follows the P3 route, the stabilizer introduces to much damping to the pole and the pole frequency becomes lower and this detracts from the synchronizing torque which could lead to poor transient stability performance. Hence it is important that the PSS is designed to ensure that each of the poles associated with the system does not have poor damping or detract from the performance of the system in any manner.

4.4.1 Eigenvalue assessment of the residue based design

Table 4.1 shows the eigenvalues for the SMIB model for all three PSS design frequencies. The stabilizer parameters are given Appendix D. The PSS gains were tuned in order to ensure that the local mode has the highest value of damping possible for the designed settings. This was done by using the derived gain equation and then manually adjusting the gain in order to find the maximum value of damping of the local mode. Assessment of Table 4.1, shows that the PSS which has the best local mode performance is that tuned at 1.0Hz, even though the mode frequencies are slightly higher than the case with no PSS and lower corner frequency of 0.65Hz.

Table 4.1: Local mode eigenvalue assessment using the SMIB model and a PSS designed using the residue approach .

Compensator tuned frequency	Local mode frequency	K_{GAIN}	Eigenvalue	Damping ratio	Damping time constant
Hz	Hz	-	-	ζ (%)	seconds
No PSS	1.042899	-	-0.6116$\pm j$ 6.5527	9.0929	1.6346
	0.9135339	-	-0.4393259 $\pm j$5.739903	7.6316	2.27622
0.65	1.237172	2.46	-1.784468 $\pm j$7.773383	22.37416	0.5603911
	0.9836276	2.46	-2.035736 $\pm j$6.180314	31.28552	0.4912229
1.0	1.298459	8.571	-2.984038 $\pm j$8.15846	34.35039	0.3351164
	0.9146028	8.571	-2.097828 $\pm j$5.746619	34.29192	0.4766836
3.0	1.289756	75	-0.7842381 $\pm j$8.103778	9.632437	1.275123
	1.143882	75	-0.6127975 $\pm j$7.187225	8.495381	1.63186

The designed settings were used in the detailed Eskom network model in order to assess the impact of the designed PSS on the inter-area mode for each of the designed corner frequency values. Table 4.2 shows the eigenvalues for the detailed Eskom model.

Table 4.2: 0.65 Hz mode eigenvalue assessment using the detailed Eskom network and a PSS designed using the residue approach.

Compensator tuned frequency	Inter-area mode frequency	K_{GAIN}	Eigenvalue	Damping ratio	Damping time constant
Hz	Hz	-	-	ζ (%)	seconds
No PSS	0.6537668	-	-0.1380342 $\pm j$4.107738	3.358451	7.24458
0.65	0.6429642	2.46	-0.4149631 $\pm j$4.039863	10.21795	2.409853
1.0	0.654691	8.571	-0.5059686 $\pm j$4.113545	12.20806	1.976407
3.0	0.7569842	75	-0.3535277 $\pm j$4.756272	7.412426	2.828633

The PSS which is designed at 1.0Hz has the highest inter-area mode damping and the highest local mode damping for the designed settings based on comparison of the results in Table 4.1 and Table 4.2. It was also noted that the stabilizer does not cause any other modes to become unstable or to have unacceptable damping. Using the analogy represented by Figure 4.4, the inter-area pole moves almost parallel to the negative $x - axis$, with a very slight upward direction, indicating that the stabilizer adds almost pure damping to this pole. The effect of the stabilizer on the local mode is also shown in Table 4.1, the slight upward direction implies that a very small amount of synchronizing torque is added to the mode, [16].

The PSS designed at the corner frequency of 1.0Hz has the most desirable characteristics as it introduces the highest local mode and inter-area mode damping, and these settings will be compared with settings designed using the other techniques.

4.4.2 Eigenvalue assessment of the participation based design

Table 4.3 shows the eigenvalues for the SMIB model for all three PSS corner frequency designs. The stabilizer parameters are given Appendix D. The PSS gains were tuned in order to ensure that the local modes have the highest value of damping possible. This was done by using the derived gain equation and then manually adjusting the gain in order to find the maximum value of damping of the local mode. Assessment of Table 4.3 shows that the PSS which has the best local mode performance is that designed at 1.0Hz, even though the mode frequencies are slightly higher than the case with no PSS and lower corner frequency of 0.65Hz

Table 4.3: Local mode eigenvalue assessment using the SMIB model and a PSS designed using the participation factor approach .

Compensator tuned frequency	Local mode frequency	K_{GAIN}	Eigenvalue	Damping ratio	Damping time constant
Hz	Hz	-	-	ζ (%)	seconds
No PSS	1.042899	-	-0.6116$\pm j$ 6.5527	9.0929	1.6346
	0.9135339	-	-0.4393259 $\pm j$5.739903	7.6316	2.27622
0.65	1.238195	2.6	-1.704932 $\pm j$7.779809	21.40681	0.5865338
	1.003832	2.6	-1.931287 $\pm j$6.307263	29.27824	0.5177896
1.0	1.286955	8.58	-2.849504 $\pm j$8.086174	33.23596	0.3509383
	0.9265217	8.58	-2.093709 $\pm j$5.821508	33.84284	0.4776214
3.0	1.43394	45.55	-2.146081 $\pm j$9.009713	23.17136	0.4659657
	1.204816	45.55	-1.938055 $\pm j$7.570085	24.8016	0.5159812

The designed settings were used in the detailed Eskom network model in order to assess the impact of the designed PSS on the inter-area mode. Table 4.4 shows the eigenvalues for the detailed Eskom model, for all three design cases.

Table 4.4: 0.65 Hz mode eigenvalue assessment using the detailed Eskom network and a PSS designed using the participation factor approach.

Compensator tuned frequency	Inter-area mode frequency	K_{GAIN}	Eigenvalue	Damping ratio	Damping time constant
Hz	Hz	-	-	ζ (%)	seconds
No PSS	0.6537668	-	-0.1380342 $\pm j$4.107738	3.358451	7.24458
0.65	0.6443857	2.6	-0.421409 $\pm j$4.048795	10.35233	2.372992
1.0	0.655823	8.58	-0.5037559 $\pm j$4.120658	12.13479	1.985088
3.0	0.729943	45.55	-0.6498329 $\pm j$4.586367	14.02868	1.538857

The PSS designed at 3.0Hz has the highest inter-area mode damping and the local mode damping offered by the design is able to meet the requirements which were set. But it can be seen that this stabilizer causes the poles to move in the upward direction, which is not desirable. The stabilizer does not cause any other modes to become unstable. It must be noted that the gain value of the 3.0Hz stabilizer is high compared to the other design cases, which is not desirable in practice as it could lead to stabilizer saturation during operation or integral windup. The PSS designed at a corner frequency of 1.0Hz,

does not cause the inter-area mode to shift upwards excessively and the damping which it provides is sufficient to meet the requirements set for both local and inter-area modes, while having a moderate value of gain. Hence this stabilizer is chosen as the best design in the participation factor based approach since all the requirements are met with the least amount of tradeoffs.

4.4.3 Eigenvalue assessment of the conventional based design

Table 4.5 shows the eigenvalues for the SMIB model for all three PSSs designed using the conventional approach. The stabilizer parameters are given Appendix D. The PSS gains were tuned in order to ensure that the local mode has the highest value of damping possible. This was done by using the derived gain equation and manually adjusting the gain in order to find the maximum value of damping of the local mode. Assessment of Table 4.5, shows that the PSS which has the best local mode performance is that designed at 3.0Hz. The stabilizer designed at this frequency causes the local mode pole to move downwards as can be seen by the slight reduction in mode frequency. This implies a slight loss of synchronizing power at the local mode frequency.

Table 4.5: Local mode eigenvalue assessment using the SMIB model and a PSS designed using the conventional approach .

Compensator tuned frequency	Local mode frequency	K_{GAIN}	Eigenvalue	Damping ratio	Damping time constant
Hz	Hz	-	-	ζ (%)	seconds
No PSS	1.042899	-	-0.6116$\pm j$ 6.5527	9.0929	1.6346
	0.9135339	-	-0.4393259 $\pm j$5.739903	7.6316	2.27622
0.65	1.22747	2.03	-2.080322 $\pm j$7.71242	26.04288	0.4806947
	0.8890753	2.03	-1.909246 $\pm j$5.586225	32.341	0.523767
1.0	1.803299	7.49	-4.142869 $\pm j$11.33046	34.34045	0.2413786
	0.7524419	7.49	-1.728272 $\pm j$4.727732	34.33387	0.5786127
3.0	1.081505	60	-3.164311 $\pm j$6.795294	42.21376	0.3160245
	0.9861994	60	-2.577886 $\pm j$6.196473	38.41103	0.3879147

The designed settings were used in the detailed Eskom network model in order to assess the impact of the designed PSS on the inter-area mode. Table 4.6 shows the eigenvalues for the detailed Eskom model, for all three design cases.

Table 4.6: 0.65 Hz mode eigenvalue assessment using the detailed Eskom network and a PSS designed using the conventional approach.

Compensator tuned frequency	Inter-area mode frequency	K_{GAIN}	Eigenvalue	Damping ratio	Damping time constant
Hz	Hz	-	-	ζ (%)	seconds
No PSS	0.6537668	-	-0.1380342 $\pm j$4.107738	3.358451	7.24458
0.65	0.639022	2.03	-0.3902516 $\pm j$4.015093	9.674025	2.56245
1.0	0.6258839	7.49	-0.5634626 $\pm j$3.932545	14.18334	1.774741
3.0	0.7180209	60	-0.8487492 $\pm j$4.511459	18.48884	1.178204

The PSS designed at 3.0Hz has the highest inter-area mode and local mode damping, and the design is able to meet the requirements which were set. Similar to the participation factor response design approach the stabilizer causes the inter-area pole to move in the upward direction, which is undesirable. The PSS designed at 3.0Hz has the desired impact on both the local and inter-area mode damping, but similar to the participation factor case the stabilizer gain is high. The PSSs designed at 0.65Hz and 1.0Hz cause the poles to move downward thus implying reduced synchronizing torque. This is undesirable as the mode could become unstable after a large disturbance under certain conditions. Hence the stabilizer which best satisfies the requirements is that designed at 3.0Hz.

4.5 Impact of the Stabilizer Parameters on Generator Behaviour

In order to assess the impact of the stabilizer parameters on the generator terminal voltage, it is important to ensure that the performance is assessed using the same ramp rate curve which the generator turbine uses to ramp up. Reference [36] states that in order to ensure that the stabilizer does not have an adverse effect on the terminal voltage and reactive power output, it is important to assess $\frac{\Delta Q_T}{\Delta P_{REF}}$. Reference [62] presents a detailed analysis of the various stabilizer parameters which influence generator terminal voltage, with an emphasis on the ramp tracking filter parameters. In practice generator units are ramped at a very specific rate which is influenced by a large number of operating conditions such as turbine steam inlet temperatures and boiler pressure. These ramp rates differ from unit to unit based on the unit capabilities. The ramp rate curves for the units at PS-KRG along with the various conditions for unit ramping are given in Appendix E.

Figure 4.5 shows the terminal voltage, field voltage and the reactive power responses of a generator for all three PSSs, for a 30MW/min ramp rate of the generator active power. This ramp was taken from the very hot turbine ramp rate curve shown in Figure E.7 of

Appendix E. In order to be able to assess the impact of the tuned PSS, various scenarios were investigated:

1. Impact of the PSS on the generator terminal voltage, field voltage, and the output reactive power,
2. Impact of the PSS on a sister unit during unit ramps, with various load levels on the sister unit,
3. Frequency domain analysis of the PSS contribution to the overall path on which it acts, $\frac{\Delta T_E}{\Delta \omega_G}$.

All of the turbine ramp curves were assessed in order to ensure that all of the designed PSSs do not cause adverse terminal voltage and reactive power fluctuations. All of the graphs for the ramp rate curves are given in Appendix E. Analysis of various graphs presented in Appendix E, and those shown in Figure 4.5, show that the residue and the participation factor based stabilizer designs behave in an almost identical manner. This observation is in line with the findings presented in [9].

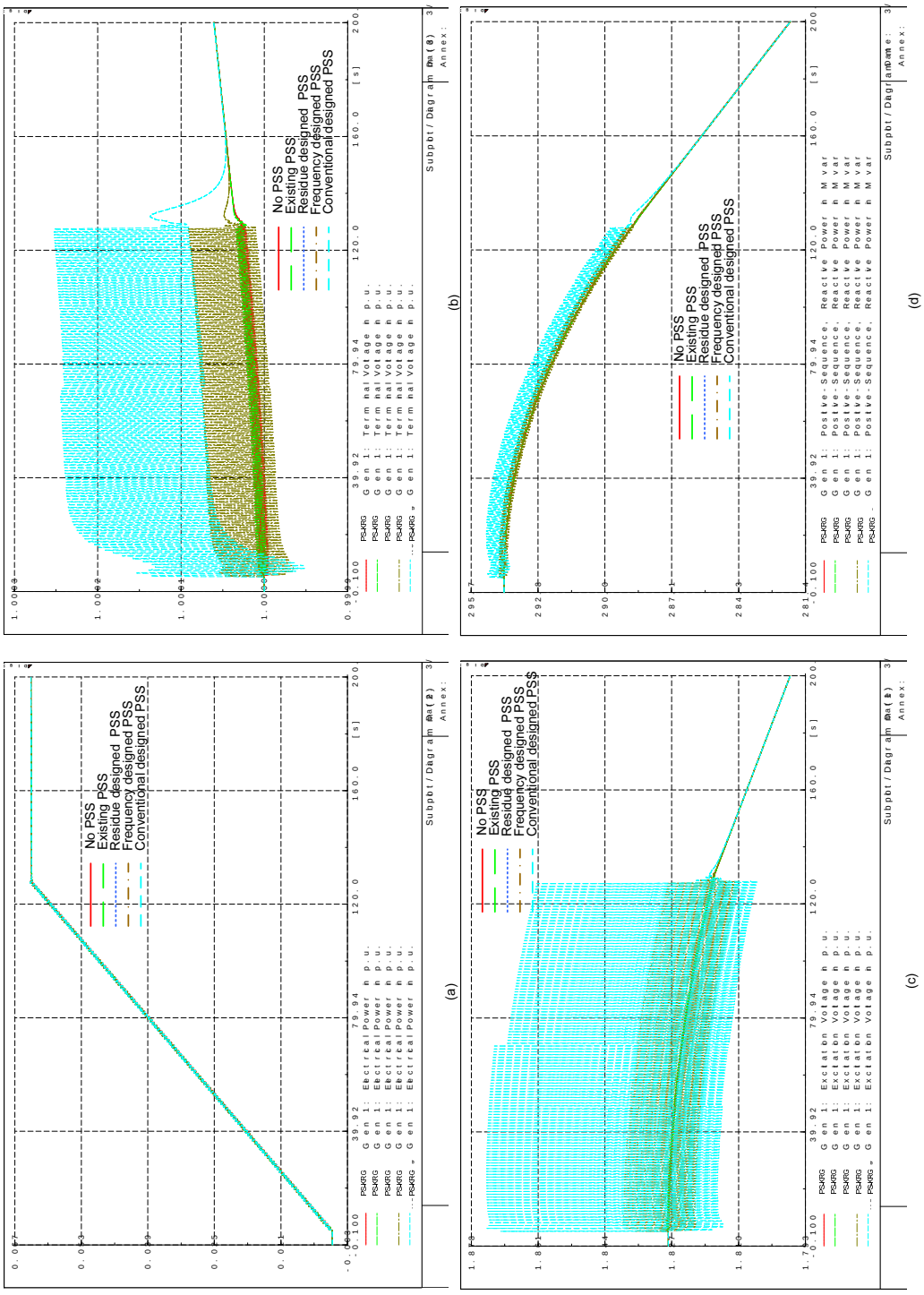

Figure 4.5: Generator parameters, (a) electrical power, (b) terminal voltage, (c) field voltage and (d) reactive power output.

The impact of the residue and participation factor based stabilizers on the terminal voltage is a slight fluctuation, as can be seen Figure 4.5 (b). Similar behaviour can also be observed on the field voltage and reactive power. The fluctuation caused by the newly designed PSSs is less than 0.00001pu, and the behaviour of the various variables does not differ much from that of the original system without a PSS and with the currently existing PSS. This implies that the PSS ramp tracking filter parameters T_8 and T_9 were chosen correctly. Reference [62] states that T_9 must be less than 0.1s to avoid excessive terminal voltage fluctuations being induced by the stabilizer.

The PSS designed using the conventional approach was also assessed in a similar manner, and the results are also shown in Figure 4.5. The performance of the conventional stabilizer design method resulted in poor terminal voltage, field voltage and reactive power performance of the unit, as can be seen in Figure 4.5 and also all of the results presented in Appendix E. The conventional design approach consistently resulted in large fluctuations of terminal voltage, field voltage and reactive power output. The main cause of the poor performance of these parameters can also be attributed to the large gain value of the stabilizer. In numerical terms the fluctuations measured were found to be of the order 0.001pu, which may not be very noticeable in simulation studies, but may be exacerbated under certain network conditions or by signal transducers used to measure these signals.

Figure 4.6 shows the performance of the sister unit parameters which were monitored as the primary unit was ramped at various load levels. In Figure 4.6 the unit was operating at full load. The sister unit performance was also assessed under different operating conditions:

1. Primary unit ramped, and sister unit operating at low load (25% load level),
2. Primary unit ramped, and sister unit operating at half load (50% load level),
3. Primary unit ramped and sister unit operating at full load (100% load level).

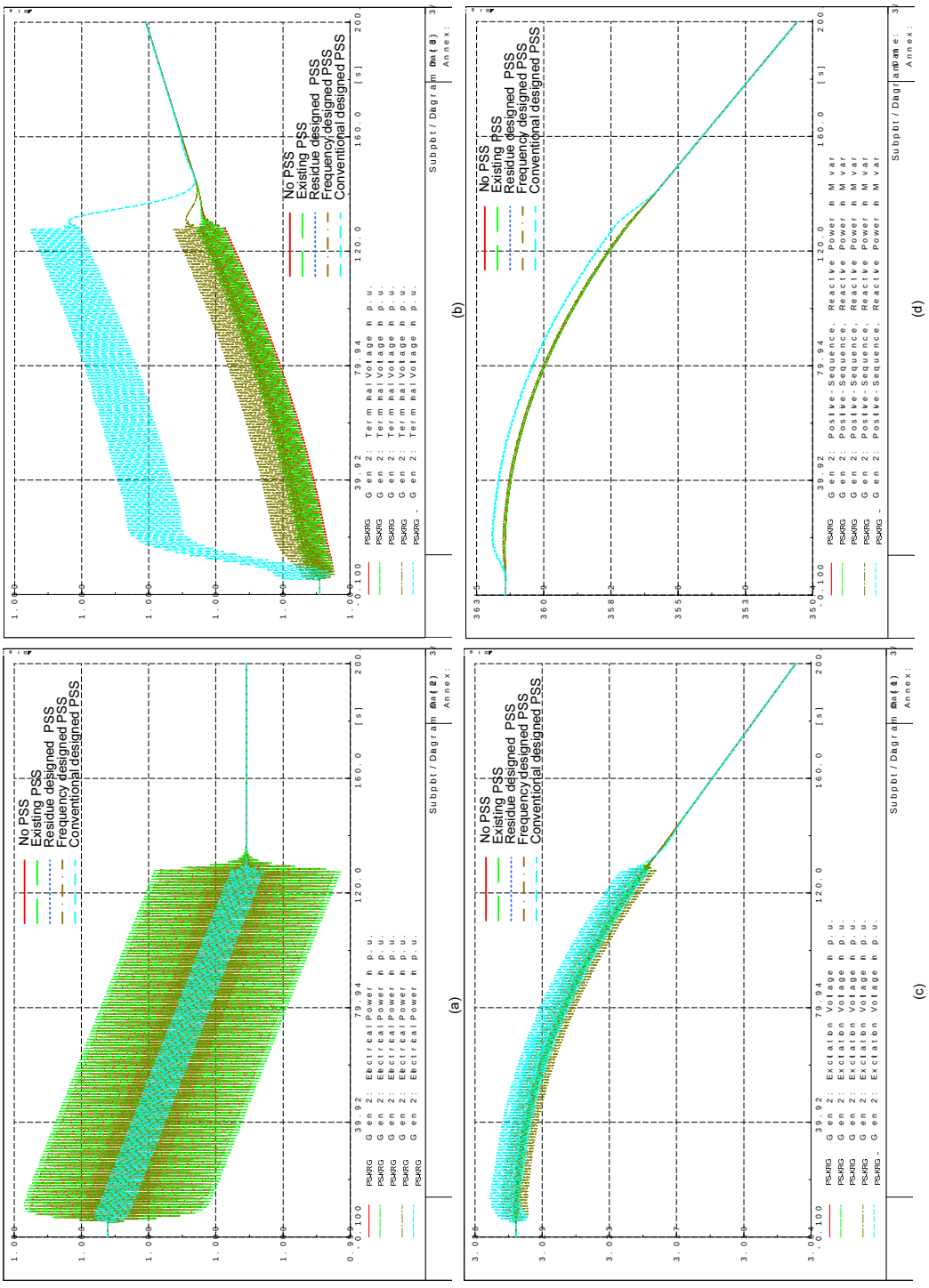

Figure 4.6: Generator parameters, (a) electrical power, (b) terminal voltage, (c) field voltage and (d) reactive power output, of sister unit, while primary unit ramped.

Figure 4.6 shows the performance of the sister unit while operating at full load. It must be stated that the sister unit was also fitted with an identical stabilizer as the primary unit for each of the tests which were conducted. As can be seen in Figure 4.6, the residue and participation factor based stabilizer designs performed identically and the fluctuations associated with the newly designed stabilizers were less than 0.00001pu, similar to the results presented in Figure 4.5. The stabilizer designed using the conventional approach was found to have poor terminal voltage, field voltage and reactive power output performance compared to residue and participation factor based stabilizer designs.

The frequency domain performance of the plant with and without all of the designed PSSs was analysed in order to assess the impact of the PSS parameters on the frequency domain performance of the plant. Reference [16] showed that the full path along which the stabilizer acts is given by $\frac{\Delta T_E}{\Delta \omega_G}$. Figure 4.7 shows the various Bode plots of the plant with and without the stabilizers. Reference [7] suggest that the frequency band which can be analysed using the Heffron-Phillips model is 0.1Hz to 3.0Hz. Above this range the model is no longer accurate and it becomes important that the generator is modelled using the Solid Iron Rotor Model (SIRM) also known as the Jackson-Winchester model which is highly complex but allows for detailed model studies of various transient phenomena which are higher than the electromechanical frequency range. This full model is given in [63]. This model is well suited to the study of torsional interactions between the PSS and the entire turbine and generator shafts. This type of analysis is beyond the scope of this dissertation and will not be considered in any of the modeling presented.

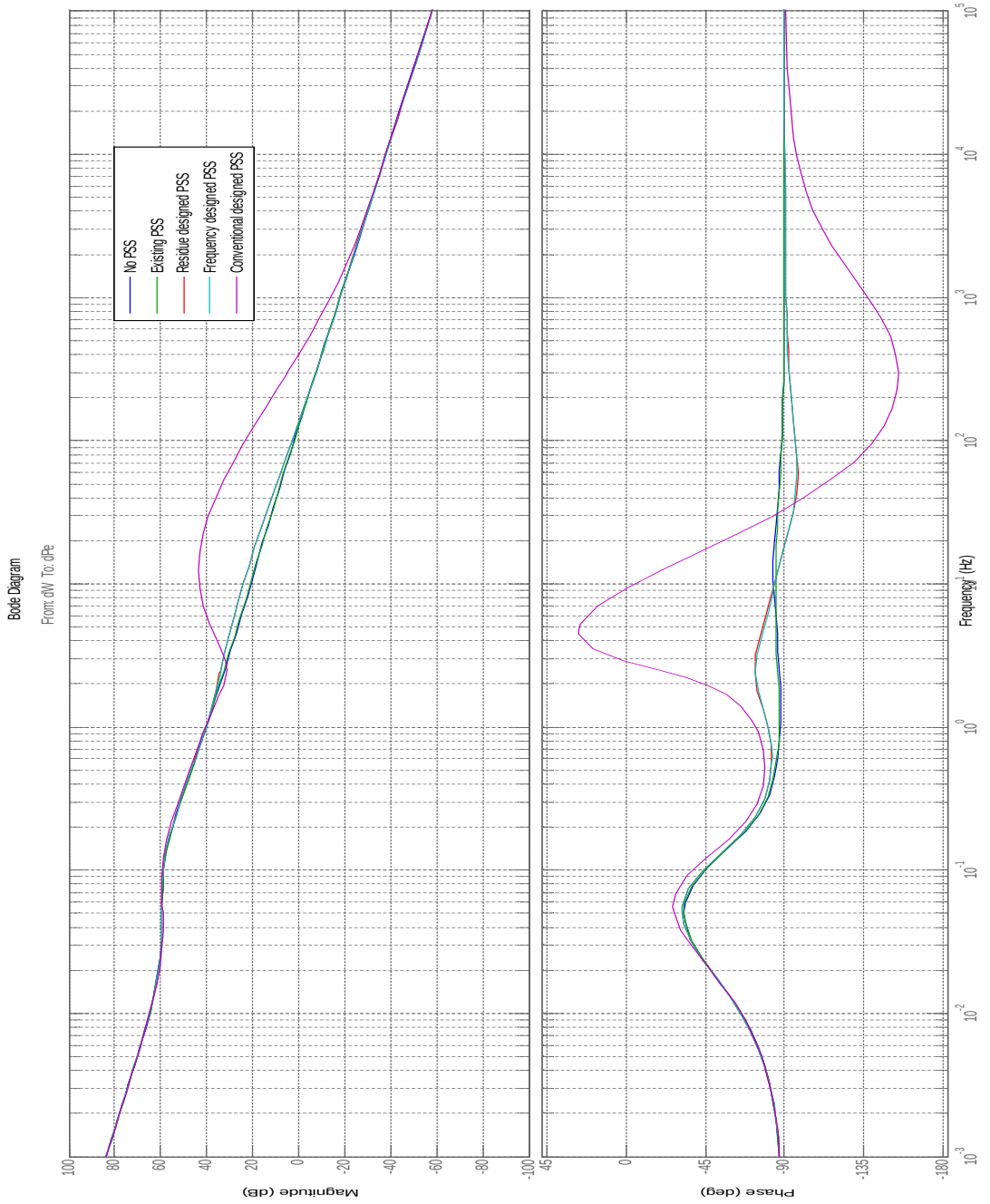

Figure 4.7: Bode plot of plant including various PSSs designed, $\frac{\Delta T_E}{\Delta \omega_G}$.

Analysis of the Bode plots shown in Figure 4.7 within the range 0.1Hz to 3.0Hz shows that the frequency response of the stabilizers designed using residues and participation

factor are identical, which is to be expected based on the modal analysis results presented earlier. The PSS designed using the conventional approach allows for higher compensation over a wider frequency range as can be seen in Figure 4.7, compared to both the residue and participation factor based stabilizers. The conventional designed stabilizer offers a higher degree of phase compensation. But what is also evident is that the conventional stabilizer design causes a large increase in the magnitude and phase of the plant at higher frequencies as shown in Figure 4.7. This is highly undesirable as the frequency range beyond 5.0Hz coincides with the natural torsional frequency band of nuclear unit shaft trains. This implies that the conventional PSS could possibly excite a torsional oscillation mode on any of the generator turbine stages resulting in damage to the unit due to torsional resonance.

Thus based on the analysis presented above, the two most suitable stabilizer designs which will be considered from here onwards are the residue and participation factor based PSS designs due to the fact that they do not produce any adverse fluctuation of the terminal voltage, field voltage, output reactive power and do not result in high gain magnitudes or phase responses within the torsional frequency band as shown in Figure 4.7.

4.6 Summary

This chapter presented a review of some of the methods which are used in the design of PSSs. The various advantages and disadvantages associated with the use of advanced techniques and their practical application in actual power systems was presented. Design methods which are commonly used in industry were also evaluated. PSSs were designed using three approaches which were found to be the best suited and most commonly used in practice. These were residue based design, participation factor based design, and the conventional based design. The criteria which were used to determine the effectiveness of the various PSSs designed were based on [30]. Three design frequencies were chosen, 0.65Hz which is the inter-area frequency of concern, 1.0Hz, which is the local mode frequency of the machines and 3.0Hz, based on suggestions presented in [16]. With each of the three methods, three stabilizers were designed and their impact on the system eigenvalues using a SMIB model and a detailed Eskom network model were analysed. The stabilizer which offered the highest amount of damping without drastically affecting the synchronizing torque of both the local and inter-area modes was chosen from each of the three design methods.

The three stabilizers from each group were then assessed to determine their impact on the generator terminal voltage, field voltage and reactive power output using the turbine ramp curves which are used on the actual power plant PS-KRG. The stabilizer designed using the conventional approach was found to induce higher fluctuations of these parameters as compared to the residue and participation factor based designs.

The frequency response of the various stabilizers was also assessed and it was found that the conventional stabilizer design introduced much more phase compensation over the desired frequency range compared to the residue and participation factor designs. But the impact of this was that the stabilizer resulted in increased gain magnitude and phase response over the torsional frequency range in which most steam driven turbines have torsional frequencies, hence increasing the risk of torsional resonance induced as a result of the stabilizer. Based on the analysis presented, the conventional stabilizer was excluded as a candidate as a result of the possible danger which may result due to torsional resonance. The residue and participation factor designs were found to perform in an identical manner to one another, both in the frequency range as well as in the SMIB models and the detailed Eskom network model.

Chapter 5

Small Signal Stability Contingency Case Analysis

5.1 Introduction

In order to be able to assess the effectiveness of the various PSSs designed it is important that various contingencies are assessed, and that these are based on parameters which have a large influence and impact on the SSS of the network and particularly the oscillation modes of concern, inter-area oscillation mode and the local oscillation mode. In order to be able to determine various transmission network contingencies it is important to fully understand the exact path over which these oscillations travel in the network. In order to be able to determine the exact path which is travelled by the oscillations of interest, a concept presented in [10] will be used. Its application will be presented using a simple example and the method will also be applied to the detailed Eskom network to determine the various oscillation paths of the inter-area mode.

The influence and the impact of load models will also be assessed, the loads which have the highest participation and observability factors of the inter-area mode will be determined using participation factor analysis and mode observability. The frequency dependance of these load models will be varied and the influence of the various stabilizers will be assessed for the various load frequency dependencies of the load models for faults applied to the system. This will be done for the SMIB model as well as the detailed Eskom network model.

5.2 Dominant inter-area mode path

With the integration of various sources of embedded generation into networks, power systems are becoming more complex in nature and the use of local control signals to damp out oscillations is no longer as highly effective on inter-area modes [64]. Understanding the exact path which oscillation modes travel within a power system enables power system controllers to identify key transmission lines and buses associated with the modes. This allows for the grid operational SSS margins to be monitored and maintained within acceptable levels for all operating conditions.

The concept of "interaction paths" in power systems was presented in [65], and it is defined as "the main path along which generators, controllers and loads interact with one another allowing for the exchange of oscillation energy". This exchange of oscillation energy must have a path which allows for it to flow. This path is provided by transmission

lines and buses. The main "interaction path" within a power system can also be defined as the corridor within the power system which carries the highest content of oscillation mode energy. Hence the interaction path implicitly has a high degree of observability of the oscillation mode of interest. References [65, 66] state that propagation paths within power systems are deterministic, hence there exist corridors which provide an optimal pathway for the propagation of oscillation energy through the network, for each individual mode within the network.

Reference [67] presents an extension of the interaction path concept through the development of the "dominant inter-area oscillation path". Similar to the interaction path the dominant inter-area oscillation paths are also deterministic [66]. Hence the most robust signals to be used in Wide Area Monitoring Systems (WAMS) can be easily determined through this type of analysis [66]. Reference [68] states that the paths with the highest content of the oscillation mode energy have their transfer capability limited. Thus identification of these corridors reveals SSS bottle-necks within the transmission network

The main limitation as to why this analysis has not received much attention is because network parameters such as voltages and currents are also influenced by reactive power control equipment such as Automatic Voltage Regulators (AVRs) and Static Var Compensator (SVCs), [69]. Network busbar voltages are also influenced by nearby loads; hence the application of these techniques is best suited to transmission network busbars without large amounts of local generation or loads [69]. The persistence of dominant inter-area oscillation paths with various types of loads has been shown not to vary much with the types of loads applied to the network [70]. Reference [70] showed that the magnitude of the oscillation energy which flows through the network lines changes as one path either carries a higher content or a particular component absorbs a larger or lesser amount of the oscillation energy. This validates observations presented in references [65, 66], that oscillation energy flow within a network is deterministic and a priori. Reference [68] also states that all dominant inter-area oscillation paths have a very high degree of persistence, implying that under various operating conditions the paths which the oscillation energy travels do not change much and they are still highly observable and robust.

5.2.1 Theoretical background [10]

As previously presented in Chapter 2, power systems can be expressed in terms of Differential and Algebraic Equations (DAEs). The linearized power system matrices given by Eq. (2.28) are used in the development of this theory. The state variables of the power system are given by the vector x_P. State variables can be chosen based on the needs of the analysis performed and are not unique. If the power system model analysed is treated as a minimal electromechanical model for an N machine network, the state space matrix will be given by:

$$x_P = \begin{bmatrix} \dot{\Delta\delta} \\ \dot{\Delta\omega} \end{bmatrix} = \begin{bmatrix} \Delta\delta_1 & \Delta\omega_1 \\ \vdots & \vdots \\ \Delta\delta_N & \Delta\omega_N \end{bmatrix} \tag{5.1}$$

-where δ_j and ω_j are the machine load angle and speed, of the j^{th} machine in the network. Assuming that $\Delta u = 0$, the power system model can be expressed as

$$\begin{bmatrix} \dot{\Delta\delta} \\ \dot{\Delta\omega} \end{bmatrix} = \begin{bmatrix} a_{11} & a_{12} \\ a_{21} & a_{22} \end{bmatrix} \begin{bmatrix} \Delta\delta \\ \Delta\omega \end{bmatrix} \tag{5.2}$$

-where $\Delta\omega$ and $\Delta\delta$ are speed and load angle state variables.Using the mode shape (observability) of the state matrix which was derived in 2.3.1 and the output state matrix C_P, the network mode shape can be defined as the product of the mode shape of the electromechanical oscillations, and the transmission network sensitivity parameters. The network mode shape serves as an indication of "how much" of each mode is distributed amongst the transmission network parameters. The output variables of interest within a transmission network are the busbar voltage magnitudes, busbar voltage angles, transmission line current magnitudes and transmission line current angles with respect to changes in the state variables of the network $\Delta\delta$ and $\Delta\omega$. The sensitivity of the busbar voltages with respect to the generator load angle $C_{V\delta}$ can be expressed as:

$$C_{V\delta} = \begin{bmatrix} \frac{\partial V_1}{\partial \delta_1} & \cdots & \frac{\partial V_1}{\partial \delta_N} \\ \vdots & \ddots & \vdots \\ \frac{\partial V_N}{\partial \delta_1} & \cdots & \frac{\partial V_N}{\partial \delta_N} \end{bmatrix} \tag{5.3}$$

The sensitivity of the busbar voltages with respect to generator speed can also be expressed using a similar approach to that of Eq. (5.3). Therefore the complete busbar voltage magnitude and voltage angle sensitivities of the network can be expressed as:

$$C_V = [C_{V\delta} \mid C_{V\omega}] \tag{5.4}$$
$$C_\theta = [C_{\theta\delta} \mid C_{\theta\omega}] \tag{5.5}$$

In the application of the concept of the dominant inter-area oscillation path, the network mode shape has to be formulated based on the use of transmission network variables of interest. The network mode shape gives the open loop observability of the network electromechanical oscillation modes of various parameters which are being analysed [68].

Network mode shapes of various network parameters are expressed as follows:

$$S_V = C_V \phi \tag{5.6}$$
$$S_\theta = C_\theta \phi \tag{5.7}$$

Eq. (5.6) and Eq. (5.7) give the network mode shape of the network busbar voltage magnitude S_V and the network mode shape of the voltage angle S_θ. Similarly the current magnitude mode shape and angle are given Eq. (5.8) and Eq. (5.9).

$$S_I = C_I \phi \tag{5.8}$$
$$S_{i\theta} = C_{i\theta} \phi \tag{5.9}$$

Dominant inter-area path mode shape properties which have been observed based on the analysis presented in [67] are:

1. Voltage magnitude mode shape S_V and voltage angle S_θ indicate the modal observability of a signal
2. The largest S_V or the smallest S_θ of networks indicates the center of the path. The center path can also be seen as the "inter-area mode center of inertia" or the inter-area pivot for the mode of interest
3. Current magnitude mode shapes S_I indicates the percentage of the content of the inter-area mode that is distributed among the transfer corridors of the network.
4. Higher values of S_I indicate the most likely path which is to be travelled by the oscillation mode energy

Appendix F gives an example which was used to demonstrate the application of the dominant inter-area oscillation mode path. The example demonstrates how the paths which contain the highest inter-area oscillation mode are identified. The example uses a very simple two-area power system model to present the application of these techniques which will now be applied on the detailed Eskom network model.

5.3 Persistence of dominant inter-area paths

The detailed Eskom network shown in Figure 5.1, shows the highlighted main corridors which carry power from the main generation pool in the North-Eastern region of the country to the South-Western region. There are two main corridors which allow for power to flow to the Western Cape region. Both corridors which go into the Western Cape emanate from the Gauteng region. Hence the lines will only be analysed from this point onwards to determine which of the two corridors carries the highest magnitude of the oscillation energy and the center of oscillation path.

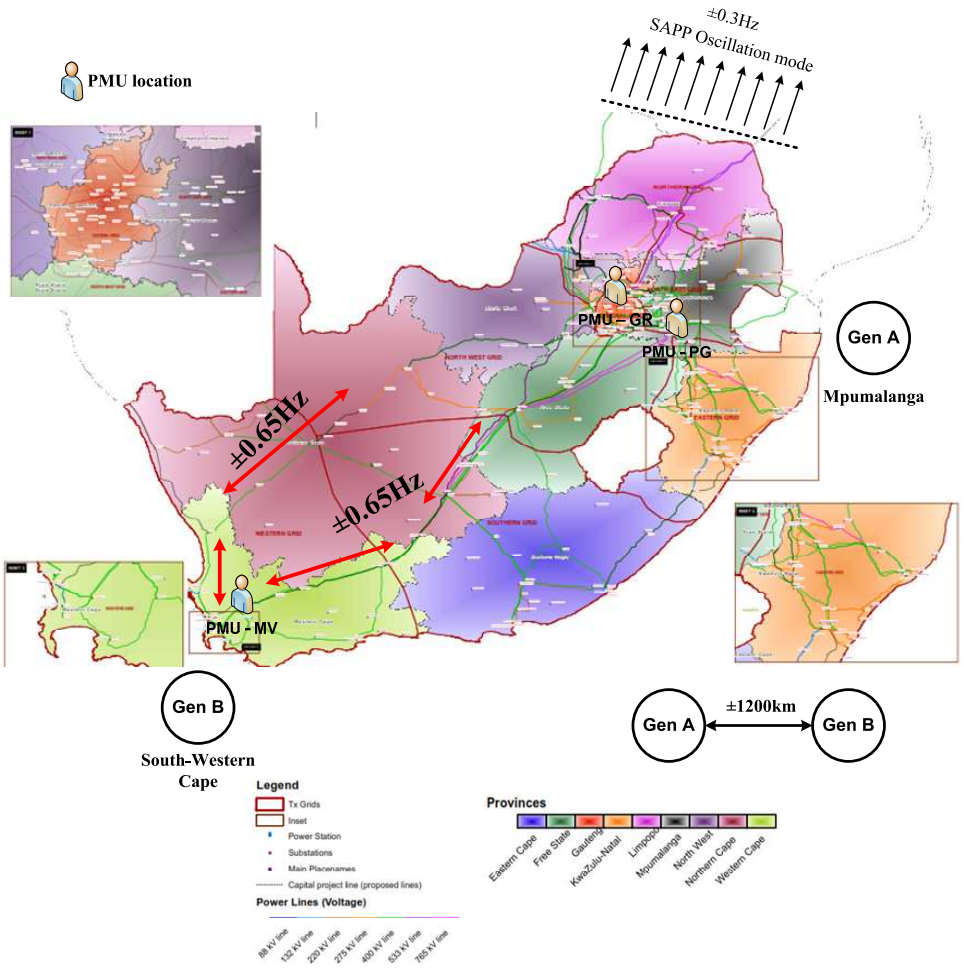

Figure 5.1: Main Eskom transmission network showing corridors between Mpumalanga and the Western Cape.

As can be seen in Figure 5.2, there is a single path labelled AB from the Gauteng region and the point whereby the transmission lines split. The transmission line path labelled as path A comes from the Northern province. The second path labelled B comes directly from the Gauteng region. In each of the identified paths, A and B, there are four main substations whereby the transmission voltage magnitudes, voltage angles, current magnitudes and current angles will be monitored to determine the dominant inter area oscillation path. Each of the various substations are labelled numerically on Figure 5.2.

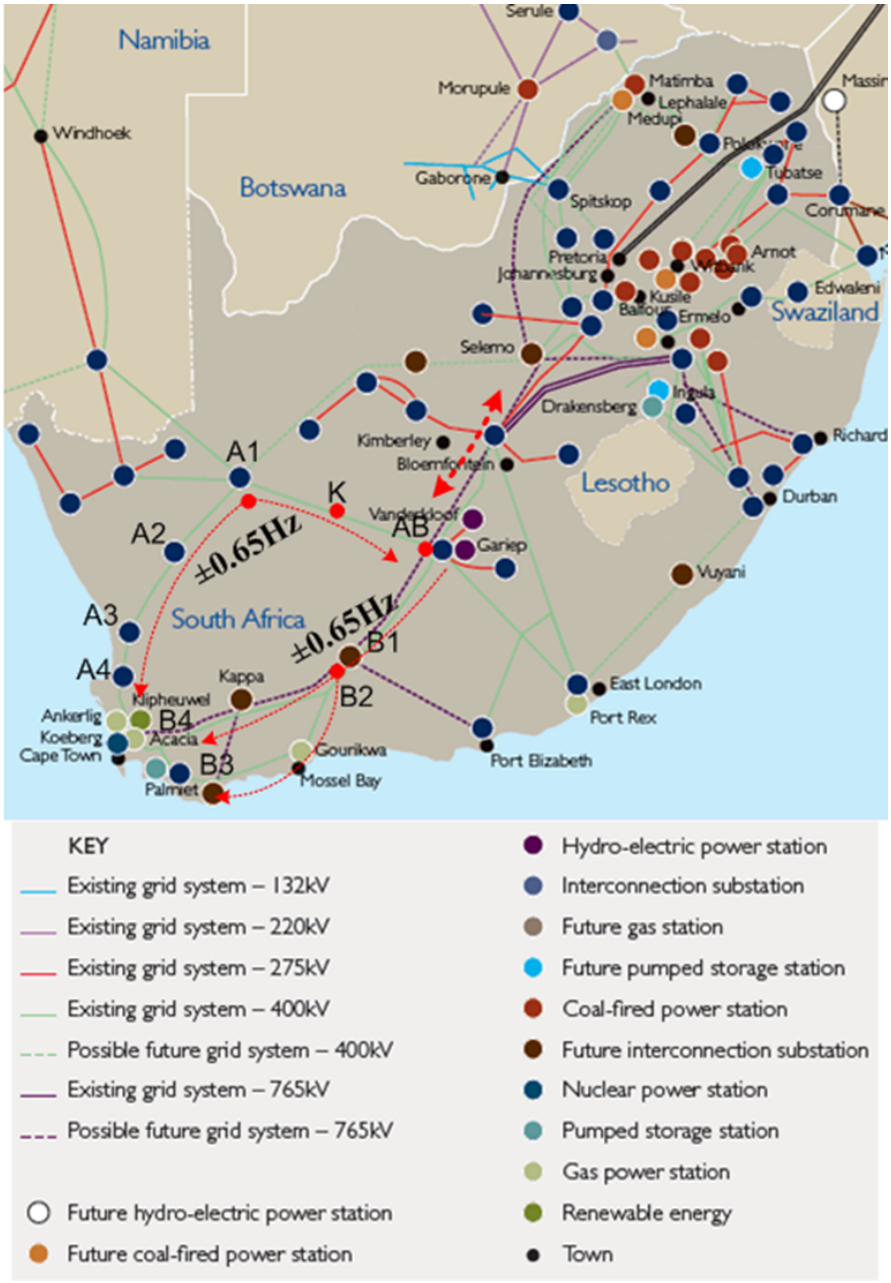

Figure 5.2: Main Eskom transmission network showing existing substation points.

Figure 5.3 shows the network mode shape along corridor A. The voltage magnitude and voltage angle are shown in Figure 5.3 (a) and (b). Analysis of Figure 5.3 (a) and (b), reveals that the busbars which have the highest observability of the mode in corridor A are busbars A1 and A2. From Figure 5.3 (b) busbar AB has the smallest voltage angle implying that this busbar also serves as the center of the path along with busbar A1 and

A2, based on analysis of Figure 5.3 (a).

Similarly Figure 5.3 (c) and (d) show the current magnitude and current angle network mode shape of the corridor A. The transmission lines between AB-K have the highest content of oscillation mode energy on the corridor A. The oscillation mode energy reduces steadily as the lines enter the Western Cape region. This indicates that even though the oscillation mode energy flows in this corridor, it is not a path that carries the highest magnitude of the oscillation mode energy.

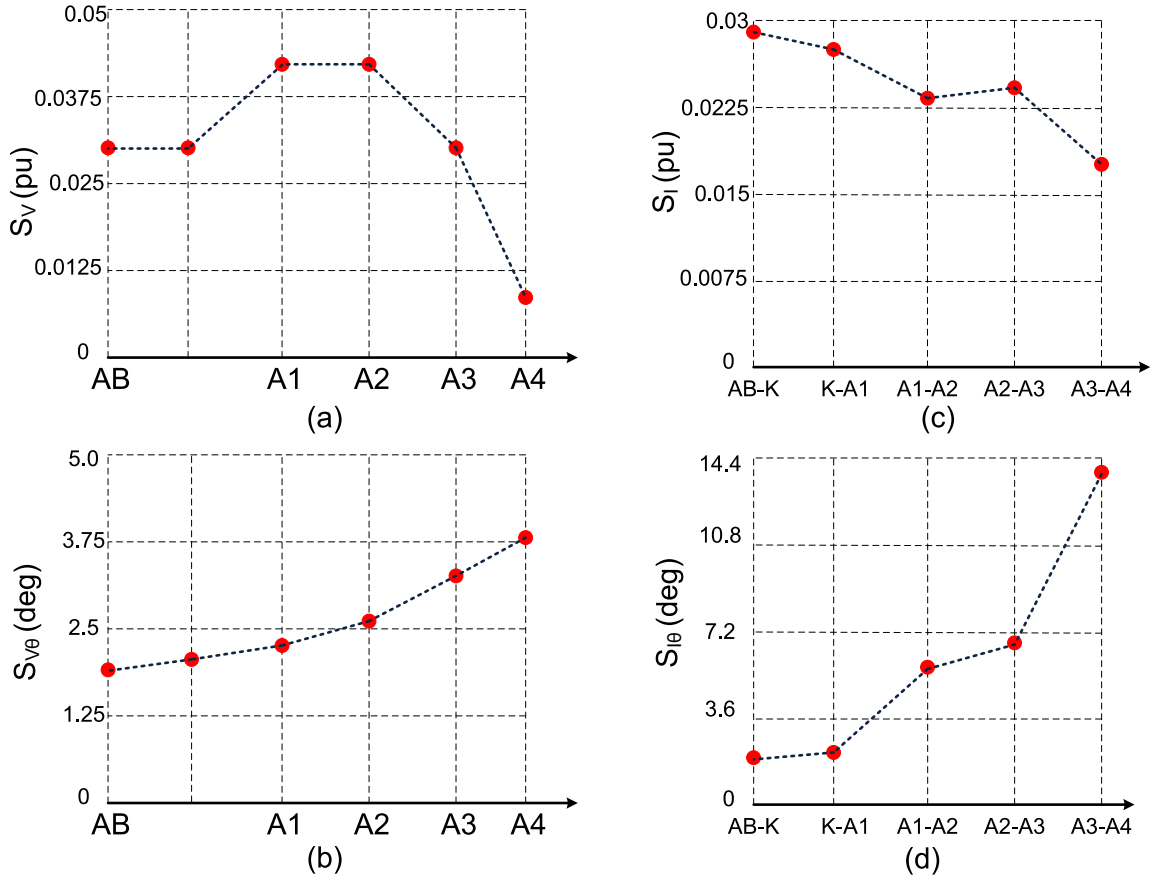

Figure 5.3: Network mode shape along corridor A.

It must be noted that some of the substations in corridor B are not connected to one another; hence some of the nodes in the figures are disconnected from one another. Some substations have two transmission lines connecting them to others and this is highlighted accordingly in the current network mode shape graphs. Figure 5.4 shows the network mode shape along corridor B, the voltage magnitude and voltage angle are shown in Figure 5.4 (a) and (b). Analysis of these figures, shows that the busbars which have the highest observability of the mode in corridor B are busbars B1 and B2. In Figure 5.4

(b) busbar AB has the smallest voltage angle similar to Figure 5.3. This implies that the busbar serves as the center of the path along with busbar B1 and B2 in corridor B. These observations are similar to those of corridor A.

Figure 5.4 (c) and (d) show the current magnitude and current angle network mode shape of the corridor B. The transmission lines between B2-B3b have the highest content of oscillation mode energy on corridor B. The oscillation mode dominant path is between AB-B1 to B1-B2 and B2-B3b, this path consistently contains higher current magnitude compared to those in corridor AB-B1 to B1-B2 and B2-B3a as well as AB-B1 to B2-B3a.

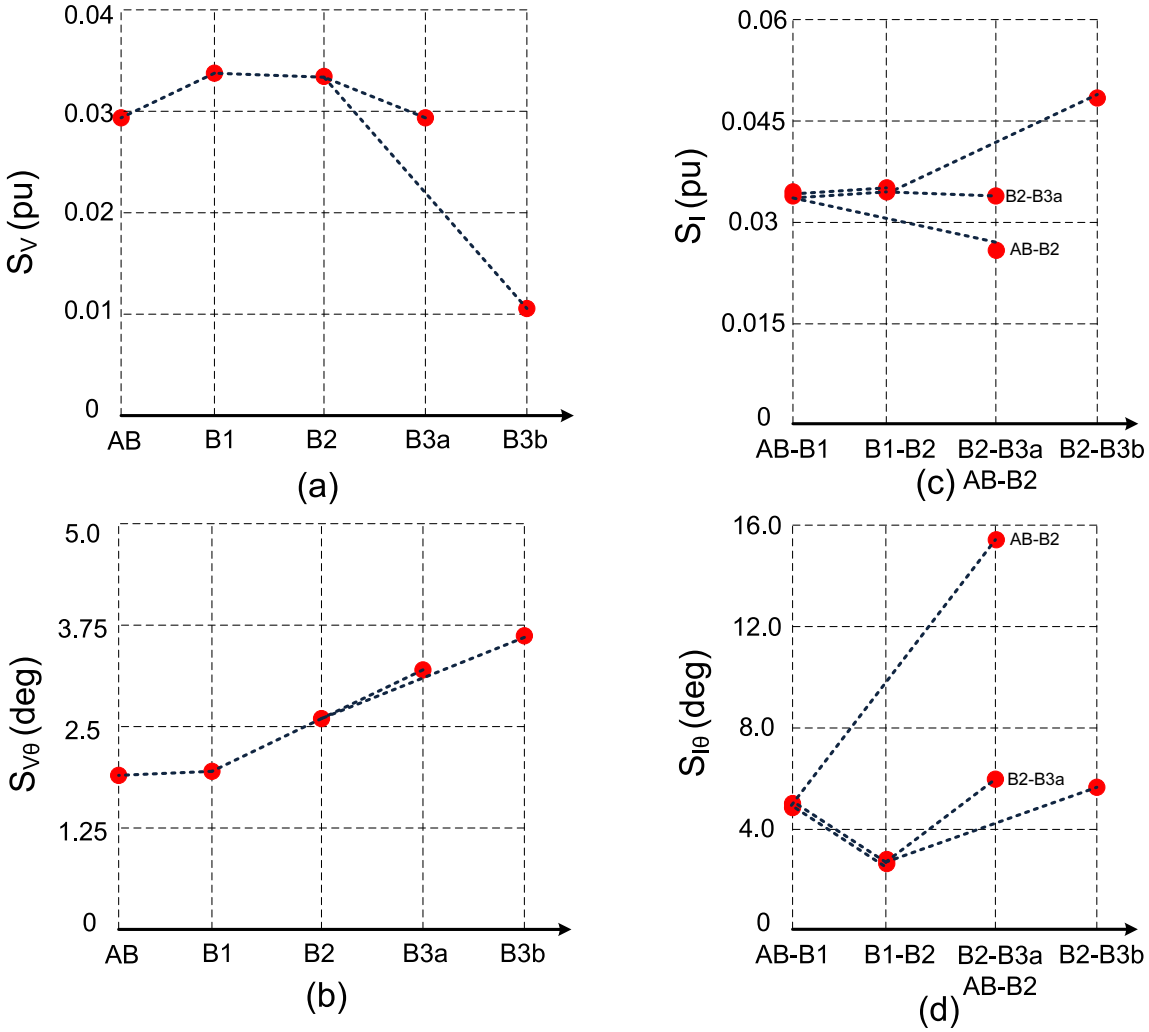

Figure 5.4: Network mode shape along corridor B.

Thus based on analysis of Figure 5.3 and Figure 5.4 the dominant inter-area mode path

rankings according to their respective magnitudes are:

1. AB-B1 to B1-B2 and B2-B3b,
2. AB-B1 to B1-B2 and B2-B3a,
3. AB-B1 to B2-B3a,
4. AB-K to K-A1 to A1-A2 to A2-A3 and A3-A4.

These paths were used in the various contingencies which were analysed. Various fault types were applied along each of these paths and in some cases some of the lines within the respective corridors were taken out of service. This was done in order to place the dominant inter-area paths under stress thus reducing the damping of the inter-area mode of concern and enabling rigorous assessment of the impact of the designed PSSs.

5.4 Impact of various load models on oscillation mode performance

5.4.1 Simplified power system model with a frequency dependent load

In order to assess the performance of the various PSSs designed, two simulation models were used. These are the simplified model with an infinite bus and the detailed Eskom network model. The simplified model which was used to assess the impact of load models shown in Figure 5.5 is marked "load L1". Induction machines were also introduced into the network to assess the impact of dynamic loads on network stability. The load frequency dependence of load L1 was set based on that of the Eskom network, which is known to be approximately $K_{pf} = 4$. The load frequency dependency is based on frequency recovery characteristics after incidents have occurred on the actual Eskom network. Load L1 was set to consume 35% of the generated active power, under all operating conditions, and the induction machines were set to consume a combined total of 22.5% of the generated active power. The induction machine consumption is based on work presented in [45], which shows that at HV transmission level, 22.5% of the load in the WECC can be modelled as a large induction machine. The final parameters of the induction machines used are given in Table 5.1.

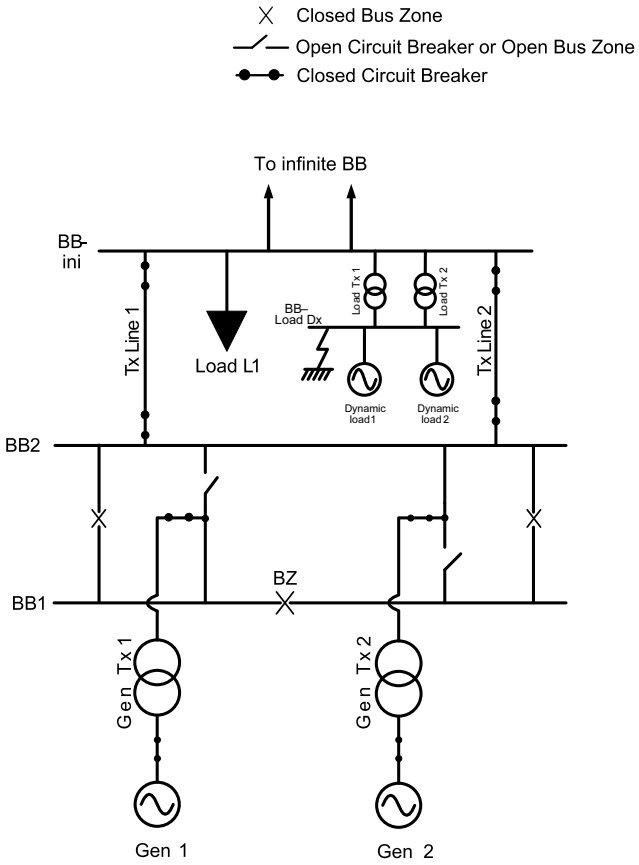

Figure 5.5: Simplified power system with load and infinite bus bar.

Table 5.1: Induction machine (dynamic load 1 and 2) parameters

R_S (pu)	X_M (pu)	X_S (pu)	R_A (pu)	X_R (pu)	H (sec.)	# poles
0.0443	10.2624	0.568	0.0584	0.068	5.25	2

The introduction of a frequency dependent load into the network, load L1, did not affect the performance of the transient or large signal disturbance performance of the network in any noticeable manner as can be seen in Figure 5.6. It can be seen in Figure 5.6 that the residue and participation factor PSSs introduce a high amount of damping which is also confirmed by the eigenvalue results presented in Table 5.2.

Eigenvalues of the simplified power system with various load models were affected slightly. For residue and participation factor designed PSS it was found that the local mode oscillation frequency increased slightly 0.02Hz and the damping increased to between 23% and 28% respectively as can be seen in Table 5.2.

Table 5.2: Local mode eigenvalue assessment using simplified power system model with load and PSS designed.

Compensator tuned frequency (Hz)	Local mode frequency (Hz)	K_{GAIN}	Eigenvalue	Damping ratio (%)	Damping time constant (sec.)
No PSS	Constant impedance load				
	1.0152	-	-0.7404 $\pm j$6.3785	11.52	1.351
	0.8984	-	0.8061$\pm j$5.7025	14.13	1.241
	4% frequency dependent load				
	1.0158	-	-0.7373 $\pm j$6.3822	11.476	1.356
	0.8988	-	0.8108$\pm j$5.6478	14.211	1.233
	4% frequency dependent load + induction motor load				
	1.0163	-	-0.7353$\pm j$6.3853	11.439	1.360
	0.8997	-	-0.8179$\pm j$5.6536	14.318	1.225
Existing PSS					
Existing PSS	Constant impedance load				
	1.0119	2	-0.6926 $\pm j$6.3582	10.829	1.4437
	0.8967	2	-0.7812$\pm j$5.7025	13.733	1.2801
	4% frequency dependent load				
	1.0126	2	-0.6896 $\pm j$6.3623	10.776	1.450
	0.8971	2	-0.7865$\pm j$5.6914	13.821	1.2713
	4% frequency dependent load + induction motor load				
	1.0131	2	-0.6875$\pm j$6.3655	10.7384	1.4544
	0.8979	2	-0.7935$\pm j$5.6421	13.927	1.2601
Residue designed PSS					
1.0 Hz	Constant impedance load				
	1.0168	8.571	-1.9228 $\pm j$6.3886	28.882	0.520
	0.9013	8.571	-1.3699$\pm j$5.6631	23.512	0.729
	4% frequency dependent load				
	1.0166	8.571	-0.6896 $\pm j$6.3623	28.889	0.5187
	0.9028	8.571	-1.3613$\pm j$5.6729	23.353	0.7345
	4% frequency dependent load + induction motor load				
	1.0165	8.571	-1.9287$\pm j$6.3872	28.907	0.5184
	0.9039	8.571	-1.3729$\pm j$5.6769	23.495	0.7284
Participation factor designed PSS					
1.0 Hz	Constant impedance load				
	1.0224	8.58	-1.9074 $\pm j$6.4241	28.463	0.5242
	0.9044	8.58	-1.3544$\pm j$5.6829	23.183	0.7383
	4% frequency dependent load				
	1.0224	8.58	-1.9121 $\pm j$6.4242	28.527	0.5299
	0.9059	-8.58	-1.3457$\pm j$5.6919	23.009	0.7430
	4% frequency dependent load + induction motor load				
	1.0224	8.58	-1.9135$\pm j$6.4236	28.548	0.5226
	0.9070	8.58	-1.3571$\pm j$5.6991	23.165	0.7368

The induction machines were also included into the network in order to assess their impact on the network. It was found that their inclusion resulted in a decrease of the modal frequency and damping of the local modes, indicating that the introduction of induction machines into the network results in poorer performance of the network. This observation is a well known fact in power systems studies and has also been widely reported in the literature, [45] etc. Table 5.2 gives the eigenvalues of the simplified power system, with load L1 initially modelled as a constant impedance load, modelled with $K_{pf} = 4$ frequency dependency, and finally $K_{pf} = 4$ frequency dependency with the dynamic load (induction machines) model.

In order to assess the various operational scenarios, the power plants shown in Figure 5.5 were operated at three levels and this was also used to assess the performance of the various stabilizers designed:

1. Full load (100% generator output),
2. Half load (50% generator output),
3. Low load (25% generator output) operation.

5.4.1.1 Operational assessment of the PSS at various load levels

The generators Gen 1 and Gen 2 were operated at full load feeding into the power system, with both the frequency dependent load and the induction machine load operated at 35% and 22.5% respectively. The large signal disturbance performance of the simplified power system was assessed by applying a single phase to ground fault on the busbar with dynamic loads, labelled "BB-load D", with the fault only lasting for 150ms. The fault durations were deliberately chosen to be large in order to increase their severity and hence their impact on the power system. Figure 5.6 shows the generator active power (a), terminal voltage (b), excitation voltage (c) with the both generators operating at full load.

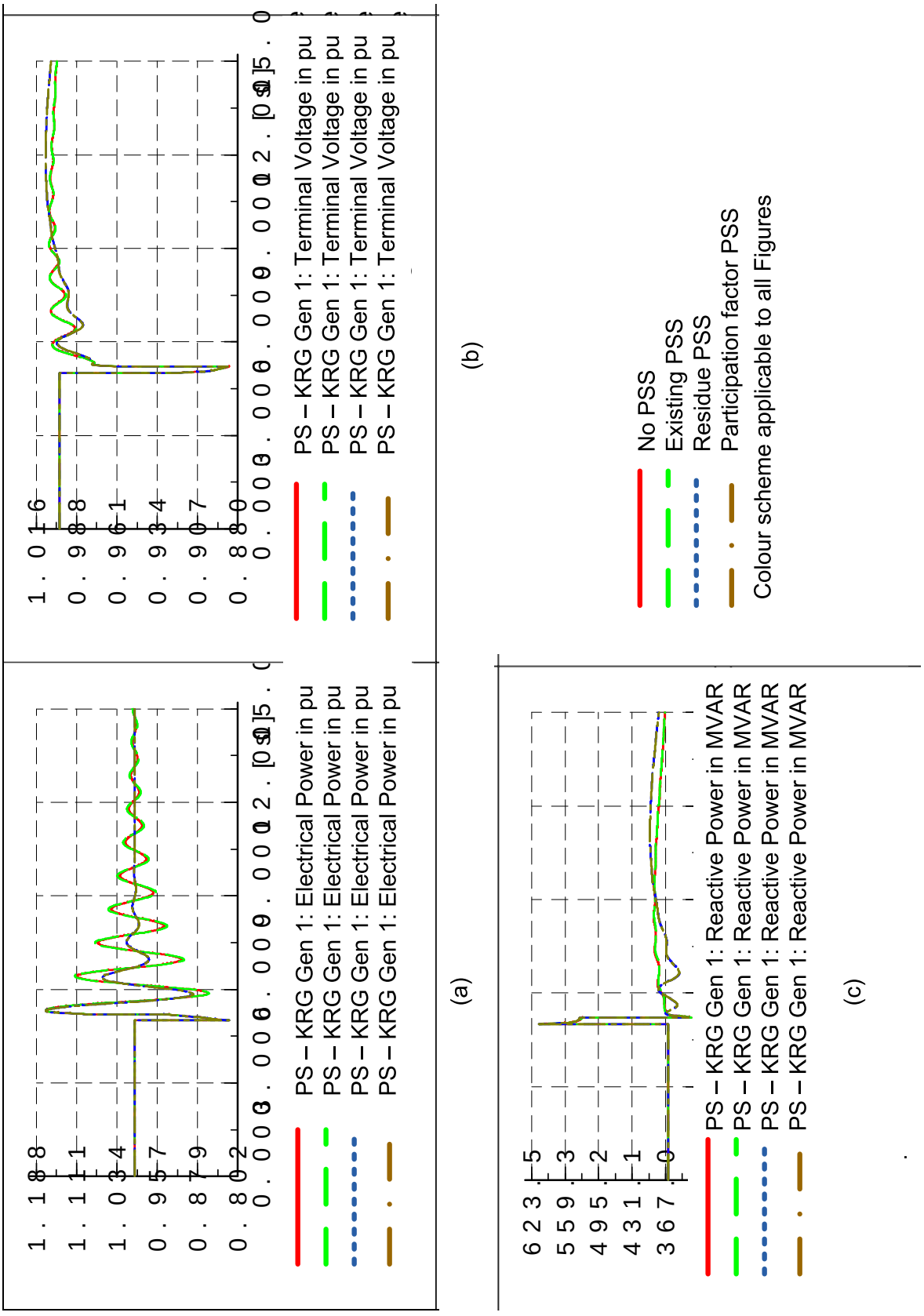

Figure 5.6: Generator operating at full load, (a) electrical power, (b) terminal voltage, (c) excitation voltage.

Assessment of Figure 5.6 (a) and (d) shows that both the residue and the participation factor based stabilizers have a much improved damping response compared with the case were there is no PSS and with that of the existing PSS. The generator terminal voltage response of the residue and the participation factor based stabilizers persist for a slightly longer duration compared to the case where there is no PSS and with the existing PSS. The largest difference between the various terminal voltage responses with the designed stabilizers compared with the existing stabilizer and compared with no stabilizer is 0.015pu.

Similar assessments were performed with the unit operating at half load and at low load. Figure 5.7 and Figure 5.8 similarly also show the generator active power (a), terminal voltage (b), excitation voltage (c).

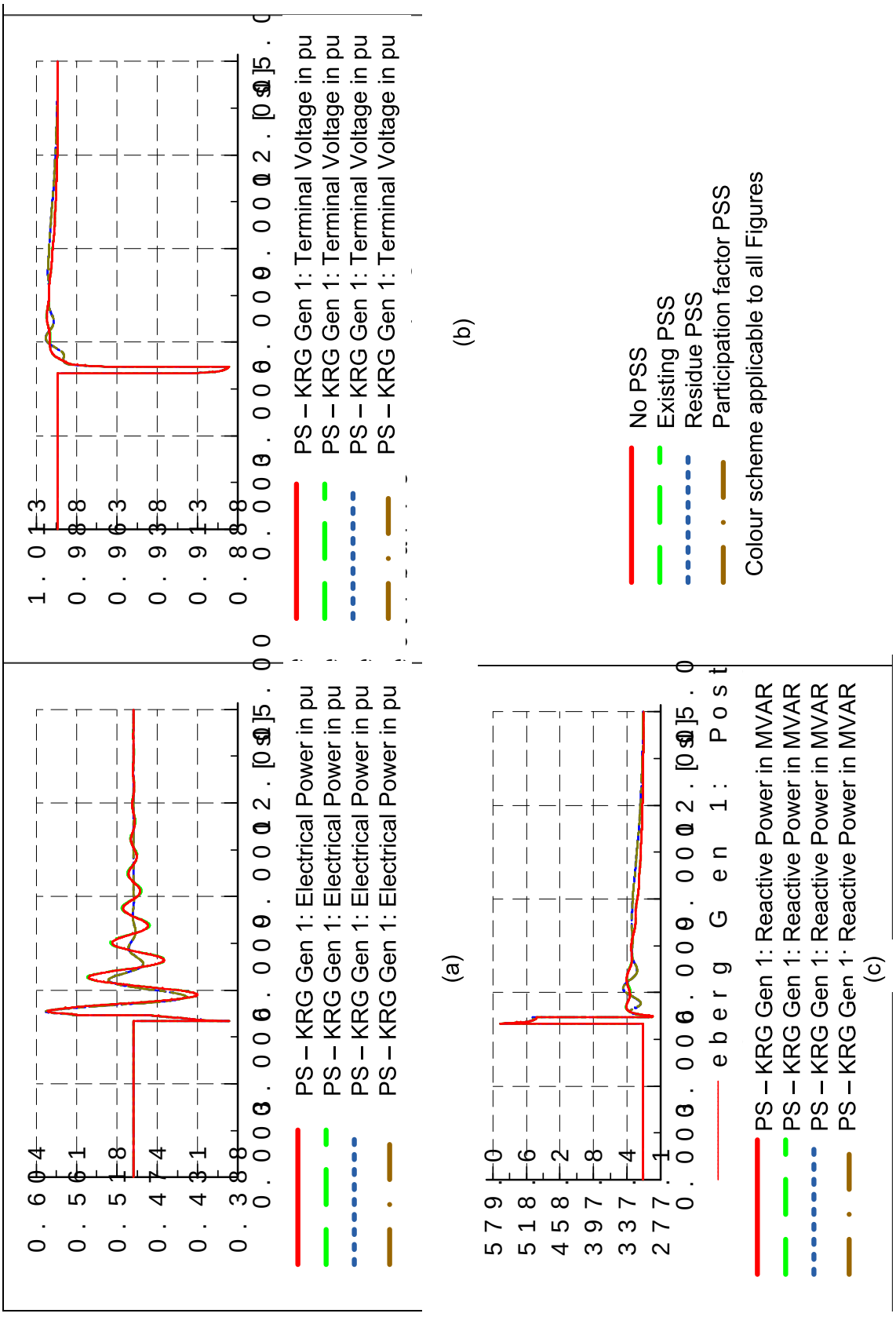

Figure 5.7: Generator operating at half load, (a) active power, (b) terminal voltage, (c) excitation voltage.

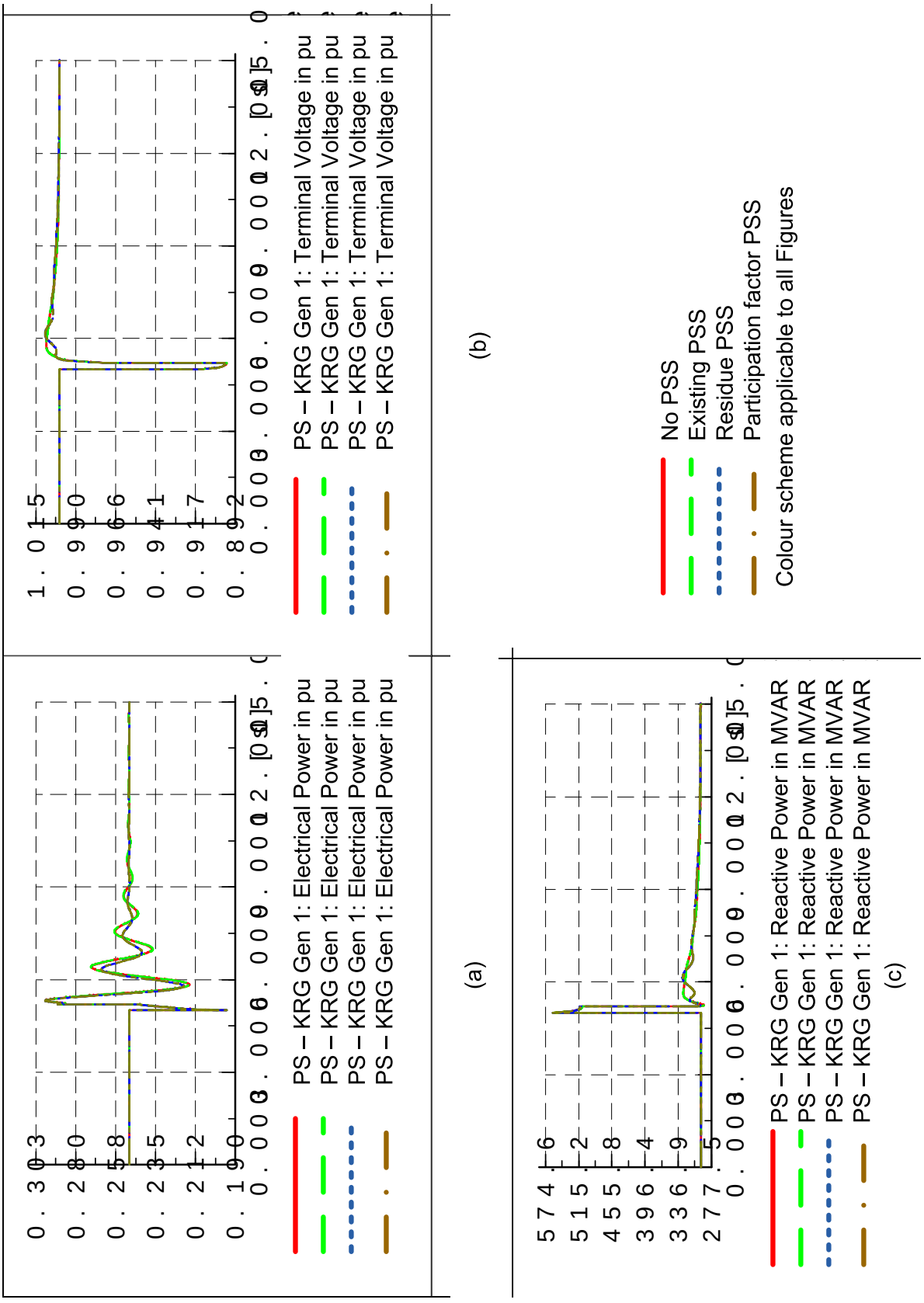

Figure 5.8: Generator operating at low load, (a) active power, (b) terminal voltage, (c) excitation voltage.

Assessment of the active power responses in both figures shows that the residue and participation factor based stabilizers have better performance as compared to the existing stabilizer as shown by the rate of oscillation mode decay in each of the figures. The terminal voltage and output reactive power responses are almost identical to the operational cases without a PSS and with the existing PSS, with the difference in peak values being 0.001pu and 1.026MVAR respectively.

Assessment of all of the three operational cases presented shows that the residue and the participation factor based stabilizer design performance are identical and that either of the methods is able to provide a high amount of damping compared to the existing PSS. This is also verified by analysis of Table 5.2. Assessment of the modal analysis results in Table 5.2 reveals that the residue based stabilizer has a slightly higher amount of damping as compared to the participation factor based design stabilizer.

5.4.2 Detailed Eskom network model with frequency dependent load model

In order to assess the performance of the designed PSSs on the actual detailed Eskom network, participation factor analysis of the 0.65Hz inter-area oscillation mode and the observability of the mode were used to identify all of the loads in the network which participate and have observability of the mode. All loads which were found to have a participation factor and observability higher than 0.001pu of the inter-area mode were set to have a load frequency dependency $K_{pf} = 4$. The impact of the load frequency dependency on the inter-area mode were analysed through modal analysis of the network. Table 5.3 shows the modal analysis results of the detailed Eskom network without the PSS, with the existing PSS, and with the residue and the participation factor based designed PSSs.

Table 5.3: Modal results of the detailed Eskom network load frequency dependency of 4%.

Compensator tuned frequency (Hz)	Mode frequency (Hz)	K_{GAIN}	Eigenvalue	Damping ratio (%)	Damping time constant (sec.)
No PSS	0.6565	-	-0.1490 $\pm j$4.1250	3.6104	6.7101
Existing PSS	0.6603	2	-0.1067 $\pm j$4.1492	2.5723	9.3661
Residue	0.6553	8.571	-0.5195 $\pm j$4.1174	12.5192	1.9247
Participation factor	0.6564	8.58	-0.5137 $\pm j$4.1245	12.3603	1.9463

Analysis of Table 5.3 shows that the residue and the participation factor based design PSSs perform rather similarly and the amount of damping which is added by both

stabilizers is almost identical and the stabilizer performance is identical. The existing stabilizer detracted from the damping of the natural mode. Hence the existing PSS is not able to adequately provide damping of the inter-area mode. The residue and the participation factor based design stabilizers are able to increase the damping of the mode by moving the pole further into the left hand side of the frequency domain even with the load frequency dependency identical to that of the actual Eskom network.

5.5 Analysis of system performance for faults acting on the dominant inter-area paths

In order to assess the performance of the tuned PSSs it is important that dominant inter-area oscillation paths are assessed for faults on the network. The contingency which was considered in all of the analysis performed in this section is the application of a three phase fault (fault duration of 150ms in each case) to a transmission line and the subsequent removal of the transmission line. The contingencies which were assessed are:

1. Loss of a transmission line far away from the dominant path,
2. Loss of a transmission line on the dominant inter-area path - corridor A,
3. Loss of a transmission line on the dominant inter-area path - corridor B.

5.5.1 Loss of line far away from dominant path

A fault was applied to a transmission line connected to a power plant that was arbitrarily selected in the Mpumalanga region, and the transmission line along with a generator at the plant were tripped. The responses of the generators at the PS-KRG power plant were monitored and are shown in Figure 5.9. Figure 5.9 shows the various responses of the generators at PS-KRG without a PSS, the existing PSS, the residue designed PSS and the participation factor designed PSS. The generator response without a PSS fitted is poor and the oscillations are sustained for long time period, the residue and participation factor designed PSS have better performance compared to the other stabilizers. This is based on analysis of the post fault eigenvalues of the network presented in Table 5.4 coupled with analysis of the transient behaviour of the generator in Figure 5.9. The active power decay response of the residue and participation factor designed PSSs has an improved response compared to that of the existing stabilizer.

Comparison of the various terminal voltage responses shown in Figure 5.9 (b) reveals that the existing PSS, residue and participation factor designed PSSs are almost identical in terms of the dynamic behaviour with the residue and participation factor PSSs having a slightly slower time response of approximately 1 to 2 seconds. The transient

disturbance response shown in Figure 5.9 implies that the residue and participation factor designed PSSs offer a higher amount of damping as the active power decay rate is higher than that of the existing PSS, this is also confirmed through modal analysis results presented in the pre-fault analysis Table 5.3 and post fault analysis Table 5.4.

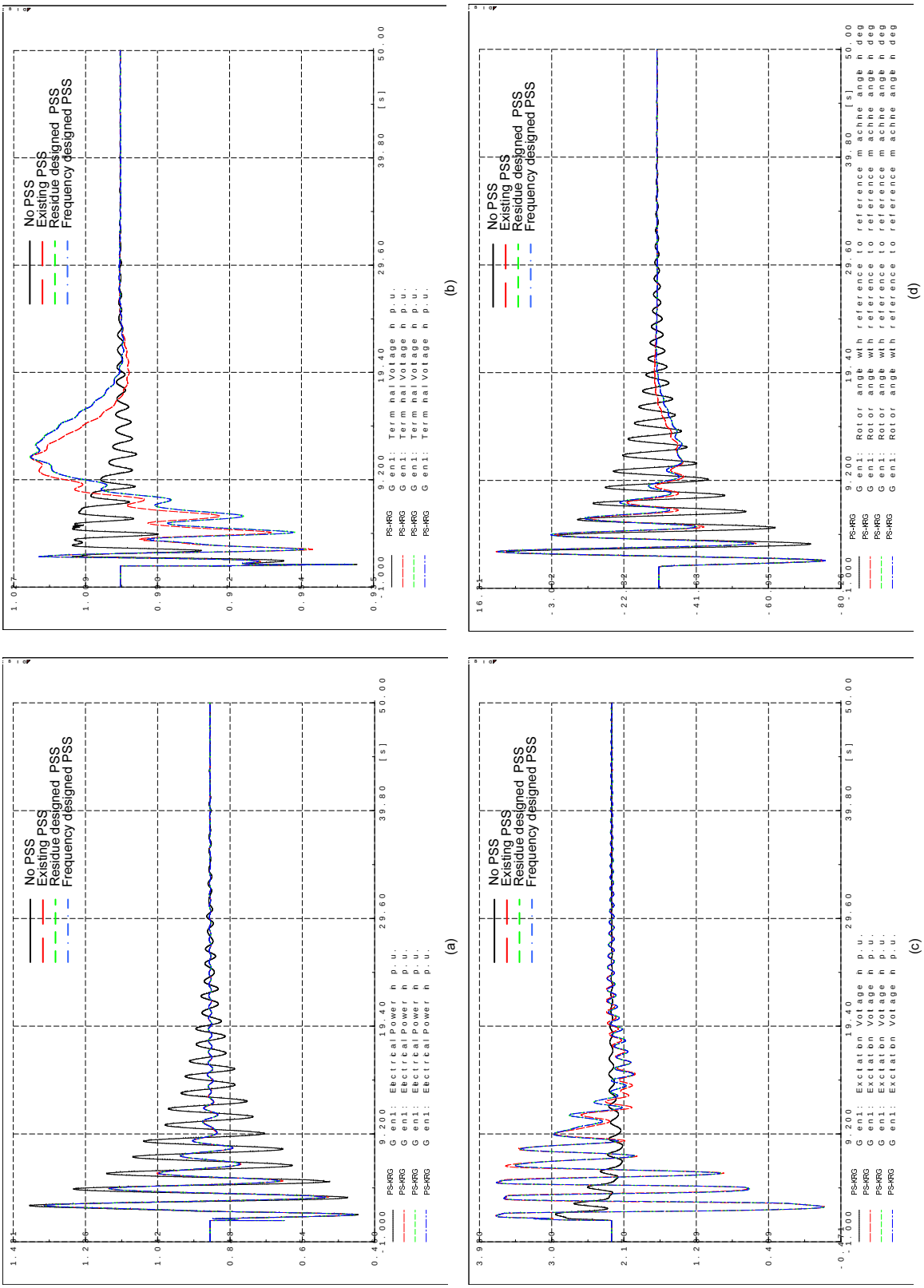

Figure 5.9: Loss of a generator and a transmission line far away from the dominant inter-area path.

Table 5.4 gives the post fault modal analysis with the line and the generator in the Mpumalanga region out of service. As can be seen in Table 5.4 the highest amount of damping of the inter-area mode is offered by the residue designed PSS, which is to be expected based on the large disturbance analysis presented in Figure 5.9. The existing PSS does reduces the natural damping of the mode resulting in a poor damping ratio which would result in oscillations being damped after a longer period of time. Both the residue and the participation factor designed PSSs are able to increase the amount of damping of the mode which results in improved damping performance of the mode for disturbances in the network.

Table 5.4: Post fault modal analysis, for the loss of a line far from dominant inter-area path.

Compensator tuned frequency (Hz)	Mode frequency (Hz)	K_{GAIN}	Eigenvalue	Damping ratio (%)	Damping time constant (sec.)
No PSS	0.65417	-	-0.1485$\pm j$4.1103	3.6119	6.7313
Existing PSS	0.65820	-	-0.1069$\pm j$4.1356	2.5863	9.3462
Residue	0.65144	8.571	-0.5176$\pm j$4.0931	12.5458	1.9319
Participation factor	0.65203	8.58	-0.5149$\pm j$4.1291	12.4694	1.9422

5.5.2 Loss of a line on the dominant inter-area path - Corridor A

In order to assess the generator response for a fault along corridor A, faults were applied along various transmission lines along the corridor. This section presents only the results of the transmission line which was found to have the biggest impact on the network SSS, which was found to be the line AB-K. All other transmission line results for faults along corridor A are presented in Appendix G.1 .

A three phase to ground fault was applied at 50% of the transmission line length for a period of 150ms, the fault was cleared by removing the line from service. The response of the generators at PS-KRG power plant was monitored, and shown in Figure 5.10. The scenario with the poorest response is obtained for the case with the PSS out of service. The existing PSS is able to provide a slightly improved response as compared to the scenario without the PSS. The residue and participation factor designed stabilizer responses were found not to be very much different from the existing PSS response. Hence it was decided to further optimize the residue and participation factor gain values in order to improve the large disturbance response of the oscillation. This was done keeping in mind that the PSS must still offer a high amount of local mode damping and increasing the gain values would decrease the local mode damping performance. Hence, as the PSS gain values were increased, both local mode and inter-area mode

oscillation eigenvalues were assessed to ensure that all the performance criteria presented in Section 4.4 were met. The PSS gain values were incrementally increased and the damping performance of the local and inter-area oscillation modes assessed along with the generator response at each interval.

The gain value which was found to offer a slightly better damped decay response of the generator parameters was $K_{GAIN} = 12.0$, this was for both the residue and participation factor designed PSSs. Figure 5.10 also shows the time domain response for the residue design PSS with increased gain. The PSSs with increased gain values do offer a slightly better response when compared to the other PSS responses, it must be noted that the increased PSS gain does not offer much in terms of improvement of the transient response.

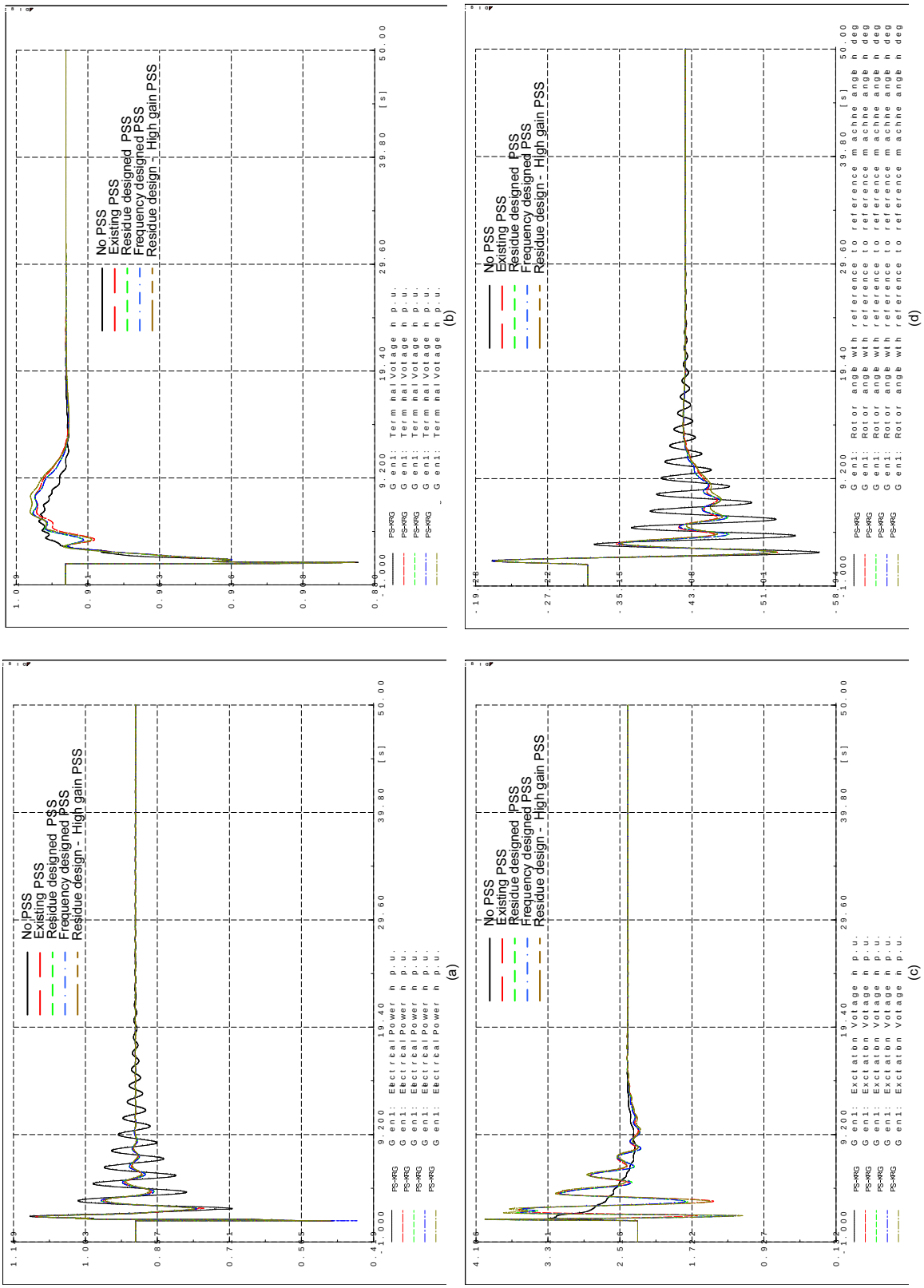

Figure 5.10: Generator response for the loss of a line on the dominant inter-area path - Corridor A.

Modal analysis of the detailed Eskom network was performed prior to the fault being applied to the network in order to determine the impact of increasing the gain on the performance of the inter-area oscillation mode. The results are given in Table 5.5. As expected, increasing the PSS gain resulted in improved performance of the inter-area oscillation mode. It must be noted that the inter-area oscillation mode frequency is reduced by 12.14mHz and 10.52mHz by the residue and participation factor PSSs respectively.

The local mode performance was assessed using a SMIB network, and as expected the PSS having a higher gain resulted in the local oscillation mode having poorer damping performance. The modal analysis results presented in Table 5.5 show both the local and the inter-area oscillation mode parameters prior to the fault being applied along corridor A. The damping performance is maintained well above 15% for the local mode and above 5% for inter-area mode oscillation, which satisfies the minimum PSS criteria set out.

Table 5.5: Pre-fault modal analysis, for the loss of a line along corridor A on the dominant inter-area path.

Compensator tuned frequency (Hz)	Mode frequency (Hz)	K_{GAIN}	Eigenvalue	Damping ratio (%)	Damping time constant (sec.)
SMIB network model					
Residue	1.5025	12.0	-2.9031±j9.4408	29.392	0.3444
	1.3152	12.0	-3.8980±j8.2639	42.661	0.2565
Participation factor	1.4782	12.0	-2.8571±j9.2879	29.402	0.3500
	0.7809	12.0	-2.3361±j4.9069	42.986	0.4280
Detailed Eskom network model					
Residue	0.65186	12.0	-0.6675±j4.0957	16.0870	1.4979
Participation factor	0.65367	12.0	-0.6595±j4.1071	15.8543	1.5163

Table 5.6 gives the modal analysis results of the post fault contingency whereby the transmission line AB-K is placed out of service considering no PSS; the existing PSS; residue designed PSS and the participation factor designed PSS. The residue and participation factor designed PSSs with increased gain were able to achieve a damping ratio approximately 15% as compared to 12% if the gain values are not increased.

The increased PSS gain improved the time domain response of the residue and the participation factor stabilizers in comparison to the existing PSS, it must be noted that increasing the gain values allows for a slightly higher amount of gain and phase to be added at higher frequencies, as well allowing larger terminal voltage and reactive power oscillations at the generator terminals. Hence the time domain response of the

generator parameters must be examined carefully online in conjunction with the torsional behaviour of the generator shaft to ensure that a large gain does not adversely affect the shaft.

Table 5.6: Post fault modal analysis, for the loss of a line along corridor A on the dominant inter-area path.

Compensator tuned frequency (Hz)	Mode frequency (Hz)	K_{GAIN}	Eigenvalue	Damping ratio (%)	Damping time constant (sec.)
No PSS	0.62514	-	-0.1521$\pm j$3.9278	3.8700	6.5736
Existing PSS	0.63087	-	-0.07847$\pm j$3.9638	1.9794	12.7423
Residue	0.61300	12.0	-0.5939$\pm j$3.8516	15.2415	1.6835
Participation factor	0.61462	12.0	-0.5889$\pm j$3.8617	15.0756	1.6980

5.5.3 Loss of a line on the dominant inter-area path - Corridor B

The exact same exercise was conducted along corridor B as was performed for corridor A. The significant difference between corridors A and B is that corridor B is the dominant inter-area path for the inter-area oscillation mode, this was presented in Section 5.3. The transmission line with the highest content of the inter-area oscillation mode along corridor B was found to be B2-B3b and Figure 5.11 shows the generator response for a three phase to ground fault along the same line, the fault was cleared by removing the line from service.

All other transmission line results for faults along corridor B are presented in Appendix G.2. The three phase to ground fault was applied fault was applied at 50% of the transmission line length for a period of 150ms. The response of the generators at PS-KRG power plant was monitored, and is shown in Figure 5.11. Similar to the results obtained for corridor A, the scenario with the poorest response is obtained for the case with the PSS out of service. The existing PSS is was assessed against the residue and participation factor designed PSSs, similar to the cases presented previously the residue and participation factor designed PSSs offered a better oscillation decay rate compared to the existing PSS.

The transient response results presented in Appendix G.2 are consistent with the observations made in Figure 5.11, the decay rate of the residue and participation factor designed PSSs is higher than that of the existing PSS, and this can be seen in Figure G.3 and Figure G.4.

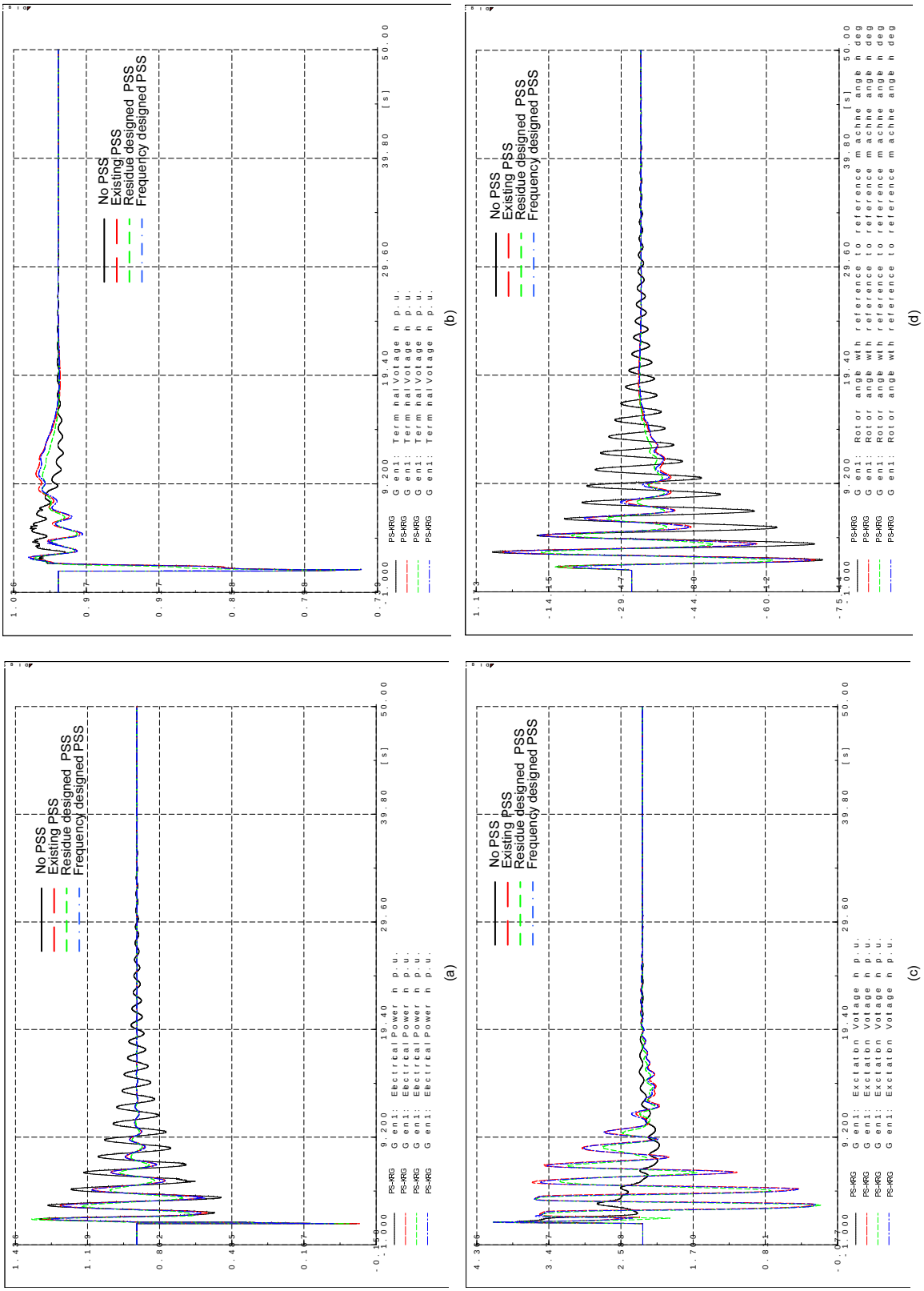

Figure 5.11: Generator response for the loss of a line on the dominant inter-area path - Corridor B.

Table 5.7 gives the post fault modal analysis with transmission line B2-B3b out of service, and as can be seen the residue and participation factor designed PSSs are able to meet the damping performance criteria for the inter-area oscillation mode. The local oscillation mode performance is identical to that given in Table 5.5 because the local mode performance was assessed using the same SMIB model. As previously stated in 5.5.2, the damping performance between PSSs optimized for the highest local mode damping performance and that with the gain increased to offer better time domain performance are not very different from one another. This is due to the fact that the gain was increased by approximately 50% in order to achieve a 3% increase in the inter-area oscillation mode damping performance, with the risk of larger generator terminal voltage, reactive power oscillations and possibly adverse interaction between the unit shaft natural torsional mode and the PSS.

Table 5.7: Post fault modal analysis, for the loss of a line along corridor B on the dominant inter-area path.

Compensator tuned frequency (Hz)	Mode frequency (Hz)	K_{GAIN}	Eigenvalue	Damping ratio (%)	Damping time constant (sec.)
No PSS	0.6203	-	-0.1516±j3.8977	3.887	6.5949
Existing PSS	0.6251	-	-0.1032±j3.9273	2.627	9.6894
Residue	0.6128	12	-0.5954±j3.8504	15.281	1.6795
Participation factor	0.6144	12	-0.5895±j3.8601	15.098	1.6961

5.6 Summary

This chapter presented a detailed analysis of various contingencies which could arise within the SMIB model and the detailed Eskom network model. In order to assess the various contingencies which could arise within the Eskom network, the dominant inter-area mode paths which exist within the Eskom network for the inter-area oscillation mode of concern was assessed using a methodology presented in [10]. The main advantage of using this methodology in the assessment of the SSS of large networks is that it determines the exact network paths which specific inter-area oscillation modes travel and the persistence of these oscillation modes on the various paths identified. With the dominant inter-area paths and the persistence of the oscillation modes along the paths known, it was then possible to identify specific transmission lines to perform contingency analysis. In the analysis of dominant inter-area paths specific contingency cases were identified as having the highest impact on the SSS of the network.

The influence of various load models used was investigated in order to determine their

impact on the oscillation mode damping. The ability of the various PSSs used to improve the oscillation mode damping performance was also investigated. The damping performance of the local oscillation mode was investigated using the SMIB power system. An induction machine was introduced into the network to assess its impact on the damping performance of the oscillation mode and the large signal disturbance performance of the network. Introduction of the induction machine load resulted in the local oscillation mode damping being reduced as expected. The ZIP load models used were modelled to have 20% of the total load being dynamic in nature in order to assess the impact on the oscillation mode damping. Reference [71] showed that the effect of load dynamics on system damping is dependent on the power system configuration and the type of load being considered. Their interaction can either result in the damping increasing or reducing depending on how the oscillation mode and the load interact either in phase with one another resulting in poorer oscillation mode damping or out of phase resulting in increased damping.

The inter-area oscillation mode damping performance was assessed in the detailed Eskom network model with the various ZIP load models being set to have a dynamic component as previously stated. Each of the transmission lines in corridors A and B were tripped to identify which of them within the respective corridors would have the largest impact on the damping performance of the oscillation mode. Once these lines were identified, the PSSs which were designed to improve the damping performance of the inter-area oscillation mode were introduced into the network to assess their impact on the damping performance. It was found that the residue and the participation factor designed PSSs were able to increase the oscillation mode damping performance above the set criteria. The time domain response of the generators at power plant PS-KRG was also monitored for each of the disturbances applied. The time domain response observed was improved by increasing the PSS gain. Increased PSS gain resulted in increased terminal voltage and reactive power oscillations. It was also observed in the Bode plots that the system gain and phase would increase over the frequency range which coincides with the unit's shaft natural mode frequencies which is highly undesirable. The PSS gains which were calculated based on optimal performance of the local mode were found to also offer the best inter-area performance with minimal adverse performance.

Chapter 6

Conclusions and Recommendations for Further Research

6.1 Conclusions and recommendations

This dissertation presented an analysis of the small signal stability of the Eskom network based on measurements. The goal of this was to identify the inter-area oscillation mode between the Western Cape and Mpumalanga networks which is known to have poor damping performance and design a PSS to improve its damping performance. Three design methods were used to optimally design a PSS which ensured that the inter-area and local oscillation modes had a sufficient amount of damping over a wide range of operating conditions.

Chapter 1 of this dissertation provided an introduction to power system stability with an emphasis placed on small signal stability within power systems. The causes of small signal instability in power systems were highlighted along with the various oscillation modes in which small signal instability may be observed in power systems, which essentially can be classified as lack of positive damping within a power system. Small signal instability in power systems can arise as a result of various scenarios and operating conditions. The frequency range in which instability may manifest itself is affected by a host of various factors. Various power system techniques and methods have been introduced and used to add damping into power system networks hence improving the small signal stability of power systems. The use of various techniques and their specific application to improve the damping performance of network oscillation modes was presented. The context and primary focus area of this dissertation is then presented, which came about as a result of small signal instability incidents observed within the Eskom network. Of primary focus and concern was the damping performance of the Western Cape and Mpumalanga inter-area network oscillation mode, which has been found to have poor damping under certain network conditions. A methodology presented in [36] was adapted to the South African network and applied in order to improve the network small signal stability performance.

Chapter 2 of this dissertation presented the basic and fundamental underlying theory applicable to the small signal stability of power systems. The use of modal analysis in the assessment of power system small signal stability was presented and how eigenvalues are used to provide information regarding the oscillation frequency and damping of oscillation modes. The effects of various generators within the network on any particular oscillation mode of interest is revealed by the participation factors; hence this information can be used to provide valuable insight into the influence of various generators within the

network. The theoretical aspect and functioning of PSSs was introduced along with how they are designed to act through the AVR by damping the generator rotor oscillations in a supplementary manner. The use of a single machine infinite bus model to determine the phase lag of the excitation control system was presented and this is the phase lag for which the PSS must compensate to ensure adequate damping within the network.

Power system model validation

Before power system models can be used it is vital that they be validated. The detailed Eskom network model was validated for both steady-state and dynamic model behaviour. The methodology used to validate the network model behaviour was adopted from reference [21].

The steady-state model behaviour was validated using measurements from the Eskom network. The dynamic network model behaviour was validated using network incident measurements. A network snapshot where an unstable oscillation mode occurred was recreated using the detailed Eskom network model in order to compare the unstable eigenvalue of the model with that obtained from network measurements. The unstable mode damping and oscillation frequency were found to be a good match to that measured in the Eskom network using PMUs. Hence the steady-state and dynamic network model behaviour was found to accurately represent the Eskom network model.

The inter-area oscillation mode between the Western Cape and Mpumalanga was confirmed by comparing the network measurements from the PMUs and the eigenvalues from the simulation model. Comparison of the inter-area oscillation mode values obtained from the Eskom network and those of the model were in good agreement. In order to find out which generators influence the inter-area oscillation mode the participation factors and controllability of the mode were calculated.

The generators at PS-KRG in the Western Cape were found to have a degree of participation in the 0.65Hz inter-area oscillation mode, and to also offer the highest degree of controllability of the oscillation mode. Hence the unit ECS was validated by comparing the open loop and closed loop results for tests which were performed and the simulated model response. This was done in order to ensure the model used was a good representation of the actual ECS at PS-KRG. The generator off-line and on-line response test comparison between the actual unit and the model were found to exhibit similar behaviour with slight differences between model and that measured. The differences observed between the model and the actual measurements show that there is behaviour of the actual plant which is not captured by the model. It must be noted that for the purposes of this study the model response obtained was considered sufficient as it the dynamic behaviour captured by the excitation system model is close to that measured on the plant.

Thus the performance of the actual Eskom network and the ECS at power plant PS-KRG were found to be very well modelled in software and this was proved through

dynamic and steady state measurements. This section of the dissertation answered research question one by presenting a detailed account of the network SSS with regards to inter-area oscillation modes of interest and which regions within the network have the highest participation in these oscillation modes.

Power system stabilizer design methods

Residue, participation factor and conventional design methods were used to design the PSS. These design methods were chosen based on a thorough analysis of their practical applicability. This was the central factor used to determine their relevance. These design methods were found to be the most commonly used in industry because of their practicality. For each of the design methods, various equations which govern the amount of phase compensation and gain to be introduced by the PSSs were derived based on the assumption that the PSS used makes use of the generator shaft speed as a stabilizing input, which is true in the case of the PSSs used at PS-KRG, which use a PSS2B.

In order to assess the impact of each of the designed PSSs, eigenvalue assessments were performed to assess the effect that each PSS had on the inter-area oscillation mode damping performance as well as that of the local mode. Each of these was compared with a set of criteria adapted from [30]. The baseline objective was set to ensure that each PSS offers the highest amount of damping for the local oscillation mode and once this baseline had been established the various PSS gain values would then be further optimized to offer a higher amount of inter-area oscillation mode damping. Once this was completed each stabilizer was assessed separately in order to determine the impact of various parameters designed on external factors such as the generator terminal voltage and reactive power fluctuations.

To assess this, actual turbine ramping curves for the units at PS-KRG were used, and it was found that the main factors which contribute to large terminal voltage and reactive power fluctuations were the washout filter time constants, PSS gain and the ramp tracking filter parameters. Hence close attention was given to the selection of all the parameters associated with each of these factors.

Assessment of the generator terminal voltage and reactive power output found that the conventional designed PSS had the highest fluctuations, and this was attributed to the fact that this stabilizer had the largest gain value out of the three designed PSSs. This was further cemented by analyzing the transfer function $\frac{\Delta T_E}{\Delta \omega_G}$. This was done to show that the conventional designed PSS introduced a large amount of gain and phase at frequencies which were above the SSS range. This frequency range was beyond the SSS frequency range and could coincide with the unit's shaft natural frequency range which is highly undesirable in practice as it could result in shaft resonance conditions. Therefore based on these observations the PSSs which were chosen as the most suitable were the residue and participation factor designed stabilizers, and the conventional designed PSS was discarded due to the numerous drawbacks it presented.

This section of the dissertation answered research questions two and three and four, where various techniques were used to design and tune the PSSs at power plant PS-KRG. It was found that residue and participation factor techniques were very able to improve both the eigenvalue damping and the time domain response of the generators of concern. The application of advanced PSS design techniques was found not to be very beneficial as most of these techniques have not been applied in industry and the drawbacks which some of these techniques present would have to be resolved before any of the advanced techniques would be applied.

Small signal stability contingency analysis

Various contingency cases were developed for the detailed Eskom network. These contingency cases involved identifying the exact paths which the inter-area oscillation energy travelled in the network. Two corridors were identified in the Western Cape which served as dominant paths for the inter-area oscillation energy flow.

Three contingency cases were developed to assess the designed PSS performance for a fault far away from the corridors and for faults along various segments of the corridors. The concept of dominant inter-area oscillation paths was presented along with the concept of the persistence of these dominant inter-area paths in power system networks. Each of these was determined for the detailed Eskom network. Since the network between the Western Cape and Mpumalanga is radial in nature the application of these concepts was straight forward. The two main corridors which deliver power to the Western Cape were assessed to determine which of them serve as the dominant path for the inter-area oscillation mode and the persistence inter-area oscillation mode along each of these various paths. One of the corridors was found to serve as the dominant path and interestingly faults along the dominant path resulted in less generator angle deviations even though it carried the highest energy flow to the Western Cape.

Further assessments conducted involved analyzing the effect of various load models on the oscillation mode damping. The load models used were allowed to have a dynamic nature. Each of the load's total consumption was set to be 20% dynamic (this value was taken from [45]). The goal of this exercise was to determine if the designed PSSs were able to improve the oscillation mode damping performance as well as the time domain response of the generators with dynamic load models in the network.

It was found that the residue and participation factor designed PSSs were both able to improve the oscillation mode damping performance. The residue and participation factor design methods were both able to improve the inter-area oscillation and local oscillation modes damping performance to a satisfactory degree with all of the performance criteria being met. The time domain performance of the designed PSSs was also found to be satisfactory for all of the network contingency cases assessed.

From all of the contingency cases analysed in this dissertation it can be seen that the application of the residue and participation factor design methods within the Eskom net-

work was be able to yield improved inter-area oscillation and local oscillation mode damping performance. Hence application of the designed PSSs should minimize the number of unstable mode oscillation incidents associated with the Western Cape - Mpumalanga 0.65Hz oscillation mode.

This section of the dissertation answered research question five. The application of advanced techniques to determine the various dominant inter-area oscillation paths was applied and with the results various network contingency cases were evaluated . This was done to determine the worst case operating scenario and optimize the performance of the designed PSSs.

6.2 Future Work

Although this dissertation presented an extensive study of the SSS performance and improvement of a particular oscillation mode within the Eskom network using PSSs, there are still areas for further research. Some of these areas include the use of the various dominant inter-area oscillation path signals to develop a wide area PSS within the Eskom network. The network mode shape voltage signal would have to be examined and the various smoothing and time delay functions which have to be incorporated must be investigated thoroughly to ensure that whichever signals are used are able to offer the best performance over a wide range of network conditions. The influence and the impact of introducing renewable energy sources into weaker parts of the networks have to be investigated, especially since various authors have shown that under some network conditions it is possible for renewable energy sources to introduce negative damping. Of particular importance must be an investigation into the various types of excitation system performances in various parts of the network in order to be able to fully understand the advantages and disadvantages of using certain excitation types in weaker or stronger parts of the network under certain network conditions.

References

[1] B. Pal and B. Chaudhuri, *Robust Control in Power Systems*. Imperial College London, United States of America: Springer Science+Business Media, 1st ed., 2005.

[2] G. Rogers, *Power System Oscillations*. Boston, London, Dordrecht, NETHERLANDS: Kluwer Academic Publishers Group, 1st ed., 2000.

[3] J. Machowski, J. Bialek, and J. Bumby, *Power System Dynamics: Stability and Control*. John Wiley & Sons Ltd, 2nd ed., 2008.

[4] Y. Song, M. Irving, and X. Wang, *Modern Power Systems Analysis*. New York, United States of America: Springer Science and Business Media, LLC, 1st ed., 2008.

[5] P. Kundur, *Power System Stability and Control*. McGraw-Hill, Inc, 1994.

[6] V. Arcidiacono, E. Ferrari, R. Marconato, J. Ghali, and D. Grandez, "Evaluation and improvement of electromechanical oscillation damping by means of eigenvalue-eigenvector analysis practical results in the central peru power system," *IEEE Transactions on Power Apparatus and Systems*, vol. Volume PAS-99, pp. 769–778, 1980.

[7] F. Demello and C. Concordia, "Concepts of synchronous machine stability as affected by excitation control," *IEEE Transactions on Power Apparatus and Systems*, vol. PAS-88, pp. 316–329, April 1969.

[8] M. Klein, G. Rogers, M. Zywno, and P. Kundur, "Application of power system stabilizers for enhancement of overall system stability," *IEEE Transactions of Power System*, vol. 4, pp. 614–626, May 1989.

[9] N. Kshatriya, *Power System Controller Design by Optimal Eigenstructure Assignment*. PhD thesis, Department of Electrical and Computer Engineering, University of Manitoba, 2010.

[10] L. Vanfretti, *Phasor measuremeas-based state estimation of electric power systems and linearized analysis of power system network oscillation*. PhD thesis, Faculty of Rensselaer Polytechnic Institute, Electric Power Engineering, 2009.

[11] IEEE and Cigre, "Definition and classification of power system stability joint task force on stability terms and definitions," *IEEE Transactions on Power Systems*, vol. Volume 19, Issue: 3, pp. 1387 – 1401, 2003.

[12] G. Rogers, M. Klein, and P. Kundur, "A fundemental study of inter-area oscillations in power systems," *IEEE Transactions on Power Systems*, vol. 6, pp. 914–921, August 1991.

[13] IEEE, "Guide for identification, testing, and evaluation of the dynamic performance of excitation control systems - 421.2 (1990)," 1990.

[14] IEEE, "Recommended practice for excitation system models for power system stability studies - 421.5 (2005)," standard, Institute of Electrical and Electronics Engineers, Inc., 2005.

[15] ABB, "Unitrol 5000 software drawings - 3bhs217423 e8i-e08." ABB excitation control system documents, January 2009. ABB User Drawings.

[16] E. Larsen and D. Swann, "Applying power system stabilizers: Part i,ii, iii," *IEEE Transactions on Power Apparatus and Systems*, vol. PAS-100, pp. 3017–3046, June 1981.

[17] EPRI, "System disutrbance stability studies for western systems coordinating council - tr108256," Tech. Rep. 1018866, Electric Power Research Institute EPRI, Palo Alto, CA: 2009., California„ 1997.

[18] EPRI, *EPRI Power System Dynamics Tutorial without Q/A section.* No. 2009:1018866, Palo Alto, CA: Electric Power Research Institute, 2009.

[19] Psymetrix, "Eskom power system a review of phasor measurement data," 2010.

[20] M. Coker, "Dynamic security assessment : Volume 1 and 2 (1997)," research report, Eskom Technology Group Report - SAPSSI (Eskom Research Innovation Centre), 1997.

[21] D. Kosterev, P. Pourbeik, and E. Allen, "Power system model validation: A white paper by nerc model validation task force of the transmission subcommittee," tech. rep., North American Electricity Reliability Council, New Jersey Princeton„ 2010.

[22] C. Taylor, D. Kosterev, and W. Mittelstadt, "Model validation for the august 10,1996 western system coordinating council system outage," *IEEE Transactions on Power Systems*, vol. 14(3), pp. 967 – 979, 1999.

[23] K. Ogata, *Modern control engineering.* Prentice Hall, 1997.

[24] R. Manicom, "Operating working procedures - moisture separator reheater system." Operating procedures of power plant PS-KRG, 2012.

[25] E. Mobil, "The outlook for energy: A view to 2040," tech. rep., Exxon Mobil, Irving, Texas, 2013.

[26] NERC, "Technical analysis of the august 14, 2003, blackout: What happened, why, and what did we learn," Final NERC Report August 14, 2003, Blackout, National American Electricity Reliability Council, Princeton Forrestal Village, 116-390 Village Boulevard, Princeton, New Jersey 08540-5731, 13 July 2004.

[27] N. Y. I. S. O. NYISO, "Interim report on the august 14, 2003 blackout," technical interim report, New York Independent System Operator, January 2004.

[28] GIMP, "Report of the enquiry committee on grid disturbance in northern region on 30th july 2012 and in northern, eastern & north-eastern region on 31 july 2012," technical report, Government of India Ministry of Power, 16 August 2012 2012.

[29] NERSA, "Inquiry into the national electricity supply shortage and load shedding," Technical Report Report by the Energy Regulator, National Energy Regulator of South Africa, 2008 2008.

[30] Cigre, "Technical brochure no 111: Analysis and control of power system oscillations task force 38.01.07," cigre task force 38.01.07 final technical report, Cigre, December 1996.

[31] C. Rajagopalan, B. Lesieutre, P. Sauer, and M. Pai, "Dynamic aspects of voltage power characteristics in multi-machine power systems," *IEEE Transactions on Power Systems, 7(3)*, vol. 7, pp. 990 – 1000, 1992.

[32] T. van Custem and C. Vournas, *Voltage Stability of Electric Power Systems*. Kluwer Academic Publishers Group, 1 ed., 1998.

[33] P. Anderson, B. Argawal, and J. van Ness, *Subsynchronous Resonance in Power Systems*. IEEE Press, 1990.

[34] M. Coker and K. Lakmeeharan, "Network stability: Research report - volume 2," research report, Eskom Resarch Innovation Center, December 1996.

[35] G. Rogers, "Demystifying power oscillations," *IEEE Computer Applications in Power*, vol. 9, pp. 30 – 35, 1996.

[36] H. Pinto, C. Gama, J. Cavalcanti, R. Leoni, R. Souto, N. Macedo, and M. E. N. Martins, "Oscillation damping analysis and control studies of the future interconnection between the north-north-east and south-east systems," *V Symposium Of Specialists In Electric Operational And Expansion Planning*, vol. SP 08, pp. 1–8, 1996.

[37] M. Ilic and J. Zaborszky, *Dynamics and Control of Large Electric Power Systems*. John Wiley and Sons, Inc, 2000.

[38] F. Hughes and M. Saidy, "Block diagram transfer function model of a generator

including damper windings," *Generation, Transmission and Distribution, IEE Proceedings*, vol. 141, pp. 599–608, November 1994.

[39] A. Lerm, A. Cañizares, and N. Mithulananthan, "Effects of limits in small signal stability analysis of power systems," *IEEE Power Engineering Society Summer Meeting, 2001*, vol. 3, pp. 1–6, 2001.

[40] L. Bu, W. Xu, L. Wang, and F. Howell, "A pss tuning toolbox and its applications," *IEEE Power Engineering Society General Meeting, 2003*, vol. 4, pp. 2090–2095, 2003.

[41] J. Paserba, J. Sanchez-Gasca, P. Kundur, E. Larsen, and C. Concordia, *Electric Power Engineering Handbook: Power System Dynamics and Stability.* CRC Press Taylor & Francis Group, 2007.

[42] D. Lee, R. Beaulieu, and G. Rogers, "Effects of governor characteristics on turbogenerator shaft torsionals," *IEEE Transactions on Power Apparatus and Systems*, vol. PAS-104, pp. 1254–1261, 1985.

[43] G. Bérubé, L. Hajagos, and R. Beaulieu, "Practical utility experience with application of power system stabilizers," *IEEE Power Engineering Society Summer Meeting, IEEE*, vol. 1, pp. 104 – 109, 1999.

[44] G. Bérubé and L. Hajagos, "Accelerating-power based power system stabilizers," *IEEE Tutorial on Power System Stabilizer Performance*, vol. 1, pp. 1–10, 2007.

[45] L. Pereira, D. Kosterev, P. Mackin, D. Davies, J. Undrill, and W. Zhu, "An interim dynamic induction motor model for stability studies in the western system coordinating council," *IEEE Transactions of Power Systems*, vol. 17, 4, pp. 1108–1115, 2002.

[46] IEEE, "Load representation for dynamic performance analysis," *IEEE Transactions on Power Systems*, vol. 8, pp. 472 – 482, 1993.

[47] Y. Mansour, "Application of eigenanalysis to the western north american power system," *Eigenanalysis and Frequency Domain Methods for System Dynamic Performanc*, vol. 90TH0292-3-PWR, pp. 97–104, 1990.

[48] C. Concordia and S. Ihara, "Load representation in power system stability studies," *IEEE Transactions on Power Apparatus and Systems*, vol. PAS 101, no. 4, pp. 969–977, 1982.

[49] W. Heffron and R. Phillips, "Effect of a modern amplidyne voltage regulator on underexcited operation of large turbine generator," *Power Apparatus And Systems, Part III. Transactions Of The American Institute Of Electrical Engineers*, vol. 71, pp. 97–2460, 1952.

[50] EPRI, "Phase ii - frequency domain analysis of low frequency oscillations in large electric power systems: Volume 1 to 5," Techinical Report EL 2348, Electric Power Research Institute, 1982.

[51] I. Hiskens and J. Milanovic, "Load modelling in studies of power system damping," *IEEE Transactions of Power Systems*, vol. 10, pp. 1781 – 1788, 1995.

[52] J. Slootweg, J. Persson, A. van Voorden, G. Paap, and W. Kling, "A study of eigenvalue analysis capabilities of power system dynamics simulation software," *Power System Computation Conference*, vol. 26, pp. 1–8, 2002.

[53] V. Vittal, N. Bhatia, and A. Fouad, "Analysis of the inter-area mode phenomena in power systems following large disturbances," *IEEE Transactions of Power Systems*, vol. PAS-6, pp. 1515 – 1521, 1991.

[54] Y. Tamura and Yorino, "Possibility of auto & hetero parametric resonances in power systems and their relationship with long term dynamics," *IEEE Transactions of Power Systems*, vol. PWRS-2, pp. 890 – 897, 1987.

[55] R. Burns, *Advanced control engineering.* Butterworth-Heinemann, 2001.

[56] M. Abido and Y. Abdel-Magid, "Robust design of electrical power-based stabilizers using tabu search," *IEEE Power Engineering Society Summer Meeting.*, vol. 3, pp. 1573 – 1578, 2001.

[57] H. Kwakernaakt, "Robust control and h-infinity optimization tutorial," *Automatica*, vol. 29, no. 2, pp. 255–273, 1993.

[58] J. Ferraz, N. Martins, and G.Taranto, "Simultaneous partial pole placement for power system oscillation damping control," *IEEE PES Winter Meeting*, vol. 3, pp. 1154 – 1159, 2001.

[59] S. D. R. Lab, "Advanced modal analysis concepts." Electronic class notes, February 1999. University of Cincinnat Structural Dynamics Research Lab course notes.

[60] F. Pagola, I. Pkrez-Arriaga, and G. Verghese, "On sensitvities, residues and participations: applications to oscillatory stability analysis and control," *IEEE Transactions on Power Systems*, vol. Volume 4, pp. 278–285, 1989.

[61] M. Klein, G. Rogers, S. Moorty, and P. Kundur, "Analytical investigation of factors influencing power system stabilizers performance," *IEEE Transactions on Energy Conversion*, vol. Volume 7, pp. 382 – 390, 1992.

[62] N. Martins, N. Z. Jr, J. Soares, G. Taranto, and J. Ferraz, "Adverse increase in generator terminal voltage and reactive power transients caused by power system stabilizers," *IEEE Transactions of Power System*, vol. 2, pp. 747–752, 2002.

[63] W. Jackson and R. Winchester, "Direct- and quadrature-axis equivalent circuits for solid-rotor turbine generators," *IEEE Transactions on Power Apparatus and Systems*, vol. PAS-88, 7, pp. 1121 – 1136, 1969.

[64] J. Sanchez-Gasca, H. Ren, S. Wang, and J. Chow, "Power system damping controller designs using multiple input signals," *IEEE Control Systems*, vol. 20, pp. 82–90, August 2000.

[65] J. Hauer, D. Trudnowski, and J. DeSteese, "A perspective on wams analysis tools for tracking of oscillatory dynamics," *IEEE Power Engineering Society General Meeting, 2007.*, vol. 1, pp. 1–10, 2007.

[66] H. Lee, J. Burns, W. Mittelstadt, K. Martin, and J. Hauer, *Integrated Dynamic Information for the Western Power System: WAMS Analysis in 2005*, ch. 14, pp. 14–1 – 14–52. Boca Raton, FL, USA: Taylor & Francis Group, 2007.

[67] L. Vanfretti and J. Chow, "Analysis of power system oscillations for developing synchrophasor data applications," *Bulk Power System Dynamics and Control (iREP) - VIII (iREP), 2010 iREP Symposium*, vol. VIII, pp. 1–17, August 2010.

[68] Y. Chompoobutrgool and L. Vanfretti, "Identification of power system dominant inter-area oscillation paths," *IEEE Transactions on Power Systems*, vol. 20, pp. 2798–2807, December 2012.

[69] L. Vanfretti and J. Chow, "Computation and analysis of power system voltage oscillations from interarea modes," *IEEE Power & Energy Society General Meeting, 2009.*, vol. 1, pp. 1–8, 2009.

[70] E. Zhou, "Power oscillation flow study of electric power systems," *Electrical Power & Energy Systems, Elsevier Science Ltd*, vol. 17, no. 2, pp. 143–150, 1995.

[71] J. Milanovic and I. Hiskens, "Effect of load dynamics on power system damping," *IEEE transactions on Power Systems*, vol. 10, pp. 1022 – 1028, May 1995.

APPENDICES

Appendix A

Excitation Control System Parameters

The AVR parameters for each of the paths identified in Chapter 2 are:

Table A.1: Unitrol 5000 AVR parameters.

T_R (s)	0.020	TC_1 (s)	2.3
KR (pu/pu)	500.0	K_E (pu/pu)	0.5
KIR (pu/pu)	0.0	T_E (pu)	0.4
K_C	1.0	E_{FD-1} (pu)	2.720
TB_2 (s)	0.160	$S_{E(EFD-1)}$ (pu/pu)	0.172
TC_2	0.40	E_{FD-2} (pu)	3.630
TB_1 (s)	57.5	$S_{E(EFD-2)}$ (pu/pu)	0.780
KIA (pu/pu)	0.0	TUC_1 (s)	3.0
TUB_2 (s)	0.1	TOB_2 (s)	0.092
TUC_2	0.25	TOC_2 (s)	0.230
TUB_1 (s)	75.0	TOB_1 (s)	5.750
TOC_1 (s)	0.230	Up_{MIN} (pu)	-21.250
V_{1-MIN} (pu)	-1.063	V_{MIN} (pu)	-0.043
E_{F-MIN} (pu)	-5.0	V_{2-MIN} (pu)	-1.063
V_{3-MIN} (pu)	-1.063	U_{P-MAX} (pu)	25.0
V_{1-MAX} (pu)	1.250	V_{MAX} (pu)	0.050
E_{F-MAX} (pu)	5.0	V_{2-MAX} (pu)	1.250
V_{3-MAX} (pu)	1.250	T_S (s)	0.004
V_{SC-MAX} (pu)	0	SES	0
K_{VC} (pu/pu)	0	V_{VC-MAX} (pu)	0
K_{SC} (pu/pu)	0	V_{COMP}	0
Shunt	0	KID (pu/pu)	0

A.1 Heffron-Phillips Model Extension [38]

In order to derive the synchronous machine extended model, the field model, quadrature axis damper model and the direct axis damper model are derived in the *s - plane.* All of the models are individually derived as transfer functions. The field model is derived as follows:

A.1.1 Field Winding Model

In order to derive the field winding model transfer function, Eq. (A.1) is transformed to the *s-domain* as given by Eq. (A.2):

$$T_{do}^{'}\dot{E}_{q}^{'} = E_{f}^{'} - E_{q}^{'} + I_{d}\left(X_{d} - X_{d}^{'}\right) \tag{A.1}$$

$$\Delta E_{q}^{'} + T_{do}^{'} s \Delta E_{q}^{'} = \Delta E_{FD} - \left(X_{d} - X_{d}^{'}\right)\Delta I_{d} \tag{A.2}$$

where:

$$\Delta I_{d} = \frac{\left(\Delta E_{q}^{''} - \Delta V_{\infty q}\right)}{\left(X_{d}^{''} - X_{l}\right)} \tag{A.3}$$

If the generator rotor position is taken as the reference, the infinite bus d-axis and q-axis voltages can be written as $V_{\infty q} = V_{\infty}\cos\delta; V_{\infty d} = V_{\infty}\sin\delta$, hence:

$$\Delta V_{\infty q} = -V_{\infty 0}\sin\delta_{0}\Delta\delta = -V_{\infty d0}\Delta\delta \tag{A.4}$$

$$\Delta V_{\infty d} = V_{\infty 0}\cos\delta_{0}\Delta\delta = -V_{\infty q0}\Delta\delta \tag{A.5}$$

Hence Eq. (A.2) can be re-written taking Eq. (A.4) and Eq. (A.5) into account, which yields:

$$\Delta E_{q}^{'} = \frac{1}{\left(1 + T_{d0}^{'}s\right)}\left[\Delta E_{FD} - \frac{\left(X_{d} - X_{d}^{'}\right)}{\left(X_{d}^{''} + X_{l}\right)}\Delta E_{q}^{''} - V_{\infty d0}\frac{\left(X_{d} - X_{d}^{'}\right)}{\left(X_{d}^{''} + X_{l}\right)}\Delta\delta\right] \tag{A.6}$$

Similarly the d-axis damper winding model can be derived. Eq. (A.7) can be transformed

into the s domain for small deviations and is given by Eq. (A.8):

$$T_{do}^{''}\dot{E_q^{''}} = E_q^{'} - E_q^{''} + I_d\left(X_d^{'} - X_d^{''}\right) \tag{A.7}$$

$$\left(1 + sT_{d0}^{''}\right)\Delta E_q^{''} = \frac{\Delta T_{d0}^{''}}{\Delta T_{d0}^{'}}\Delta E_{FD} - \left[\left(X_d^{'} - X_d^{''}\right) + \frac{\Delta T_{d0}^{''}}{\Delta T_{d0}^{'}}\left(X_d - X_d^{'}\right)\right]\Delta I_d + \left[1 - \frac{\Delta T_{d0}^{''}}{\Delta T_{d0}^{'}}\right]\Delta E_q^{'} \tag{A.8}$$

Hence substituting for ΔI_d and $\Delta E_q^{'}$ from Eq. (A.3) to Eq. (A.6) and rearranging one obtains:

$$\Delta E_q^{''} = g_1\left(s\right)\Delta E_{FD} + g_2\left(s\right)\Delta\delta \tag{A.9}$$

-where

$$g_1\left(s\right) = \frac{\left(X_d^{''} + X_l\right)\left(1 + sT_{d0}^{''}\right)}{\left(X_d + X_l\right) + \left[T_{d0}^{'}\left(X_d^{'} + X_l\right) + T_{d0}^{''}\left(X_d^{''} + X_l + X_d - X_d^{'}\right)\right]s + T_{d0}^{'}T_{d0}^{''}\left(X_d^{''} + X_l\right)s^2} \tag{A.10}$$

$$g_2\left(s\right) = \frac{-V_{\infty d0}\left[\left(X_d - X_d^{''}\right) + \left\{T_{d0}^{'}\left(X_d^{'} - X_d^{''}\right) + T_{d0}^{''}\left(X_d - X_d^{'}\right)\right\}s\right]}{\left(X_d + X_l\right) + \left[T_{d0}^{'}\left(X_d^{'} + X_l\right) + T_{d0}^{''}\left(X_d^{''} + X_l + X_d - X_d^{'}\right)\right]s + T_{d0}^{'}T_{d0}^{''}\left(X_d^{''} + X_l\right)s^2} \tag{A.11}$$

Similarly the q-axis damper winding model can also be can be derived from Eq. (A.12) and can be transformed into the s domain for small deviations and is given by Eq. (A.13):

$$T_{qo}^{''}\dot{E_d^{''}} = E_d^{'} - E_d^{''} - I_q\left(X_q^{'} - X_q^{''}\right) \tag{A.12}$$

$$\Delta E_d^{''} + T_{q0}^{''}s\Delta E_d^{''} = \left(X_q - X_q^{''}\right)\Delta I_q \tag{A.13}$$

Making use of Eq. (A.5) leads to

$$\Delta E_d^{''} = \frac{K_{4q}}{1 + bT_{q0}^{''}s}\Delta\delta = g_3\left(s\right)\Delta\delta \tag{A.14}$$

-where b and K_{4q} can be expressed as:

$$b = \frac{X_q'' + X_l}{X_q + X_l} \tag{A.15}$$

$$K_{4q} = V_{\infty q0} \frac{\left(X_q - X_q''\right)}{(X_l + X_q)} \tag{A.16}$$

A.2 Heffron-Phillips Extended Model Validation

The extended Heffron-Phillips model derived in [38] was validated using results which were presented in the paper. The power system used to study the behaviour of the generator model is a SMIB model, and a similar model is shown in Figure A.1. The results presented in [38] were reproduced in order to ensure that the application of the extended Heffron-Phillips was identical to that presented in [38].

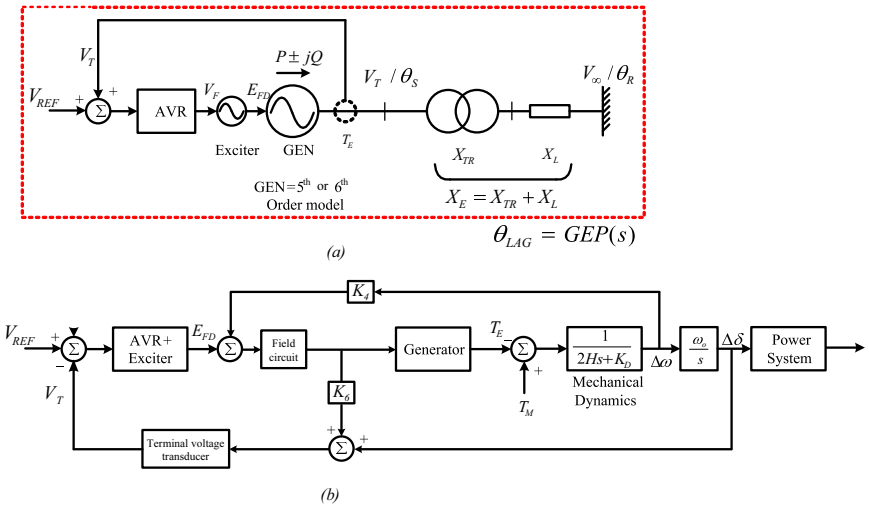

Figure A.1: SMIB model used to validate the extended Heffron-Phillips model.

Appendix B

Dynamic Network Snapshot

B.1 Snapshot of Network Conditions

The network operating conditions, generation, transmission and the various load centers were all taken from the network SCADA system and used in the software simulation model to recreate the network conditions.

Network Conditions prior to the unstable mode being observed (05:24 am)

Table B.1 shows the total generation and system losses within the network prior to the unstable oscillation mode being observed in the network.

Table B.1: Total generation and system losses of the network prior to the unstable mode being observed.

Total Generation	24579.11	MW	1559	MVAr
Total Load	23554.00	MW	4317	MVAr
Total Losses	1025.11	MW	-2758	MVAr

Figure B.1 shows the load profile of the network prior to the unstable oscillation mode being observed in the network.

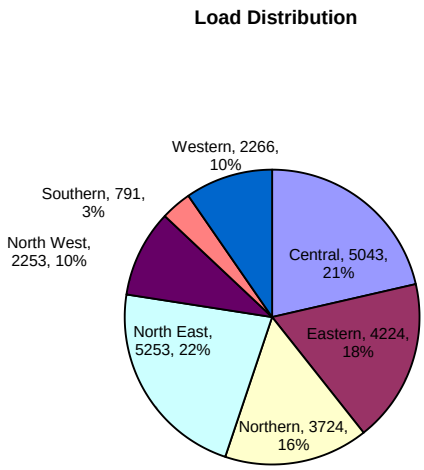

Figure B.1: Network regional load profile prior to the unstable mode being observed.

Network Conditions when the unstable mode existed but before it had been excited being excited (06:30 am)

Table B.2 shows the total generation and system losses within the network when the unstable oscillation mode existed in the network but before it had been excited.

Table B.2: Total generation and system losses of the network when to the unstable mode existed but before it had been excited.

Total Generation	26900.00	MW	911.4	MVAr
Total Load	25274.00	MW	4401	MVAr
Total Losses	1626.00	MW	-3490	MVAr

Figure B.2 shows the load profile of the network when the unstable oscillation mode existed in the network but before it had been excited.

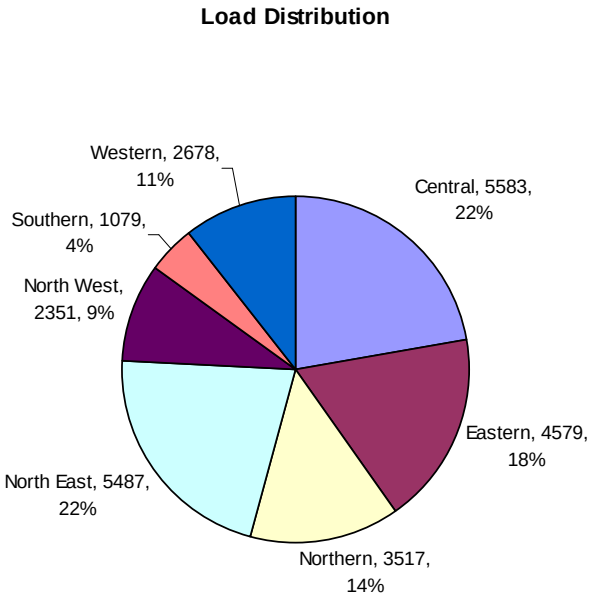

Figure B.2: Network regional load profile prior to the unstable oscillation mode being excited.

B.2 Network events observed during the unstable mode presence

Table B.3: Sequence of network events on 10 January 2011.

Time	Event description
05:24am	PS-MAJ unit 6 400kV breaker open. Unit islanded from 654MW (including aux). Frequency: 50.07 – 49.91Hz
05:24am	At ALP, transmission line ALP-MAJ 400kV breaker tripped on backup earth fault
05:26am	MAJ – TUT 400kV breaker tripped on buszone
	PS-MAJ 400kV section breaker 4 tripped on buszone
	PS-MAJ 400kV section breaker 5 tripped on buszone
	PS-MAJ unit 5 400kV breaker tripped on buszone
	PS-MAJ unit 5 22kV breaker tripped on generator protection.
06:34am	Large Western Cape unit reported power swings of +/- 45MW on the unit. At the same time, other power plants in Mpumalanga reported a reluctance to synchronize units due to power swings being experienced at the station.
06:40	PS-DRA unit 1 tripped from SCO mode after experiencing power swings on the network.
06:40	PS-DRA unit 2 tripped from SCO mode after experiencing power swings on the network.
07:21	PS-MAJ Unit 6 synchronized.
08:11 – 08:23	PS-DRA units 1 – 4 were taken to GEN mode for frequency control and to alleviate power swings
08:24	MAJ – PEG 400kV line taken off transfer and left out of service so that MAJ 400kV busbar could be coupled for the return of other MAJ units
08:47	MAJ 400kV busbar coupled via bus coupler A and bus coupler B. Bus section breakers 4 and 5 remain open.
09:47	MAJ – TUT 400kV breaker closed by National Control after linking PS-TUT to bus bar 2 at PS-MAJ.

Appendix C

Power Plant unit model validation

C.1 Low-load circuit model validation

Figure C.1 shows the ECS response test performed on the unit for step inputs into the AVR with the unit operating at low load. Figure C.1 (a) shows the terminal voltage response and (b) shows the field voltage response. Similar to other tests performed, the simulated terminal voltage response compared well with the measured unit response and the response of the model was considered to sufficiently accurate for the purposes of this study. The field voltage response also compared quiet well, despite the response positive and negative step response peaks and the waveform behaviour when the step is applied.

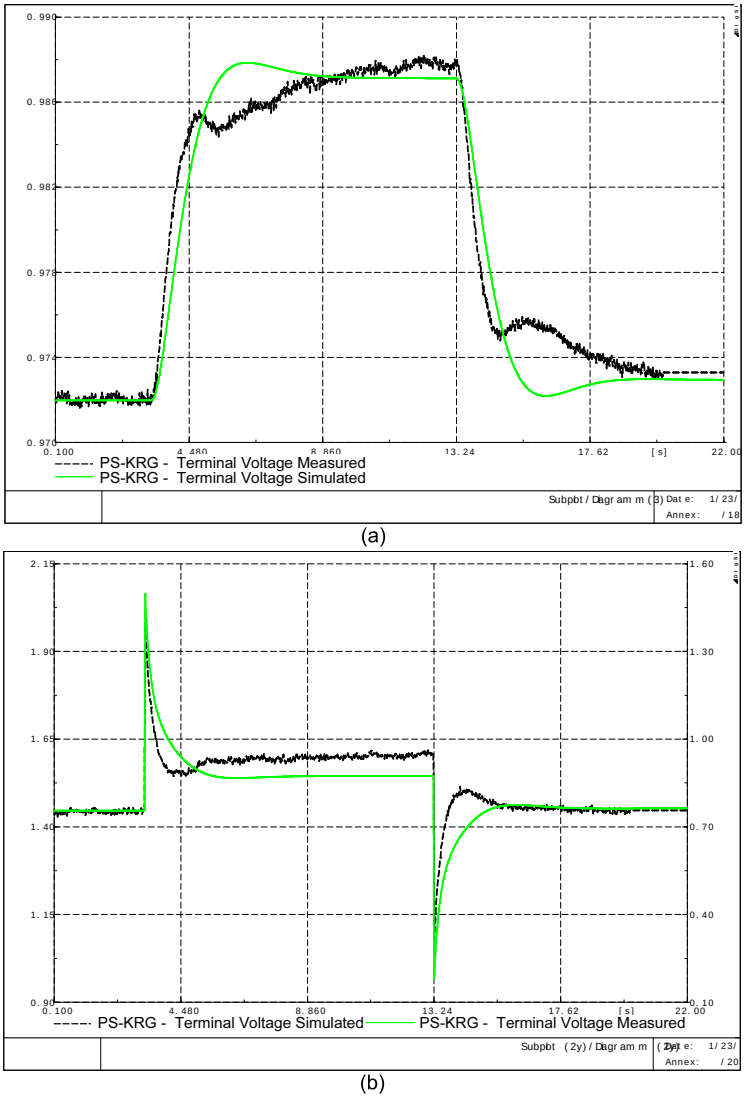

Figure C.1: Low load response to AVR step input changes. (a) Unit terminal voltage response, (b) Unit field voltage response.

C.2 Full-load model validation

Figure C.2 shows the ECS response measured for step inputs into the AVR with the unit operating at full load. Similar to other tests performed, the simulated terminal voltage response compared well with the measured unit response and the response of the model was considered to sufficiently accurate for the purposes of this study. The field voltage response also compared quiet well, despite the response positive and negative

step response peaks and the waveform behaviour when the step is applied.

The terminal voltage response was observed to be slightly sluggish and this was attributed to the fact that the simulation model used to verify the unit response was an SMIB model and hence the actual grid conditions were not adequately captured to mimic the terminal voltage response.

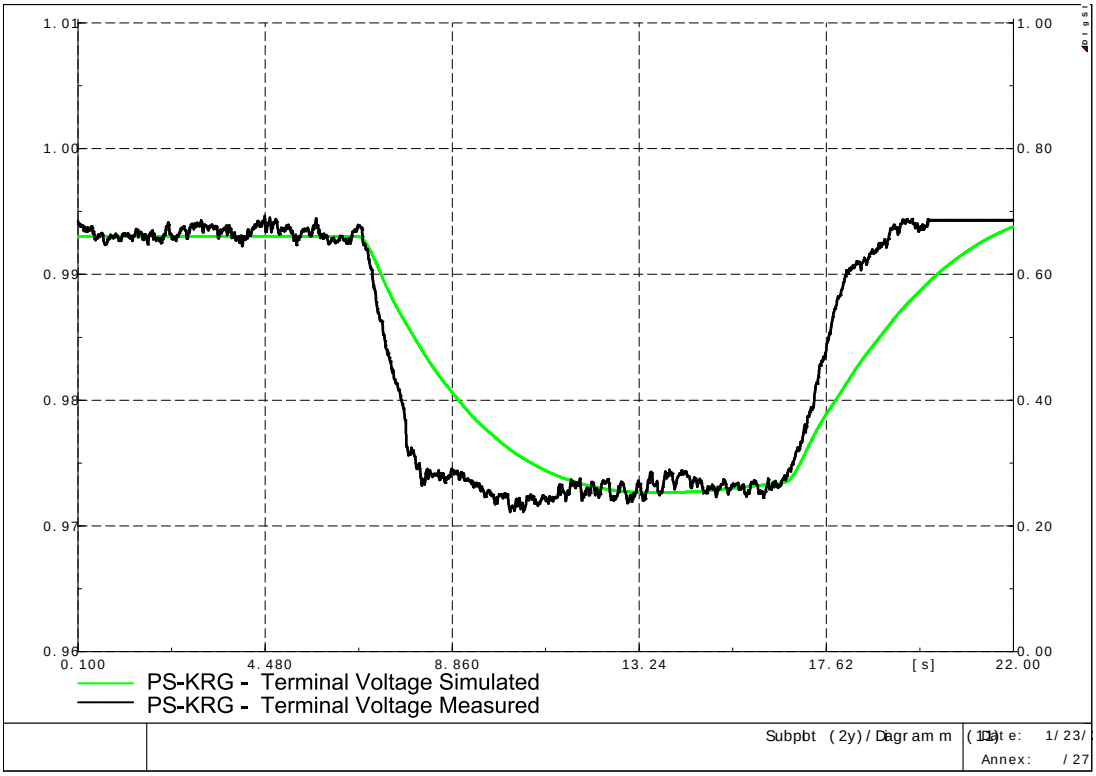

Figure C.2: Terminal voltage response to AVR step input changes with unit at full load.

Appendix D

Power System Stabilizer Design Calculations

The design of the PSSs was presented in section 4.3, where the various equations which were used for each of the particular design methods were presented. This section outlines the application of the various design equations derived for the various oscillation mode frequencies.

D.1 Residue based stabilizer design

The extended Heffron-Phillips model was implemented in MATLAB and used in order to determine the phase lag between the various input and output paths for the design of the compensator. Eq. (D.1) was used to determine the phase lead to be introduced by the stabilizer. The gain of the stabilizer was calculated using Eq. (D.2).

$$\angle G_P(\lambda_j) = \pi - \angle R_j - \angle G_W(\lambda_j) \tag{D.1}$$

$$K_{GAIN} = \frac{|\Delta\lambda_i|}{|R_i|\,|G_W(\lambda_j)|\,|G_P(\lambda_j)|} \tag{D.2}$$

The PSS gain was used as a preliminary value and further optimized based on the eigenvalue analysis of local, inter-area, and intra-plant oscillation modes. The PSS gain was optimized based on findings presented by [16] which show that the most optimal stabilizer gain which satisfies both inter-area and and local mode damping requirements is generally equal to one third of the instability gain. The instability gain is defined as the value of gain at which any of the modes associated with the generator becomes unstable.

Table D.1 shows the residue and washout filter phase values which were calculated using the extended Heffron-Phillips model at each of the corner frequencies used to design the various stabilizer parameters. Only one calculation example will be used to illustrate

the application of the various equations associated with the controller design, and the results of the other modes will be presented in a table format.

Table D.1: Phase parameters obtained using the extended Heffron-Phillips model.

Frequency	$G_W(\lambda_j)$	$R(\lambda_j)$
Hz	degrees	degrees
0.65	9.83	43.1
1.0	6.4	52.0
3.0	2.14	75

$$\angle G_P(0.65Hz) = 180^o - 9.83 - 43.1^o = 127.07^o$$

-the amount of phase compensation which must be provided by the stabilizer is 127.07^o.

As previously stated, a single lead/lag block can provide a maximum of 65^o and since PSS2B has three lead/lag blocks. The phase will be equally divided between the blocks.

$$\begin{aligned} \angle\theta_{BLK} &= \frac{127.07^o}{3} = 42.3567^o \\ \alpha &= \frac{1 - sin\theta_{BLK}}{1 + sin\theta_{BLK}} \\ &= \frac{1 - sin(42.3567)}{1 + sin(42.3567)} = 0.19493 \end{aligned}$$

Using phase lead design theory for lead compensation presented by [55], the phase lead compensator time constants are designed as follows:

$$\begin{aligned} T_2 &= \frac{1}{2\pi f_c\sqrt{\alpha}} \\ &= \frac{1}{2\pi(0.65Hz)\sqrt{0.19493}} = 0.55458sec \\ T_1 &= \alpha T_2 \\ &= (0.19493)(0.55458sec) \\ &= 0.10810sec \end{aligned}$$

-where T_1 is the lag time constant, and T_2 is the lead time constant. For the lead/lag

compensator blocks it must be noted that $T_1 = T_3 = T_{11}$, which are the lag time constants and $T_2 = T_4 = T_{10}$ which are the lead time constants. Table D.2 shows the various lead/lag time constants which were designed for each of the controllers at the various mode frequencies. The stabilizer gains were optimized to give the highest amount of damping for the local mode. The optimal stabilizer gain was found to be $K_{GAIN} = 2.46$. The stabilizer gain must still be optimized for the inter-area mode.

Table D.2: Residue based design lead/lag block time constants.

Frequency	$\angle G_P$	α	$T_1 = T_3 = T_{11}$	$T_2 = T_4 = T_{10}$	K_{GAIN}
Hz	degrees	-	seconds	seconds	-
1.0	121.60	0.2122	0.07337	0.3455	8.571
3.0	102.86	0.27932	0.02804	0.10038	75

D.2 Participation factor based stabilizer design

The extended Heffron-Phillips model implemented in MATLAB was also used in order to determine the phase lag between the various input and output paths for the design of the compensator. Table D.4 was used to determine the phase lead to be introduced by the stabilizer. The gain was of the stabilizer was calculated using Eq. (D.4). The PSS gain was used as a preliminary value and further optimized based on the eigenvalue analysis of local, inter-area, and intra-plant oscillation modes. The PSS gain was optimized based on findings presented by [16] which show that the optimal stabilizer gain which satisfies both inter-area and local mode damping requirements is generally equal to one third of the instability gain. The instability gain is defined as the value of gain at which any of the modes associated with the generator becomes unstable.

$$\angle G_P(\lambda_j) = -\left[\angle p_{ij} + \angle G_W(\lambda_j) + \angle G_{EXC}(\lambda_j) + \angle G_{GEN}(\lambda_j)\right] \quad \text{(D.3)}$$

$$K_{GAIN} = \frac{2H\,|\Delta\lambda_i|}{|p_{ij}|\,|G_W(\lambda_j)|\,|G_{PSS}(\lambda_j)|\,|G_{EXC}(\lambda_j)|\,|G_{GEN}(\lambda_j)|} \quad \text{(D.4)}$$

Table D.3 shows the ECS phase lag, participation factor phase angle and washout filter phase angle. The extended Heffron-Phillips model was used to obtain $\angle G_W$ and $\angle G_{ECS}$ at the corner frequencies of interest. The participation factor phase angle was obtained from the detailed Eskom network. Only one calculation example will be used to illustrate the application of the various equations associated with the controller design and the results of the other modes will be presented in a table format.

Table D.3: Phase parameters obtained using the extended Heffron-Phillips model.

Frequency	$G_W(\lambda_i)$	$\angle p_{jj}$	$\angle G_{ECS}$
Hz	degrees	degrees	degrees
0.65	9.83	91.925	133.0
1.0	6.4	91.0	142.0
3.0	2.14	91.02	165.0

$$\angle G_P(0.65Hz) = -[91.925 + 9.83 - 133.0] = -234.75^o = +125.245^o$$

- the amount of phase compensation which must be provided by the stabilizer is 125.245^o.

As previously stated, a single lead/lag block can provide a maximum of 65^o and since PSS2B has three lead/lag blocks, the phase will be equally divided between the blocks.

$$\begin{aligned} \angle\theta_{BLK} &= \frac{125.245}{3} = 41.7483^o \\ \alpha &= \frac{1 - sin\theta_{BLK}}{1 + sin\theta_{BLK}} \\ &= \frac{1 - sin(41.7483)}{1 + sin(41.7483)} = 0.2006 \end{aligned}$$

Using phase lead design theory for lead compensation presented by [55], the phase lead compensator time constants are designed as follows:

$$\begin{aligned} T_2 &= \frac{1}{2\pi f_c \sqrt{\alpha}} \\ &= \frac{1}{2\pi(0.65Hz)\sqrt{0.19493}} = 0.5467sec \\ T_1 &= \alpha T_2 \\ &= (0.2006)(0.5467sec) \\ &= 0.10967sec \end{aligned}$$

Table D.4 shows the various lead/lag time constants which were designed for each of the controllers at the various mode frequencies. The stabilizer gains were optimized to give the highest amount of damping for the local mode. The most optimal stabilizer gain was found to be $K_{GAIN} = 2.60$. The stabilizer gain must still be optimized for the inter-area

mode.

Table D.4: Participation factor based design lead/lag block time constants.

Frequency	$\angle G_P$	α	$T_1 = T_3 = T_{11}$	$T_2 = T_4 = T_{10}$	K_{GAIN}
Hz	degrees	-	seconds	seconds	-
1.0	120.6	0.2155	0.073873	0.3428	8.58
3.0	101.86	0.28327	0.050351	0.18728	45.55

D.3 Conventional stabilizer design

The extended Heffron-Phillips model implemented in MATLAB was also used in order to determine the phase lag between the various input and output paths for the design of the compensator. Table D.6 was used to determine the phase lead to be introduced by the stabilizer. The gain of the stabilizer was calculated using Eq. (D.6). The PSS gain was a preliminary value and was further optimized based on the eigenvalue analysis of local, inter-area, and intra-plant oscillation modes. The PSS gain was optimized based on findings presented in [16] which show that the most optimal stabilizer gain which satisfies both inter-area and and local mode damping requirements is generally equal to one third of the instability gain. The instability gain is defined as the value of gain at which any of the modes associated with the generator becomes unstable.

$$\angle G_P(\lambda_i) = [0 + 0 + \angle G_{EXC}(\lambda_i) + \angle G_{GEN}(\lambda_i)] \tag{D.5}$$

$$K_{GAIN} \approx \frac{2H|\Delta\lambda_i|}{|G_{PSS}(\lambda_i)||G_{EXC}(\lambda_i)||G_{GEN}(\lambda_i)|} \tag{D.6}$$

Table D.5 shows the phase lag values of the ECS at the frequencies of interest. Only one calculation example will be used to illustrate the application of the various equations associated with the controller design and the results of the other modes will be presented in a table format.

Table D.5: Phase parameters obtained using the extended Heffron-Phillips model.

Frequency	$\angle G_{ECS}(\lambda_i)$
Hz	degrees
0.65	133.0
1.0	142.0
3.0	165.0

$$\angle G_P\,(0.65Hz) = [133.0] = +133.0^o$$

- the amount of phase compensation which must be provided by the stabilizer is 133.0^o

As previously stated, a single lead/lag block can provide a maximum of $65^o$and since PSS2B has three lead/lag blocks, the phase will be equally divided between the blocks.

$$\begin{aligned}
\angle\theta_{BLK} &= \frac{133.0}{3} = 44.333^o \\
\alpha &= \frac{1 - sin\theta_{BLK}}{1 + sin\theta_{BLK}} \\
&= \frac{1 - sin\,(44.333)}{1 + sin\,(44.333)} = 0.1773
\end{aligned}$$

Using phase lead design theory for lead compensation presented by [55], the phase lead compensator time constants are designed as follows:

$$\begin{aligned}
T_2 &= \frac{1}{2\pi f_c\sqrt{\alpha}} \\
&= \frac{1}{2\pi\,(0.65Hz)\,\sqrt{0.1773}} = 0.58150sec \\
T_1 &= \alpha T_2 \\
&= (0.1773)\,(0.58150sec) \\
&= 0.1031sec
\end{aligned}$$

Table D.6 shows the various lead/lag time constants which were designed for each of the controllers at the various mode frequencies. The stabilizer gains were optimized to give the highest amount of damping for the local mode. The optimal stabilizer gain was found to be $K_{GAIN} = 2.03$. The stabilizer gain must still be optimized for the inter-area mode.

Table D.6: Conventional based design lead/lag block time constants.

Frequency	$\angle G_P = \angle G_{ECS}$	α	$T_1 = T_3 = T_{11}$	$T_2 = T_4 = T_{10}$	K_{GAIN}
Hz	degrees	-	seconds	seconds	-
1.0	142.0	0.1525	0.065215	0.40755	7.49
3.0	165.0	0.09941	0.016726	0.16826	60

Appendix E

Unit Ramp Rate Performance Data

The unit ramp up rates are all dependent on the turbine temperatures for the units at PS-KRG, there are four start up or ramping conditions, and these are adapted from [24]:

- Cold turbine start up - initial rotor temperature $< 65^oC$
- Hot turbine start up - initial rotor temperature 120^oC
- Hot turbine start up - initial rotor temperature 150^oC
- Very hot turbine start up - initial rotor temperature $> 160^oC$

Figure E.1 shows the cold turbine start up curve with an initial temperature of less than 65^oC which is used to ramp up the unit to rated operating load, adapted from [24]. Figure E.2 shows the simulated response of the unit with the sister unit operating at full load.

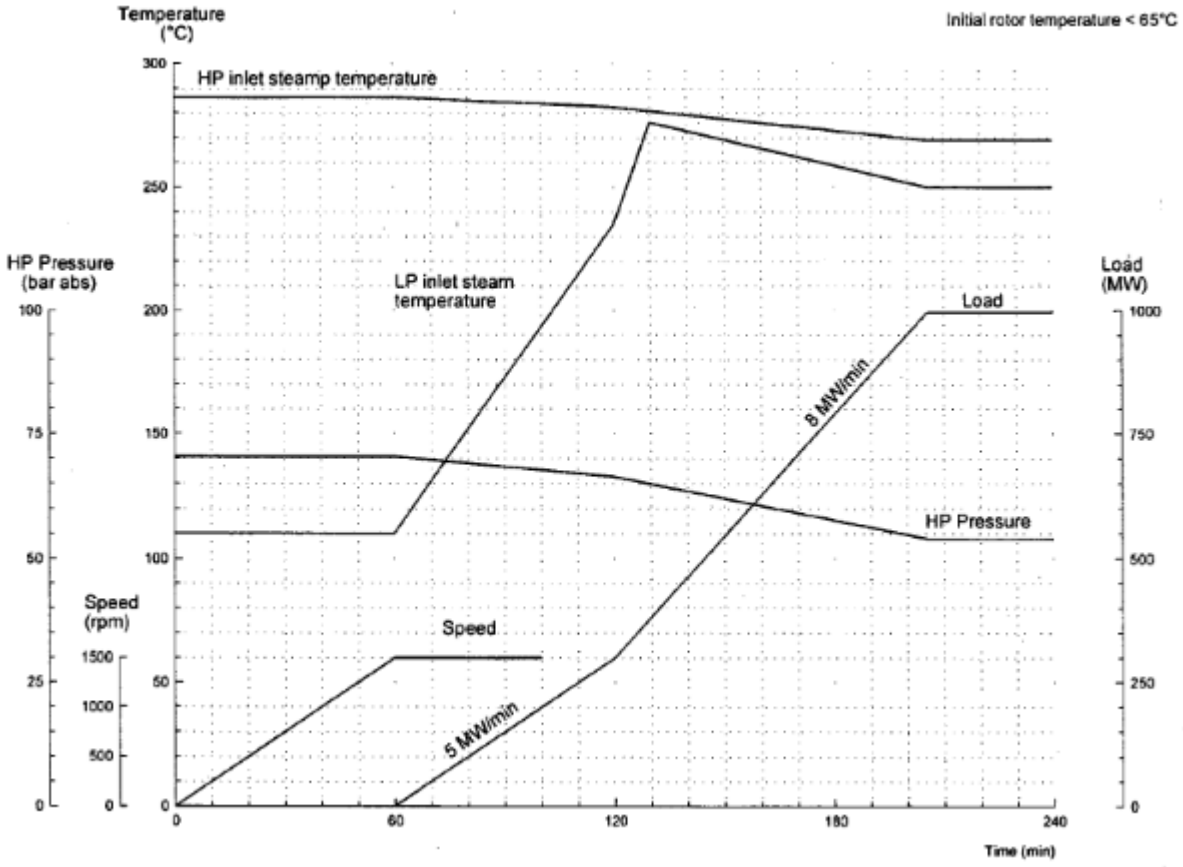

Figure E.1: Cold turbine start up curve with an initial rotor temperature of $< 65^oC$, adapted from [24].

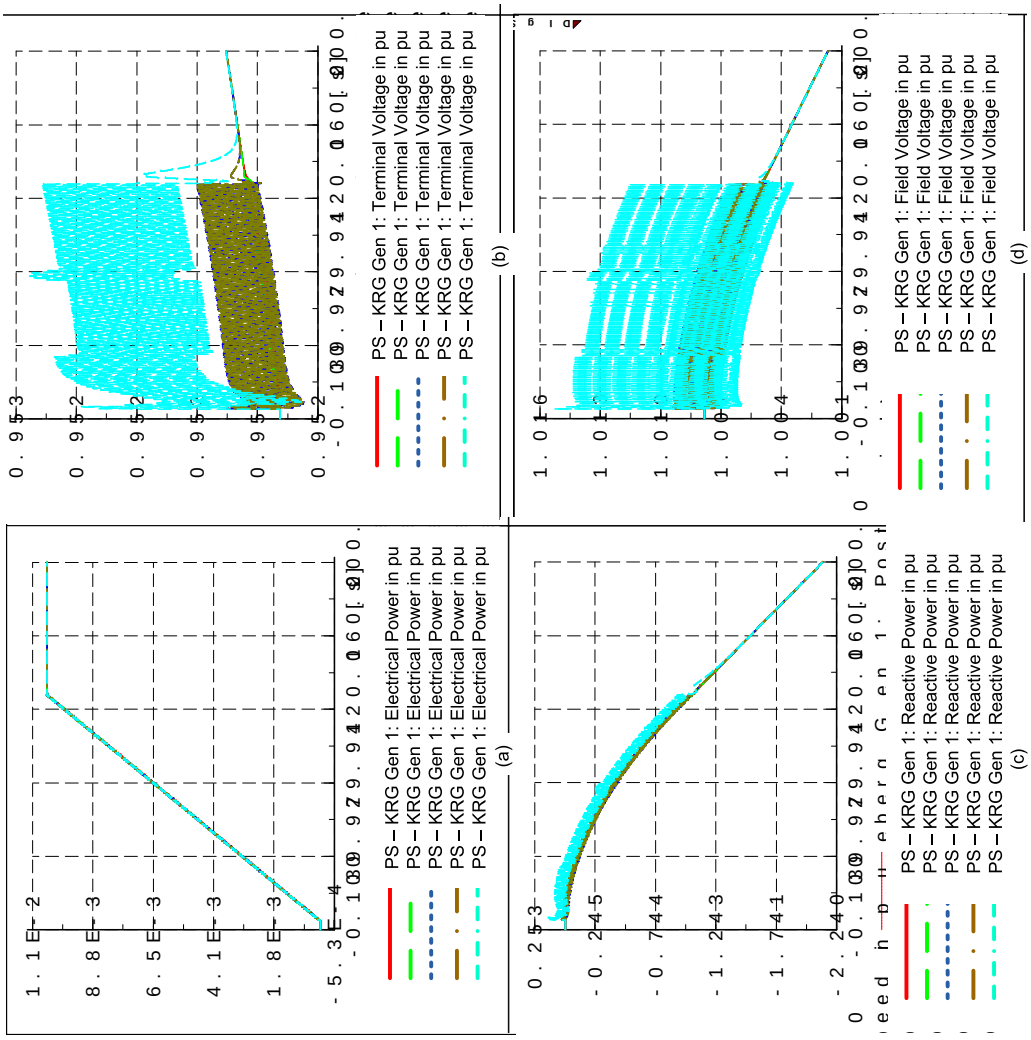

Figure E.2: Cold turbine start up curve with sister unit at full load and ramp rate of 5MW/min.

E.1 shows the hot turbine start up curve with an initial rotor temperature of 120^oC which is used to ramp up the unit to rated operating load, adapted from [24]. Figure E.4 shows the simulated response of the unit with the sister unit operating at full load.

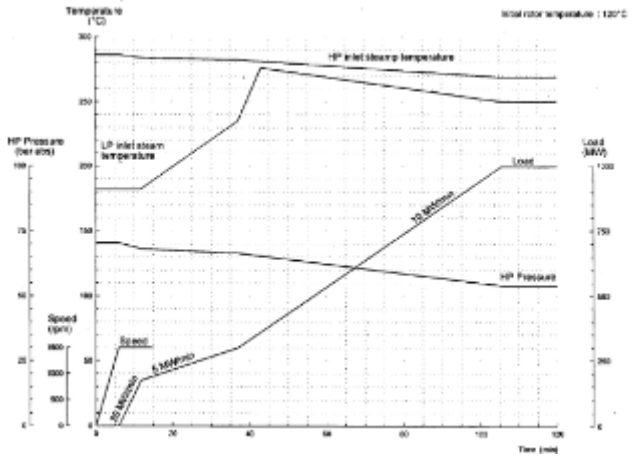

Figure E.3: Hot turbine start up curve with an initial rotor temperature of 120^oC, adapted from [24].

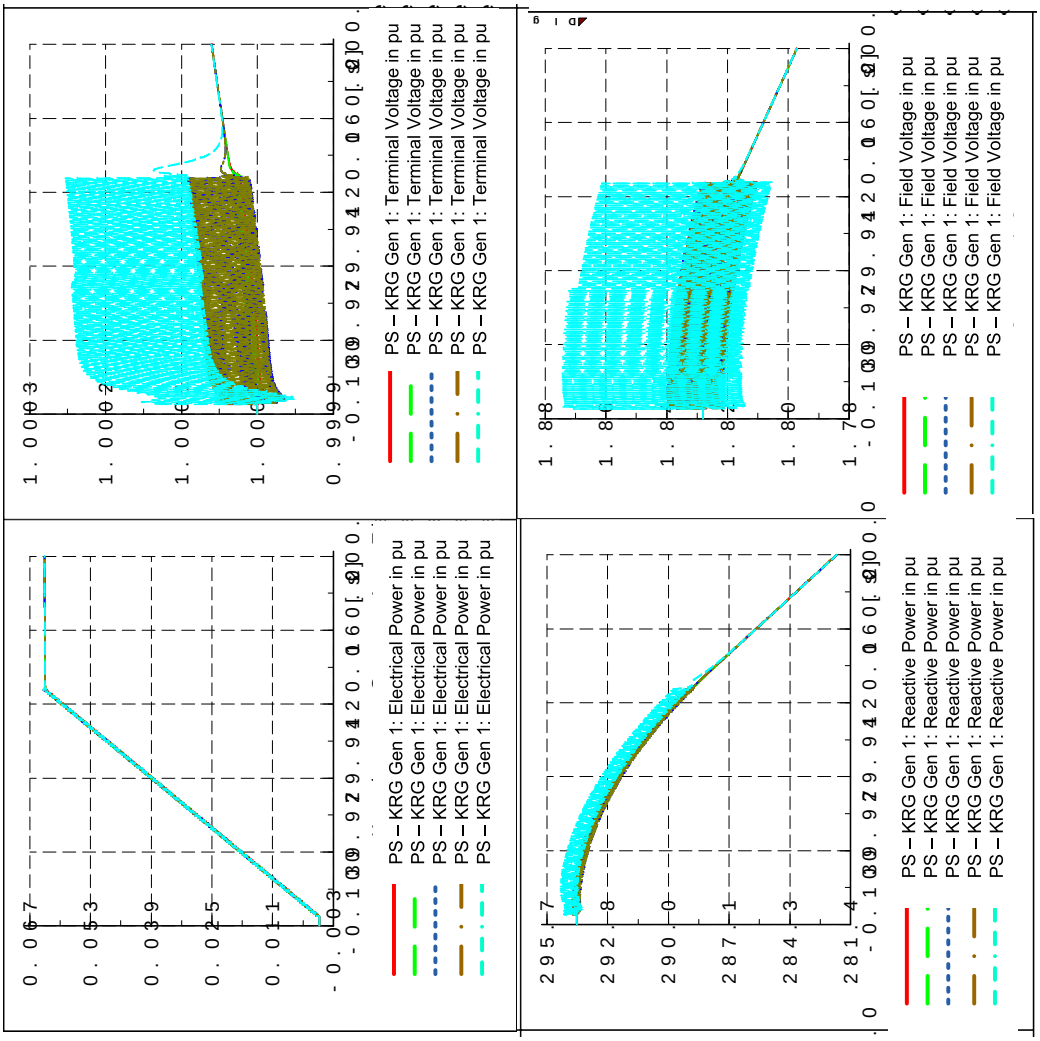

Figure E.4: Hot turbine 120^oCstart up at a ramp rate of 30MW/min with sister unit at full load.

Figure E.1 shows the hot turbine start up curve with an initial rotor temperature of 150^oC which is used to ramp up the unit to rated operating load ,adapted from [24]. Figure E.6 shows the simulated response of the unit with the sister unit operating at full load.

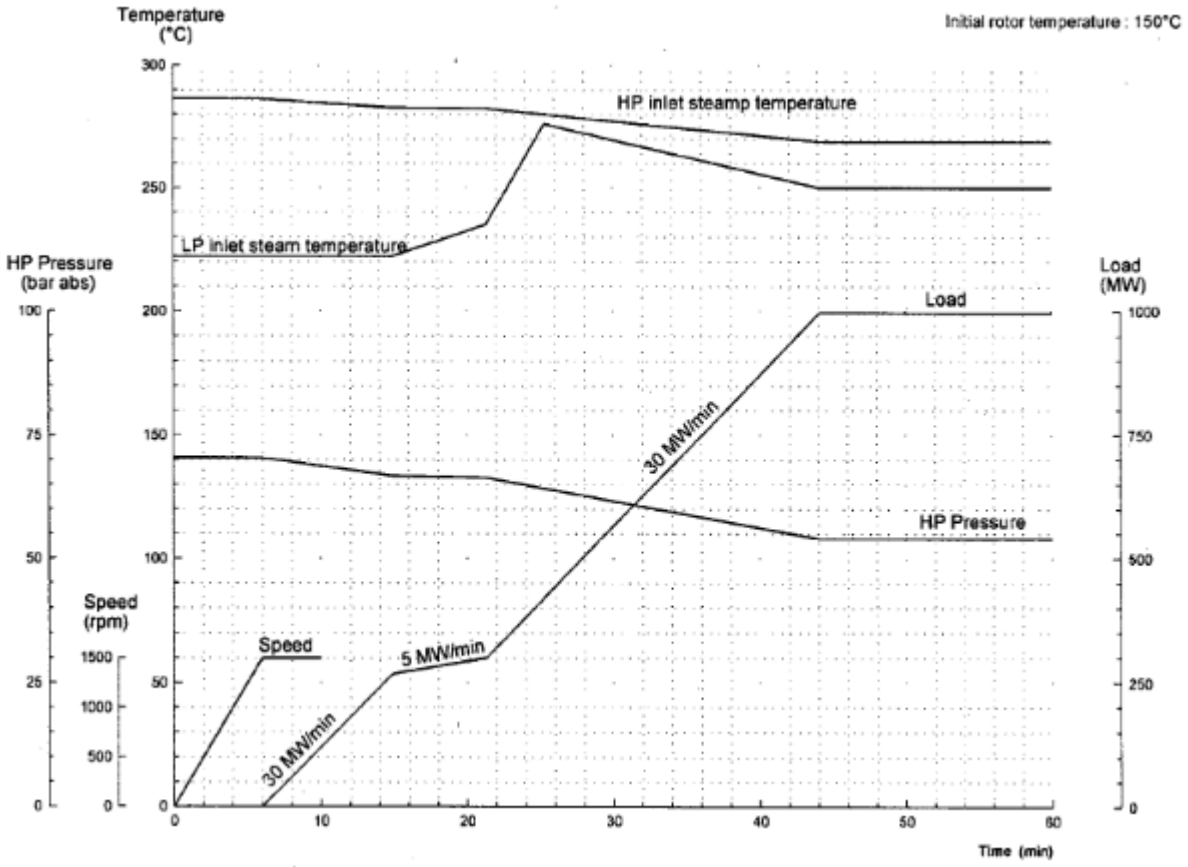

Figure E.5: Hot turbine start up curve with an initial rotor temperature of 150^oC, adapted from [24].

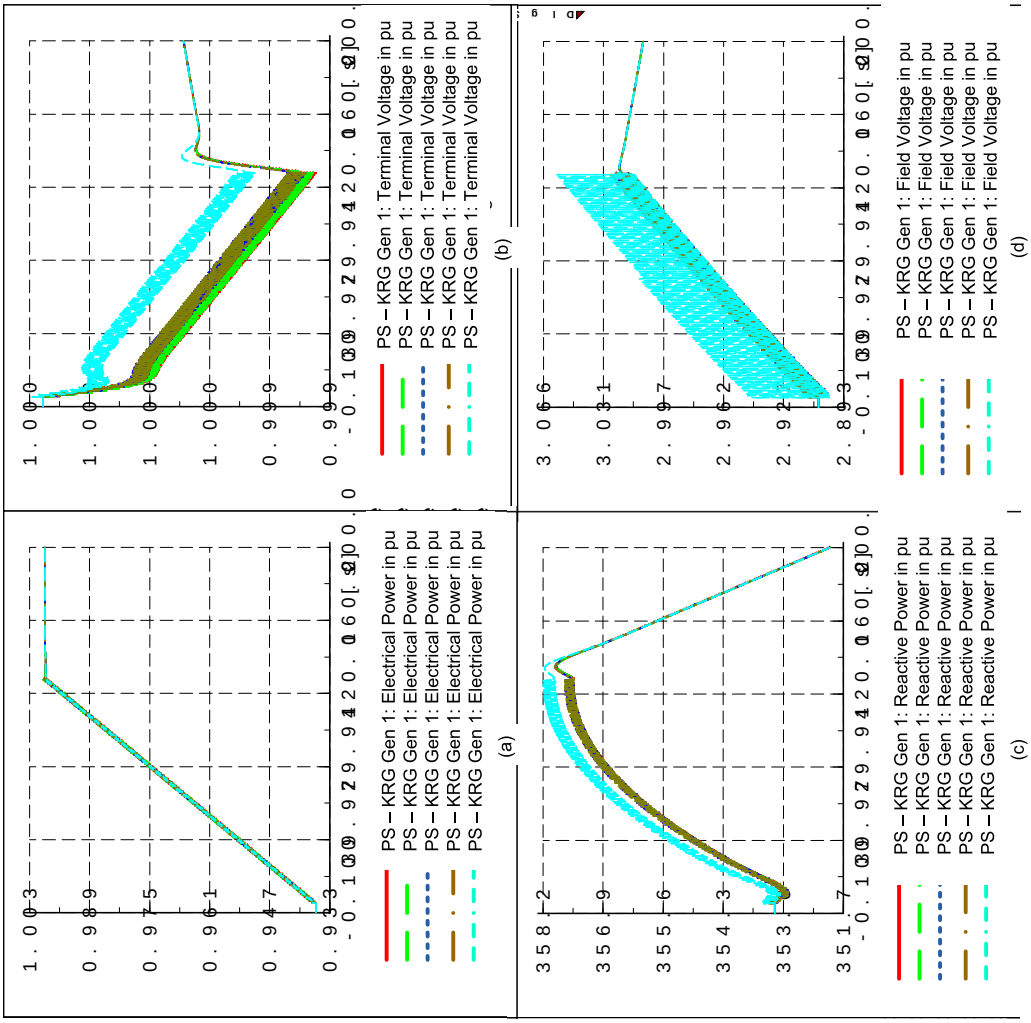

Figure E.6: Hot turbine start up 150^oC with a ramp rate of 30MW/min and sister unit on full load.

Figure E.1 shows the very hot turbine start up with rotor temperature greater than 160^oC which is used to ramp up the unit to rated operating load, adapted from [24]. Figure E.8 shows the simulated response of the unit with the sister unit operating at full load.

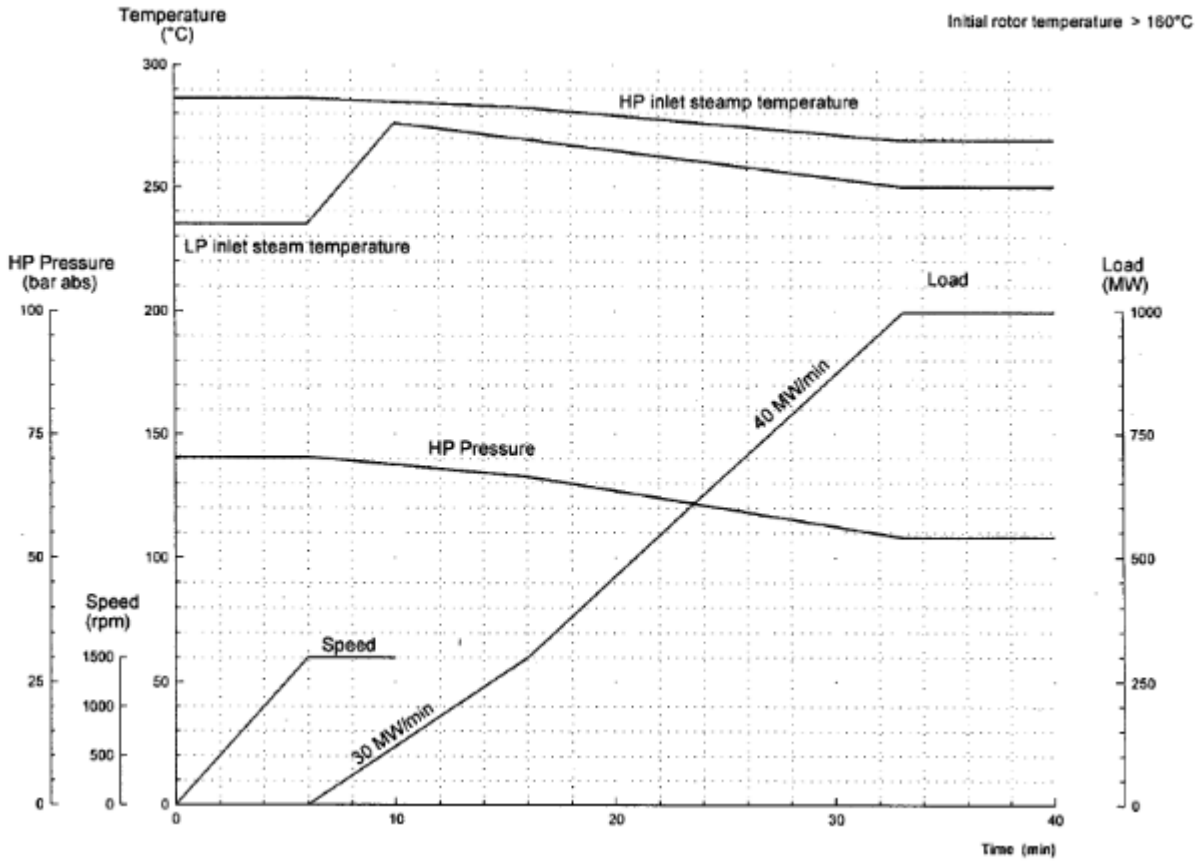

Figure E.7: Very hot turbine start up curve with an initial rotor temperature greater than 160^oC, adapted from [24].

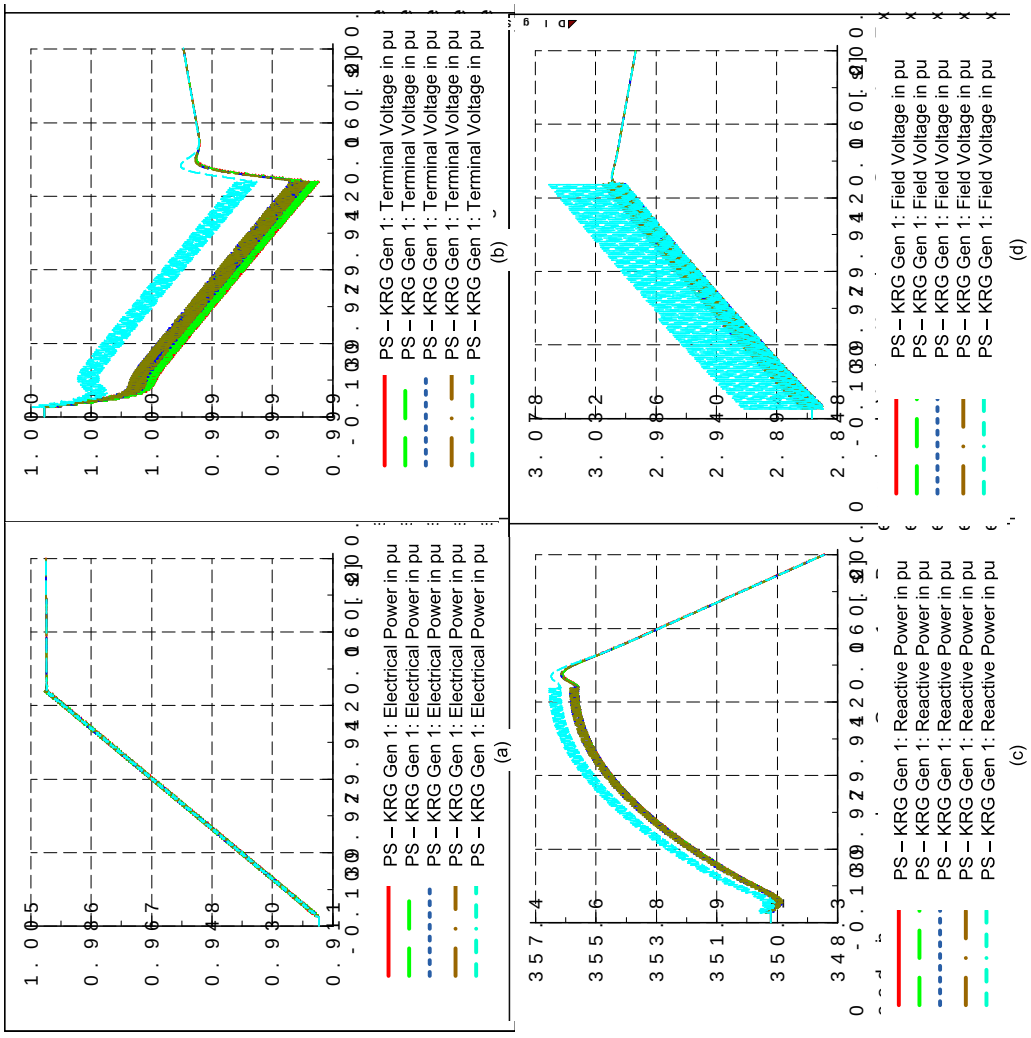

Figure E.8: Very hot turbine start up with a ramp rate of 40MW/min and the sister unit at full load.

Appendix F

Dominant inter-area oscillation mode example

The system which was used to demonstrate the application of the proposed algorithms is the well-known two area network example which was taken from [5]. Figure F.1 adapted from [5] shows a simple two area system with power flowing from area one to area two.

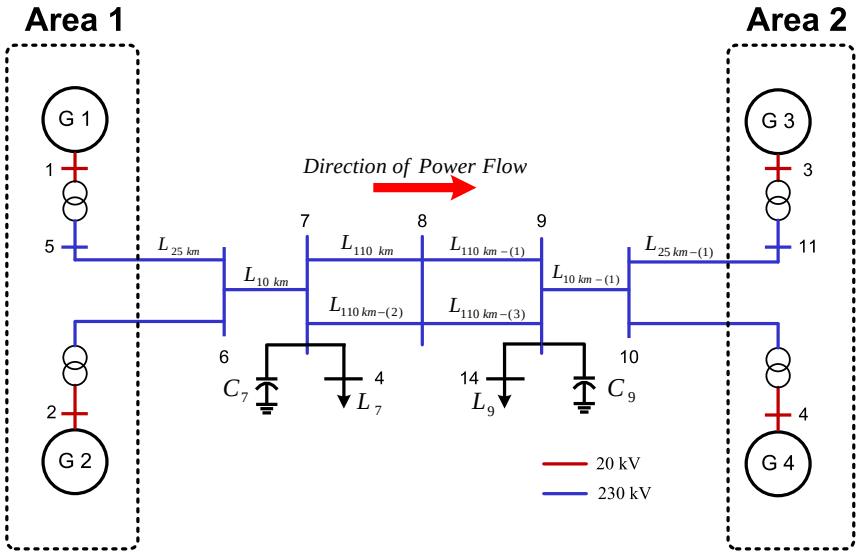

Figure F.1: Simple two area system adapted from [5].

Based on the eigenvalue results given in Table F.1, a single inter-area mode with poor damping was found. The various bus voltage and current sensitivities were calculated using Eq. (5.6) to Eq. (5.9). The observability of the inter-area mode of concern was then used to calculate the network mode shape of the various busbar voltages and currents of the network. It was found that the dominant inter-area oscillation path corridor occurs along bus bars 6-7-8-9-10 as expected.

Table F.1: Eigenvalue analysis results for rotor oscillation modes (without PSS).

Load flow	Eigenvalue (Frequency in Hz and Damping Ration)		
	Inter-area Mode	Area 1 Local Mode	Area 2 Local Mode
400MW	+0.027±j3.46 (ζ = −0.00786, f = 0.551Hz)	-0.647+j6.277 (ζ=+0.102, f=1.00Hz)	-0.659±j6.473 (ζ=+0.101, f=1.04Hz)
200MW	-0.033±j3.68 (ζ=+0.008, f=0.586)	-0.861±j6.153 (ζ=+0.139, f=0.99)	-0.648±6.537 (ζ=0.099, f=1.041)

Figure F.2 (a) shows the normalized voltage magnitude mode shape and Figure F.2 (b) shows the network voltage angle mode shape. Artificial network busbars were added to the network in order to improve the resolution of the graph shown in Figure F.2.

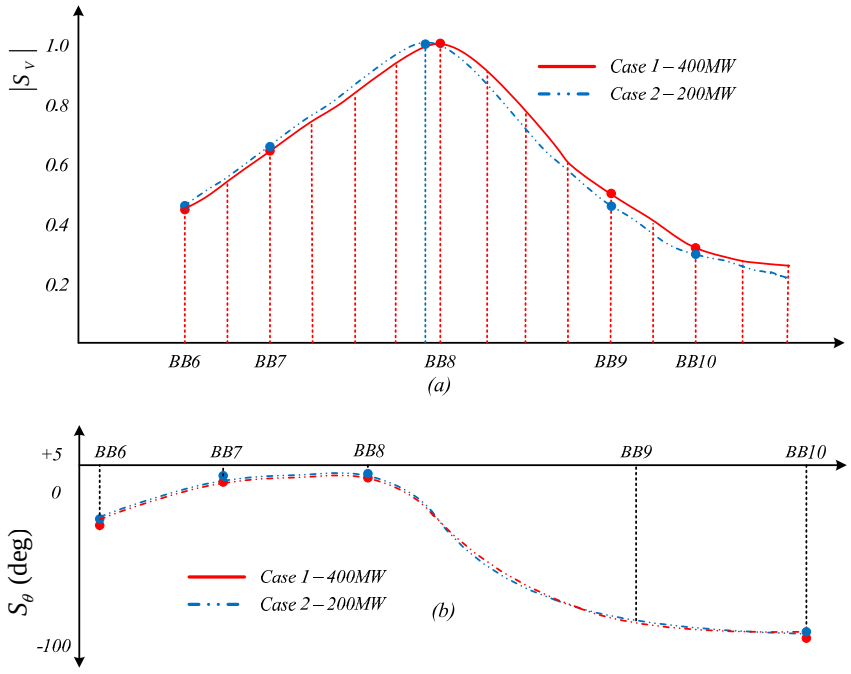

Figure F.2: (a) Normalized network voltage mode shape (b) Voltage angle mode shape.

It can be seen in Figure F.2 that the peak of the normalized voltage magnitude shifts to the left as the active power transferred from area one to area two is reduced. Reference

[69] states that this is a result of the AVR adjusting for different reactive power levels of the network.

It can be seen in Figure F.2 (b) that busbar (8) serves as the pivot of the inter-area oscillation flow. This is based on the observation that the smallest value of $S_{v\theta}$ occurs at busbar 8.

Appendix G

Dominant inter-area path fault assessment in the Eskom network

G.1 Fault impact analysis along corridor A

Figure G.1 shows the generator response for the loss of a line along corridor A. Transmission line AB-K was tripped and taken out of service.

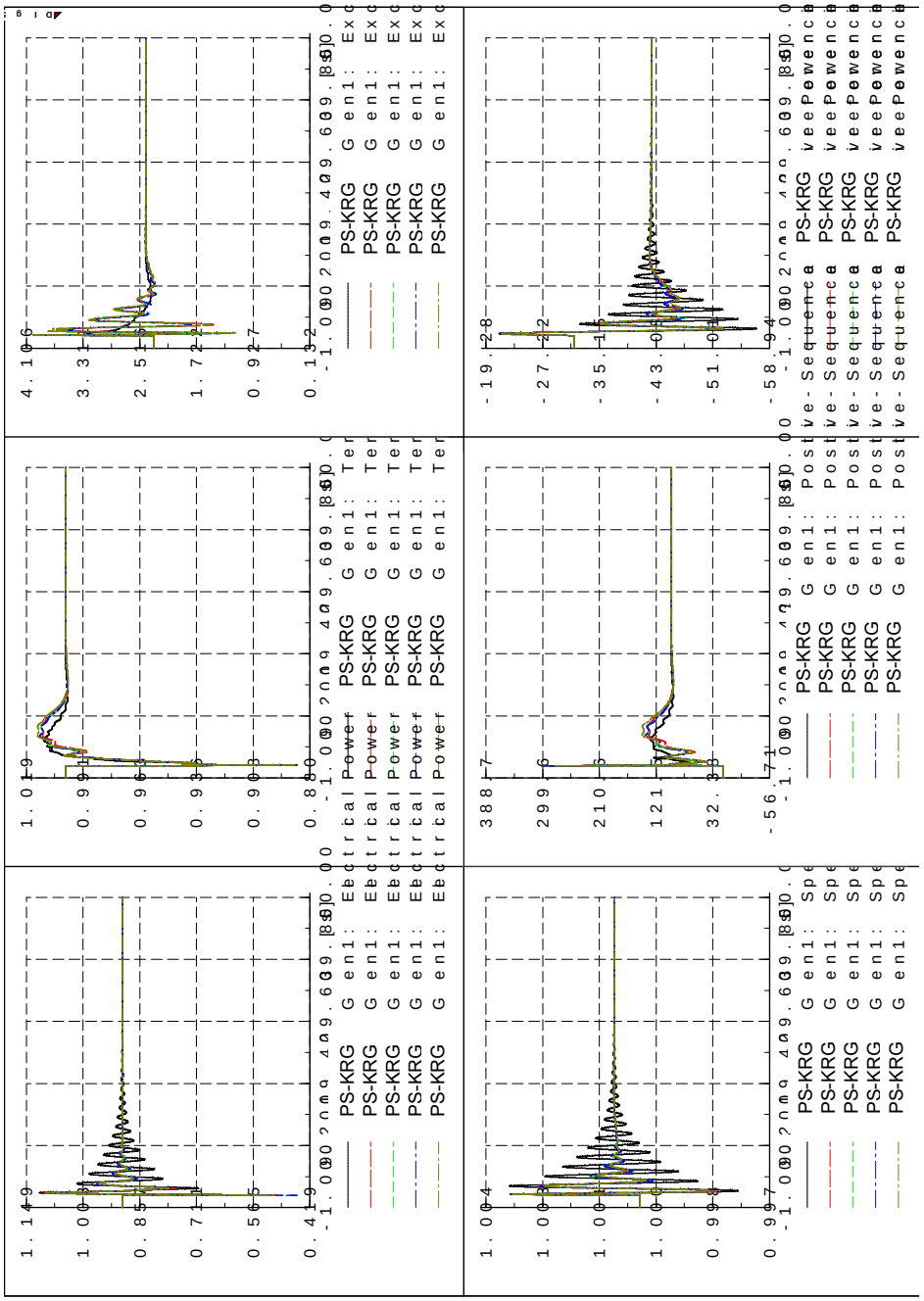

Figure G.1: PS-KRG generator response for a loss of a line in corridor A, line AB-K.

Figure G.2 shows the generator response for the loss of a line along corridor A. Transmission line AB-K was tripped and taken out of service.

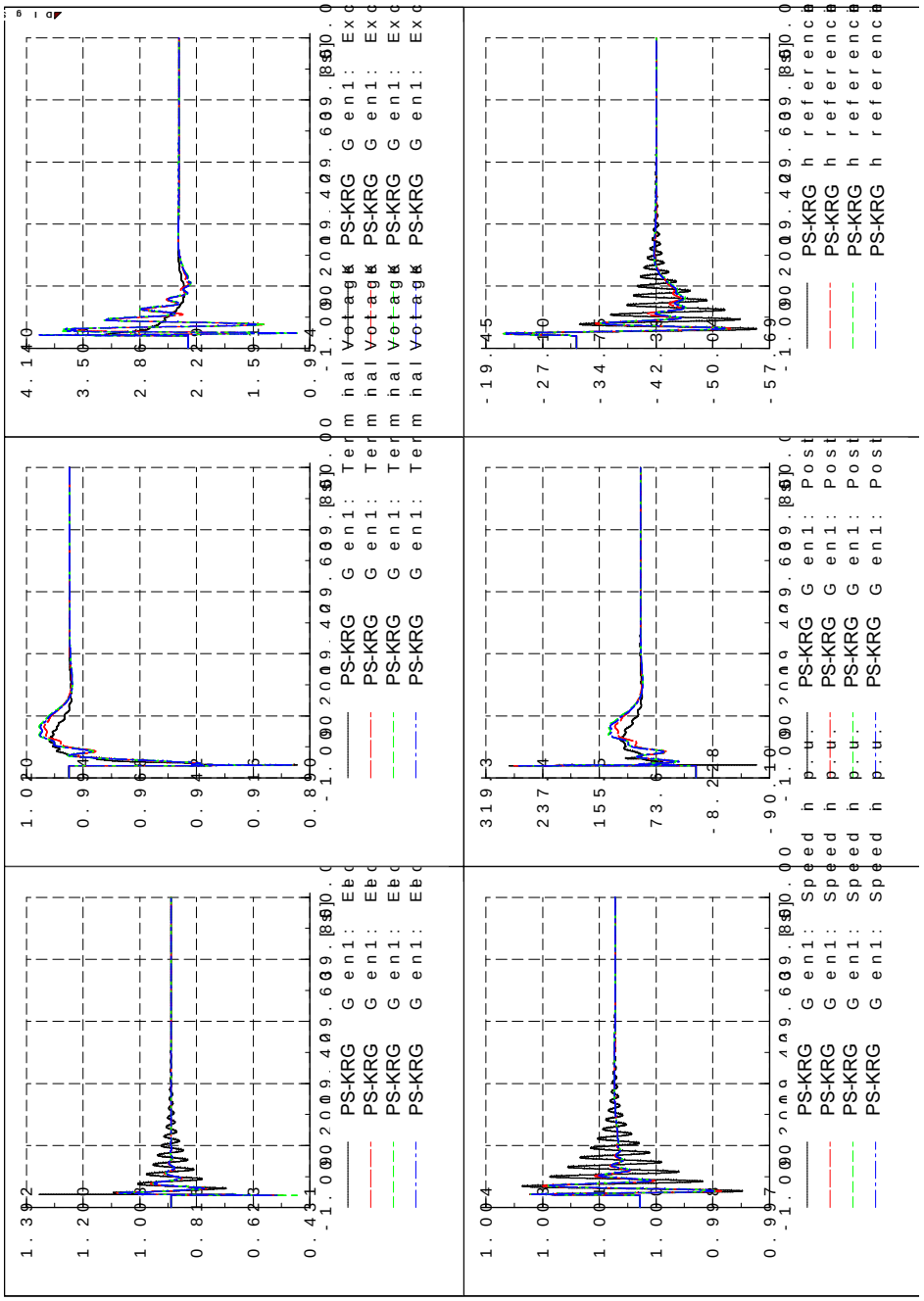

Figure G.2: PS-KRG generator response for a loss of a line in corridor A, line K-A1.

G.2 Fault impact analysis along corridor B

Figure G.3 shows the generator response for the loss of a line along corridor B. Transmission line B1-B2 was tripped and taken out of service.

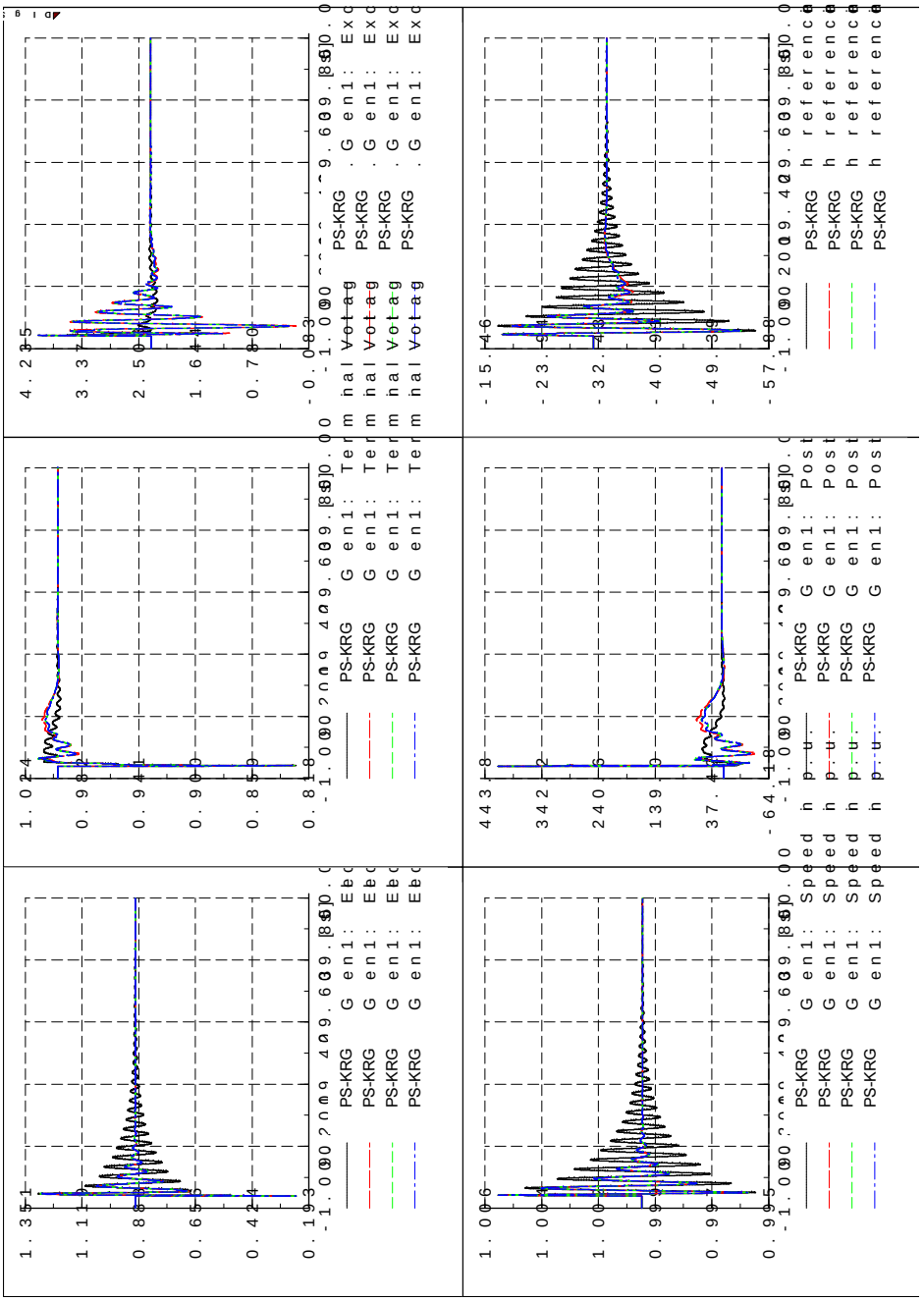

Figure G.3: PS-KRG generator response for a loss of a line in corridor B, line B1-B2.

Figure G.3 shows the generator response for the loss of a line along corridor B. Transmission line B2-B3b was tripped and taken out of service.

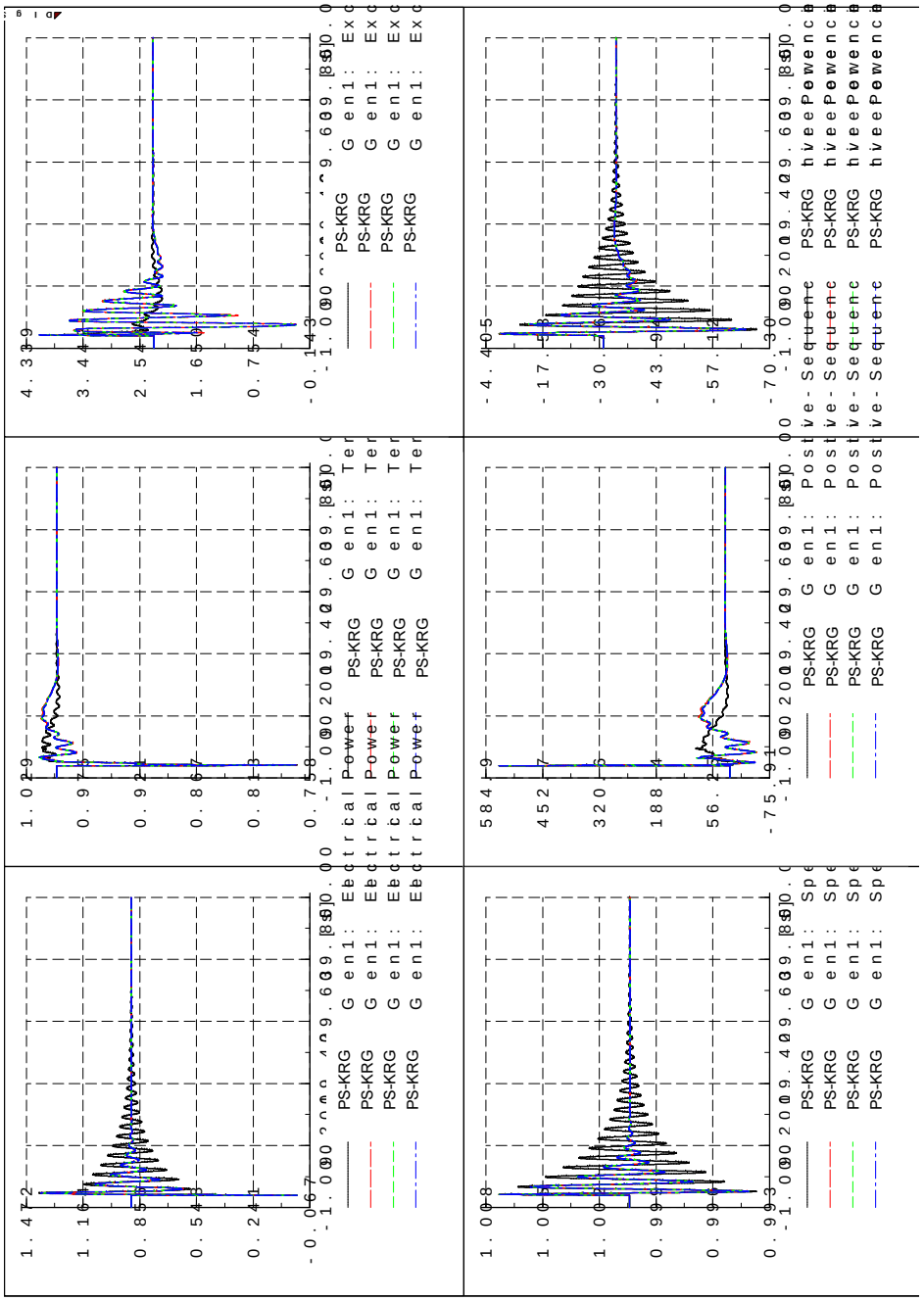

Figure G.4: PS-KRG generator response for a loss of a line in corridor B, line B2-B3b.